BRNO UNIVERSITY OF TECHNOLOGY

VYSOKÉ UČENÍ TECHNICKÉ V BRNĚ

FACULTY OF CIVIL ENGINEERING

FAKULTA STAVEBNÍ

INSTITUTE OF TECHNOLOGY OF BUILDING MATERIALS AND COMPONENTS

ÚSTAV TECHNOLOGIE STAVEBNÍCH HMOT A DÍLCŮ

BEHAVIOUR OF CEMENTITIOUS COMPOSITES EXPOSED TO HIGH TEMPERATURES

STUDIUM CHOVÁNÍ CEMENTOVÝCH KOMPOZITŮ PŘI PŮSOBENÍ VYSOKÝCH TEPLOT

DOCTORAL THESIS

DISERTAČNÍ PRÁCE

AUTHOR — Ing. Iveta Nováková

AUTOR PRÁCE

SUPERVISOR — doc. Ing. LENKA BODNÁROVÁ, Ph.D.

VEDOUCÍ PRÁCE

BRNO 2020

ABSTRACT

Fire resistance is becoming increasingly important along with the development of new concrete types with high strength and dense structure with reduced porosity. Such concrete types are susceptible to fire spalling and extensive crack formation. At the moment, there are a limited number of methods for enhancement of fire resistance of existing structures, which could be applied in underground structures with restricted space and limited air exchange, such as tunnels, underground garages or nuclear powerplants.

This work is focused on the development of two methods, and both are dealing with porous structure modification. The first method is intentional heat treatment (IHT) method, suitable for the enhancement of fire resistance of existing structures. The second method emphasized the design of air-entrained concrete (AeA-FiResCrete) with the use of “new generation” air-entraining agents suitable for enhancement of fire resistance of newly designed concrete. Testing of compressive strength, porous structure modification was completed by the analysis of “moisture clog,” which contributes to explosive spalling and extensive cracking. The efficiency of developing methods was verified during large-scale testing according to modified ISO834 (m-ISO) curve.

No extensive crack formation or explosive spalling was observed during the exposure period during the large-scale testing of slabs with the applied IHT method. The total thickness of the IHT method with configuration IHT200/2, composed of IHT zone and IHT transition zone, penetrated to the depth of 25,5 to 43,0 mm depending upon various concrete types. Moisture clog in AeA-FiResCrete was more significant than in the case of slabs with applied IHT method, and it could be concluded that the IHT method enhances fire resistance of concrete exposed to elevated temperatures without influencing its compressive strength and durability. Results from AeA-FiResCrete testing showed only a slight improvement of its fire resistance.

KEYWORDS

Fire resistance of concrete, intentional heat treatment (IHT) method, air-entrained concrete (AeA-FiResCrete), silica fume, polymer microspheres, porous structure, modified ISO 834 (m-ISO) curve.

ABSTRAKT

Trendem moderního stavitelství je časté používání vysokohodnotných a vysokopevnostních betonů. Spolu s vysokou pevností tyto betony obsahují malé množství vzduchových pórů, což může způsobit explosivní odpýskávání betonu a následný kolaps konstrukce. Dalším problémem jsou stávající konstrukce, které často nevyhovují současným zvýšeným požadavkům na požární bezpečnost. Využití existujících metod pro zvýšení požární odolnosti stávajících betonových konstrukcí, například nátěry a předsazené protipožární konstrukce, je limitované. Vývoj nových metod pro ochranu betonových konstrukcí je nezbytný, a to hlavně se zaměřením na aplikaci v tunelech, podzemních garážích a jaderných elektrárnách.

Tato práce se zabývá vývojem dvou metod pro zvýšení odolnosti betonů vůči působení vysokých teplot, se zaměřením na modifikaci pórové struktury. První metoda je záměrné předehřívání betonu (IHT method) pro zvýšení požární odolnosti stávajících betonových konstrukcí. Druhá metoda se zaměřuje na návrh provzdušněného betonu (AeA-FiResCrete) s vhodnými požárními vlastnostmi s použitím provzdušňujících přísad „nové generace“. Při experimentech byla kromě pevnosti a modifikaci pórové struktury sledována přítomnost tzv. vodní bariéry „moisture clog“. Účinnost vyvíjených metod byla ověřena testováním betonových desek dle modifikované teplotní křivky ISO 834 (m-ISO).

Desky ošetřené IHT metodou nevykazovaly při testování dle m-ISO křivky žádné nadměrné praskání ani explosivní odprýskávání. Celková tloušťka IHT metody skládající se z IHT zóny a IHT přechodné zóny byla v rozmezí 25,5 a 43,0 mm při konfiguraci IHT200/2. Při testování AeA-FiResCrete byla vodní bariéra výraznější než v případě desek s aplikovanou IHT metodou, a proto lze usuzovat, že IHT metoda přispívá ke zvýšení požární odolnosti, a to bez negativního vlivu na pevnost a trvanlivost betonu. Testované AeA-FiresCrete betony vykazovaly pouze nepatrné zlepšení odolnosti vůči působení vysokých teplot.

KLÍČOVÁ SLOVA

Požární odolnost betonu, metoda záměrného předehřívání betonu (IHT method), provzdušněný beton (AeA-FiResCrete), mikrosilika, polymerní mikrosféry, pórová struktura, modifikovaná ISO 834 (m-ISO) křivka.

BIBLIOGRAPHIC REFERENCES

Ing. Iveta Nováková *Behaviour of cementitious composites exposed to high temperatures.* Brno, 2020. 191 p. Doctoral thesis. Brno University of Technology, Faculty of civil engineering, Institute of technology of building materials and components. Supervisor doc. Ing. Lenka Bodnárová, Ph.D.

BIBLIOGRAFICKÁ CITACE

Ing. Iveta Nováková *Studium odprýskávání cementových betonů vlivem působení vysokých teplot.* Brno, 2020. 191 s. Disertační práce. Vysoké učení technické v Brně, Fakulta stavební, Ústav technologie stavebních hmot a dílců. Vedoucí práce doc. Ing. Lenka Bodnárová, Ph.D.

DECLARATION OF CONFORMITY OF PAPER AND ELECTRONIC FORM OF DOCTORAL THESIS

I declare that the electronic form of the submitted doctoral thesis entitled Behaviour of cementitious composites exposed to high temperatures is identical to the submitted paper form.

In Narvik on 31. 08. 2020

Ing. Iveta Nováková
author

PROHLÁŠENÍ O SHODĚ LISTINNÉ A ELEKTRONICKÉ FORMY ZÁVĚREČNÉ PRÁCE

Prohlašuji, že elektronická forma odevzdané disertační práce s názvem Studium odprýskávání cementových betonů vlivem působení vysokých je shodná s odevzdanou listinnou formou.

V Narviku dne 31. 08. 2020

Ing. Iveta Nováková
autor práce

DECLARATION

I declare that I have prepared the doctoral thesis entitled Behaviour of cementitious composites exposed to high temperatures independently and that I have listed all used information sources.

In Narvik on 31. 08. 2020

Ing. Iveta Nováková
author

PROHLÁŠENÍ

Prohlašuji, že jsem disertační práci s názvem Studium chování cementových kompozitů při působení vysokých teplot zpracovala samostatně a že jsem uvedla všechny použité informační zdroje.

V Narvik dne 31. 08. 2020

Ing. Iveta Nováková
autor práce

ACKNOWLEDGMENT

I would like to express my sincere thanks to my supervisor, doc. Ing. Lenka Bodnárová Ph.D. for supervision and support during the whole time. Furthermore, I would like to thanks prof. Ulrich Diederichs and prof. Olafur Wallevik for providing me their laboratories for experimental work, their support and essential advisory work during my PhD studies. Finally, I would like to thanks all colleagues and experts who supported me during my research activities and internships including my family and friends.

CONTENT LIST

INTRODUCTION

Concrete is one of the basic building materials, and its composition is under constant development. Almost every building or structure contains concrete; annual production is about $3{,}8 \cdot 10^9$ -$10 \cdot 10^9$ tons (1, 2). Many centuries have passed from the time when the first concrete structures were built. The earliest recordings of concrete structures are being dated back to 6500 BC by the Nabataea traders in regions of Syria and Jordan.

Nevertheless, Romans are more known for the use of Roman concrete due to its widespread utilization. The technique for making puzzolan cement was lost since the fall of the Roman Empire in 476 AD until the year 1414, when the manuscript was found again. Development and research focused on cement and concrete technology took an endless 410 years, until the invention of Portland cement by Joseph Aspdin in the year 1824 in England (3). Since that time, the main ingredients as aggregates, cement and water were supplemented by admixtures, additions, various types of fibres and rebars to improve concrete properties. The most significant progress in concrete design took place in the last 90 years due to more sophisticated analyses and new technologies for testing and evaluation of concrete properties. Nowadays the names such as high-performance concrete (HPC), self-compacting concrete (SCC) or fibre reinforced concrete (FRC) are widely used not only in the scientific community but also in the construction sector.

The most important properties of fresh concrete which have to be considered during the design process are consistency, air content and workability loss. Great emphases are given to those properties of fresh state concrete to reduce or eliminate mistakes caused by workers during the processing of concrete on a construction site. Improper processing of fresh concrete could degrade the final properties of hardened concrete, and even if the concrete is excellently designed, properties of hardened concrete could be insufficient. There are many properties of hardened concrete which are evaluated by numerous tests, but the most important are compressive strength and durability. Durability is likely increasing along with compressive strength, and newly developed concrete types such as HPC or UHPC (ultra-high performance concrete) are reaching compressive strength from 70 MPa up to 200 MPa and even more. Concrete, which is classified as a UHPC, should have a minimum compressive strength of 120 MPa (4). High compressive strength is achieved by good packing design, reduction of water-cement ratio, and an increase of powder components. All those factors result into reduction and modification of the air void system. Upgrade of one characteristic might have a negative impact on some other characteristic, and in the case of HPC and UHPC, it is fragility and decrease of fire resistance. These particular types of concrete are susceptible to explosive spalling more than standard concrete. Khory described spalling as a violent or non-violent breaking off of layers or pieces of concrete from the surface of a structural element when it is exposed to high and rapidly rising temperatures, as experienced in fires with heating rates typically 20–30°C/min (5).

Concrete is inhomogeneous non-plastic material, composed of aggregates, cement paste and air voids. If it is exposed to elevated temperatures over 100°C, each component has different thermal expansion or shrinkage, which results in disruptions of internal concrete structure and microstructure. There are three main phenomena, which are causing cracking and damages of microstructure, namely water molecule migration, chemical changes of cement paste, and incompatibility of cement paste and aggregates volume changes. If the moisture content of the concrete element in the natural environment is under 3%, explosive spalling is unlikely to occur as the moisture migration is not excessive (6). If the concrete is exposed to climate conditions in northern or central Europe, the moisture content is usually above 3%, and fire resistance precautions have to be made while designing new concrete structures. By simple computation it can be calculated that 75 l of free water in 1 m^3 of concrete with 3% moisture content, in the surface layer with an area 1 m^2 and thickness 10 mm (minimum allowed cover layer thickness for reinforcement) there is 0,75 l of unbonded water. In case of a fire event this free water is going to transform into vapour and migrate into

surrounding ambient. Transformation of water into vapour in pores of cement paste is accompanied by the rise of pressure, one of the main factors of explosive spalling. The first chemical changes in cement paste as dehydration of ettringite and dehydration of calcium silicate hydrates (CSH) gels terminate at temperatures above 80°C. Damage of the concrete microstructure reduces strength, and the spalled cover layer of reinforced concrete exposes the steel rebars and can result in collapse of the whole structure.

Fire is one of the four elements of nature, and it is almost impossible to predict its behaviour. Nevertheless, there are documents which are focusing on structural fire design and fire resistance testing. These documents might seem very strict and exaggerated, but Chapter 1" “reviews fire events which exceeded all expectation and caused excessive damages of structures and caused numerous life losses. The main objectives of Eurocode 2: Design of concrete structures - Part 1-2: General rules - Structural fire design (6) are a restriction of fire spread and inhibition of collapse of the entire structure. The European standards EN 1363-1:2012 and EN 13823:2010+A1:2014 are focused on fire resistance tests and determination of the behaviour of individual elements and structures subjected to defined heat traffic and the period until they divert from their characteristic strength (7, 8). The riskiness is even higher in road tunnels and underground garages, where the ventilation system is needed for smoke removal, and heat is accumulating in the location of the fire. Nowadays, the traffic in large cities is diverted into tunnels to reduce traffic in the streets, and this means that tunnel linings carry a higher burden of responsibility for safety. In the case of fire event and consequent collapse of tunnel lining not only people and structures underground are endangered but also on the surface above the tunnel which can lead towards catastrophic consequences. The development of concrete with better fire resistance characteristics is not going to prevent the occurrence of the fire events but could contribute to higher residual strength of affected structural elements and cost reduction of the reparations of damaged structures.

This PhD thesis is focussed on the design of a new method to increase the fire resistance of existing concrete structures and innovative design concrete mixes. In the past, when admixtures and additions were not used, a concrete structure was more “open” and characterised by a more extensive air void system. New types of concrete like HPC and UHPC have a significantly reduced air void system due to high strength gain, and that has a negative impact on fire resistance. It was validated that capillary pores highly contribute to the better fire resistance of concrete and reduces fire spalling (9). One of the main objects within this research is connected to the development of the intentional heat treatment (IHT) method for porous structure development in existing concrete structures, and its consequent evaluation if it contributes to better fire resistance and reduction of the explosive spalling occurrence.

I. THE THEORY

1 FIRE EVENTS AND IMPORTANCE OF FIRE PROTECTION FEATURES

Throughout the years and decades, hundreds of smaller or larger scale fires have been recorded. Fire is one of the four elements and it is hard or sometimes even impossible to get it under control. Fire propagation depends on the materials present and local conditions. If the fire event takes place in open space, the type of flaming material, direction, and speed of wind play a major role. Access of firefighters is not restricted, and they can use various techniques such as water jets or sprinkle from the air with the use of cranes or planes. Other techniques for extinguishing a fire such as dry powder extinguishers and compressed air foam systems (CAFS) can be used in case of dealing with fire events which cannot be extinguished by water. When the fire occurs in an area where access is restricted, then the techniques and methods for extinguishing the fire are more complicated, and can lead to more rapid development of temperatures in the centre of fire. Fire spread in restricted areas such as closed underground car parks or road and rail tunnels depends on the quantity of inflammable materials in the area surrounding ignition of the fire and air velocity. Parameters of fire regarding temperature development and maximum temperature can cause significant damage to the structure. However, for evacuation and rescue of victims from the fire event the smoke is more severe, which is complicates not only evacuation but also visibility during the extinguishing of fire by firefighters, see Fig. 1 (10).

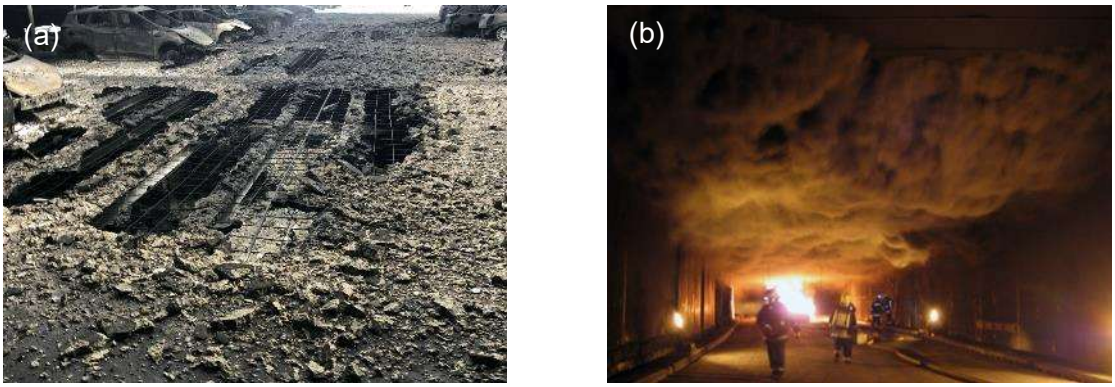

Fig. 1: (a) Structural damage caused by fire; (b) The smoke stratification in the initial moments of the fire (11, 12).

Fire safety in tunnels is improving and adjusting to the present situation concerning vehicles and their technological developments. In the past there were vehicles with either petrol or diesel engines, nowadays there are vehicles with gaseous fuels, electric and hybrid-electric engines which are characterized by different fire scenario and requires different rescue operations. A brief discussion of various fuels and their risk can be found in section 1.2.

Every fire event leads to an improvement in knowledge and development of new and innovative fire protection methods. Furthermore, with the development of high-tech technologies and various types of software for modelling of fire protection systems, structures could be designed with higher efficiency. In those advanced modelling programs, fire spread can be based on tests performed in the laboratory; in other words, first fire test then modelling. Alternatively, another way round based on modelled fire scenarios, structures or fire safety systems can be tested in the laboratory to prove the accuracy of the models (13–15); in other words modelling before fire testing.

1.1 Fire events

Fire events could be classified in various manners, but no matter how severe the fire scenario is, there are always damages of structure, and sometimes even loss of human lives. The cause of a fire could be intentional, initiated by arsonists, or originate accidentally from defects in electrical installation, incorrect work procedures, human fatigue, or inattention. The location of a fire could be in highly populated urban areas and human life can be endangered, on road infrastructure in or outside of the towns, remote place and countryside, where the victims are animals.

Fires in the city could be small, and firefighters are able to get it under control within a few hours, or the fire is massive and quickly spreads around multiple structures. Large scale fires were more common in middle age times, for example, the Great Medieval fire of London in 1135 or the Great fire of Gouda in Netherlands 1438 (16). From the beginning of the 19th century, at least one big fire accident has been recorded every year. Fires from recent years worthy of mention are:

- fire at container storage station at the Port of Tianjin, China 2015, where there were 173 accident victims (17).
- Grenfell Tower fire, West London, England 2017. Fire damaged whole high-rise building and spread very quickly most probably due to low fire resistance of cladding (16).
- Notre-Dame de Paris fire, France 2019, world heritage building caught in a fire and entire wooden structure of the roof and some sections of stone vault underneath collapsed (18).

Fire events involving road structures, in particular tunnels, are going to be described in detail in section 1.1.2. Large scale vegetation fire events are taking place every year in Australia, California, and other countries (19, 20). It is very challenging to get such large scale fires under control, and large numbers of firefighters and heavy techniques and interventions are needed.

Fig. 2: (a) Typical Australian bushfire scenario (21)*; (b) Notre-Dame de Paris fire* (22)*; (c) Grenfell Tower in flames* (23)*.*

1.1.1 Parking garages

Fire in underground garages can arise from more sources than in the case of tunnel fires, which are always caused by vehicles or trains. According to MSB's statistics in Sweden (24) and astudy carried out in New Zealand, the most common cause of the reported fires are arson and electrical or technical failures. Fires in parking garages are often limited to one vehicle, only in 3% of cases fire spreads to other vehicles mostly due to insufficient ventilation (25). In Sweden between the years 2011 and 2014, roughly 40 vehicle fires took place in multi-storey parking facilities or large garages every year. French researchers stated that between 1995 and 1997, 98% of garage fires involved fewer than four cars and 95% of those fires were extinguished in less than 60 minutes. By contrast, 8% of garage fires between 2010 and 2014 involved more than five vehicles and 6% involved more than seven vehicles. Furthermore, only 40% were extinguished in less than an hour, 30% took more than 2 hours and 10% took more than 4 hours (12).

In some cases, fire can spread from one parked vehicle to another even over one free parking spot between the parked vehicles. Vehicles currently produced contain about 50% of plastic by volume, which represents 10% by weight (12). Plastic melts at lower temperatures than steel and is also more combustible, which contributes to faster fire development. Those statistics clearly point towards the increased risk of modern cars build with polymer-based composite materials and new types of fuels.

King's Dock, Liverpool, England, 2017

The fire started during New Year´s Eve when everyone was at the stadium. Thanks to that, there were no major losses of lives. All floors of multi-storey parking garage caught fire and 1 400 vehicles were completely destroyed bythe fire. Water which was sprayed over the garages to extinguish the fire was draining through the individual floors as they were ruptured to a great extent. The temperature of the fire reached 1 100°C which is severe for a concrete structure and contributes to the collapse of the entire building (12, 26, 27). This event created opportunities for large scale research programs and verification of new fire safety systems and models (28).

Fig. 3: King´s Dock: (a) External CCTV image; (b) Ramp from level 6 to level 7 (27).

Helsingborg, Sweden, 2013

An electric car with a nickel-cadmium battery caught fire for unknown reasons. During the fire, three other cars were destroyed entirely and another 75 were damaged by smoke and soot (29).

Gretzenbach, Switzerland, 2004

A car parked in the garage, which was a part of an apartment complex. The roof of the garage which served as a playground with trees and park benches, collapsed shortly after 11 firefighters entered the garage. The collapse of the roof killed 7 firefighters (30).

San Diego, California USA, 2018

Fire in an underground garage in the basement of a residential building. Smoke from the fire spread up to the second floor (31).

1.1.2 Road and rail tunnels

According to the statistic from several countries including France, Italy and Germany, accidents seem to occur more frequently on open roads and less in tunnels. The reason behind that could be a better focus of drivers and higher control of the tunnels when compared to open roads. According to French statistics, there will only be one or two car fires (per kilometer of the tunnel) for every hundred million cars that pass through the tunnel (32). Those numbers are extremely low, but every fire event in a tunnel has a destructive impact not only on the vehicle but also on tunnel structure. As tunnel structures are equipped with many installations and the tunnel lining has to dispose of certain load-bearing capacity, exposure to high temperatures can significantly decrease its strength and result in the collapse of the entire structure. Refurbishing works and installations in tunnels are expensive and reparation of tunnels can be demanding both financially and in terms of time.

Fire events in road tunnels are more frequent than in rail tunnels, but the accidents in rail tunnels are usually more severe in relation to human victims. Further, in this chapter, several examples of accidents in road and rail tunnels are going to be reviewed. About two thirds of fires in rail tunnels are caused by an electrical or mechanical failure, while in road tunnels the proportion attributed to these elements is approximately half. Approximately one-third of fires in road tunnels were caused by human behaviour (errors and wrong decision-making). Accidents in tunnels involving large scale fires and deaths always get more publicity, but as we are focusing on the damage to structures, every event in a tunnel involving elevated temperature counts.

One example for all is Norway, with its high number of tunnels. Norway is a country that constructs the most road tunnels, over 1 100 tunnels with a total length of 1 134 km (33, 34). A study performed by Norwegian public road administration map vehicle fires in tunnels between the years 2008 and 2015. In the study many parameters were evaluated and taken into account, such as length of the tunnels, time of the fire, location of the fire in the tunnel, involved vehicles, injuries to people and damage of vehicles, and action of tunnel service operators and emergency services. Other pieces of information about fire events were the duration of the fire and resulting refurbishment works, effect of the fire ventilation, and estimated fire load in megawatts (MW). Subsea tunnels, about 14,5% of tunnel kilometers in Norway, are a special case as there is a gradient higher than 5%. A combination of high gradient and heavy goods vehicles is a cause for about 46% of accidents in Norwegian tunnels between 2008 and 2015. Summary of fires and smoke without fire accidents in Norwegian tunnels is presented in Fig. 4 (33, 34). In only Oslofjordtunnelen 16 fire events during an 8 year period (2008-2015) were investigated by the Accident Investigation Board, Norway, and led to the establishment of many safety recommendations (35).

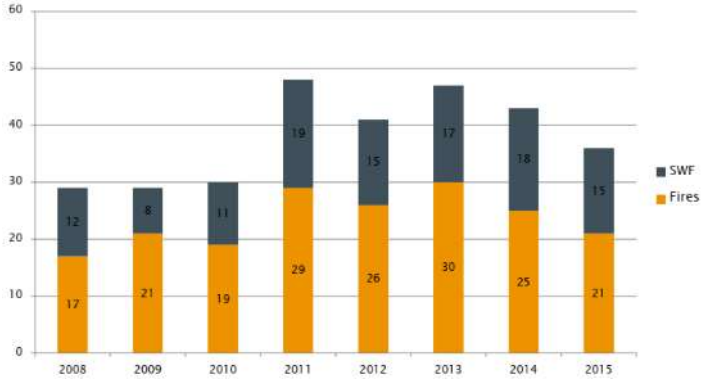

Fig. 4: Fires and smokes without fire (SWF) per year in tunnels in Norway (34).

Channel Tunnel, France and the United Kingdom, 1996, 2006 and 2008

Heavy goods vehicles (HGVs) carrier shuttle caught fire even before entering the tunnel. The fire size was established to about 1,5 MW when entering the tunnel and elevated to 350 MW at its maximum. Fire events in 1996 and 2008 have a similar scenario, flames spread over several HGVs and carriages, but in 2006 only one HGV was entirely destroyed but did not spread to either of the adjacent vehicles. Nevertheless, the tunnel lining was affected to the depth of 30 mm and the catenary parted over the length of 10 m. During the fire in 2008, 650 m of tunnel lining and installations were damaged. The refurbishment of the tunnel took about 5 months and cost 60 million euros (32).

Mont Blanc Tunnel, France and Italy, 1999

A HGV traveling through the tunnel caught fire possibly due to overheating of the engine. In total 25 vehicles were trapped in the tunnel, and 38 tunnel users and firefighters died as a result of the extensive fire which spread over 1,2 km length of the tunnel. Severe damage was caused to the tunnel lining over a length of 900 m and the maximum temperature during the fire event was estimated to 1 000°C. The fire lasted for 53 hours and even after 5 days, the centre of fire was still closely watched. It was extremely challenging to fight due to a large amount of dense smoke. Several significant factors contributed to such an extensive fire including goods carried in the HGV, wind direction from the south, different ventilation regimes at either end of the tunnel, and speed of the ventilation at 1 m/s. The fire in Mont Blanc Tunnel on 24th March 1999 was the eighteenth HGV fire recorded since the tunnel opened in 1965 (32).

Tauern Road Tunnel, Salzburg Austria, 1999

A car accident of 60 individual vehicles was the cause of a fire in the tunnel in which 12 people were killed and 42 injured. The incident occurred when a truck collided with a column of a stationary vehicles waiting at traffic signal. A high contribution to the rapid development of the fire was a HGV carrying spray cans and paints. Fire destroyed 16 HGVs and 24 cars. The large scale fire was boosted by escaping fuel and hazardous materials on one of the involved vehicles. The fire (with a duration of 15 hours) significantly damaged the tunnel, and reparation and improvement of structure, ventilation and fire safety systems lasted for 3 months. The fire duration was rather short as the transverse ventilation system worked very well, but damages were significant due to rapid temperature development (36, 37).

Summit tunnel, Littleborough UK, 1984

A train carrying 1 million liters of petrol derailed in the tunnel, and fire flames went through a ventilation shaft 120 m high. This event is referred to as a most severe event, as the temperature was reaching values so high, that brick walls and all steel components were melting down (36).

An important lesson has been learned from every fire event in a tunnel or underground garage, and both active and passive fire protection methods are still developing and improving. One of the examples could be Burnley tunnel, Melbourne, Australia, where a correctly designed fixed fire-fighting suppression system prevented the spread of a fire caused by a standing HGV.

1.2 Fuels and their risks

When it comes to fuels and types of engines currently in use, the variety is much greater than 20 or 50 years ago. Back then, the choice was limited to either a benzine or diesel engine, and in case of an accident, fire related scenarios were well known. Nowadays, with new types of engines with power supply from electrical batteries, gaseous fuels, or other alternative fuels, the fire scenarios vary. Additionally, the worldwide tendency is to abandon fossil fuels and become a fossil-fuel independent society by 2030 (10). It is a big issue for fire safety and the design of passive and active fire protection, but also for firefighters and techniques they use

for extinguishing fires. Hybrid or fully electric cars are trendy nowadays, as these cars are more ecological and do not contribute to the production of CO_2 by their usage. The negative impact of their manufacturing and use of scarce minerals for the production of electric batteries and the innovative design of the engine is a different issue that is not the subject of this study. The most common type of battery is the Li-ion battery, which in case of damage and subsequent combustion can burn for several days, and even when successfully extinguished, it might re-ignite without any external factors after several days (38). The burning process of electric batteries used in hybrid and electric cars is highly dangerous for firefighters due to different techniques for extinguishing and recognition of electric vehicles in an accident with or without fire occurrence. Besides the various types of fuels in the cars, the content of plastic and polymer-based composite materials in the vehicle construction rose from 200 kg to 350 kg during the last six years (12).

2 METHODS AND ASSESSMENT OF FIRE RESISTANCE

Fire resistance of structures is an extremely important feature, and as most structures are constructed from concrete or steel, there are prescriptive Eurocodes for their design. There are three types of assessment of concrete structure fire resistance, namely fire testing, prescriptive methods and performance-based methods. The first method, fire testing, is the most critical and expensive but has high importance as the other two methods are based on results from this test.

In this chapter, all three methods are going to be described in detail and evolution in the use and development of those methods will be stated. Innovative approaches and development of new testing setups and numerical models lead to the improvement of fire resistance design. Therefore, new structures can be designed more efficiently and in case of a fire event they will be safer and more resistant.

2.1 Definition of fire resistance

Fire resistance of material could be explained in many different ways. According to the EU standard EN 13501-1 building materials and products are ranked from A to F in proportion to their fire behaviour (energetic contribution to fire). Criteria such as smoke, flaming droplets or particles are the decisive features when the building material or product is classified. Concrete belongs to class A1: non-combustible material, which properties are preserved over a certain period when exposed to elevated temperatures. Concrete exposed to flames or elevated temperatures does not produce harmful and hazardous smoke emissions. Furthermore, there are no burning droplets within the first 10 minutes (39).

Fire resistance is defined in “1991-1-2 (2002): Eurocode 1: Actions on structures - Part 1-2: General actions - Actions on structures exposed to fire” as an ability of a structure, a part of a structure or a member to fulfil its required functions (load-bearing function and/or fire separating function) for specified load level, fire exposure and duration (40).

2.2 Fire testing

Every material behaves differently under exposure to elevated temperature. The main objective of fire testing is the testing of concrete and partly reinforced concrete. Results from fire testing serve as constant or variable input parameters for prescriptive and also performance-based methods. Even though fire testing is the most challenging and complex method, without it, none of the following two fire design methods would exist. Fire testing should be document precisely and provide full detail of every step, starting with the preparation of samples through aging to fire exposure itself and cooling, and should be fully traceable. Moreover, fire testing requires a high level of safety and precautions against fire in the laboratory or facility.

Suitably designed fire testing is a key factor in obtaining reliable results. As concrete is a composite material composed of aggregates and cement paste, its behaviour in elevated temperatures can be easily influenced, especially by variable water content. The purpose of testing should be clearly defined before the selection of shape and dimensions of test samples. If the mix design, shape and size of test samples, and curing conditions are incorrectly chosen, monitored characteristics could be influenced by other phenomena occurring during the fire testing, and obtained measurements may be incorrect. When the samples are ready for fire testing, parameters such as actual moisture content, loading during the fire test or types of measurements taken during the fire tests must be clearly defined.

Various types of concrete are characterized by different fire behaviour thanks to a high number of variables, such as type of cement, w/c ratio, aggregate type, used admixture and its amount, the presence of dispersed fibre reinforcement and many others. Concrete design and performance of various concrete types will be described in chapter 3, Concrete in elevated temperatures. Reinforced concrete or concrete containing structural fibres is a slightly different case in which concrete's primary role is the protection of steel reinforcement.

The other aspect is the harshness of the fire scenario, particularly fire propagation, maximum exposure temperature, speed of cooling and length of the test. Another parameter is the duration of individual stages (heating- dwell-cooling). Fire testing could be performed according to predefined time-temperature fire scenarios based on real fire fuelled by different materials such as wood, gas or fossil fuels. The standard curve used for structures is ISO 834, and is founded on cellulose fire, more harsh fire scenarios are used for fire design of tunnels, e.g., RABT curve, HC or RWS curve. The other types of testing scenarios follow a pr eset ramp rate to a defined maximum temperature with specified temperature dwell and controlled cooling. Those regimes are used to classified individual phenomena that happen at exact temperature levels.

Data collection and processing are an integral part of fire testing. Knowing the setup and tested samples will lead to correct processing and understanding of gained values. Many factors could influence collected data, and if any is omitted, an incorrect conclusion could be reached, and a set of valuable data spoiled.

2.2.1 Preparation and curing of specimens prior to the fire testing

Concrete mixes or samples taken from the existing structure should be designed or taken in such a way that results will emphasise the investigated parameter. In other words, if we would like to monitor moisture migration due to fire exposure, a series of concrete with different porous structures shall be prepared, and the porous structure evaluated before the fire test. If the sample is taken from an existing structure, location in structure and size of the sample are directive parameters. Every property of the concrete, such as porosity, aggregates type, w/c ratio, or its compressive strength, influences data gained during fire testing, and if not processed carefully, misleading conclusions could result.

Specimens prepared for fire testing or full structures must have defined shape, dimensions and eventually weight. Dimensions are critically important because if the specimens are too small, some phenomena will not even occur during the fire testing, and the test would not be representative of the full structure made of the tested concrete. For example, fire spalling caused by moisture clog formed at a certain depth would not happen if the total thickness of the tested sample is smaller than that certain depth. If the same concrete mix was tested in structure or used a larger sample, moisture clog could be formed and completely different measurements obtained. Another example worth mentioning is the thermal expansion of aggregates and cement paste, which can be acceptable in the case of small samples but cause cracking in large samples.

Besides the shape of samples, the way in which the sensors for measuring the temperature development or other properties are incorporated or attached to the sample is very important. Inappropriate installation of sensors can again lead to false results. It is convenient to place

the thermocouples for measuring of temperature development in the tested sample during the casting. If the thermocouple probes are attached subsequently by some mortar or other material, the temperature is measured in different materials, and disconnection to the tested sample can appear.

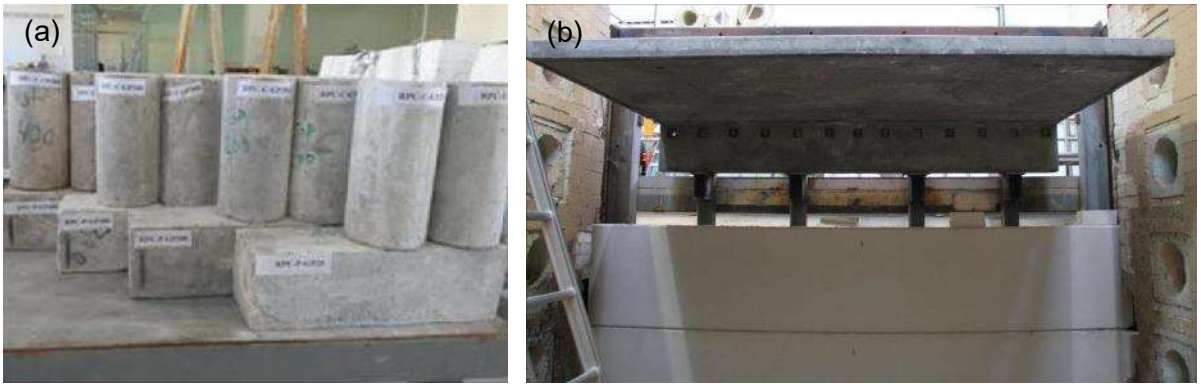

Fig. 5: Various samples for fire testing of concrete: (a) small scale testing samples (41)*; (b) setup of large scale testing* (42)*.*

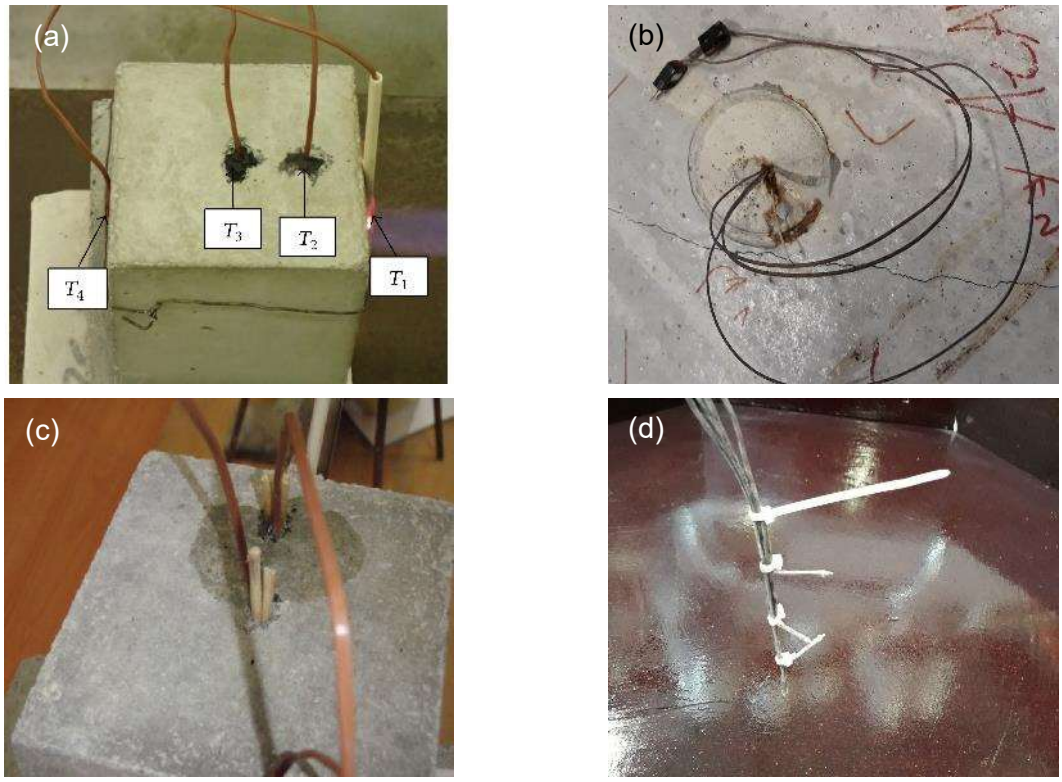

Fig. 6: Incorporation of thermocouples in specimens for fire testing: (a), (c) subsequent installation of thermocouples (43)*; (b), (d) Placement of thermocouples during the casting.*

The casting of samples or extraction of samples from a structure is followed by curing/aging/conditioning. The period between demoulding or taking samples from the structure and fire testing is decisive, especially in connection to moisture content. Curing of samples prior the fire test could be in laboratory conditions, water storage or drying. The most suitable conditions of samples are those, which are closest to the exposure conditions in real time and place. The moisture content of specimens is gradually decreases if they are cured in laboratory conditions. If the specimens are fully submerged in water or exposed to 100% relative humidity (RH), the moisture content will be high, and results from fire testing will be strongly influenced by water migration. Another possibility is to dry the samples before the testing to omit explosive spalling and water migration and analyse chemical changes in

concrete, particularly in cement paste. The moisture content of concrete under 3% is recommended by Eurocode 2 (6) to inhibit spalling. In reality, 3% of moisture content is rather low value and hardly reachable (44, 45). Furthermore, measurements of moisture content of samples by surface moisture meters may not be representative for the whole volume of the sample, and standard drying procedure of reference specimens is advisable. The following Fig. 7 describes moisture content in concrete based on RH and temperature of surrounding ambient conditions.

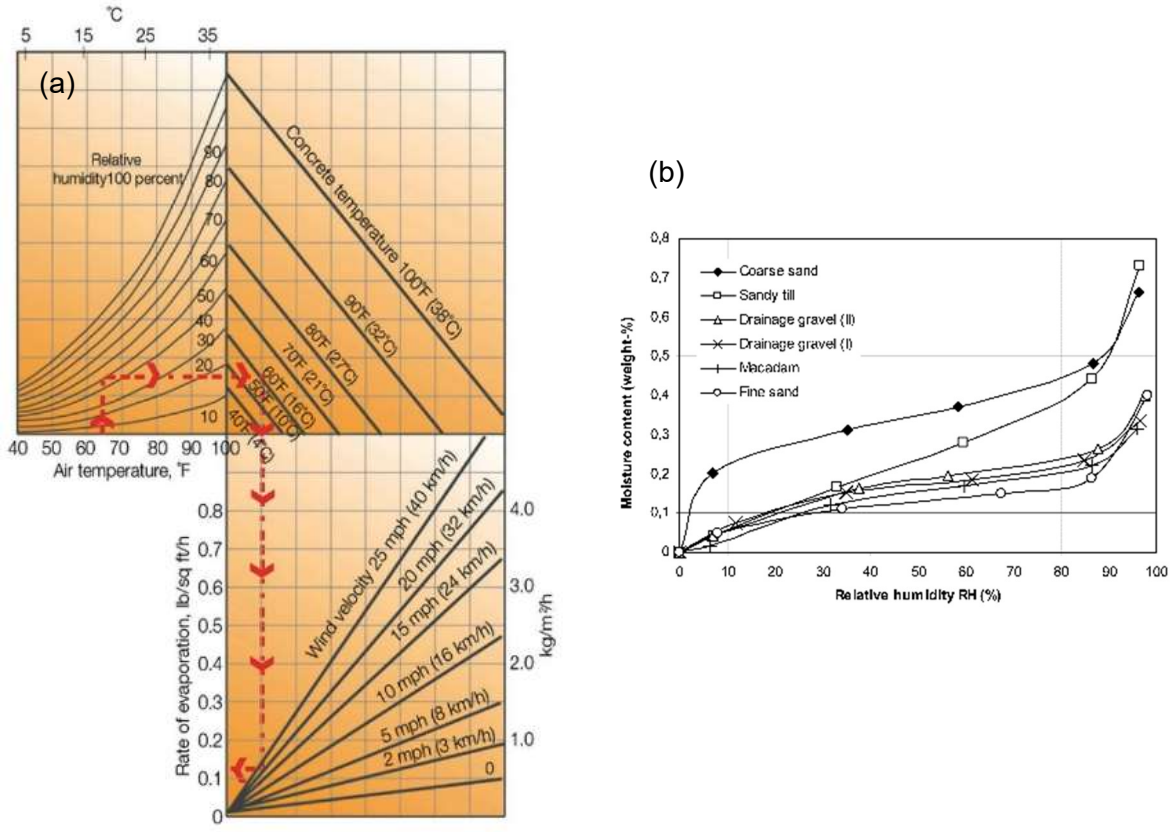

Fig. 7: (a) Effect of concrete and air temperatures, relative humidity, and wind velocity on the rate of evaporation of surface moisture from concrete (44, 46)*; (b) Hygroscopic equilibrium moisture content curves in wetting for the studied materials. Temperature T ≈ +20°C* (45).

2.2.2 Time-temperature scenarios and predefined heating regimes

Fire testing is sensitive to any parameter change and therefore, several predefined time-temperature curves were developed and used for testing across the world. The most widely used fire scenario is the standard time-temperature curve ISO 834. The testing curve was first introduced in 1975 and based on wood (cellulose) fuel source. Nowadays, buildings are equipped with thermoplastic materials, synthetic foams and fabrics which, in case of fire, create a completely different fire scenario than a wood-fuel fire. Those materials strongly contribute to the speed of the fire and heat release rate, and in this manner increasing fire severity beyond that of the standard ISO 834 fire curve. A large number of fire tests were performed according to the standard time-temperature fire curve, and extensive database, Fire Resistance Rating (FRR), was developed over the years to enhance safe evacuation and rescue activities. Modernization of living space and furnishings of today´s apartments triggered research concerning material composition and composition of fire loads was estimated as follows in Tab. 1.

Tab. 1: Composition of fire loads (47).

Room Usage	Fire load Percent Weight (kg)			Fuel load Percent Fire Load (MJ)		
	W	P	T	W	P	T
Kitchen	87	14	<<1%	80	20	<<1%
Living Room	66	33	1	57	41	1
Dining Room	73	27	1	65	34	1
Primary Bedroom	42	26	31	38	34	28
Secondary Bedroom	40	30	30	35	38	27
Basement Living Room	61	39	0	52	48	0

Note: W: Wood and Paper; P: Synthetic Plastic materials (including polyurethane foam); T: Textiles (including clothing); <<1%: much lower than 1%.

Inspired by these findings, various “realistic fire time-temperature curves” were introduced based on different parameters, see Fig. 8. Accuracy of newly developed realistic fire time-temperature curves were verified by fire test of light gauge steel frame wall panels, and compared to tests performed under standard ISO 834 fire curve. The conclusion of the fire testing was drawn out, and the necessity of further testing for a better understanding of the characteristics of realistic fire profiles is recognised (48).

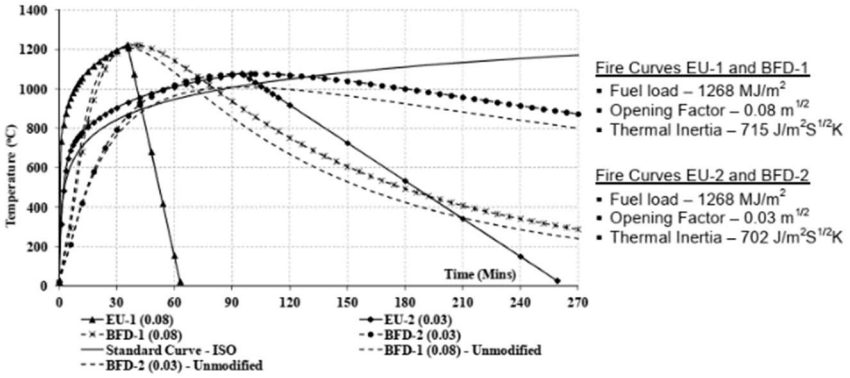

Fig. 8: Realistic fire time-temperature curves (48).

As the variety of fuel sources, locations and conditions of fire events changed throughout the years, more harsh fire scenarios such as hydrocarbon curve, modified hydrocarbon curve, Rijkswaterstaat fire curve or RABT German fire curve were introduced. All fire scenarios are described in detail in this chapter.

The predefined time-temperature fire curves serve for the overall behaviour evaluation of test sample, element or full structure, but predefined heating regimes are used for the description of individual changes in concrete based on specific exposure temperature. Predefined heating regimes commonly follow constant temperature ramp up to the requested maximum temperature, which is held for a predefined period and then cooled naturally or again according to the prescribed temperature ramp. Subjects of those predefined heating regimes are detail evaluation and general principle explanation of moisture migration, chemical changes of cement paste and aggregates, thermal expansion and shrinkage of cement paste and aggregates of concrete exposed to elevated temperatures.

Standard time-temperature fire curve ISO 834

The testing curve was first introduced in 1975 and based on wood (cellulose) fuel source. Since that time, significant changes with respect to ISO 834:1975 have been made. For example, the accuracy of measuring equipment, tolerances applied to the deviation of the curve, pressure conditions for vertical and horizontal elements, specification of test load,

conditioning, application of instrumentation and criteria respecting loadbearing capacity. All those parameters are mentioned in ISO 834-1:1999 and, in addition to this ISO, ISO 834-2 to ISO 834-14 are available for specific elements of building construction (48, 49). Conditions such as conditioning and specification of test load are highly important in case of testing non-reinforced concrete elements.

As mentioned earlier, a standard time-temperature fire curve or cellulosic curve is based on wood fuel-burning furnaces and up to now was slightly modified to give faster temperature gain during the first few minutes. Currently used gas-fired furnaces are more powerful, and able to follow faster temperature gain from the beginning of the test. The ISO 834 time-temperature curve is used for buildings, and prescriptive methods given in Eurocode 1 and 2 are based on this fire scenario. Further parameters and accuracy limits of testing are stated in EN 1363-2 (50). Temperature development is described by equation (1 (1).

(1 (1)

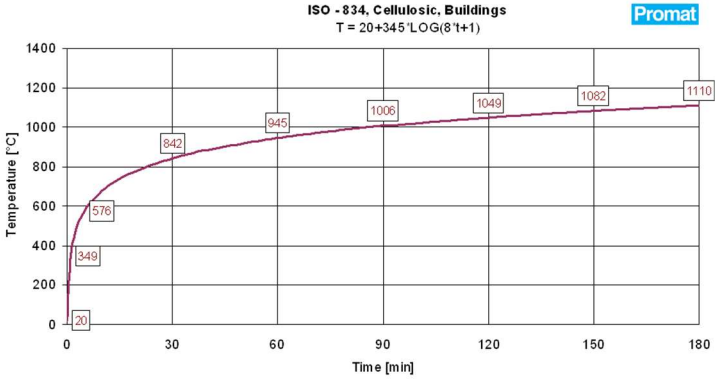

Fig. 9: Standard time-temperature curve, ISO 834 (50).

Hydrocarbon curve and modified hydrocarbon curve

These fire scenarios were developed in the 1970s for offshore and petrochemical industries. The burning rate of petrol gas and chemicals so-called hydrocarbon fuels is more severe than wood-fuelled fire, and characterised by rapid temperature rise in the first 5 minutes up to 900°C (rate of 176°C/min) (5, 50). Fast developing temperature gradient in the first minutes of the hydrocarbon fuel-based fires (HC, MHC and RWS) are the cause of spalling and explosive spalling of concrete structures. The following equations describe hydrocarbon (2) and modified hydrocarbon (3) curves:

$$T = 20+1080*(1-0{,}325*e^{-0{,}167*t}-0{,}675*e^{-2{,}5*t}) \quad (2)$$

$$T = 20+1280*(1-0{,}325*e^{-0{,}167*t}-0{,}675*e^{-2{,}5*t}) \quad (3)$$

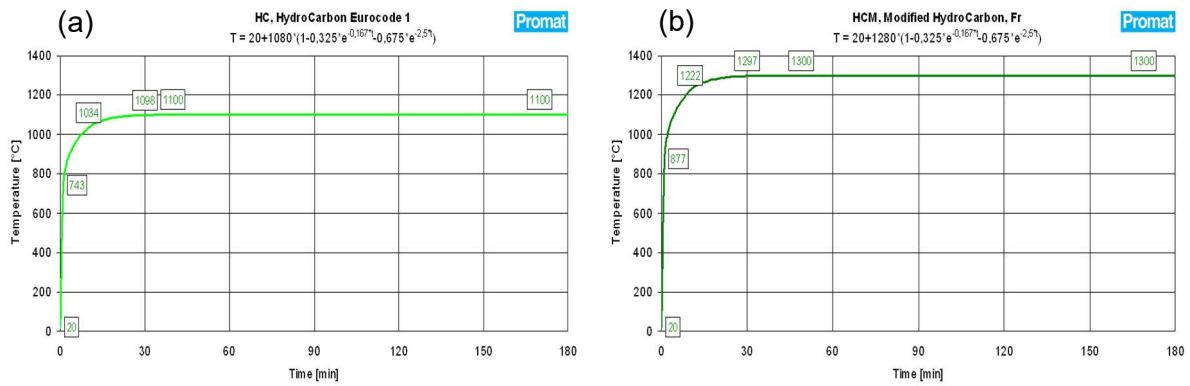

Fig. 10: Fire testing curves: (a) hydrocarbon curve; (b) modified hydrocarbon curve (50).

Rijkswaterstaat (RWS) fire curve

This fire testing scenario was developed for fires in tunnels by the Ministry of Transport in the Netherlands. The Centre for Fire Research (TNO) has established a testing scenario for evaluation of passive protecting materials in tunnels, and it assumes a fire event involving HGV with 50 m^3 tank carrying oil or petrol fuel, which produces 300 MW fire load and lasts up to 120 min. A full-scale test re-evaluated the correctness of the RWS fire curve as a design curve for tunnels in the Runehamar tunnel in Norway, and its correctness was reconfirmed (5, 50, 51). Temperature development of RWS fire curve is described by the following co-ordinates:

RWS, RijksWaterStaat	
Time (minutes)	Temperature (°C)
0	20
3	890
5	1140
10	1200
30	1300
60	1350
90	1300
120	1200
180	1200

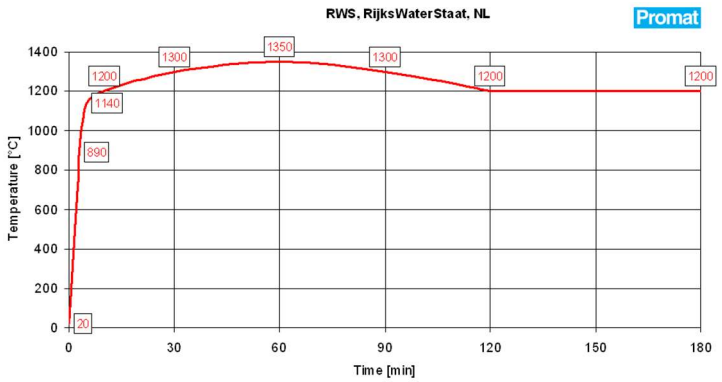

Fig. 11: Temperature development co-ordinates and graphical interpretation of RWS fire scenario (50).

RABT German fire curve

The RABT fire curve was developed on the basis of RWS but represents less severe fire scenarios in tunnels reaching the maximum temperature 1200°C (melting point of some aggregates) and sustained for 60 min before decaying to ambient temperature. The RABT curve is also termed as a ZTV-fire scenario and has two variations, for railway tunnels and road tunnels, see Fig. 12. The failure criterium for elements exposed to RABT-ZTV fire curve is that the temperature of the reinforcement should not exceed 300°C (5, 50, 51).

RABT-ZTV (railway)	
Time (minutes)	Temperature (°C)
0	15
5	1200
60	1200
170	15
RABT-ZTV (road)	
Time (minutes)	Temperature (°C)
0	15
5	1200
30	1200
140	15

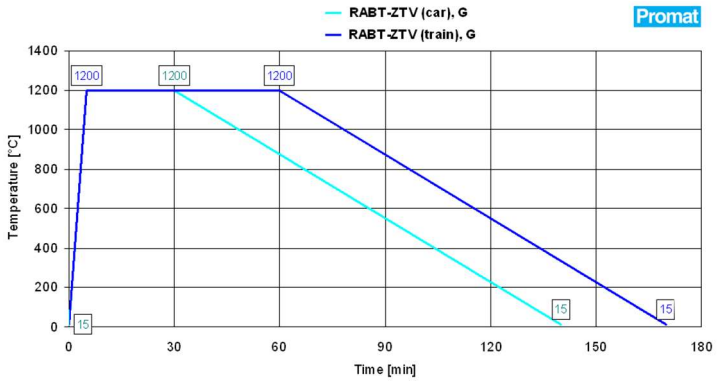

Fig. 12: Temperature development co-ordinates and graphical interpretation of RABAT-ZTV fire scenario (50)

To conclude on fire curves based on time-temperature fire development, it is important to update them according to material and structure design progress. Furthermore, each fire event in tunnels, e.g., Channel (1 100°C), Great Belt (800°C) or Mont Blanc (1 000°C), initiated reconsideration of the severity of testing fire curves. The latest innovation in the fire testing in tunnels is a newly modified and increased hydrocarbon curve, which is supposed to serve for fire testing instead of RWS and RABT scenarios. Parameters of the modified HC curve are fire

load of 345 kW/m^2, temperature rise to 1 200°C in less than 10 minutes and maximum temperature 1 300°C after approx. 20 min from initiation of the fire test and severe fire supposed to last less than 120 min.

Predefined heating regimes

Those regimes are used for monitoring of individual mechanisms such as water transformation and migration, chemical changes, and deterioration of inner structure due to incompatibility of cement paste and aggregates behaviour under the thermal load. As some of those mechanisms are taking place simultaneously, it is not always possible to decouple them and monitor them individually. Regimes which, have constant predefined temperature gain, maximum temperature, temperature dwell and controlled cooling commonly serve for an understanding of changes of concrete and explanation of overall behaviour of concrete under thermal load. Speed of loading could be slow such as 1°C/min or rapid such as exposure to flame, instant extreme heat e.g. 1 300°C by a gas burner (5, 43).

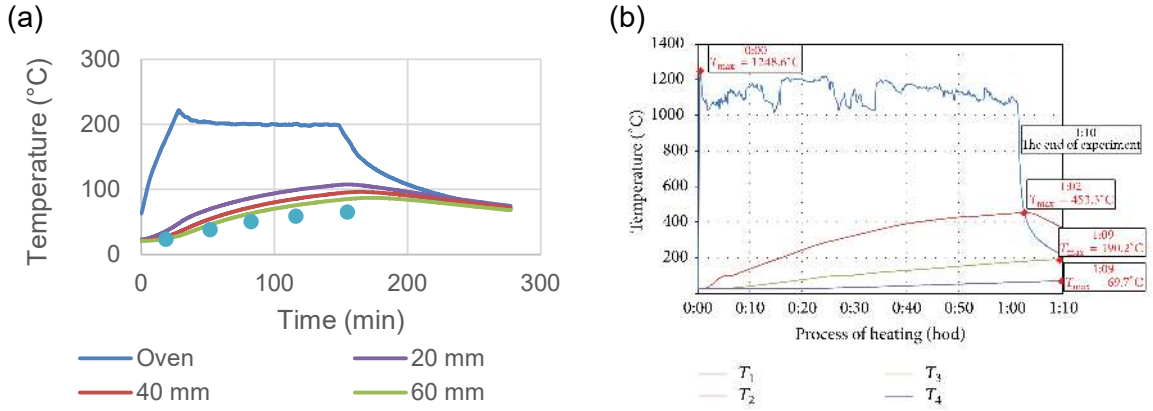

Fig. 13: Predefined fire regime (a) temperature ramp 5°C/min; max temperature 200°C; temperature dwell 2 hours; natural cooling; (b) exposure to open flame (43).

2.2.3 Conditions during the fire testing

Conditions during the fire testing means the scale of the test, type of the oven, placement of samples and loading rate during the fire regime. The specimens could be entirely heated when placed inside the oven or exposed to elevated temperatures from one side. Those two setups are usually smaller scale fire testing, the third one, large-scale testing in tunnels or existing structures, is the most complex arrangement and is rarely performed. Oven types can also vary based on their size, shape and fuel source. In recent years, it is a trend to test samples under load, which brings in new aspects and behaviour of concrete during the fire exposure. Testing of concrete under load creates thermal strains, which better represent the real conditions of concrete in structures.

Large-scale fire tests

These tests were held in several research institutes to collect as much data during the fire event as possible. One of those tests was performed within the METRO project in an abandoned rail tunnel with a length of 276 m. The three commuter train carriages were subjected to fire and development, duration, and extinguishing of fire were monitored. The full-scale test was performed to have a comparison to reduced scale tests and real fire events in rail tunnels (52, 53). Loading of the concrete structure during the fire testing could be calculated. However, monitoring of the change during large-scale fire tests is somewhat limited, and therefore small-scale laboratory tests with predefined loading and monitoring of the load-bearing capacity of test elements during the fire exposure are essential.

Small-scale fire tests

These tests are performed in laboratories, and test progress can be regulated and closely monitored. As was mentioned earlier, some behaviour of fire cannot be observed on small samples, and therefore it is wise to start with smaller samples and then scale-up and compare obtained results. Small-scale fire tests are performed under two regimes Fig. 14 (54):

- Steady-state tests, where the sample is first thermally loaded according to the thermal regime and then mechanically loaded while the temperature is constant, heat-then-load (HTL). (T=constant, σ= varying)
- Transient tests, where the specimen is mechanically loaded prior to the heating. The material is load-then-heat (LHT). (T=varying, σ= constant) (46)

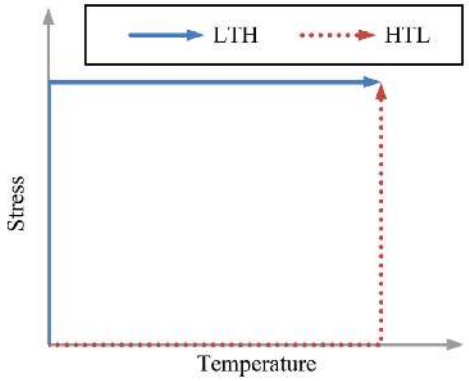

Fig. 14: Schematic diagram of the temperature and stress history of specimens subjected to LTH and HTL tests (46).

Types of the oven

For most of the tests ovens with gas burners and open flame burners are used as a source of the heat. Gas burners can develop high heat in a short time, but to maintain the temperature at a certain level is more challenging. When performing tests according to predefined heating regimes with slower heat development and target temperatures, electric ovens could be more suitable. Electric ovens can be more easily regulated, and also transition between temperature increase and stable exposure temperature could be maintained without extensive overheating. In the past, the burning of wood was used as a source of heat, and this is the basis for the standard testing curve ISO 834. Ovens with wood or fossil fuels are not used nowadays for small scale tests but widely used for large-scale testing.

Heat exposure conditions

Samples could be exposed to heat from all sides or only from one side. When the entire samples are exposed to elevated temperatures, heat penetrates evenly, and the coldest point is theoretically in the centre of the sample. The movement of the water molecules is again towards warmer and colder areas, and if the vapour is restricted, spalling occurs. If the moisture content in tested samples is far above 3% or thermal expansion of individual concrete components is exceeded, the whole sample could be disintegrated, see Fig. 15.

The other case of heating exposure condition is from one side of the sample, commonly slab. In those samples the temperature gradient between the heated and cold surface could be monitored. Water in all forms (liquid and gaseous) migrates through the structure and is responsible for first crack formation in the concrete structure and microstructure. The temperature and moisture content on both surfaces is developed differently and induces different strains in one side heated sample, than if the sample is entirely exposed to heat. One side heated samples also behave differently during the cooling stage; uneven cooling of heated surface and core of the sample can again cause thermal strains that do not occur with entirely heated samples.

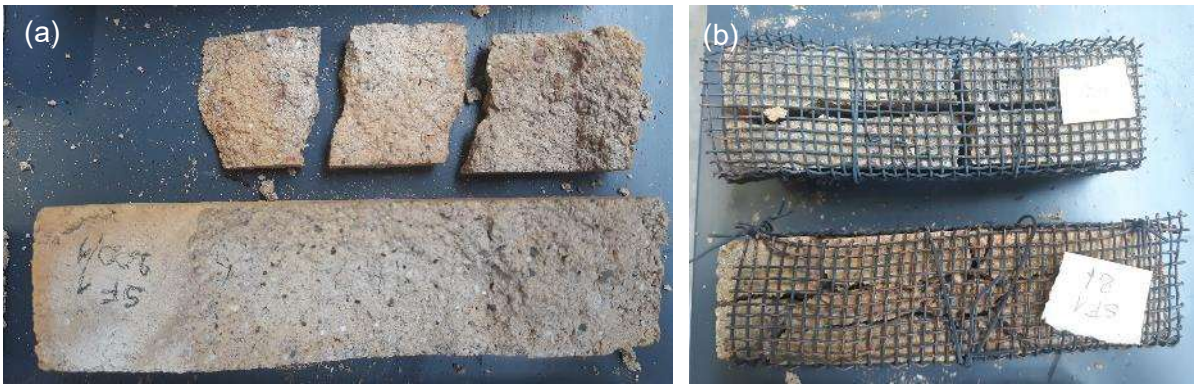

Fig. 15: Full exposure of samples to the heat (a) surface spalling; (b) full disintegration due to thermal load.

Loading of individual samples

The loading rate during fire exposure is usually defined as a percentage of the nominal strength of tested concrete. Standard load ratios are from 10 to 55% (54) of nominal strength. These samples are under restrained volume expansion or shrinkage, and investigation of its behaviour is more complex but comparable to the real conditions. New parameters that are stepping in are a behaviour of sample in loaded and unloaded direction, if uniaxially loaded, and behaviour of sample if multi-axially loaded.

Elastic strains in the concrete structure due to the expansion of aggregates and shrinkage of the cement paste are increasing in severity when the concrete is heated over 100°C and still does not break. That was a big concern for a scientist up to the 1970s before the 'transient creep' was introduced (55). Transient creep, more precisely load-induced thermal strain (LITS), develops during the first heating (and not during the cooling) when the test specimen is loaded. LITS, above 100°C is a function of the temperature and not of time (5, 54).

Load-induced thermal strains (LITS)

LITS is a phenomenon that is not recognizable in temperatures under 100°C. The strain in heated concrete starts occurring between 100 and 250°C, and they are strongly influenced by moisture/vapour migration. Furthermore, they are aggregate type independent up to 400°C. Analysis of the existing multiaxial test data showed that LITS is the result of a considerably confinement-dependent phenomenon and that laboratory experiments on concrete exposed to triaxial compressive load and elevated temperatures above 250°C are needed. Based on the results from various laboratory tests, for temperatures up to approx. 400°C LITS seems to be mainly due to chemical reactions and microstructural changes that are happening in the cement paste, such as dehydration, migration and state of water in the cement paste. Thermomechanical damages that are occurring due to the thermal incompatibility of cement matrix and aggregates during the exposure to high temperatures contribute significantly to the development of LITS (54).

Incorporation of LITS in the modelling of a concrete structure and structural analysis will yield erroneous results, especially for columns exposed to fire (5). In terms of temperature, LITS is mainly irrevocable, and the thermal incompatibility of aggregates and cement paste may cause damage of an inner structure during the cooling phase. The existence of the LITS is demonstrated by fire testing of specimens under uniaxial or multiaxial load.

When the concrete sample is heated from one side without loading, free thermal strain (ε_0) takes place. Several cases of testing non-loaded specimens showed that the thermal expansion behaviour of concrete is highly nonlinear with temperature (56, 57). The elastic strain at ambient temperature ($\varepsilon_{ela,0}$) is introduced, if the concrete sample is loaded prior to fire testing. Interaction of free thermal strain and elastic strain at ambient temperature results in load-induced thermal strain (ε_{lits}), and LITS can be experimentally estimated as follows:

$$\varepsilon_{lits} = \varepsilon_{tot} - \varepsilon_0 - \varepsilon_{ela,0} = \varepsilon_{tot} - \varepsilon_{th} - \varepsilon_{sh} - \varepsilon_{ela,0} \qquad (4)$$

where: ε_{lits} load-induced thermal strain

ε_{tot} total strain

ε_0 free thermal strain

$\varepsilon_{ela,0}$ elastic strain in ambient temperature

ε_{th} thermal expansion strain

ε_{sh} shrinkage strain

For simplicity, the strains are shown only in longitudinal direction Fig. 16.

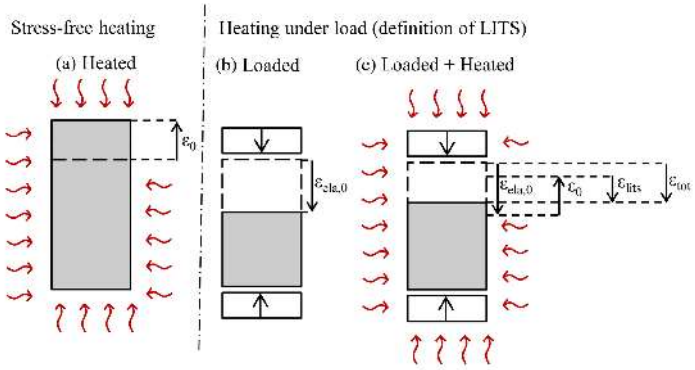

Fig. 16: Definition of εlits: schematization of the strain components developing in a concrete specimen subjected to (a) stress-free heating (b) mechanical loading (c) heating under constant mechanical load (54).

The results of load-then-heat (LTH) tests performed for different stress levels are often expressed by plotting the strain that develops during the heating phase ε_{heat}, usually referred to as thermal strain, against the average temperature of the specimen T, where ε_{heat} is evaluated as:

$$\varepsilon_{heat} = \varepsilon_{tot} - \varepsilon_{ela,0} \quad (5)$$

According to the definition above, ε_{lits} may be seen as the difference between the strain developed during the heating phase ε_{heat} and the free thermal strain ε_0:

$$\varepsilon_{lits} = \varepsilon_{heat} - \varepsilon_0 \quad (6)$$

Thus, if on the same chart, the values of ε_{heat} for different stress levels are plotted together with the unloaded control specimen behaviour (for which $\varepsilon_{heat} = \varepsilon_0$), a curve expressing LITS as a function of temperature is produced. For each stress level it is the difference between the curve expressing ε_{heat} for that particular stress level and the curve obtained for the unloaded control specimen Fig. 17 (54)

As was mentioned, LITS is a phenomenon that is starting to develop after 100°C, and is most probably connected to drying of the cement matrix, which takes place between 100 and 200°C. The influence of cement matrix properties does not vary as much as the influence of various types of aggregates, and for that reason up to about 300°C the dehydration of cement matrix, drying, and migration of water in various forms have the main influence. Between 300 to 450°C the type of the aggregate begins to influence LITS development. Incompatibility of cement paste and aggregates results in the formation of cracks, i.e., thermomechanical damages and contribution to transient thermal creep in this temperature range, see Fig. 17 (54).

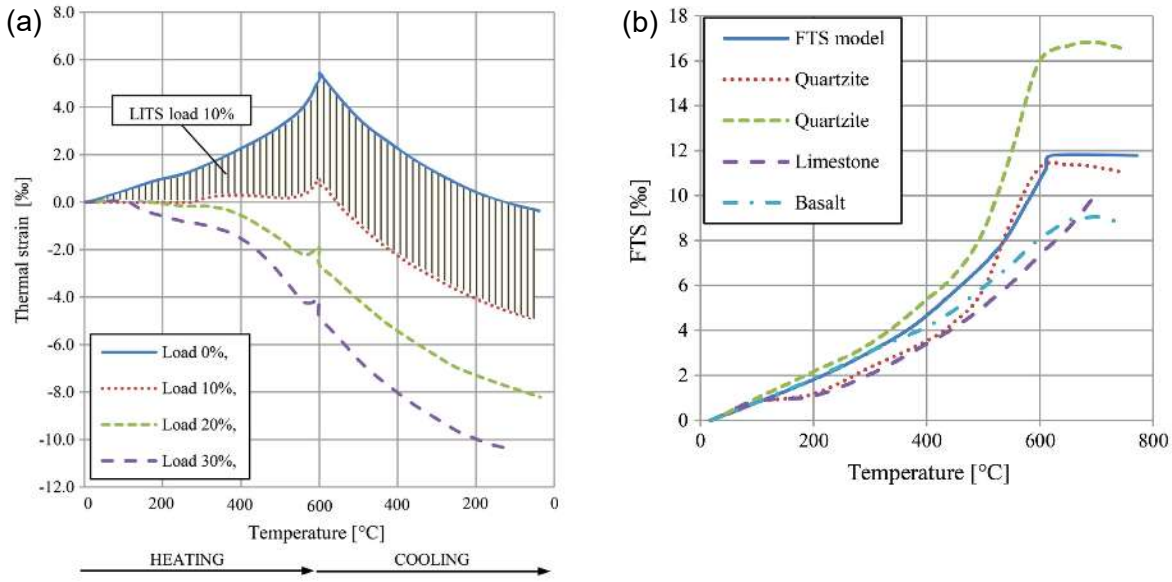

Fig. 17: (a) Total thermal strain measured during a LTH test, expressed as a function of temperature, for different load levels. Aggregate: basalt. Heating rate: 1°C/min; (b) Experimental Free thermal strain (FTS) vs temperature for various concretes (58) *and the curve obtained by the free thermal stain model exposed in* (54, 59, 60).

As the LITS is a phenomenon that is taking place simultaneously with many other changes in the concrete structure during the elevated temperature, it is not easy to adequately measure its extension. Nevertheless, many laboratory tests were performed, and the measured values were used as input parameters for various models that explain LIST based on the outcome of the mathematical models. The LITS mathematical models started to be widely developed from around 1976 and are uniaxial or multiaxial, where parameters such as a free thermal strain (FTS), temperature, thermal expansion coefficient, load ratio are used. Worth mentioning are uniaxial explicit LITS models from Anderberg and Thelandersson's TS model (61), Nielsen's LITS model (59), and Diederichs' LITS model (62). The Thelandersson's LITS model (63), De Borst & Peeter's LITS model (64) and Pearce's LITS model (65) from 2004 belong in the group of multiaxial explicit models. Those listed mathematical models are limited by the various hypotheses which might not match real behaviour of concrete exposed to heat, and behaviour in certain temperatures is not yet fully understood experimentally (5, 54).

2.2.4 Data collecting before, during and after fire testing

Type and methods for collection of data depend on the main purpose of the test; in other words, parameters we want to verify. Nevertheless, most common properties monitored during the fire testing are temperature development in the oven or/and samples themselves and moisture loss assessed mostly gravimetrically. Visual assessment of formed cracks or discolouration of concrete also indicates a scale of damage. Those three properties (temperature, moisture and visual changes) are the most common and easily recordable parameters, and equipment with measuring techniques will be described in detail.

Other properties such as changes of a porous structure, crack formation inside the sample, volume changes, water migration, and chemical changes of cement paste and aggregates can be measured by equipment dedicated to individual characteristic analysis. All those changes of structure result into the loss of strength, which could be evaluated by comparison of reference sample without heat exposure, and sample after fire testing. Some parameters are not measurable after fire test due to extensive damage of test sample or low strength, e.g., microscopical determination of parameters of the air-void system in hardened concrete (ASTM C457M-16, EN 480-11), water permeability by TORRENT permeability tester, initial surface absorption test (ISAT), or compressive strength measured by non-destructive methods (Schmidt hammer). Furthermore, if the sample is fire-tested under load (uniaxial or multiaxial),

load level can change due to expansion, shrinkage or weakening of the inner structure of heated concrete.

Data collecting before fire testing

Samples can be cured under various conditions prior to the fire test, and therefore it is necessary to measure all the requested parameters immediately before the initiation of a fire test. The temperature of samples could be measured by laser infrared thermometer or thermocouples integrated inside the sample. If samples are dried in the oven to 100°C before the fire test, it is essential to let them cool down to ambient temperature, and then start the fire test. Also, drying to 100°C is not advisable as water located at gel pores and CSH interlayers starts to evaporate at around 60°C.

The moisture content of samples could be gravimetrically measured by drying of the "reference" sample, which was cured under the same conditions until the fire testing as the sample to be exposed to elevated temperatures. Another possibility is surface moisture meter, but that is not fully representative for the whole sample. Nevertheless, if the tested sample is exposed to heat from one side, this device can be used for monitoring moisture during the fire test.

Visual evaluation prior to the heating could be done with the naked eye or using an optical microscope. In the case of large samples, some drying cracks or other damages could be visible only by an optical microscope. Photo-documentation due to colour and structure is advisable.

Data collecting during fire testing

The most suitable way of recording of temperature during fire testing is by thermocouples probes and a datalogger. Thermocouples could be integrated into the sample and record temperature change in the sample or placed in the oven and record temperature, to which the samples are exposed. By obtaining temperature around and in the sample, the thermal gradient of concrete could be calculated. Measurement of the temperature inside the sample could indicate the scale of dehydration of cement paste, connected to chemical changes, and also volume changes. Furthermore, moisture migration could be followed on one-side heated samples as the temperature could change based on water/vapour migration towards the heated and non-heated surface.

Monitoring of moisture during the fire testing could be performed in the case of one-side heated samples by a surface moisture meter or by advanced laboratory equipment such as in-situ neutron tomography, which can operate while heating the sample (66). Moisture changes of entirely heated samples are not possible unless samples could be gravimetrically controlled during the heating. In the case of one-side heated samples, moisture could be recorded on the non-heated surface by moisture meter or visually by escaping water or vapour through formed cracks or more significant pores close to or on the surface.

Visual evaluation during the fire test again depends on the test setup and apparatus used for fire testing. The monitoring of crack formation accompanied by vapour evaporation could be done on one-side heated samples. Crack development could be recorded, and also thickness and length of cracks can be measured. Cracks serve as migration channels for water or vapor, and steam coming out from cracks or formation of wet spots on the non-heated surface can be observed. All these processes, the formation of cracks, vapor/water migration, and discolouration, are changing during the individual fire test phases (heating-exposure maximum temperature-cooling), and therefore monitoring through the whole period of the test is highly recommended.

During the fire test spalling or explosive spalling of the tested concrete can also occur; in this case, "sound" evaluation could take place. Cracking or popping of smaller or greater parts of the sample can be a sign of inner structure deterioration.

Data collecting after fire testing

Measurements of temperature after fire tests are not highly relevant. Measurements of weight loss are important because that might be the first indication of changed proportion due to fire exposure. If the weight loss is significantly higher than the loss measured prior to the fire test, then chemically bonded water is realized, and strength of cement paste rapidly influenced. Differential thermal and thermogravimetric analyses could be used for a more precise evaluation of chemically bonded water loss.

Visual analysis of samples after fire exposure is essential, and many assumptions made, which can serve for the selection of suitable tests needed to be performed to gain valuable information about the behaviour of given material (concrete) in the fire. The optical microscope could be used for cracks analyses and discolouration assessment. If the spalling took place, the volume of spalled material and type of spalling could be determined.

2.3 Prescriptive methods

Prescriptive methods are based on fire assessment of individual elements, parts of structures or entire structures, and apply on every structure, but only partly to tunnels where the fire events have different scenarios. Fire protection methods are divided into two types; active and passive. Passive fire protections are considered to be polypropylene fibres in the concrete, thickness of rebar cover layer, insolation against high temperatures, fire resistance paint, protective walls, and other shielding structures. Some types of active fire protection are sprinklers, fire alarms, smoke detectors, fire resistance doors and windows. Documents used by engineers for structural fire design in Europe are Eurocodes, international and national standards, and council directives.

In this chapter a detailed review of documents used for structural fire design and fire testing will be given. Furthermore, an overview of passive and active methods for fire protection will be described. The capture will be concluded by fire design dedicated for tunnels and structures with limited ventilation and access possibilities.

2.3.1 Documents used for structural fire design

In this section, documents for structural fire design for member countries of the European Union and European Free Trade Association are going to be presented. The Commission of the European Community decided to prepare documentation based on article 95 of the Treaty in 1975. There were two main objectives, to eliminate technical obstacles of trade and harmonize the technical specifications. It took about 15 years to prepare full documentation for structural design within which two parts are dedicated to the fire design of concrete structures. Parts which are focussing on fire design of concrete structures are "1991-1-2 (2002): Eurocode 1: Actions on structures - Part 1-2: General actions - Actions on structures exposed to fire" (EN 1991-1-2) (40) and "EN 1992-1-2 (2004): Eurocode 2: Design of concrete structures - Part 1-2: General rules - Structural fire design" (EN 1992-1-2) (6). Both documents are harmonized with “Council Directive 89/106/EEC” (67), particularly “Essential Requirement N°1 Mechanical resistance and stability”, and “Essential Requirement N°2 - Safety in case of fire”. Synchronised documents to Eurocode 1 and 2 are ISO23932-1:2018 Fire safety engineering - General principles (68).

The first part of both EN 1991-1-2 and EN 1992-1-2 are similar and describe general information regarding content, scope, normative references, the distinction between principles and application rules, assumptions, terms and definitions and symbols used for individual values or parameters.

In addition to those EU documents, the national annex can contain only certain information such as values and/or classes where Eurocodes allowed alternatives. Country-specific data, and the procedures to be used where the Eurocodes approve alternative procedures.

Safety requirements described in EN 1991-1-2 consist of Construction Products Directive 89/106/EEC which gives the following essential requirement for the limitation of fire risks: “The construction works must be designed and built in such a way, that in the event of an outbreak of fire:

- the load-bearing resistance of the construction can resist for a specified period,
- the generation and spread of fire and smoke within the structure are limited,
- the spread of fire to neighbouring constructions is limited,
- the occupants can leave the structure or can be rescued by other means,
- the safety of rescue teams is taken into consideration” (40).

Moreover, another actions, which are specified by competent authorities. Those are, for example, maintenance and installation of sprinkler systems and the use of approved insolation and coating materials, including their maintenance.

Design procedures for structural fire design would consider the behaviour of the structural system at transient temperatures, the potential heat exposure, and the beneficial effects of passive and active fire protection systems. Those three features, in combination with the purpose of a structure, are key parameters for the full analytical procedure of structural fire design. A comparison of different types of design procedures, such as the prescriptive method or the performance-based method, is presented in both EN 1991-1-2 and EN1992-1-2.

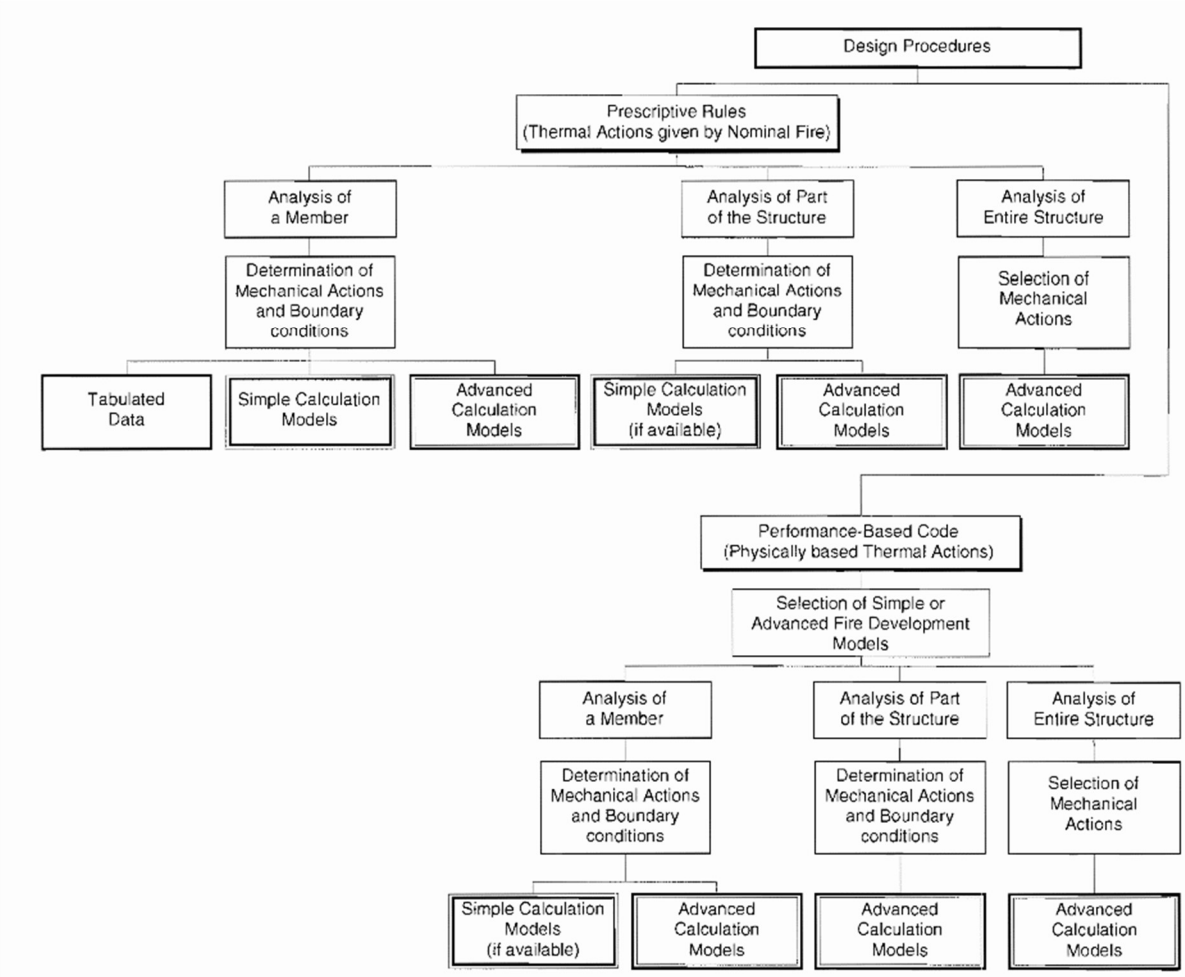

Fig. 18: Alternative design procedures (40)

Design objectives given in EN 1991-1-2 are expected to be adopted by interested external organizations. Also, the text of EN 1991-1-2 includes the most important principles and rules for the description of thermal and mechanical actions on structures.

Eurocode 1: Actions on structures - Part 1-2: General actions - Actions on structures exposed to fire (1991-1-2) (2002)

The 1991-1-2 is focused more on generic information and description of overall phenomena, which take place during the fire event and reasons for the importance of appropriate fire design. The document is divided into 4 parts and includes annexes A to F. Individual parts are General (Section 1), Structural fire design procedure (Section 2), Thermal action for temperature analysis (Section 3), and Mechanical actions for structural analysis (Section 4). For a demonstration of content, several parts are going to be interpreted here.

A structural fire design analysis has to take into account steps as a selection of the relevant design fire scenarios, determination of the corresponding design fires, calculation of temperature evolution to which individual structural elements are exposed, and calculation of mechanical behaviour of the structure exposed to fire. Moreover, fire exposure of structure is classified as accidental action.

Load levels are a critical feature for structural fire design calculation as they induce additional phenomena LITS and changing behaviour of a concrete structure when exposed to elevated temperatures. If the load levels are specified in a given table, the load level corresponds to the design value of the load of the element at normal temperature multiplied by the coefficient specifying the load level for fire design.

Different fire development is expected in different structures, and therefore rates of heat release are given in EN 1991-1-2, see Tab. 2. Abbreviation RHR_f stands for the maximum rate of heat release per square meter.

Tab. 2: Fire growth rate and RHRf for different occupancies (40)

Max Rate of heat release RHR_f			
Occupancy	Fire growth rate	t_α [s]	RHR_f [kW/m^2]
Dwelling	Medium	300	250
Hospital (room)	Medium	300	250
Hotel (room)	Medium	300	250
Library	Fast	150	500
Office	Medium	300	250
Classroom of a school	Medium	300	250
Shopping centre	Fast	150	250
Theatre (cinema)	Fast	150	500
Transport (public space)	Slow	600	250

Eurocode 2: Design of concrete structures - Part 1-2: General rules - Structural fire design (EN 1992-1-2) (2004)

The EN 1992-1-2 is a guideline for structural fire design by a prescriptive method and consists of six parts.

- General information (Section 1) is very similar to EN 1991-1-2.
- Basic design (Section 2) verifying methods from elements analysis through analysis of parts of structure and terminate with global structural analysis.

- Material properties (Section 3) focused on changes in behaviour and strength development of concrete under standard fire load.
- Design procedures (Section 4) which could be simplified or advanced calculation methods, additionally there are also stated changes in shear, torsion and anchoring behaviour under fire load, spalling, joints and protective layers.
- Tabulated data (Section 5) presents input values obtained mostly from fire testing according to standard time-temperature ISO 834 curve of columns, walls, slabs, tensile members and beams.
- High strength concrete (HSC) (Section 6) which behaves slightly differently under thermal load and its thermal properties and higher susceptibility to spalling requires different structural design.

Structural fire design according to a prescriptive method is extremely complex, and as it is not the main subject of this doctoral thesis, only several figures and tables are going to be given as an example. An envelope of resisting bending moments over supports for fire conditions; temperature profiles (°C) for a column, dimension 300 x 300 mm – R30; minimum width of cross-section as a function of fire resistance (for standard fire exposure) see Fig. 19.

(a)

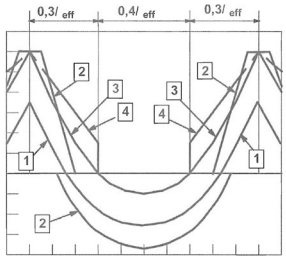

Explanation:

1 Diagram of bending moments for the actions in a fire situation at $t = 0$
2 Envelope line of acting bending moments to be resisted by tensile reinforcement according to EN 1992-1-1
3 Diagram of bending moments in fire conditions
4 Envelope line of resisting bending moments according to Expression (5.11)

(b)

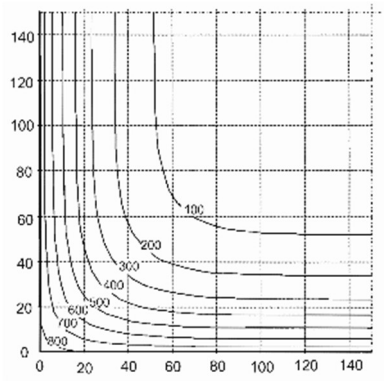

(c)

Fire resistance	R 60	R 90	R120	R180	R240
Minimum width of cross-section mm	90	120	160	200	280

Fig. 19: Data for structural fire design (a) Envelope of resisting bending moments over supports for fire conditions; (b) Temperature profiles (°C) for a column, dimension 300 x 300 mm – R30 and (c) Minimum width of cross-section as a function of fire resistance (for standard fire exposure) (6).

To contribute to fire resistance of structure not only by well-performed structural fire design, but also passive and active fire protection could be considered. Visual presentation of active and passive fire protection measures is presented in Fig. 20 (69).

(a)

(b)

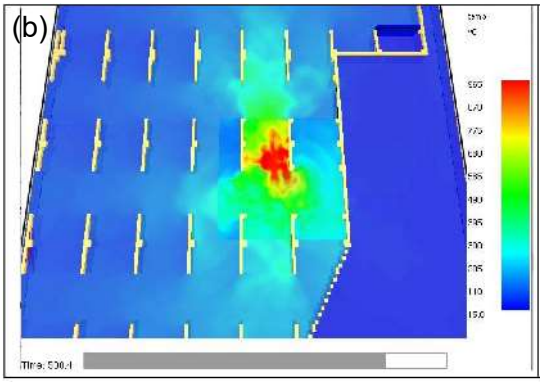

Fig. 20: (a) Difference between passive and active fire protection measures (69)*; (b) Numerical simulations of an underground car park – ceiling temperature* (15)

2.3.2 Passive fire protection measures

Passive building security is already in place when designing buildings, especially by properly designing fire compartments, providing escape routes, limiting the spread of fire to neighbouring buildings, and finally, choosing suitable structural materials. Choosing the right construction materials is very important. In case of concrete, it is necessary to design concrete mix to not only withstand high temperatures for as long as possible but also to avoid excessive explosive spalling, which would accelerate the penetration of heat towards steel reinforcement in the case of a reinforced concrete structure causing faster loss of strength. Another type of passive protection used for an increment of the fire resistance of existing buildings is the creation of various protective structures, the application of paints and sprayed cementitious materials. The extent of fire damage of structure can be reduced by passive fire protection measures and contribute to easier, faster, and less expensive repair work.

Fire doors

Fire doors are categorized by the fire-protecting rating, based on which they are classified for how long s period of the time they can withstand the fire exposure. Their main task is prevention or delays to the spread of fire and smoke in between individual compartments.

Firewalls, floors and ceilings

Firewalls, floors and ceilings have the same purpose as fire doors in preventing the spread of fire and smoke through the structure as well as their primary structural purpose. When suitable materials are used for their design, such as non-combustible structural materials or materials with an improvement of material properties by polypropylene microfibres in case of concrete, fire safety can be ensured.

Fire and smoke dampers

Fire and smoke dampers are used in heating, ventilation, and air conditioning ducts to prevent the spread of fire inside the ductwork, closing automatically if the temperature rises. They can also be linked to fire alarm systems (69).

Coating materials

Coating materials epoxy or cementitious based are the most common for the protection of structural elements. Spray-applied epoxy intumescent and subliming coatings are frequently used for steel and concrete surfaces and can protect the structure up to 80°C. Other available types of passive fire protection are coatings, which include phenolic foam, glass fibres, or elastomer rubber (70).

The design of concrete

The design of concrete can prevent explosive fire spalling and reduce overall structure damage. The use of polypropylene microfibres, aggregates with low thermal expansion or creation of a highly interconnected poroue system, could be used.

Most of the earlier mentioned methods must be utilized during the construction phase, and only a few of them can be additionally applied, especially in tunnels. In the tunnels, the area for application of passive fire protection features is highly restricted, and if an epoxy coating is used and the fire event exceeds its exposure temperature, the coating material melts and droplets can occur. Furthermore, it could lead to dangerous gas production and complicate rescue actions. This fact gives way for further development and introduction of new passive protective methods primarily focused on application in tunnels.

2.3.3 Active fire protection measures

Various smoke detection devices, electronic fire alarms, and other reporting devices can be used as an active means of protection. In many buildings, a sprinkler system is installed, which uses water as a fire extinguishing medium. Another active measure is to provide heat and smoke removal, a perfected evacuation plan, and easy access for rescue teams. Furthermore,

a sufficiently designed and used ventilation system can contribute to the faster extinguishing of fire, especially in tunnels, where natural ventilation is absent. Active fire protection measures are divided into detection and suppression categories.

Fire detection solutions

Fire detection solutions are smoke alarms that inform about the fire event. They could be based only on local alerts by intensive sound beeping or connected to the fire department or/and police. In tunnels, besides smoke alarms, cameras are commonly installed to have information about a cause of the fire.

Fire suppression measures

Fire suppression measures include fire extinguishers, automatic or manual sprinkler systems, standpipe systems, preventive foam, or even non-toxic gaseous agents that are used for extinguishing the flames.

Hypoxic air systems

Hypoxic air systems are quite new methods that prevent ignition or spread of fire. They work on the basis of oxygen reduction in a specific space where the fire hazard is suspected. This method can fully replace standard fire extinguishing equipment, has no environmental impact, and has easy installation and low maintenance levels (71). Hypoxic air systems are beneficially used in server rooms and other rooms with a high amount of electric installations.

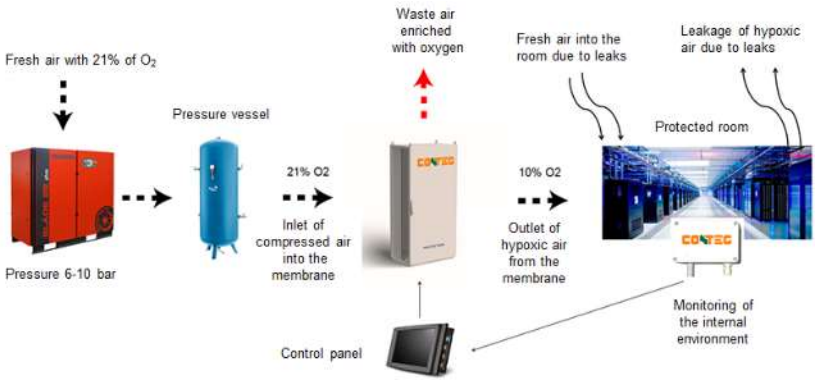

Fig. 21: Technical solution of hypoxic air fire preventive system (71)

2.3.4 Regulations dedicated to tunnel fire design

Nowadays, the borders of the building industry are being pushed to the limits, and tunnelling engineering is no exception. The development of drilling techniques and advanced geotechnical/geological knowledge allow building massive underground structures. Traffic and fire safety are indispensable parts of planning underground structures, which are becoming more complex and sophisticated due to modern communication technologies. An example is given to emphasize the necessity of fire safety in tunnels. The Laerdal tunnel is the longest tunnel in the world, 24,5 km, and without proper traffic and fire safety features, it would not be safe to operate.

Based on the reviewed legislation and directives, there are almost no guidelines for tunnel design published by the EU. At the moment, tunnel design engineers follow Eurocodes, particularly EN 1992 “Design of concrete structures,” EN 1997 “Geotechnical design” and EN 1990 “Basic of structural design,” but none of the mentioned document contains guidelines for tunnel design (72). The “Directive 2004/54/EC on minimum safety requirements for tunnels in the Trans-European Road network” (73) is the only document published by the EU, and dedicated clearly to tunnels. Otherwise, the national standards for tunnel design are used. Currently, there is an attempt to prepare a new European tunnel standard and/or guideline, which would foster harmonization of design rules between countries.

The Czech national standards and technical guidelines used for tunnel design (including fire safety design) are TP98, TP229 issued by Ministry of transport (74, 75), and Government Regulation No. 264/2009 Coll. “Government order on safety requirements for road tunnels longer than 500 meters” (76). Furthermore, documents from some other countries such as Norway, Japan, USA, and guidelines issued by international associations RILEM and FIB (51, 77–81) are available and used.

The driving force for fire resistance precautions and innovations in tunnels are traffic accidents and fire events. Data from such events are collected and used in best practice and development of fire protection and safety features in tunnels. Transport Research Information Database (TRID) is an incorporated database that combines the records from the Transportation Research Information Services Database and the Joint Transport Research Centre’s International Transport Research Documentation Database. TRID provides access to more than 1,25 million records of transportation research worldwide (82).

2.4 Performance-based methods – numerical modeling

Performance-based methods (PbM) were developed by engineers focused on fire design of structures and are based on the calculations with input factors such as temperature, the pressure developed inside the concrete structure during the water transformation, mechanical damages due to volume changes of individual components in the concrete and concrete mix design. These methods were first introduced around the 1970s by Bažant and Thonguthai (83) when computers started to be used in the field of civil engineering. The “one-phase model” describing a state and transport of pore water (84) serves as a basis for many successive models. In comparison to prescriptive methods PbM are more flexible and adjustable to individual structures. Using PbM leads commonly towards salvage of the material and larger freedom for architects.

The evolution of PbM is based on phenomena possible to combine or models separately developed and then merged. The first attempts of modelling were based purely on thermal analysis, followed by thermo-mechanical models and thermo-hydro-mechanical models, and the latest trend is a thermo-hydro-chemo-mechanical model. The evolution of modelling is driven by more complex laboratory fire testing where decoupling of individual phenomena could be measured by innovative laboratory techniques such as in-situ neutron tomography (66) or ^{29}Si magic-angle spinning nuclear magnetic resonance (^{29}Si MAS-NMR) supported by X-ray diffraction and thermogravimetric analysis (85).

Prescriptive based methods are the main subject of fib Bulletin 38 “Fire design of concrete structures – materials, structures and modelling” (51) published by fib (The International Federation for Structural Concrete), and RILEM (International Union of Laboratories and Experts in Construction Materials, Systems and Structures) technical committee 256-SPF: Spalling of concrete due to fire: testing and modelling (86) in proceedings from the workshop which takes place every two years. Those two organizations fib and RILEM, are very active in gathering researchers investigating the same problem and by sharing the knowledge, accelerating the understanding of the behaviour of concrete under thermal load, which is extremely complex.

2.4.1 Thermal analyses

Thermal analyses were used as the first attempt when calculating fire resistance of concrete elements or concrete structures. The time-dependent temperature distribution is necessary for structural analysis. Anderberg proposed one of the first thermal analyses and the key hypothesis was that the cross-section of the element which is not heated over the 500°C retain the same strength and modulus of elasticity as design (87). This method is highly dependent on concrete type as the behaviour of individual types of concrete differ a lot.

There are several programs developed by professional software houses, such as ABAQUS, ANSIS in the USA or LUSAS in the UK Research workers designed the other group of thermal analyses, and those are FIRES-T3 developed in 1977 in the USA, and TEMPCALC developed in 1986 by Anderberg in Sweden (5).

2.4.2 Thermo-mechanical models

Thermo-mechanical models are usually interfaced and not integrated. The thermal calculation is carried out first for the whole duration of the fire exposure and then integrated into the mechanical analysis program to calculate the stresses and strains for the element or structure. There is no interaction between the two analyses, and moisture effect is omitted. Regardless of those factors, thermo-mechanical models provide accurate results, and transient creep (LITS) is particularly integrated for columns. As the moisture migration is not incorporated in the calculation, explosive spalling cannot be predicted by those models.

The development of thermo-mechanical models started in 1974 at the University of California by Backer & Bresler (88) and was called FIRES-RC. The program was later improved, and the outcome was a more realistic concrete behaviour model. Several more programs such as CONFIRE developed in Norway in 1982, CEFICOSS introduced in 1987, FIREXPO developed in 1999 by contractor Bouygues within project HITECO, and Kodur et al. in 2009 (89).

2.4.3 Thermo-hydro-mechanical models

Thermo-hydro-mechanical models could be used for modelling of explosive spalling, which is a very complex mechanism. Commonly, models that involve more parameters are based on the previously developed models, such as the model from Tenchov & Purnell, which is based on the model from Ortiz introduced in 1985 but with the addition of two parameters, permeability and relative humidity of concrete. Another model that is essential because it incorporates the inhomogeneity of concrete as one of the factors. Zhao introduced a model based on the use of steam tables for the calculation of pore pressure (90).

HITECOSP (high-temperature concrete spalling) is a fully coupled nonlinear model, designed to predict the behaviour, and potential for spalling, of heated concrete structures for fire and nuclear reactor applications. In this model, concrete is considered as a multiphase material consisting of a solid phase, two gas phases and three water phases (5). This type of model is most commonly used for new types of concrete, such as HPC and UHPC, because their porous structure significantly differs from standard concrete, and explosive spalling occurrence is more probable in case of a fire event.

2.4.4 Thermo-hydro-chemo-mechanical models

Thermo-hydro-chemo-mechanical models analyse the behaviour of concrete and are based on four balance equations: a) mass of dry air, b) mass of the water state (liquid + vapor, taking phase changes into account), c) enthalpy of the whole medium (including latent heat of phase changes and heat effects of hydration or dehydration processes) and d) linear momentum of the multiphase system. Gawin et al. (84) presented a model which introduces different spalling criteria on a failure mode: shear failure, buckling failure, simplified fracture failure and integral failure. Another thermo-hydro-chemo-mechanical model was developed based on two thermo-hydro-mechanical models (91, 92), and a fully coupled approach is used to describe the behaviour of the multiphase partially saturated porous material, where all of the main phase changes are taken into account. Furthermore, two critical parameters should not be omitted; thermal exchange at boundaries, and thermal-fluid-dynamics of the surrounding environment of the analysed structure element (51).

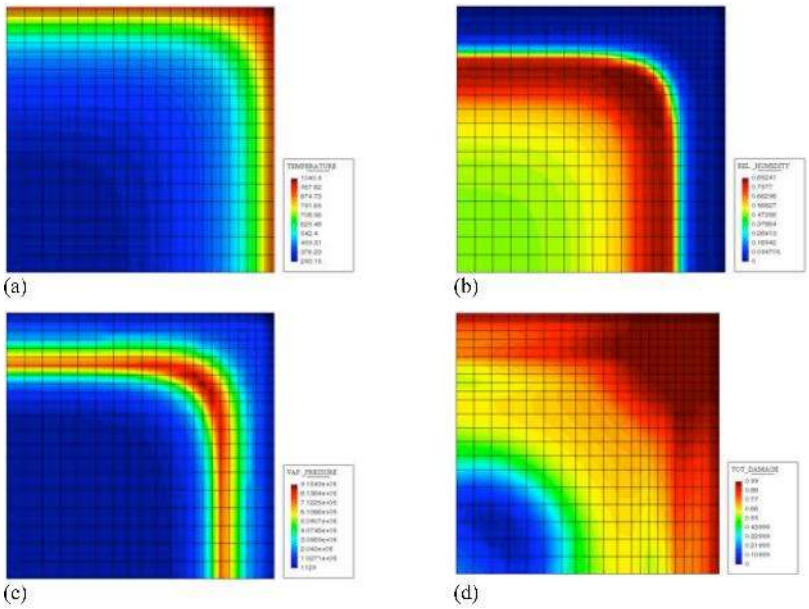

Fig. 22: Example of a quarter HSC column section distribution of (a) temperature, (b) relative humidity, (c) vapour pressure, (d) damage exposed when to a mix of radiative and convective heating conditions (51, 92, 93).

To summarise the development of all types of performance-based models, it could be stated that since the 1970's when the field was discovered, many researchers came up with models concerning one, two or more factors. Models which include many factors could predict the behaviour of concrete and its susceptibility to explosive spalling quite precisely, but there are still a few limiting factors restricting further investigation and development of mathematical models. Sophisticated models have high computational and time demands; still, some limitation of availability of material properties from experimental laboratory measurements are missing, and assumption of concrete homogeneity (macroscopic models for concrete) (51, 94).

3 CONCRETE IN ELEVATED TEMPERATURES

Fire resistance of concrete can be rapidly improved by an appropriate selection of input materials and concrete design. Emphases are given to materials with higher thermal stability. Unfortunately, such materials are not available in all locations, and the quality of input materials is frequently compromised, and locally available materials used. One concern is the selection of individual input materials, but the overall design and interaction of individual input materials under fire load is another issue. Additionally, load stresses, heating regimes, the shape of elements, and other parameters can cause the failure of structure build from well designed concrete mix with suitable input materials.

As is well-known, concrete is composed of the cement matrix, aggregates, and air pores. Those three main components have various behaviour under thermal load, and their interaction defines the fire resistance of concrete. In this section, the behaviour and contribution of individual input materials to the fire resistance of concrete will be described in detail. Apart from the description of materials and their behaviour, the role and influence of the porous system and the interfacial transition zone (ITZ), which is located between the cement matrix and individual grains of aggregates, will be explained. Nowadays, it is common to use various types of dispersed fibres or admixtures to modify the concrete mix and improve particular properties. Chapter 3 will be concluded by a list of rules, which are essential for the design of concrete with improved fire resistance.

3.1 Cement matrix

Cement matrix commonly represents 30 to 40% of the concrete volume, and is composed of cementitious hydration products, unhydrated cement grains, sand, pores and water. The characteristics of the cement matrix of ITZ differ slightly from the bulk cement matrix, and therefore it will be described in a separate subchapter. Optional materials present in the cement matrix are supplementary cementitious materials (SCM) and admixtures. Dispersed fibres are practically part of the cement matrix, but they mostly do not react chemically with cement mortar, and for this reason, will be described in the separate section 3.2. Properties of individual components and their behaviour, when exposed to elevated temperatures, will be described in detail.

3.1.1 Cement

Cement is the hydraulic material consisting of Portland cement clinker and is the main binding component in concrete due to its chemical reaction with water. During the reaction hydration products are formed, which give strength to cement paste. In general, there are more types of cement, mostly based on their composition from a chemical perspective, such as white cement, alite cement, high belite cement, high alumina cement, or blended cements where Portland cement is partly substituted by SCM. The differences of various cement types are plotted on the CaO-Al_2O_3-SiO_2 ternary diagram in Fig. 23.

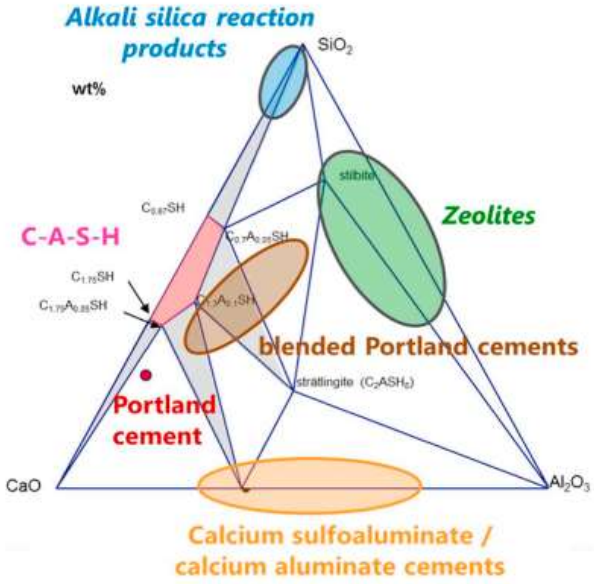

Fig. 23: The dominance area of Portland cement, blended types of cement, calcium sulfoaluminate and calcium aluminate types of cement, zeolites and ASR products plotted on the $CaO–Al_2O_3–SiO_2$ ternary diagram of cementitious materials (95).

Blended cements are not going to be discussed in detail, and focus will be given predominantly to the hydration mechanism and formation of hydration products, its structure and behaviour under thermal load. Water content and porous structure in hydrated cement paste depend on hydration, extend closely connected to water/cement (w/c) ratio and curing age, see Fig. 24.

Water is present in cement paste either in the form of chemically bonded water in hydration products, or water present in CSH interlayer space, gel pores, capillary pores and surface-adsorbed water in empty macropores (96). The gel pores represent about 28% of cement paste (97). Water used for hydration of cement also serves for the workability of fresh cement paste, and unless plastifying admixture is used, water is in abundance and evaporates during the hardening phase. The excessive amount of mixing water or the use of cement with accelerated hydration, so-called rapid cements, can result in the formation of less dense CSH gel, in other

words, higher porosity of cement paste. In such cases, porosity could be maintained by the addition of SCM (98, 99).

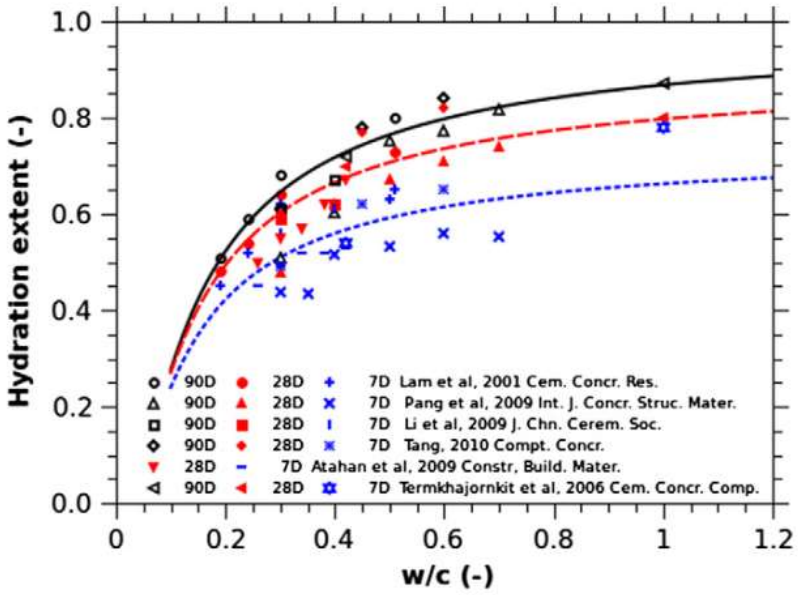

Fig. 24: Relation between hydration extent and w/c ratio for different curing ages of cement pastes (99).

The range of coefficient of thermal expansion for hydrated Portland cement paste in room temperature varies from 10,8 to 16,2 $\cdot 10^{-6}$/°C (100). When the cement paste is exposed to elevated temperatures, the thermal expansion is changing according to exposure temperature. This problem is going to be explained in detail below in the section entitled “Behaviour of Portland cement exposed to elevated temperatures”.

Chemical composition of clinker and its hydration process

The clinker is composed predominantly by alite, belite, tricalcium aluminate and tetracalcium aluminoferrit listed in Tab. 3, among the other less significant chemical and mineralogic components. Both chemical composition and hydration process will be focused only on the most important features, which are crucial for fire resistance of concrete (101, 102).

Tab. 3: Typical chemical composition of clinker (102).

Compound	Formula	Shorthand form	% by weight
Tricalcium aluminate	$3CaO \cdot Al_2O_3$	C_3A	10
Tetracalcium aluminoferrite	$4CaO \cdot Al_2O_3 \cdot Fe_2O_3$	C_4AF	8
Belite or dicalcium silicate	$2CaO \cdot SiO_2$	C_2S	20
Alite or tricalcium silicate	$3CaO \cdot SiO_2$	C_3S	55
Sodium oxide	Na_2O	N	up to 2
Potassium oxide	K_2O	K	
Gypsum	$CaSO_4 \cdot 2H_2O$	$C\underline{S}H_2$	5

Individual compounds have different reaction times and roles during the hydration of clinker (Portland cement), and four main reactions are going to be described.

One of the initial reactions is performed by tricalcium aluminate (C_3A) and is characterised by high heat development, little strength contribution, and its rapid reaction can be retarded by

the addition of gypsum. Gypsum reacts with C_3A and forms ettringite on the surface of C_3A grains (103). The reaction of C_3A hydration (equation 7) and the formation of ettringite (equation 8) follow:

$$3CaO \cdot Al_2O_3 + 6H_2O \rightarrow 3CaO \cdot Al_2O_3 \cdot 6H_2O \quad (7)$$

$$3CaO \cdot Al_2O_3 + CaSO_4 \cdot 2H_2O \rightarrow 3CaO \cdot Al_2O_3 \cdot 3CaSO_4 \cdot 32H_2O \quad (8)$$

Tricalcium silicate (Alit, C_3S) is mostly responsible for the initial setting of cement and early strength gain. Hydration products from its reaction are CSH gel and calcium hydroxide ($Ca(OH)_2$, Portladite). Its reaction follows equation (9):

$$2(3CaO \cdot SiO_2) + 6H_2O \rightarrow 3CaO \cdot 2SiO_2 \cdot 3H_2O + 3Ca(OH)_2 \quad (9)$$

Dicalcium silicate (Belite, C_2S) is responsible for the gain of strength after approx. seven days. Hydration products from its reaction are CSH gel and calcium hydroxide. Its reaction follows equation (10):

$$2(2CaO \cdot SiO_2) + 4H_2O \rightarrow 3CaO \cdot 2SiO_2 \cdot 3H_2O + Ca(OH)_2 \quad (10)$$

Last, but not least is the reaction of Tetracalcium aluminoferrit (Ferrite, C_4AF), which reduces the maximum melting temperature during clinker production and does not contribute much to the strength of cement paste. The reaction of C_4AF is rapid due to the presence of alumina. The addition of gypsum or calcite could retard the reaction in a same manner as in the case of C_3A. The reaction is more complex, and highly dependent on the presence of $Ca(OH)_2$, gypsum or calcite. Equation (11) explain the formation of calcium aluminates hydrates (CAH) in the presence of $Ca(OH)_2$. If carbonates (calcite) or sulphates (gypsum) are present in system, calcium carbo- and sulpho-aluminiate (ferrite) hydrates are formed, Equation (12) (104–106).

$$4CaO \cdot Al_2O_3 \cdot Fe_2O_3 + 4Ca(OH)_2 + (2n-4)H_2O \rightarrow 2(4CaO \cdot 0{,}5Al_2O_3 \cdot 0{,}5Fe_2O_3 \cdot nH_2O \quad (11)$$

$$4CaO \cdot Al_2O_3 \cdot Fe_2O_3 + CaSO_4 \cdot 2H_2O \rightarrow 3CaO \cdot Al_2O_3 \cdot CaSO_4 \cdot nH_2O \quad (12)$$

Hydration products forming hardened cement paste are mainly CSH gel ($3CaO \cdot 2SiO_2 \cdot 3H_2O$) representing about 60%, and $Ca(OH)_2$, which constitute about 15 to 25%. The rest of hardened cement paste is constituted by unhydrated cement grains, ettringite, and other types of hydration products. The most common methods used for the identification of the extent of cement hydration are thermogravimetry analysis (TGA), X-ray diffraction analysis (XRD), backscatter electron image analysis (BES/IA), scanning electron microscope or ^{29}Si MAS-NMR (85, 99, 107).

Behaviour of Portland cement exposed to elevated temperatures

Hydration products of Portland cement do not consume all mixing water during the preparation of Portland cement paste, and also hydration extent of Portland cement is commonly between 0,45 to 0,8 (99, 108, 109). Therefore, there is free water and physically bonded water along with chemically bonded water in hydration products. Evaporation of free water takes place up to temperature 374°C (critical point of water), but a significant part of free water is released between 95 and 105°C (83). Evaporation of free water will be extensively described in section 3.1.1.3 and 3.2. In this section, release of physically bonded water in CSH gel and chemically bonded water in hardened Portland cement paste will be discussed.

The first chemical reaction taking place is decomposition, or more preciously loss of crystalline structure, of Ettringite between 70°C and 120°C, but the greatest part of the reaction occurs suddenly at 114°C (saturated water vapour pressure 1,63 bar) (51, 85, 110–113). Chemical reaction,

$$3CaO \cdot Al_2O_3 \cdot 3CaSO_4 \cdot 32H_2O \rightarrow Ca[Al(OH)_6]_2SO_4 \cdot 8H_2O + 2CaSO_4 \cdot 0{,}5H_2O + 17H_2O \quad (13)$$

during which is released water, formed monosulphates, and the second product is either bassanite or γ-anhydrite characterised by linear thermal expansion 42 · 10^{-6}/°C (113).

The temperature range of dehydration of CSH gel varies a lot in literature as there are more types of water to evaporate. Some authors state evaporation from 105°C up to 1 000°C (114, 115), while others state the beginning of dehydration of CSH at 250°C up to 800°C (51, 85, 97). The reaction,

$$(CaO)_a \cdot SiO_2 \cdot (H_2O)_b \leftrightarrow (CaO)_a \cdot SiO_2 \cdot (H_2O)_{b-c} + c \cdot (H_2O)^{vapour} \quad (14)$$

evaporation of water from CSH ($3CaO \cdot 2SiO_2 \cdot 3H_2O$) is reverse reaction and happening in multiple steps. Each step is characterised by different activation energy (83,7-372 kJ/mol) needed for the water molecule to be released. The first is realised water attached to the outer side of CSH layer group, called globule or water in CSH gel pores. When the temperature continues to increase, more energy is developed, and interlayer water is evaporating. Individual CSH backbone layers approach each other and becoming denser, see Fig. 25, where two different principles are described (114, 116, 117). The crystalline form of βC_2S (Larnite) is formed between 120 and 200°C and decomposes during the last stage (117–120). Hager states in her article that the last phase of decomposition of CSH is between 600 and 800°C, and results in formation of βC_2S (115). Formation of βC_2S is also recorded by X-Ray diffractogram (see Fig. 27) from Alonso and Fernandez (85). As CSH gel represents approximately 60% of hydrated cement paste, evaporation of water from its structure causes great volume changes characterised by the formation of microcracks. Microcracks extend the interconnection of the porous system, which serves better for the vapour migration. As dehydration of CSH gel is a reverse reaction, water can re-enter the interlayers already if the relative humidity of surrounding ambient is more than 20% (96).

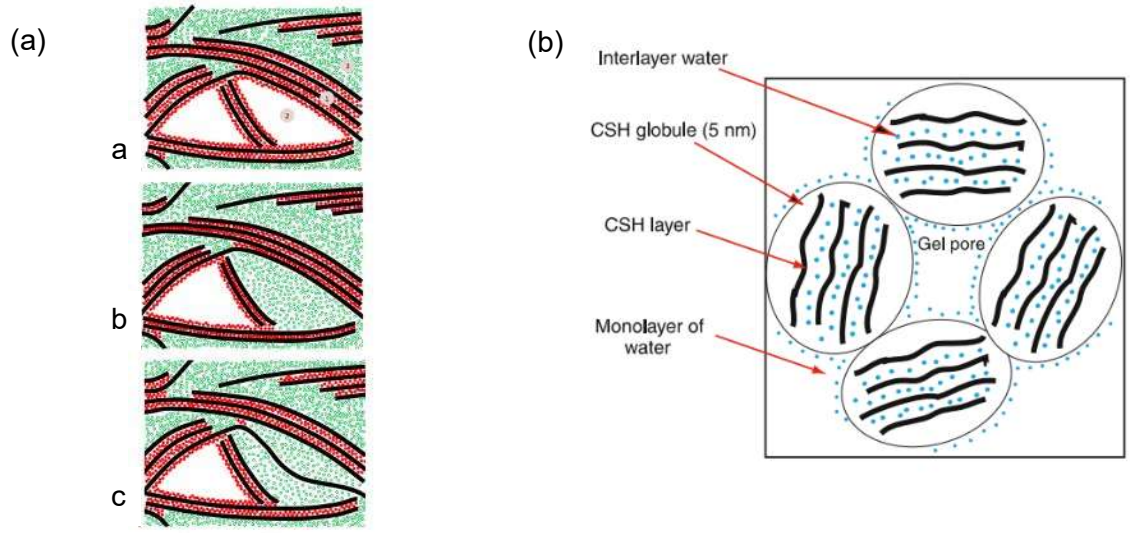

Fig. 25: CSH gel – (a) Schematic representation of the CSH microstructure during temperature changes (in detail described below); (b) A schematic of globulous structure of CSH gel. (114, 116).

Schematic representation of the CSH microstructure during temperature changes (a) Original microstructure before temperature change. A state corresponding to partial desaturation of the gel pores (at 50−90% RH) is depicted. The solid lines represent CSH backbones. The backbone spacing is ca. 1,4 nm, and the interlayer spaces (marked as ①) are about 0,7−0,9 nm wide. Full red circles represent interlayer water between CSH backbone sheets or adsorbed water on the surface of larger, but empty pores, that in NMR manifests as interlayer water. Empty green circles represent water in filled gel pores. Gel pores are about 2,5 nm in size. Larger gel pores (marked as ②) are empty of water, while smaller gel pores (marked as ③) remain full. Water molecules in vapour phase are not presented. (b) Microstructure after heating according to the water migration model (c) Microstructure after heating according to the pore rearrangement model. In part b, the number of red circles

between layers is less than in parts a and c, whereas in part c the number of true interlayers and surface layers that give rise to red circles is reduced. The total number of circles is kept constant between the schemes so as to represent constant water content in the samples during temperature changes (116).

Another significant chemical reaction is the dihydroxylation of calcium hydroxide (Portlandite, $Ca(OH)_2$). This reaction is a single-step reaction with activation energy approx. 151,8 kJ/mol, and the variation of activation energy is very low (114). The reaction takes place between 390 and 476°C, and is extremely sensitive to the texture, the form of the particles and to the heating rate (121). The apparent activation energy, in other words, the heat needed for dehydroxylation of Portlandite,

$$Ca(OH)_2 \leftrightarrow CaO + H_2O^{vapour} \quad (15)$$

can be experimentally evaluated by thermal-analytical experiments at different heating rates, or by calculation according to numerical models such as differential (Friedman) and advanced (Vyazovkin) iso-conversional methods (Model-Free). Fig. 26 presents the decomposition of Portlandite based on the heating rate, which is also connected to the scale of microstructure damages. If the heating process is fast, build-up of pressure caused by a great volume of released water searching for migration channels, can cause less or more violent damage to the microstructure. The amount of Portlandite in hydrated cement paste varies from 15-25% and could be decreased by the addition of pozzolan reactive supplementary cementitious materials.

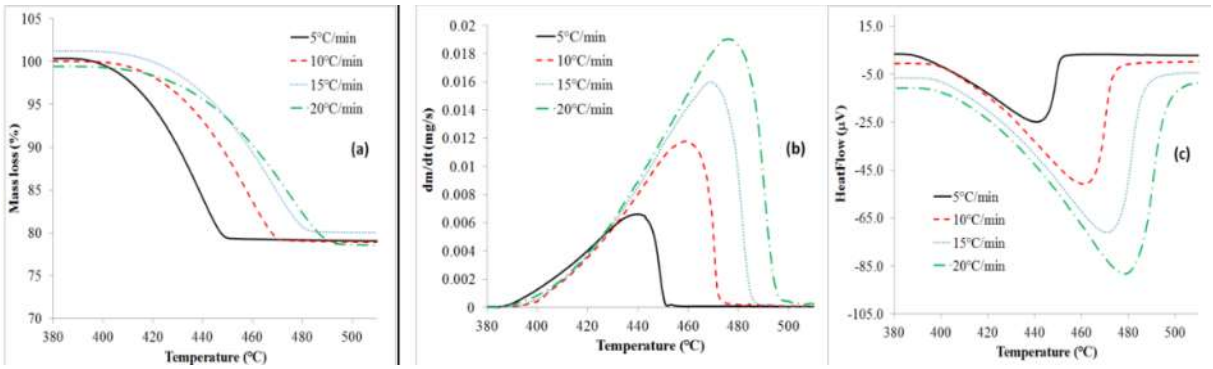

Fig. 26: TG/DTG/DTA curves of thermal decomposition of Ca(OH)2 at different heating rates (121).

The dihydroxylation of Portlandite is a reverse reaction, and if the formed calcium oxide (CaO) gets in contact with water, even in the form of air humidity, reaction characterised by volume increase by 44% takes place, and Portlandite is formed (51).

The last most significant chemical reaction due to thermal exposure of Portland cement paste is decarbonisation of calcium carbonate (Calcite, $CaCO_3$), which initiates around 650°C. Content of calcite in hydrated Portland cement is not high, and therefore reaction,

$$CaCO_3 \rightarrow CaO + CO_2 \quad (16)$$

does not cause significant damage to the microstructure. Content of calcite could be influenced by carbonation of a sample during its preparation. This reaction is again reverse, and calcium oxide can spontaneously react with atmospheric CO_2.

Chemical changes of Ettringite ($3CaO \cdot Al_2O_3 \cdot 3CaSO_4 \cdot 32H_2O$), Portlandite ($Ca(OH)_2$), calcite ($CaCO_3$), Brownmillerite ($Ca_4Al_2Fe_2O_{10}$) or Larnite (C2S) can be analysed by X-ray diffraction analysis but for dehydration of CSH gel ^1H nuclear magnetic resonance (NMR) relaxometry, supported by X-Ray diffraction (XRD) and thermal analysis (TGA/DTA) is more suitable. The decomposition of crystalline phases of hydrated Portland cement exposed to 20, 100, 200, 450 and 750°C, are presented in Fig. 27. It is important to keep in mind that results from analysis of hydrated Portland cement can be influenced by the preparation procedure and ambient in which the sample was prepared. The most common issue and cause of many minor

mistakes in results, is atmospheric carbonation reaction, which can increase measured calcite content in a sample (99, 121).

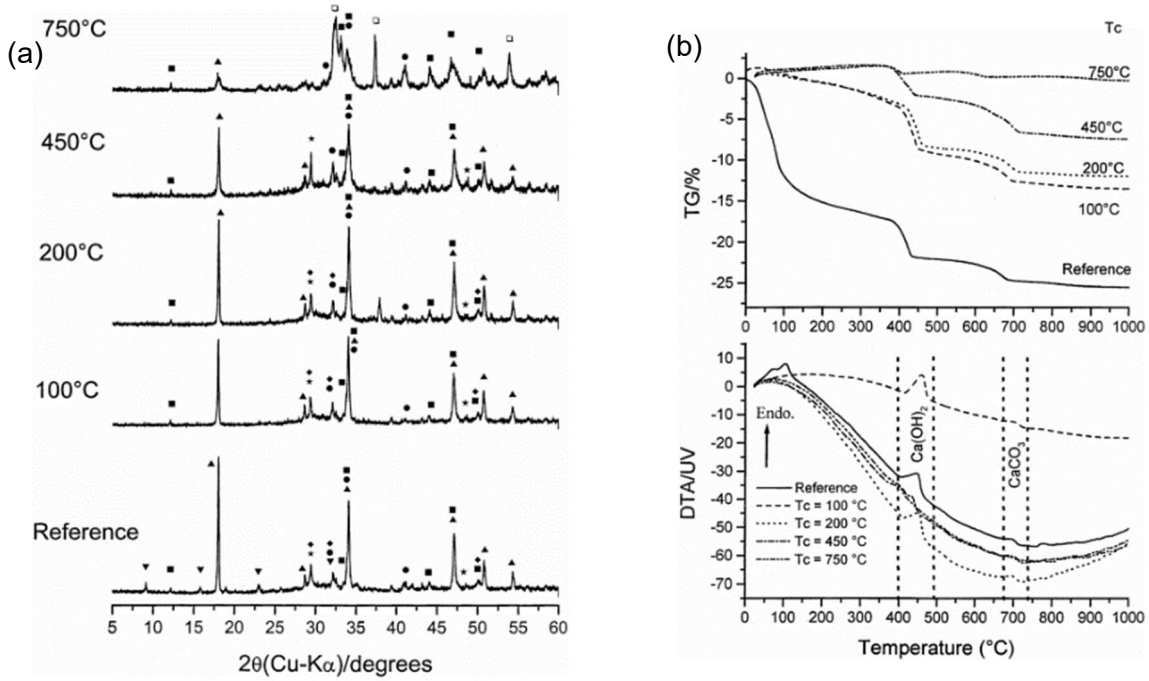

Fig. 27: XRD and TA of hydrated Portland cement: (a) X-ray diffractograms of the reference specimen (initial cement paste), and the heated specimens at various temperatures. Key to phases: Larnite (•); Portlandite (▲); Calcite (*); Brownmillerite (■); Ettringite (▼); $Ca_{1,5}\ SiO_{3,5} \cdot xH_2O$ (♦); lime (□); (b) Thermogravimetric analysis (TG and DTA) of the reference specimen (initial cement paste) and the heated specimens at various temperatures (Tc) (85).

All the chemical changes and evaporation of water from the Portland cement paste are accompanied by volume changes, which are characteristic for different exposure temperatures (55). A thermal strain of Portland cement paste exposed to a temperature range from 27°C to 871°C was described in detail by Cruz and Gillen (122). They experimentally measured coefficient of linear thermal expansion of Portland cement paste (w/c ratio 0,40) and stated that between 27 and 149°C paste expands 14,8 · 10^{-6}/°C and then shrinks between 149 and 871°C, 32,8 · 10^{-6}/°C, see Fig. 28.

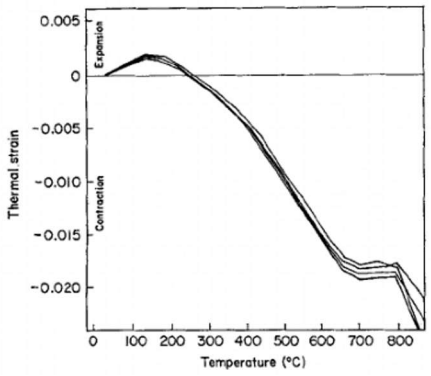

Fig. 28: Thermal strain of Portland cement paste (w/c=0,40, 4 tests) (122).

Furthermore, different thermal expansion is stated for cooling of cement paste, when the value of the linear thermal coefficient is 27 · 10^{-6}/°C for cement paste without access to additional water. If there is access to water located in capillary pores or external moisture flowing into CSH gel, the resulting expansion (during or after cooling) is about 11,6 · 10^{-6}/°C (123).

3.1.2 Supplementary cementitious materials (SCMs)

Supplementary cementitious materials are used as a replacement for Portland cement with the aim to reduce the carbon footprint of cement and still preserve its properties. The origin of SCM is mostly from various industries in the form of waste, changed, with or without treatment, into secondary raw materials, which are beneficially used in cement or concrete production. The most widely used SCMs are fly ash (FA), ground granulated blast furnace slag (SL) and silica fume (SF), more alternative types are calcinated clay, ground glass, pumice, or rice husk ash. Nowadays, the trend is highly focused on existing and new SCMs, as a consequence of emphasizing the reduction of CO_2 emissions, the use of environmentally friendly materials, the circularity of materials by reuse of waste from various industries and reduction of landfilling.

The most important property of SCM is the content of the amorphous (glassy) phase, which is reactive under certain conditions, and contributes to the strength and other properties of cement paste. Other properties influencing reactivity of SCMs are fines, the shape of particles, chemical composition, replacement level, water/cementitious materials ratio. For example, fly ash (FA) is one of the most common SCMs in the cement and concrete industry, but only 20% of FA is suitable as Portland cement replacement, the other 60% could be used for earthwork, and the rest has no use and is landfilled. Another reason why it is essential to keep testing the potential of new materials that could become SCMs is due to the closing of thermal power plants producing by-product FA.

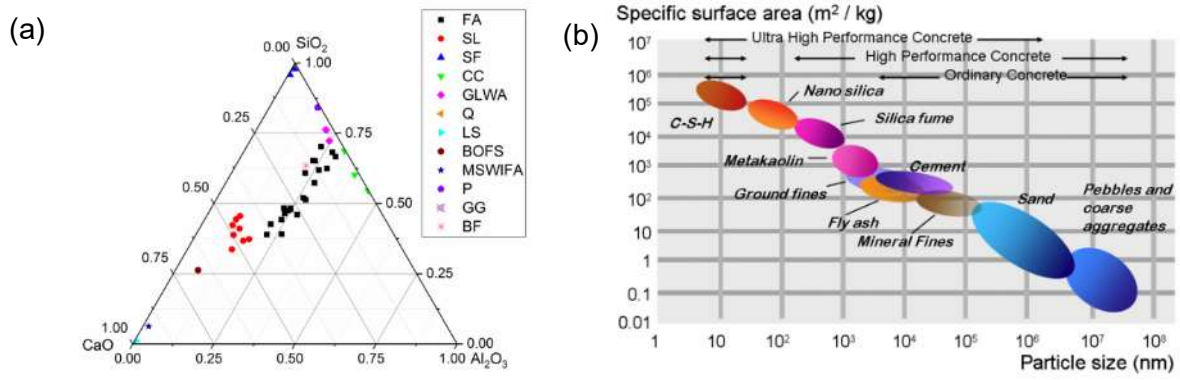

Fig. 29: Characteristic of SCMs: (a) Ternary phase diagram showing SiO_2, Al_2O_3 and CaO amounts for various SCMs. Key to SCM types: fly ash (FA), ground granulated blast furnace slag (SL), silica fume (SF), calcinated clay (CC), ground lightweight aggregates (GLWA), quartz (Q), ground limestone (LS), basic oxygen furnace slag (BOFS), municipal solid waste incineration fly ash (MSWIFA), ground pumice (P), ground glass (GG) and basalt fines (BF); (b) specific surface area of several selected SCMs (124, 125).

Reactivity is a factor that sorts SCMs into inert, latent hydraulic or pozzolanic type, and they can be blended directly in clinker during the cement production or as an addition during concrete production. If they are homogenised with clinker directly during cement production, then we refer to blended cements characterised by C/S ration (CaO/SiO_2 ratio), see Tab. 4. Presented chemical composition is for exact types of FA, SL and OPC. Therefore, it is not possible to generalise those examples.

Tab. 4: Overview of several blended cements and their C/S ratio. Key to SCM types Fig. 29 (126).

Material	CaO	SiO2	C/S ratio
Ordinary Portland cement (OPC)	63	22	2,86
OPC + 25% F-FA	48	29	1,66
OPC + 25% C-FA	52	25	2,08
OPC + 25% SL	57	25	2,28
OPC + 40% SL	53	27	1,96
OPC + 25% CC	50	26	1,92

Reactivity of SCMs could be improved by the addition of sulphate constituent (gypsum) and carbonate constituent (lime). Reactivity of individual SCMs is possible to analyse by various test methods. There are tests specifically for FA and SL described in ASTM and EN, but based only on comparison of strength properties to reference mix (127–129). Other methods, such as Chapelle test, the Frattini test, the strength activity index test, and the SCM dissolution test, have been introduced. Those methods are useful, but they are not able to distinguish whether the SCM is pozzolanic or latent hydraulic reactive. Therefore, isothermal calorimetry and thermogravimetry analysis or “rapid, relevant, and reliable” test method were introduced (124, 130, 131).

Pozzolanic SCMs

The main characteristic of pozzolanic material is a higher content of amorphous silica and alumina, which need for their reaction calcium hydroxide and water. The reactivity could be classified based on heat release during the reaction, amount of consumed calcium hydroxide, or amount of bonded water, into less or more reactive SCM groups. The pozzolanic reaction is initiated later than hydration of clinker, and therefore, pozzolanic products are formed in pores of cement paste. The delayed pozzolanic reaction could last for several months or even years, depending on the available chemical components and water. As the microstructure is becoming denser, penetration or ingression of water and aggressive chemicals dissolved in water is restricted and contributes to higher durability of concrete. On the other hand, denser microstructure has negative impact on fire resistance of concrete.

The most common pozzolanic reactive SCMs are silica fume and calcinated clay. Those are highly reactive and contribute, for example, to strength and prohibit the initiation of alkali-silica reaction. Less, but still pozzolanic reactive, are some types of silica fumes, fly ash, ground pumice, ground glass or rice husk ash (124, 132, 133).

Latent hydraulic SCMs

This material is also used for carbon footprint reduction of cementitious based materials, but the reaction must be initiated by alkali activators. Latent hydraulic SCMs can react with water when activated via high pH, mechanical grinding, temperature, or other techniques. Calcium hydroxide is not consumed during the reaction. As pH of hydrated clinker (pH >11) or calcium hydroxide (pH 12,8) is high, they are used as alkali activators. As in the case of pozzolanic materials, reactivity could be supported by sulphate and carbonate components and lead to the formation of additional hydrate phases. The higher release of heat during the reaction is characteristic for latent hydraulic SCMs. Furthermore, the contribution of this type of SCMs is very similar to pozzolanic reactive SCMs.

The main representative of latent hydraulic SCMs is ground granulated blast furnace slag, a by-product of pig iron manufacturing. Other, more alternative materials in this group, commonly less reactive, are some types of slags from other metallurgy industries or incineration of various materials (109, 124, 134, 135).

Inert SCMs

Inert SCMs are powder materials that are not reactive or reactive to a very law degree. They are purposefully used to increase fines in the concrete and ensure workability in fresh state. Furthermore, those materials can be beneficially used if the available fine aggregates are crushed and contain very little fines under 0,125 mm. The disadvantage of inert SCMs is their water absorption and need of water for surface wetting. The water needed for their wetting is not fully used for chemical reactions and remains in the structure as free water. This water might be used with delay for hydration of cement and complete the hydration of unhydrated particles. Nevertheless, those particles might be covered by an impermeable layer of hydrated cement and restrict additional hydration. If the inert SCMs are used, more mixing water is needed due to higher total specific surface of powder material. Greater surface area needs to be covered by water film, and the remaining water, which was not used for hydration of cement, form more capillary pores.

As inert SCMs any ground mineral material could be used, for instance, quartz, basalt fines, limestone powder and non-reactive fly ash and ground granulated blast furnace slag. A most frequent reason for low reactivity is a high content of the crystalline phase of calcium, silica and alumina.

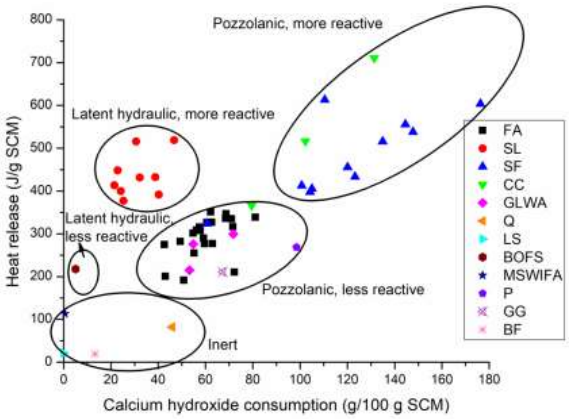

Fig. 30: Results from isothermal calorimetry and thermogravimetry analysis on various types of SCMs and their classification (124).*Note: Key to SCM types Fig. 29.*

Behaviour of SCMs exposed to elevated temperatures

The thermal behaviour of SCMs is closely related to Portland cement behaviour as those two components are forming cement paste when blended with water. This mix also can include admixtures and fines from aggregates, but for simplification, only a blend of Portland cement and SCMs will be considered.

The benefits and disadvantages of SCMs are closely related to the individual type of material, replacement ratio of Portland cement and w/c ratio. Therefore, general contribution or negative impact of SCMs to fire resistance of concrete could not be clearly stated. It can be stated, however, that the lowest impact on behaviour of cement paste is attributed to fly ash, followed by ground granulated blast furnace slag and the most significant change of fire resistance is seen with silica fume, micro and nano silica.

Furthermore, the benefit of pozzolanic reactive SCMs is the consumption of calcium hydroxide, which in the case of dehydroxylation forms CaO and consequent exposure to moisture sources causes its hydration, characterised by 44% volume expansion (51). Contrarily, silica fume consumes calcium hydroxide during its reaction, but in the longer term, it produces dense CSH gel and calcium hydroxide during its continuous hydration. Fly ash forms less dense CSH gel as its reactivity is lower compare to silica fume (136, 137). According to the reviewed studies, silica fume does not show a significant influence on fire resistance up to 10% content, but greater amounts form a denser structure of CSH gel and fill a large amount of pores in hydrated Portland cement paste (138, 139). Another widely used SCM is ground granulated blast furnace slag, which contains more CaO in its chemical composition and is able to form more dense CSH gel over time, which makes it, again, non-beneficial for fire resistance (140, 141).

A significant drawback of SCMs is the delayed reaction during which the hydration products are formed in the pores of already shaped cement paste, and by that, the interconnection of the porous system is decreased and overall porosity reduced. Newly formed CSH gel and crystals are dividing capillary pores and filling gel pores. The reduction of capillary pores is going to contribute to reduced mobility of evaporating water, namely, free physically and chemically bonded water, and encourage high-pressure development. The pressure of water and vapour will increase up to the level of the tensile strength of cement paste, and cause fractures and cracks in the microstructure. If the hydration products formed by SCMs reaction

provide high strength, for example, silica fume or micro silica (138), the cracking will be more violent and destructive for the microstructure.

Inert SCMs could be beneficial for fire resistance of concrete as they have water adsorbed on their surface and do not react, so the water is providing the space between the individual particles. In other words, higher content of free or adsorbed water might contribute to the greater interconnection of the pores, especially capillary pores. A higher presence of unbonded water, which needs to evaporate during the exposure to high temperatures might cause nonviolent cracking as the pressure will not build up. The benefit could be the space which will remain free after water evaporation. The benefit or disadvantage of inert SCMs is highly related to its type, water absorption, amount in the concrete mix and many other factors, so it is not possible to draw a clear conclusion.

3.1.3 Mixing water

One of the main ingredients for cement mortar and concrete is water, which first serves for the workability of fresh cementitious based materials, and then for hydration of cement and formation of binding between individual aggregate particles. The amount of water is expressed by the amount of water in relation to cement content, termed water/cement ratio (w/c ratio). The w/c ratio necessary for full hydration of cement is 0,23, and the rest is needed for filling the pore space (about 30%) that is present in cement paste (142, 143). The workability of fresh cementitious material could be also provided by various types of plasticizers and superplasticizers. Before the use of plasticizers became standard practice, only water was used for maintenance of fresh properties of cementitious materials, and therefore, older concrete has a higher porosity and lower strength. The strength of concrete is highly dependent on water content; see Fig. 31.

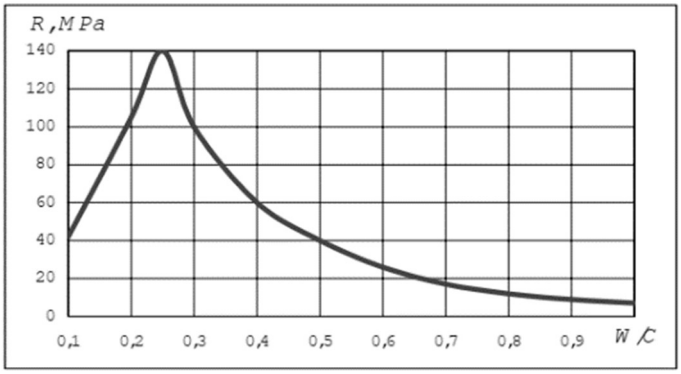

Fig. 31: The dependence of 28 days cement paste strength R on water/cement ratio (143).

Higher w/c ratio provides higher content of pores in the concrete, but it does not necessarily mean better fire resistance as the pores might be of non-suitable size.

Nowadays, the trend is reduction of water/cement or water/binder (if SCMs are used) ratio to achieve high strength of cementitious materials and workability is provided by plasticizers or superplasticizers. The gain of high strength and better durability of concrete is also achieved by optimal packing density, which is again contributing to the reduction of pores and lowering the degree of interconnection of a porous system (144, 145). The model of distribution of cement particles in cement paste with different water/cement ratios is presented in Fig. 32.

Some blended cements or cements with the high surface area have higher water demand, and if the present SCM is, for example, micro silica, the microstructure of concrete becomes extremely dense, which, in case of a fire event, is going to lead to high pressure build-up and explosive spalling. Furthermore, water absorption of aggregates also plays an important role in w/c ratio design. If aggregates with higher water absorption are used, prewetting or higher amounts of mixing water are needed. Water absorbed in aggregates could be released during the aging process of cementitious materials and complete the hydration of cement. In case of

a fire event, water from aggregates must evaporate through the cement paste, and if the amount of water is greater, damage to cement paste might also be more significant.

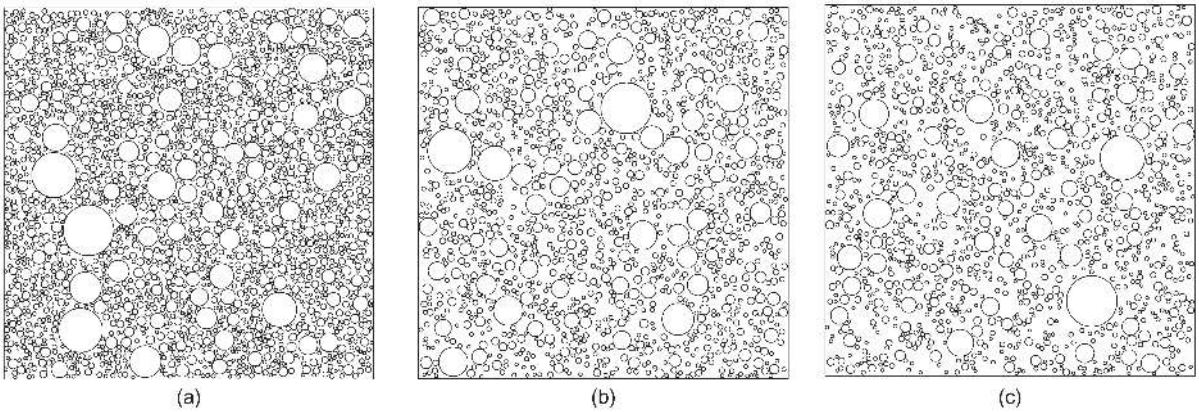

Fig. 32: Distribution of cement particles for different w/c. (a) w/c = 0,3; (b) w/c = 0,5; (c) w/c = 0,7 (146).

3.1.4 Admixtures

Admixtures are chemical agents commonly in a liquid state, used for the improvement of selected properties of fresh or hardened cementitious materials. Use of admixtures is changing microstructure of cement paste which can, in larger or smaller degree, influence its fire resistance. The most common admixtures are plasticizers for improvement of workability of fresh concrete and air-entraining agent (AeA) for porous structure adjustment for better frost resistance. Other types of admixtures are accelerators for greater development of hydration process, set-retarders for the opposite effect. The water proofing admixture improves durability and water tightness of concrete. Only the AeA will be described in detail as that can have a major influence on fire resistance of concrete.

Air-entraining agent is modifying porous microstructure by increasing the number of pores with diameter of 10 to 300 μm (this value varies a lot in literature) (147–149), reducing the distance of individual pores, and resulting in improving freeze-thaw durability of concrete. Pores created by AeA with specific diameter are densely dispersed in cement paste and partly filled with water adsorbed on the pore surface. Owing to surface tension and capillary pore pressure, the pores are not fully filled with water and space serves for ice crystals formation (150, 151). Connection between freeze-thaw resistance and fire resistance of concrete is the overlap of suitable pore size for either formation of ice crystals or evaporation of water. Capillary pores serve as a migration channels for escaping water vapour and their higher interconnection is beneficial (150, 152). Though there are many different classification systems of pores based on their diameter, the general rule could be ration of water in the pores and the ability of water molecules passing through the pores (83, 96). A problematic area exists around the ice formation, water or vapour migration based on moisture content and temperature. In particular, if the ambient temperature is rising around the concrete structure, mobility of water is increased in order to equalise temperature in the concrete structure, and the water or vapour migrates through the least restricted way – capillary pores. Example for ice crystals formation due to decrease of ambient temperature around the concrete structure would be again based on migration of water, in this case water suction, in order to equalise temperature. If the moisture content of structure is high or is fully submerged in water, more ice crystals are formed, and higher damage of concrete is generated.

Traditional AeA works on the principle of surface-active agents content that have two poles: one is hydrophobic and the other hydrophilic, see principle in Fig. 33. The air void is formed on interphase between water and air, and the surface tension is lowered, so the air voids can stabilise once they are formed. Commonly, alphatic or aromatic hydrocarbons are used for hydrophobility, and carboxylic acid or sulphonic acid groups ensure the hydrophilicity. The AeA foams in mixing water, and produced air voids which are locked in the paste during the hardening process (149).

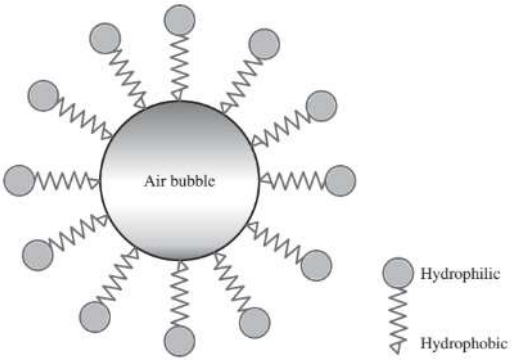

Fig. 33: Mechanism of traditional air-entraining agent (149).

The new types of AeA are based either on polymer microspheres or on chemical process. Those two new approaches are introduced by largest concrete admixtures producers such as Sika, BASF or MC Bauchemie. Product from Sika, SikaControl AER-200 P, is powder which produces air voids of required size by chemical reaction with the mixing water (149). Second type of newly developed AeA is based on introduction of polymer microspheres in cement paste and was presented by MC Bauchemie (Centrament Airpolymer) and BASF (153, 154). The hollow spheres have uniform diameter smaller than 100 μm, high resilience, tough but flexible polymeric shell, so the content of air voids is stable and easier to maintain.

Behaviour of concrete with AeA exposed to elevated temperatures

The air-entrained concrete is predominantly investigated in ambient temperature or for performance under exposure to freeze-thaw cycles with or without the presence of deicing agent. Influence of AeA on concrete, particularly normal strength concrete and high strength concrete, properties in elevated temperatures has been investigated by very few researchers, namely Khalig et. al. and Holan et al. (155–157). Preliminary study on normal strength concrete showed negative influence on compressive strength of air-entrained concrete exposed to 200°C, but between 200°C and 800°C the performance of air-entrained concrete was similar to non air-entrained concrete (157). Investigation of air-entrained high strength concrete (AeA-HSC) showed improved properties between 100 and 400°C exposure temperature, other wise the behaviour was mostly identical to non air-entrained HSC. Properties of Elastic modulus and stress-strain response were not significantly influenced by temperature as the highest difference was caused by entrained air itself (155–157).

In general, the addition of air in concrete decreases significantly compressive strength and therefore it might be challenging to evaluate the influence of AeA on concrete behaviour under elevated temperatures as the strength of reference HSC (1,3% of air in fresh concrete) was higher by approximately 30% in comparison to AeA-HSC (8% of air in fresh concrete) (155, 156). One possibility of how to compare concrete with and without AeA with the same initial strength, is an adjustment of mix design, but that would introduce more variables and complicate the evaluation of gained results.

3.1.5 Porous system in the cement matrix

Pores in concrete are its indispensable part, and the minimum pore content standardly used for mix design calculation is 2%. If the individual phases of concrete are evaluated, pores could be present in aggregates or cement paste. The porosity of aggregates varies from 0,4% (granite, gabbro) up to 67% (close porosity with water absorption about 16%) of high porous aggregates such as lightweight aggregates or extrusive igneous rocks (young volcanic basalt up to 24% porosity). More important for concrete properties are pores in cement paste, which are either empty, partly or completely filled with free or physically bonded water.

Powers, in his study, described dependency of hydration level and porosity and stated that porosity of fully hydrated cement, is about 26% with minimal w/c ratio 0,2 (158). In other

literature sources, the minimum w/c ratio 0,42, where 0,23 is for hydration of cement (chemically bonded water) and 0,19 for filling the gel pores is stated (159). The gel pores and a certain quantity of capillary pores (micro capillary pores) are inevitable, larger capillary pores and macropores can be omitted entirely. The number of capillary pores depends on w/c ratio, particularly on the water which is not consumed by the hydration process and evaporates either during the hardening process, later on, or remains in the hardened cement paste structure. Macropores are the large pores, which result from the mixing process and are formed during the casting of concrete. The presence of water in macropores is highly dependent on the relative humidity of surrounding ambient, but typically they are empty with water adsorbed to their walls. Bažant also explained water bridges, which partly restrict the mobility of water unless the concrete is exposed to elevated temperatures (83).

In general, pores could be classified as micropores (<2 nm), mesopores (2-50 nm) and macropores (>50 nm), as referred to in Fig. 34, including the methods suitable for analyses of various pore sizes (151).

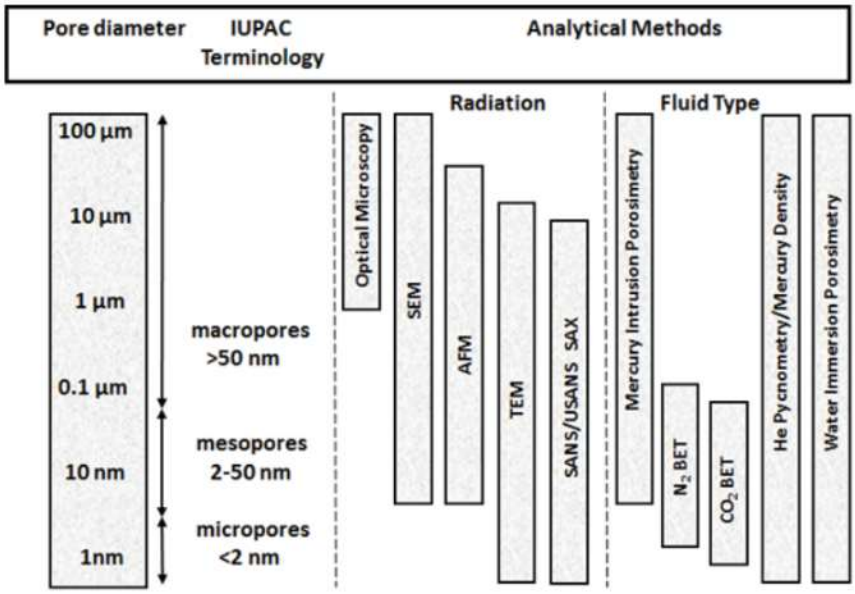

Fig. 34: Methods used to determine porosity and pore size distribution (151).

Classification of pores in cement paste is specific due to the direct reflection of their formation (origin). Terminology for pores in cement paste is as follows; gel pores (present in CSH gel) capillary pores and macropores. Those three groups can be further subdivided, and CSH interlayer water added as the water present between individual CSH layers is not chemically bonded and evaporates around 105°C. It is essential to mention that different literature sources state slightly different pore size classification and terminology, one of the classification systems is presented in Fig. 35 (150).

The porous structure could be changed by (i) addition of air-entraining admixture, causing an increase of capillary pores with diameter from 1 to 50 µm; (ii) w/c ratio, higher w/c ratio higher content of capillary and macropores; (iii) addition of SCM, which form hydration products with delay in gel and capillary pores; (iv) mixing and placing of concrete, especially connected to the formation of macropores and caverns; (v) addition of fibres, which increase the volume of ITZ characterised by higher permeability and presence of capillary pores, and (vi) design of concrete mix, packing density of aggregates on which the new types of concrete such as HSC, HPC or UHPC are based.

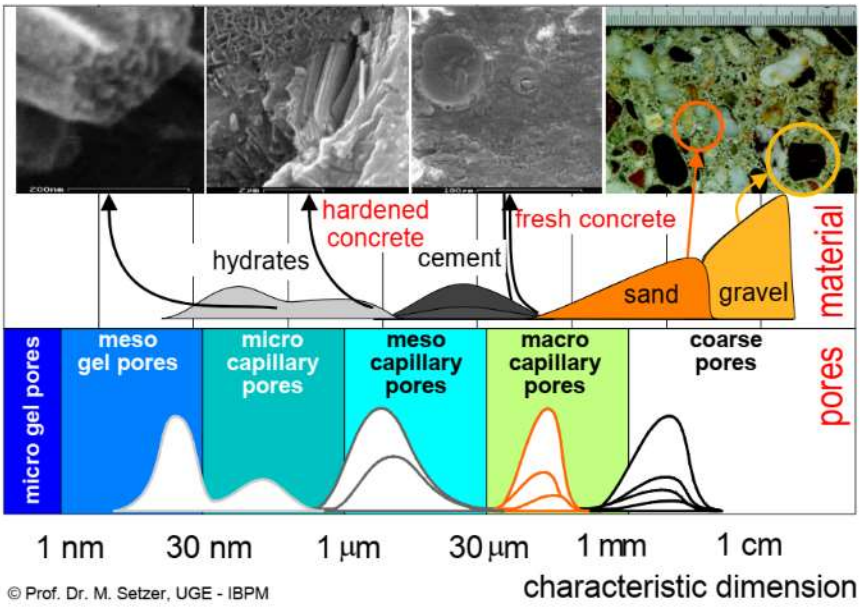

Fig. 35: Pore sizes in concrete (150).

Migration of water through the concrete structure is influenced by many factors, such as heating regime (rapid or gradual), the direction of water migration (towards warmer or colder surface), state of water (liquid, gaseous), a form of water (chemically bonded, physically bonded or free water), the inner structure of concrete (ratio between cement paste and coarse aggregates, the maximum particle size of aggregates), amount, rate of interconnection and type of pores (gel, capillary, macro pores), and thermal properties of concrete. The presence of bigger aggregates can accelerate crack formation and drying process (66). There is an extensive number of factors influencing the presence of evaporable water in the concrete pore structure, general mechanisms of water migration due to exposure to elevated temperature are described below. The term "evaporable water" is used for water, which is lost at 105°C under steady-state temperature conditions (97); see illustration Fig. 36. Upon heat exposure, water present in CSH interlayers passes to gel pores, then to capillary pores and macropores, on its way out through heated surface or to equalise temperature towards the cold surface.

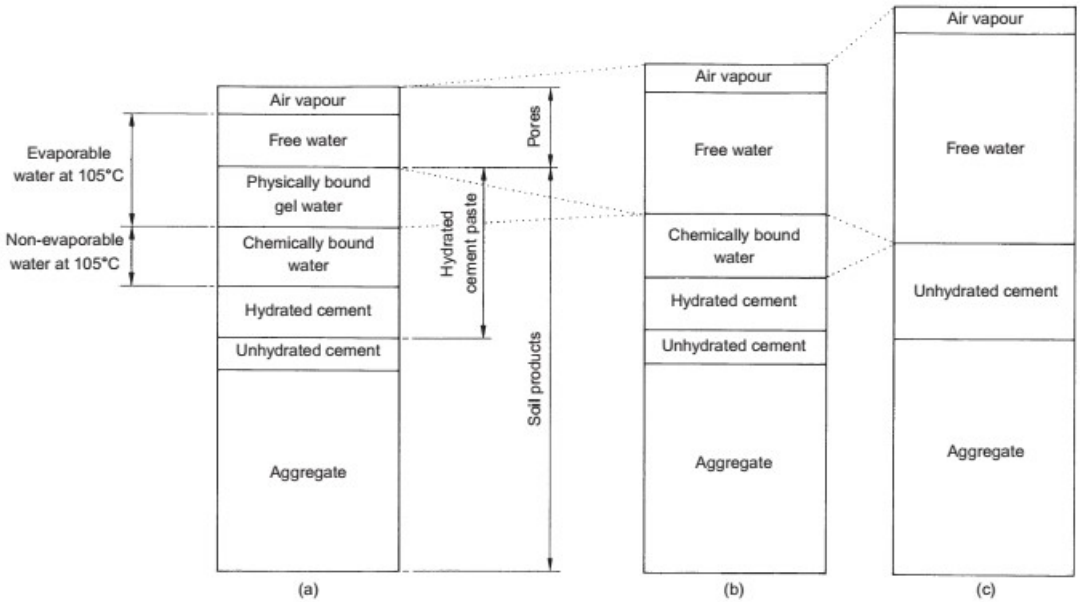

Fig. 36: Types of water in concrete related to the concrete constituents and temperature (a) 20°C; (b) 105°C; (c) 850°C (97).

CSH interlayers

The intrinsic structure of amorphous CSH gel is always filled with water molecules that are not chemically bonded but physically bonded in between the CSH layers by van der Waals' forces. When concrete is heated, physical van der Waals' forces are weakened by expanding water molecules, and results in an extension of the space between individual CSH layers (5). This phenomenon is only recognisable during the heating, and it is not apparent after cooling of concrete. When the water evaporates from CSH interlayer into gel pores, individual CSH layers agglomerate and enlarge the number of gel pores (0,01 - 0,1 μm) and also influence microcapillary pores (0,1 - 1 μm). This phenomenon is explained in detail in chapter 3.1.1 Cement, subchapter "Behaviour of Portland cement exposed to elevated temperatures".

Gel pores

Gel pores, or also called micropores, are pores present in the structure of the CSH gel phase (160). Smaller gel pores with a diameter smaller than 1,5 nm are filled with water; the bigger gel pores with a diameter of about 2,5 nm are empty. This statement is dependent on temperature and humidity in the surrounding environment, especially relative humidity. Water in gel pores is present if exposed to relative humidity between 50 and 100% (114).

The dimensions of gel pores vary based on the literature source, but in general, it could be stated that their diameter is smaller than 30 nm. Gel pores can be divided by size into small gel pores with diameter 2,5 - 10 nm and micropores with diameter from 0,5 to 2,5 nm (160). Another source states meso gel pores with diameter from 1 nm to 30 nm and micro gel pores smaller than 1 nm, and that they are always filled with water evaporable at 105°C (150).

Capillary pores

Capillary pores are evenly dispersed in hydrated cement paste, and due to their diameter from 30 nm up to 1 mm are suitable for water and vapour migration in heated concrete. According to Brameshuber, capillary pores can be divided into micro capillary pores (30 nm to 1 μm), meso capillary pores (1 μm to 30 μm) and macro capillary pores (30 μm to 1 mm) (150). Another source states diameter of capillary pores between 10 and 100 nm and that the pores are empty unless the RH of surrounding ambient is higher than 85%. The filling of pores greater than 100 nm is difficult, unless the RH is very close to 100% (96). The dimension of capillary pores varies in literature probably the most from all of the pores present in concrete.

Macro pores

The presence of macropores in concrete is highly unwanted, but due to the mixing process and concrete work, their content is pervasive due to the imperfection of concrete handling. The diameter of macro pores is from 1 mm and larger (150). Unless the concrete is fully submerged in water, macropores are empty or with water adsorbed on pore walls, depending on concrete actual moisture content.

Pore pressure

The free water is mobilised due to thermal exposure of concrete, and the pores are used as migration paths. Water migration in concrete is monitorable by in-situ neutron tomography, but to monitor pore pressure during the thermal exposure is highly challenging. Though the capillary pressure and build-up of pore-water pressure are commonly processed by theoretical models. They are based on known parameters such as pore-water content, heat flux vector, the mass flux of moisture and thermodynamic properties of water (66, 83, 161). One of the first model was introduced by Bažant and Thonguthai in 1987 based on Darcy´s law. Model describes three different temperature areas for water migration (0-95°C, 95-105°C and 105°C-higher) and development of water/ vapour pressure. From the presented data, Fig. 37, is visible that the highest pore pressure is in the are with an actual temperature around 200°C, demonstrated by calculation, and also obtain from laboratory testing. Dauti et al. associated the water loss between 200 and 250°C to the kinetics of dehydration and the influence of vapour pressure (66).

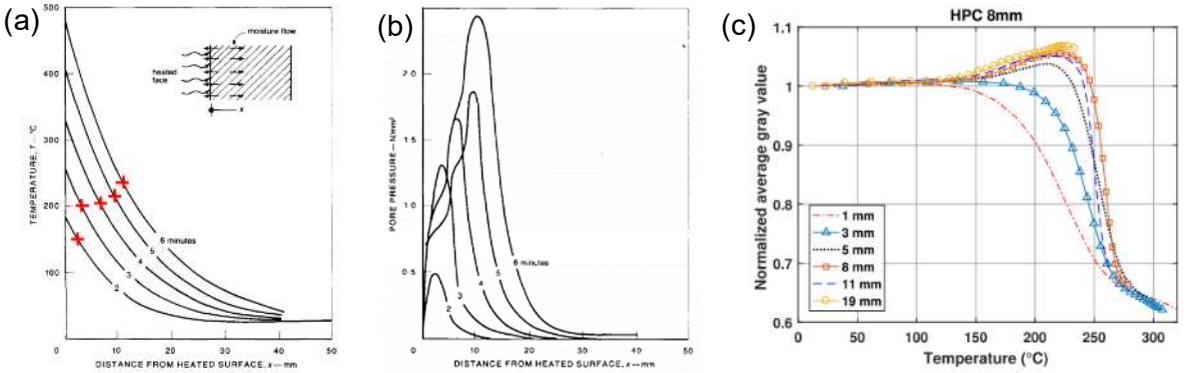

Fig. 37: Relationn between temperature and pore pressure, and distance x from heated surface: (a), (b) Model introduced by Bažant and Thonguthai (83)*; (c) Measured data by in-situ neutron tomography by Dauti et al.* (66)

Another study from Davie et al. (161) introduced the Modified Model, which is based on modification and extension of the Tenchev Model. Tenchev hasn't included in his model adsorbed water (up to 50-60% of free water at the room temperature), and focused explicitly on capillary pressure, which resulted in a conservative approach when utilised in the prediction of mechanical damages and spalling. After the integration of adsorb water in the model, it was concluded that capillary pressure has little or no effect on the transport behaviour in concrete exposed to intensive heating.

3.1.6 Interfacial transition zone

Concrete is composed of smaller and larger particles, and the zone between cement paste and larger particles like aggregates or fibres is termed the interfacial transition zone (ITZ). The thickness of ITZ is about 9-51 μm (146) and is characterized by higher porosity due to locally higher water/cement ratio. The ITZ is present in all types of concrete, and cement paste characteristics define its properties and dimensions. In normal strength concrete, the ITZ zone is commonly weak as the cement matrix has more porous structure due to higher water-cement ratio, and lacking smaller particles to fill up those pores, for example, products from pozzolanic reaction or micro-fillers. The design of concrete with higher strength (over 50 MPa) is based on good packing density and low porosity of the cement matrix, including the ITZ zone (144). Scanning electron microscopy and processing of second electron and backscattered electron images are suitable methods to analyse ITZ in detail (162, 163).

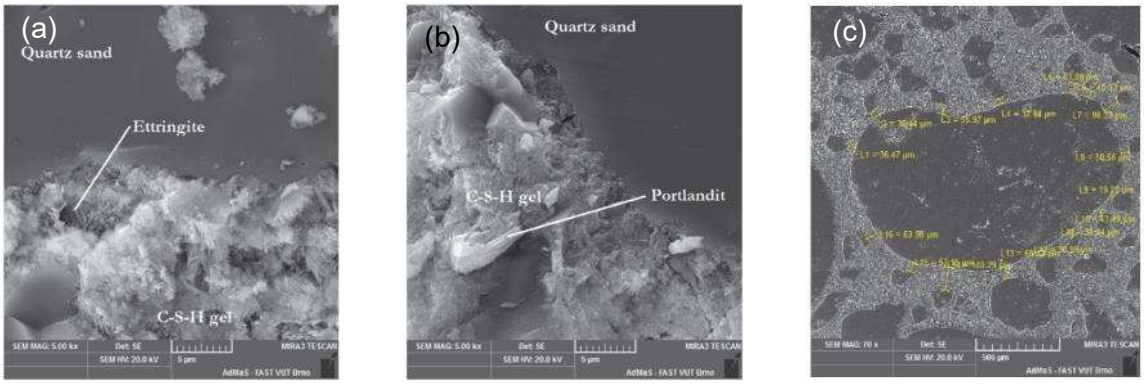

Fig. 38: (a), (b) Microstructure of fracture surface at aggregate–cement paste interface by detection of SE with magnification 5000×; (c) Distances between grains of aggregate measured using SEM with detection of SE, magnification 70× (163)*.*

Porosity in ITZ is commonly interconnected and can serve as a migration system for vapour through the concrete structure when exposed to elevated temperatures. Furthermore, a tensile strength of ITZ is lower and could prevent explosive spalling as vapour pressure has a limited chance to build up. In other words, if the vapour pressure exceeds the tensile strength of ITZ, which is lower than for the bulk cement matrix, microcracking occurs, and vapour pressure is

reduced by expansion to the larger space and reaches another barrier. This mechanism could be slightly different if the structure is under load, and LITS mast be taken into account.

The other reason for locally higher water/cement ratio or, to be more precise, the presence of micro-bleeding (cement particles dissolved in a higher amount of water) is vibration during the casting and placing of concrete (164). The use of various types of vibrators induces the motion of concrete, especially bigger particles, correspondingly coarse aggregates. Bigger particles oscillate and move through the cement matrix to form a denser structure, but an improvement of overall strength by compaction (moving the coarse aggregates closer to each other) is accompanied by the formation of the area filled by cement milk (solution of cement particles and water). This area is commonly under the aggregate particle, and its extent is based on water/cement ratio, and the presence of SCMs. Furthermore, the parameters of vibration, such as frequency, duration and intensity, are influencing factors for the formation of larger ITZ.

After the hardening process, water evaporates or is chemically bonded, and drying pores are formed at a greater scale, than in the other locations of concrete volume. From one point of view, it could be of benefit for fire resistance as the porous system is bigger, due to presence of larger crystals of Portlandite strongly oriented in parallel to the aggregate surface (123, 165), and is characterised by a higher degree of interconnection, which results in better permeability properties. On the other hand, dry ITZ is predominantly composed by Ettringite and Portlandite crystals, which can grow big as space is available (locally higher w/c ratio), see Fig. 39. The CSH gel is present in much lower amount.

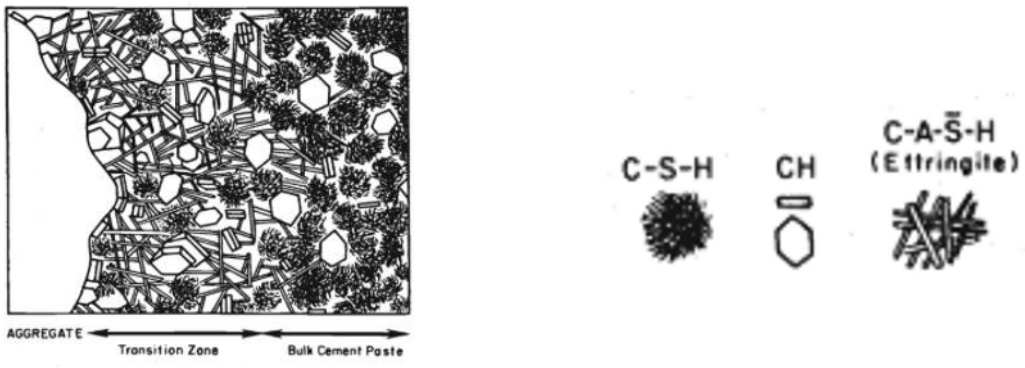

Fig. 39: Representation of the transition zone at a paste/aggregate interface in concrete, showing a more coarsely crystalline and porous microstructure than that of the bulk paste (165).

If the hardened paste in ITZ is exposed to elevated temperatures, changes initiate around 50°C by evaporation of water, followed by decomposition of Ettringite at around 114°C (expansion action) and dihydroxylation of Portlandite at about 400°C. Those phenomena are enough to weaken the concrete inner structure and influence overall strength. The inevitable part of thermal exposure is a cooling phase, where reverse or other reactions are happening. Besides water regain in capillary, gel and interlayer CSH gel pores, the rehydration of CaO is characterised by 44% volume gain (51). All described chemical processes have a significant impact on the integrity of the concrete structure exposed to elevated temperatures.

Concrete is in general material with low modulus of elasticity, and regarding the stresses in concrete structure due to thermal expansion of individual components, ITZ it affected the most. The three main volume changes caused by elevated temperatures are expansion and subsequent shrinkage of the cement matrix, expansion of H_2O in liquid or gas phase in pores, and predominantly an expansion of aggregates. Each mentioned action takes place at different temperatures, volume changes are not synchronized, and highly incompatible, which leads to cracking of concrete inner structure predominantly at the weakest point, interfacial transition zone.

3.2 Fibres

The first attempt to use a dispersed fibre reinforcement in concrete was aimed to improve the tensile strength of concrete. For this purpose, steel fibres were used, and intensive investigation of their influence on concrete properties started by a team around Romualdi and Baston in the United States in 1963 (166). Nowadays, steel fibres are widely used for industrial floors, high-performance concrete and sprayed concrete. The second most common fibres are macro polymer fibres used for drying shrinkage and creep reduction. Polymer fibres have a positive influence on concrete properties and are also widely used, but due to their negative environmental impact, the new solutions and alternative types of fibres are investigated. Alternative types of fibres based on the material type are glass, carbon, basalt, natural wood or cellulose. According to size of the single fibres they can be divided into macro and micro fibres (based on their diameter), and described by cross-section (diameter), length or aspect ratio.

The type, material, shape, dimensions, dose, and other parameters of fibres are decided based on their expected role in concrete. For structural purposes, the general rule is the length of fibres, which are supposed to be 3,5 of the maximum particle size of used aggregates (167). The regulations for fibres in concrete with the purpose of increasing fire resistance are slightly different, and also the principle of their action varies. One of the theories, and yet the most recognised one, is the creation of micro-network of fibres which will eventually evaporate, and the formed porous system will serve for release and migration of water vapour. The other principle is the strengthening of the cement paste to prevent excessive cracking of cement paste and to increase its tensile strength.

In this chapter, the most relevant fibres tested for fire resistance improvement will be described, and several research results presented. At the moment, polypropylene microfibres (PPF) are considered as best practice of passive fire protection for concrete (5, 51, 168, 169), and therefore a larger part of this chapter will be dedicated to them.

3.2.1 Macro fibres

As was mentioned earlier, macro fibres serve mostly for structural purposes or as a protection of early age shrinkage and creep. Nevertheless, an attempt to test their influence on fire resistance and fire spalling of concrete was carried out. The main idea of macrofibres contribution to fire resistance is the increase of tensile strength of cement paste and prevention of formation of larger cracks. The surface of the fibre is commonly finished with a coating agent that can, in a smaller or greater degree, react with the surrounding cement paste (low surface tension) and form a strong bond. Identically to the case of aggregates, the interfacial transition zone is formed between fibre and cement paste and is characterised by higher porosity through which vapour can eventually migrate. The most common materials for macro-fibres are steel, polymer and composite polymer-based glass or basalt fibres, see Fig. 40.

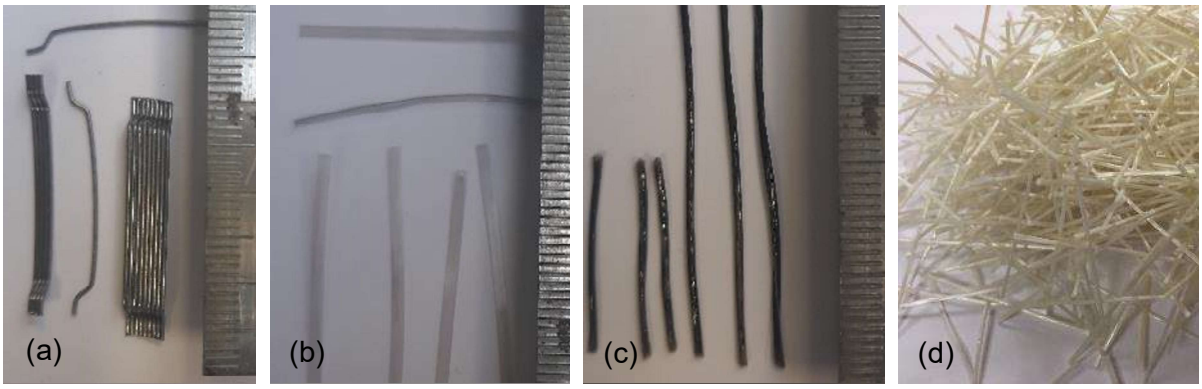

Fig. 40: Macro-fibres (a) steel, (b) polymer, (c) composite basalt, (d) composite glass (170).

Steel fibres

Steel fibres have demonstrated only minor influence on fire resistance of concrete, but in combination with PPF, fire spalling was reduced or entirely prevent (168, 169, 171, 172). A study presented by Yermak et al. states results from testing of smaller non-loaded samples heated in an electrical furnace. The higher degree of spalling and crack formation was observed in the case of samples containing only steel fibres or reference sample with no fibres. The best performance was shown by the sample with 0,75 kg of PPF and 60 kg of steel fibres, where no spalling and sufficient residual strength was measured (172).

Research presented by Kodur et al. and Kahanji et al. is focused on larger scale testing of beams made of ultra-high performance concrete with steel fibres (length 13 mm and diameter 0,2 mm). Results from beams with 1,5 volume% of steel fibres testing showed spalling of beams in the compression zone, which contrasts with normal strength concrete and high-strength concrete. The addition of 1,6 kg of PPF significantly reduced fire-induced spalling, see Fig. 41 (169, 171).

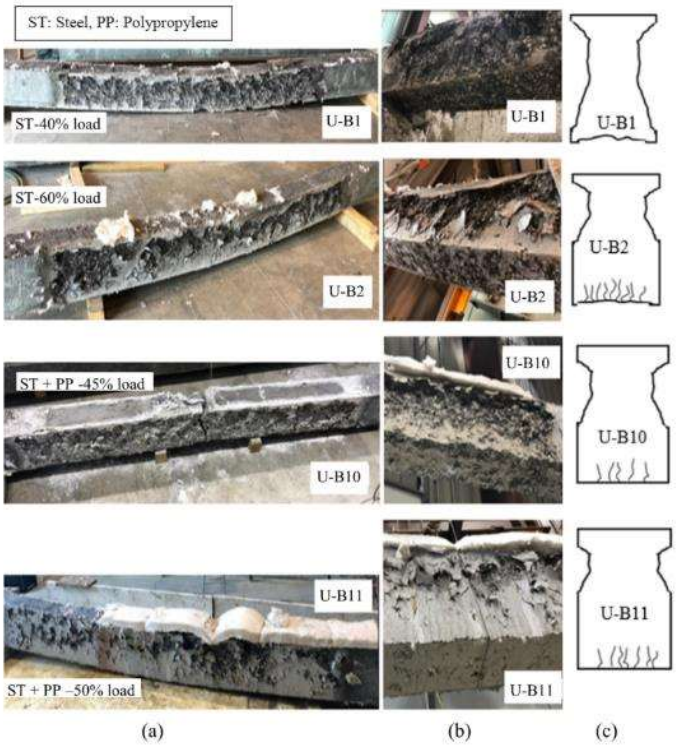

Fig. 41: Fire test results: (a) state of UHPFRC beams after fire tests, (b) bottom surface in tested beams, (c) schematic illustration of spalling and cracking pattern in tested beams (169).

The study focused on beams made of ultra-high performance concrete with steel fibres and PPF, performed by Kahanji et al., and presents two different doses of fibres (2 and 4 volume %) and three different beam loading levels (20, 40 and 60%). Spalling of UHPC under higher load was reduced most probably by the presence of already formed microcracks, but a complete collapse of the tested beam occurred earlier. More spalling was observed in the case of load at 40%, than beams loaded by 20%. Spalling was not observed when PPF were added in dosee of 4 kg/m^3 (168).

Composite fibres

Testing of composite fibres with a focus on fire resistance and prevention of fire spalling is rare, and from the reviewed literature, only composite basalt fibres were subjected to investigation.

The high-performance concrete reinforced by basalt macro and micro fibres were exposed from one side to elevated temperature and extension of fire spalling investigated. Results showed that basalt fibres cannot prevent HPC from fire spalling, but do not increase fire spalling and do increase rebar protection (173).

3.2.2 Micro-fibres

Several types of micro fibres were tested either in concrete (173–175) or mortar (176) to evaluate their contribution to fire resistance of cementitious materials. As mentioned earlier, the most commonly used micro fibres are polypropylene fibres (PPF) as they have a low melting point in comparison to the other material type fibres. PPF could be melted at a temperature of 130°C or slightly higher 165°C and provide interconnected channels for water and vapour migration. The other principle of micro fibres and their contribution to the fire resistance of cementitious materials is the prohibition of microcracks formation. The higher the tensile strength of cement paste is, the higher the pressure of water vapour it can withstand and prevent crack formation. On the contrary, the build-up pressure can reach higher values and cause explosive spalling. Therefore, this principle might be suitable only in certain cases and in places with a lower probability of fire event occurrence.

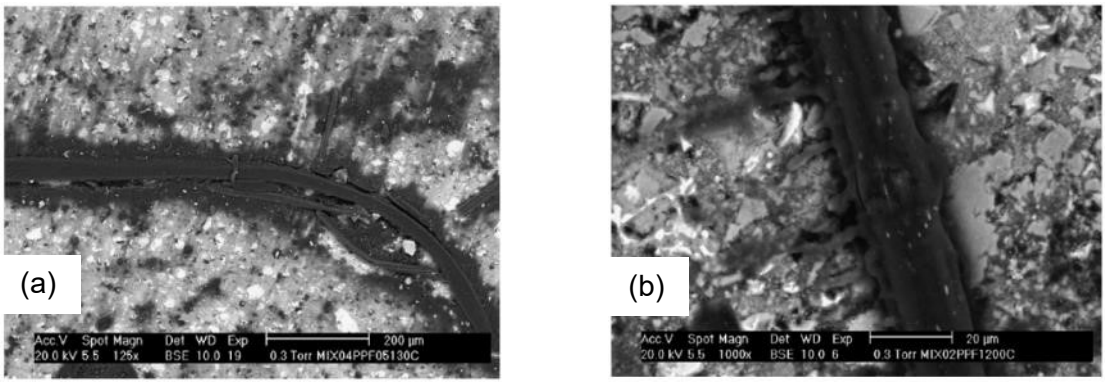

Fig. 42: Microscopic photo of (a) PPF in HPC heated at 130°C; (b) PPF in SCC heated at 200°C (177).

Nevertheless, one of principles is the same for all of them. Every type of fibre is coated with a dispersant agent to allow good dispersion during the mixing and casting. The coating of the fibre decreases its surface tension and improves hydrophilic properties. A thin water molecule layer is formed on the fibre surface, which is later eventually consumed by hydration of non-hydrated cement particles, or remains as free water in hardened concrete. The space around the micro fibre can serve as a migration channel for vapour during a fire event; this phenomenon was explained in detail by Khoury et al. (174).

Polypropylene fibres

The problem with explosive spalling and extensive damages of concrete due to fire exposure accompanied the use of plasticizers and superplasticizers. The possibility to develop concretes with reduced porosity such as high strength concrete, self-compacting concrete, high performance and ultra-high performance concrete brought a necessity for a new solution for fire resistance enhancement.

In the early 1990s, tests have shown an increase in fire resistance of concrete due to the addition of PPF with minor impact on compressive strength or other properties. In a short period of time, PPF became the normal practice for tunnel lining and other structures with a higher probability of fire events. Many countries and international associations, such as Sweden, Britain, Fib or RILEM, implemented the use of PPF as passive fire protection, and recommended dosage in the range from 1 to 3 kg/m^3 (51, 178). Although the benefits of PPF were recognized and proven by many research teams across the world, the detail of the principle was not known until 2008 when Khoury and Willoughby described the entire process (97, 174). The detailed description of PPF performance in concrete during exposure to

elevated temperatures provides important input data for thermo-hydro-mechanical numerical modelling. In the last two decades, numerical modelling has become more and more popular and used for the fire design of more complex structures.

There are two main principles which describe the contribution of PPF to fire resistance of concrete.

The first principle is employed from the beginning of heating up to the point when the fibres start to melt at 150°C or PPF with the reduced melting temperature at 130°C. Action is based on poor adhesion of PPF to cement paste and the formation of less dense ITZ. The space for water and vapour migration through concrete microstructure is extended by the low density of ITZ around the PPF and introduced as a pressure induced tangential space (PITS), see Fig. 43 (97, 174).

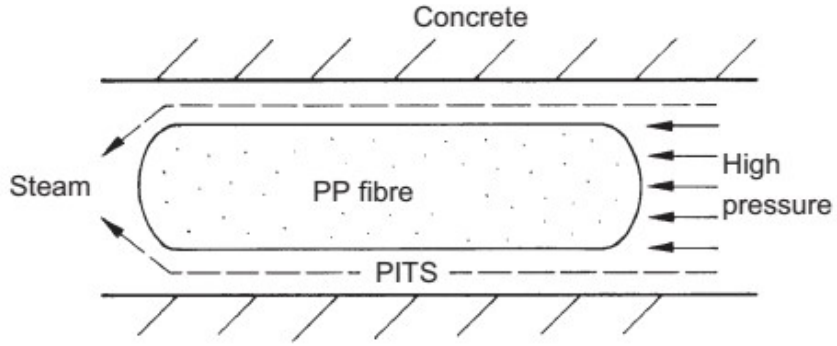

Fig. 43: Oversimplified representation of steam pressure release around a poorly wetted fibre owing to vapour pressure induced rupture of interfacial contact (PITS = pressure-induced tangential space)(97, 174).

The second principle is melting and consequent volatilization of PPF. The solid-state PPF is composed of 55% of crystalline phase and 45% of the amorphous phase with an average density of 0,91 g/cm^3. The molecular structure of PPF at room temperature (20°C) is an isotactic polymer with total length approx. 739 nm composed by individual polymer molecules of length 14 nm, schema presented below (Fig. 44).

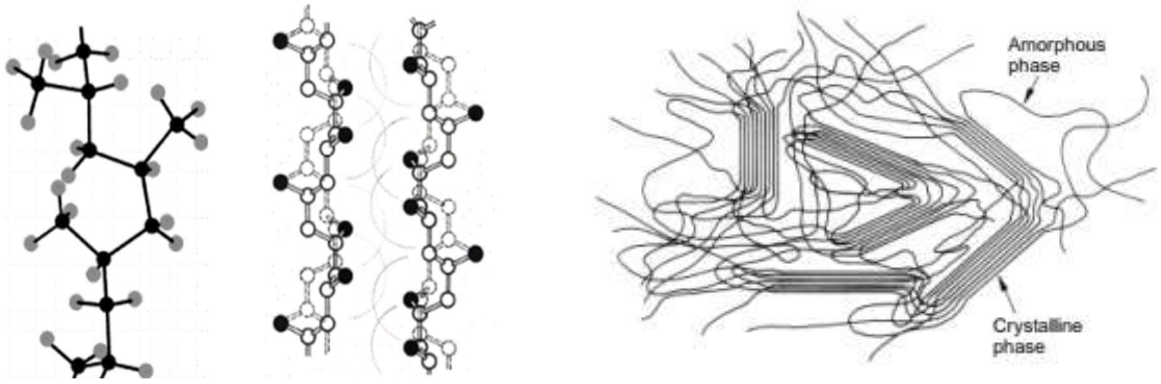

Fig. 44: Representation of (a) single turn of i-PP helix; (b) packing of i-PP helices showing van der Waals radius (179)*; (c) fringed micelle representation of a semi-crystalline polymer* (180).

(a) (b) (c)

Melting of standard PPF starts at 150°C, but lately, fibres with a lower melting point (130°C) have been introduced to the market. In this work, the principle will be explained for standard PPF with the initiation of melting at 150°C. Due to increasing exposure temperature, PPF structure becomes fully amorphous, and the dimension of the polymer molecule would be around 14 nm long. The maximum melting rate takes place at 165°C, and the last crystals decompose around 176°C, when the melting of PPF is completed. The melted mass remains in the created channels or penetrates in capillary pores (diameter approx. 1 μm) as the

molecules of melted PPF are still too large to fill gel pores with diameter from 1,5 to 2,5 nm (117, 181). Furthermore, melted mass is more likely to flow towards the heated zone, where evaporation initiates at temperature 350°C. Vapour phase of PPF is between 350°C and 475°C, and the molecule size decreases to 0,68-1,08 nm, which is small enough to penetrate into the gel pores (97, 174).

The empty channels formed after PPF melting and volatilization are interconnected, and the scale of interconnection depends on PPF dosage and size. As smaller diameter and higher dose gets, the greater the total length of formed channels is. The detailed calculation of the channel length based on various parameters (dose, length, diameter, number of fibres) is provided by Khoury (97). Some selected data are presented in Fig. 45, and shows the total number of fibres and length for dose of 1 and 2 kg/m^3 of PPF.

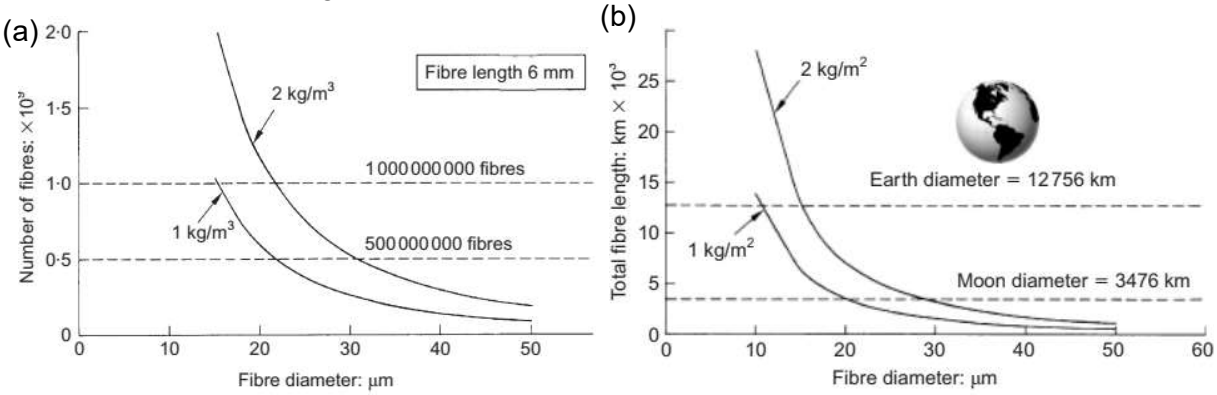

Fig. 45: (a) Total number of fibres as a function of fibre diameter for 1 and 2 kg/m^3 fibre content of concrete and 6 mm fibre length; (b) Cumulative fibre length as a function of fibre diameter for 1 and 2 kg/m^3 fibre content of concrete (97).

To conclude on PPF and its contribution to fire resistance of concrete and prevention of spalling, many studies were conducted concerning different types of concrete with higher or lower porosity. Small and large scale tests were carried out, and variable measuring methods employed (40, 48, 156, 167, 178, 180–183). One of those is a study from Huismann et al. who used acoustic emission and ultrasound analysis and concluded that empty channels after melted PPF behaves as homogenously dispersed cracks and lowers thermal strain in concrete structure (182).

Other fibres

Other material types of fibres investigated under thermal load are glass, basalt, carbon and polyvinyl alcohol (PVA). There hev been a few studies on the various length of glass micro fibres with a length of 6, 12 and 25,4 mm added in various doses, but their contribution was significant only up to about 500°C. A higher dose in the case of 6 mm long fibres reduced strength in general, but longer fibres (25,4 mm) in a dose of 0,5 and 1,0% of cement weight performed better at room temperature and up to 500°C (175, 184). Fire spalling was also not influenced by the addition of 12,7 mm long basalt fibres (173).

An extensive study was performed by Cavdar, who tested four different material types of fibres in four different doses exposed to 100, 450 and 650°C. Most significant results from this study were that the lowest decrease in compressive strength was recorded in the case of carbon fibres in doses from 0,5 to 1,5% by volume, the optimal dose of polypropylene and glass fibre was 0,5% by volume, and optimal PVA fibre dose was between 0,5 and 1,5% by volume (176). None of the fibres mentioned in this section were introduced to the market as fibres increasing fire resistance of concrete.

3.3 Aggregates

Aggregates constitute about 70% of concrete, and their properties could influence the behaviour of concrete exposed to elevated temperatures on a large scale, especially by their thermal instability coupled with volume changes. There are many influencing parameters when the aggregates are evaluated in connection to cement paste, therefore in this chapter, only the behaviour of aggregates themselves and the influence of their chemical and mineralogical nature will be discussed. Properties such as water absorption and release, mineralogical and chemical changes result in crack formation and disintegration of individual grains. Listed properties and behaviour under thermal load are characteristic for both fine and coarse aggregates, but more significant for coarse aggregates. Fine aggregates are part of the cement matrix, and changes of cement paste overshadow their reaction to elevated temperatures.

The most widely used aggregates types are siliceous and calcareous, and therefore, data concerning these two types are presented in Eurocode 2 (6). Aggregates could be classified into four groups according to their stability in elevated temperatures.

Crushed fire bricks and fused aluminium oxide (corundum) belong in the most resistant class, followed by less resistant aggregates types such as expanded slag, shale, slate and clay. Finally there are the more conventional rock types like grained igneous rock basalt, calcareous and siliceous aggregates, or their combination (silico-calcareous, sediments) (123, 185). Some types of rock are more stable in a fire, but the quarries with suitable rock type might not be located close to the building site of the structure with increased fire risk, and compromises are therefore needed. Nevertheless, igneous rock such as basalt is established as one of the most suitable and available options for the preparation of concrete which is stable in elevated temperatures. An exception would be basalt with extrusive nature, as it can contain an amorphous glass phase (known as a lava pillow), which melts at lower temperatures. Last, but not least, are artificial and natural lightweight aggregates, that perform well in heated concrete unless they contain an extensive amount of moisture in their inner structure.

3.3.1 Siliceous aggregates

Siliceous aggregates are recognised as the least resistant to an elevated temperature due to the transformation of the quartz from the α to β polymorph at 573°C, which is accompanied by volume increase by 0,85%.

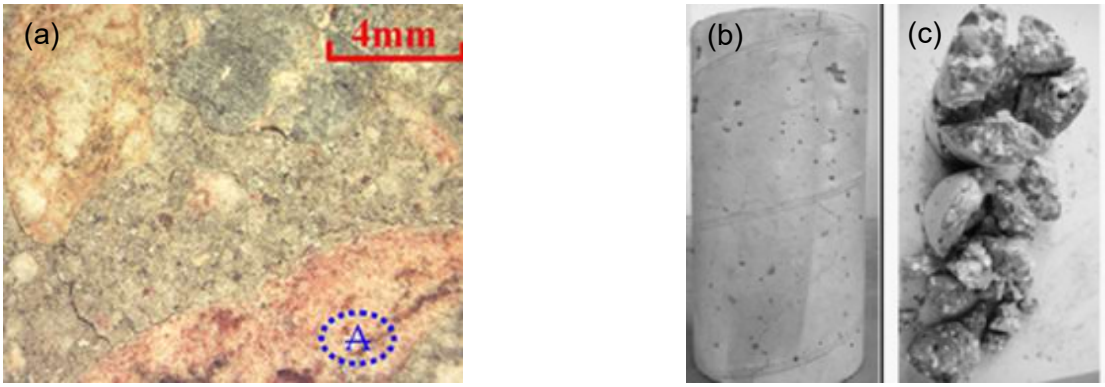

Fig. 46: Siliceous (S) aggregates (a) Cracking at the paste–aggregate interface for a concrete (w/c = 0,6) heated at 750°C, (A aggregate); (b) No spalling of 6/7 HPC-SC samples; (c) Spalling of 1/7 HPC-SC samples (186, 187).

3.3.2 Siliceous-calcareous aggregates

The representative for siliceous-calcareous aggregates is flint, which is composed partly by quarts but with different microstructure than quartzite, and that leads to earlier crack formation and spalling around 450°C while quartzite is stable up to 600°C (187). The damages and properties reduction of concrete with flint aggregates were recorded between 300°C and 700°C. The conclusion drawn by Xing was that it is important to take into account both mineralogical and chemical nature when evaluating the fire stability of aggregates (186–188).

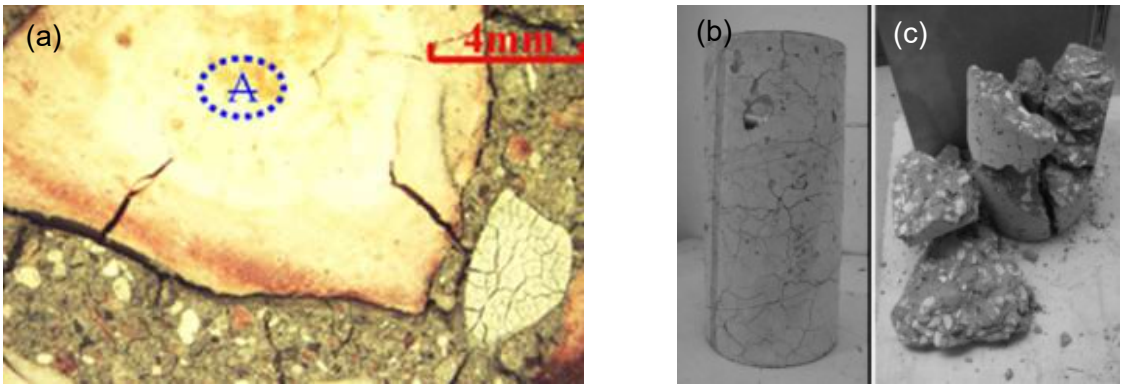

Fig. 47: Siliceous-calcareous (SC) aggregates (a) Cracking at the paste–aggregate interface for a concrete (w/c = 0,6) heated at 750°C, (A aggregate); (b) No spalling of 7/9 HPC-SC samples; (c) Spalling of 2/9 HPC-SC samples (186, 187).

3.3.3 Calcareous aggregates

Calcareous aggregates such as limestone contain in their chemical structure carbonates, which are released from structure between 660°C and 979°C. Coefficient of thermal expansion of calcite range from 4,5 to 5 · 10^{-6}/°C and only the surface is impacted by heat. Problems arise after the cooling phase when the free CaO, formed during the decomposition, comes into contact with atmospheric CO_2 or humidity. Equations 17 and 18 explain the volume expansion upon rehydration or carbonation, which is also demonstrated in Fig. 48 (b) 3 days after heating of calcareous aggregates to 750°C (186, 187, 189).

$$CaO\ (1\ cm^3) + H_2O \rightarrow Ca(OH)_2\ (1{,}93\ cm^3)\ (17)$$

$$CaO\ (1\ cm^3) + CO_2 \rightarrow CaCO_3\ (2{,}14\ cm^3)\ (18)$$

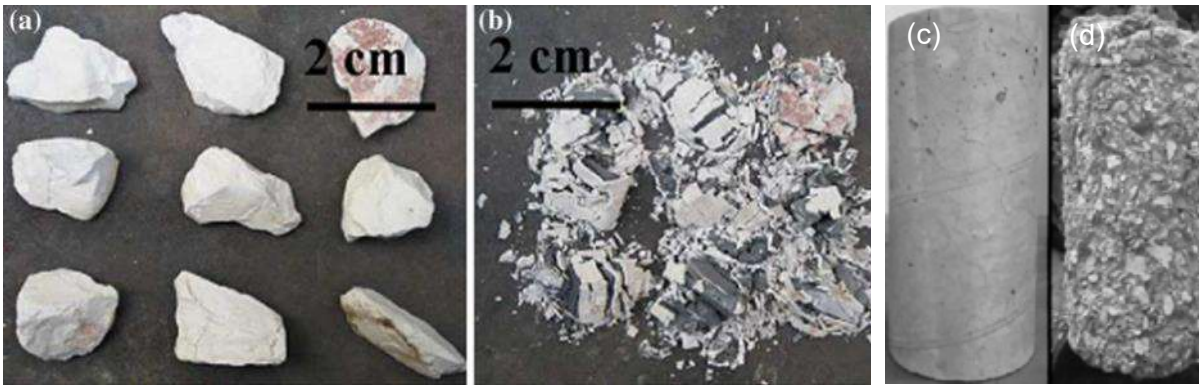

Fig. 48: Comparison of calcareous aggregates and HPC-C before and after transformation from CaO to portlandite after heating at 750°C, (a)(c) Immediately after heating–cooling cycle at 750°C; (b)(d) 3 days after heating–cooling cycle at 750°C (186, 187).

The following graphs in Fig. 49 and Fig. 50 present data comparing the concrete compressive strength degradation of various concrete and aggregates types and thermal elongation of concrete.

As calcareous and siliceous aggregates are most common, Eurocode 2 gives coefficient only for those two, unless the data are given only for siliceous aggregates which is the most conservative approach due to their poor performance when exposed to elevated temperatures (6).

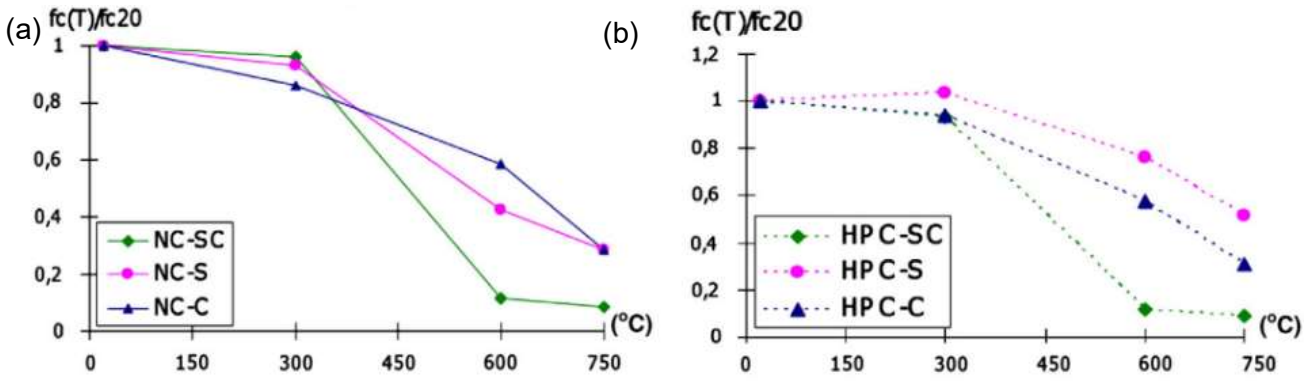

Fig. 49: Compressive strength degradation of (a) normal strength concrete (NS) and (b) high performance concrete (HPC) with various aggregates (186).

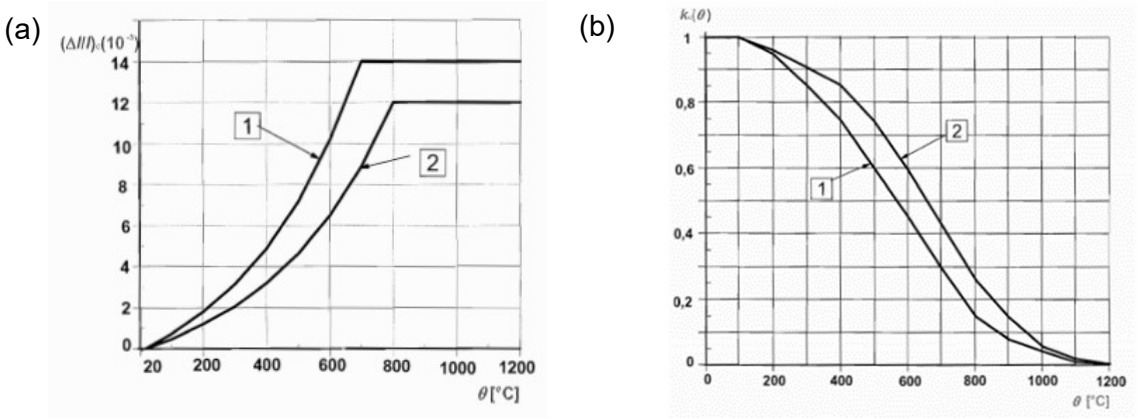

Fig. 50: Thermal behaviour concrete with siliceous [1] and calcareous [2] aggregates (a)Total thermal elongation of concrete; (b) Coefficient k_c (θ) allowing for decrease of characteristic strength (f_{ck}) of concrete (6).

3.3.4 Other aggregate types

Basalt

Basalt is an intrusive or extrusive igneous rock, and in nature, could be found in the form of compact, dense material with low porosity, or in the form of porous but strong material. In most locations the first mentioned type of basalt can be found, intrusive igneous rock type, which has beneficial properties during exposure to elevated temperatures, such as low coefficient of thermal expansion ranging from 5,5 to 8· 10^{-6}/°C and thermal stability up to approx. 900°C (51, 115, 123). Basalt aggregates are adventurously used in research to avoid the influence of aggregates on fire resistance of concrete, and allow decoupling of individual processes which are taking place at different temperatures and phases of concrete.

Light-weight aggregates (LWA)

Natural and artificial clay expanded lightweight aggregates are highly suitable for the production of fire resistance concrete (fireplace inserts). LWA have a low coefficient of thermal expansion, and are stable up to approx. 1000°C, but problems can occur if the concrete with LWA has high moisture content. The mixing process of concrete with aggregates with high water absorption includes pre-wetting process of LWA, or preparation of concrete with low consistency class for the precast vibro-compaction process. If the LWA are pre-wet before mixing, water remains in the LWA structure, and in case of fire exposure, violent explosive spalling occurs (190).

Sandstone

As sandstone is sedimentary rock, it is composed predominantly of quartz, feldspar, muscovite and other rock fragments in lower percentage (191). In a study from Kompaníková et al. it was identified by testing two different sandstones that their thermal stability is up to

400°C, and is connected to the mineralogy composition and porosity of sandstone. The stability to thermal exposure is increasing with lower porosity and higher content of minerals stable in elevated temperatures (192).

3.3.5 Significant properties of aggregates in elevated temperatures

The most significant properties of aggregates connected to thermal behaviour are the coefficient of thermal expansion, thermal conductivity, diffusivity and specific heat. Thermal conductivity, diffusivity and specific heat are more connected to heat transfer and strongly depend on moisture conditions of aggregates, concrete or both. Due to thermal exposure, the water content (free or chemically bonded) is decreasing, and more empty pores are present, filled by air, which has lower heat conductivity than water. Thermal conductivity of concrete highly depends on aggregates mineralogy and moisture content, but in general, thermal conductivity of saturated concrete ranges between 1,4 and 3,4 W/m°C (100, 123). Low thermal conductivity could slow down the heating of concrete elements, which is beneficial in the case of reinforced concrete. On the other hand, a faster equalising of the temperature in bulk concrete can prevent formation of moisture clog, resulting in explosive spalling.

The coefficient of thermal expansion is defined as a change in length of unite per degree of temperature. The following values are characteristic for concrete and aggregates in ambient temperature, but when exposed to elevated temperatures, those values are changing. The value for concrete ranges between $5{,}8 \cdot 10^{-6}$/°C and $14 \cdot 10^{-6}$/°C and in the case of aggregate it varies between $5{,}0 \cdot 10^{-6}$/°C and $12 \cdot 10^{-6}$/°C, but in some exceptional cases can reach values of $25{,}8 \cdot 10^{-6}$/°C (100, 123). Namely, quartz is significant by its higher thermal expansion, while calcite and potassium feldspar have anisotropic behaviour (calcite can have a linear thermal coefficient of expansion as great as $25{,}8 \cdot 10^{-6}$/°C parallel to its C-axis and as low as $-4.7 \cdot 10^{-6}$/°C perpendicular to this direction). The more significant the difference of coefficient of thermal expansion between cement paste and aggregates, the higher is the probability of explosive spalling and crack formation.

The research dedicated to fire resistance, stability, and degradation mechanisms of aggregates exposed to elevated temperatures is extensive, and therefore, it is challenging to give a brief overview. Tab. 5, Fig. 51 and Fig. 52 give a summary of properties and behaviour of most common minerals and rock types exposed to elevated temperatures.

Tab. 5: Average linear coefficient of thermal expansion of some common rocks and minerals in ambient temperature (193).

Mineral	Coefficient of thermal expansion [10^{-6}/°C]	Rock	Coefficient of thermal expansion [10^{-6}/°C]
Quartz	11,5 - 12,0	Quartzite, silica shale, chert	11,0 - 12,5
Orthoclase, microcline	6,5 - 7,5	Sandstones	10,5 - 12,0
Pyroxenes, amphiboles	6,5 - 7,5	Quartz sands and pebbles	10,0 - 12,5
Olivine	6,0 - 9,0	Argillaceous shales	9,5 - 11,0
Albite	5,0 - 6,0	Dolomite, magnesite	7,0 - 10,0
Calcite	4,5 - 5,0	Granites and gneisses	6,5 - 8,5
Oligoclase, andesine	3,0 - 4,0	Syenite, andesite, diorite, phonolite, gabbro, diabase, basalt	5,5 - 8,0
Labradorite , Bytownite	3,0 - 4,0	Marbles	4,0 - 7,0
Anorthite	2,5 - 3,0	Dense, crystalline, porous limestones	3,5 - 6,0

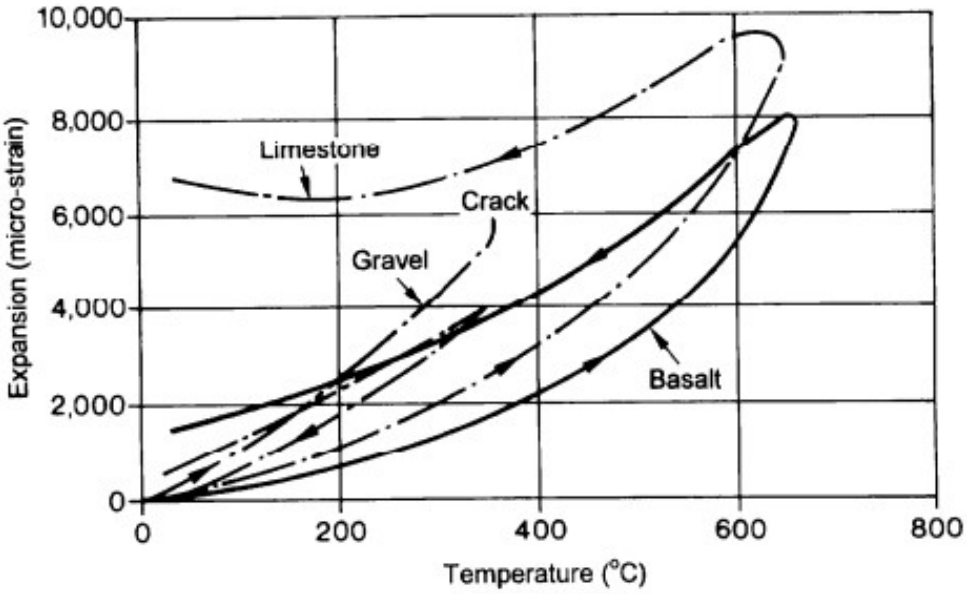

Fig. 51: Thermal strain during the first heat cycle (2°C/min) of three rectangular aggregates (20-30 mm) showing a break-up of Thames river gravel at 350°C, and the lower thermal stability of the limestone than the basalt (56).

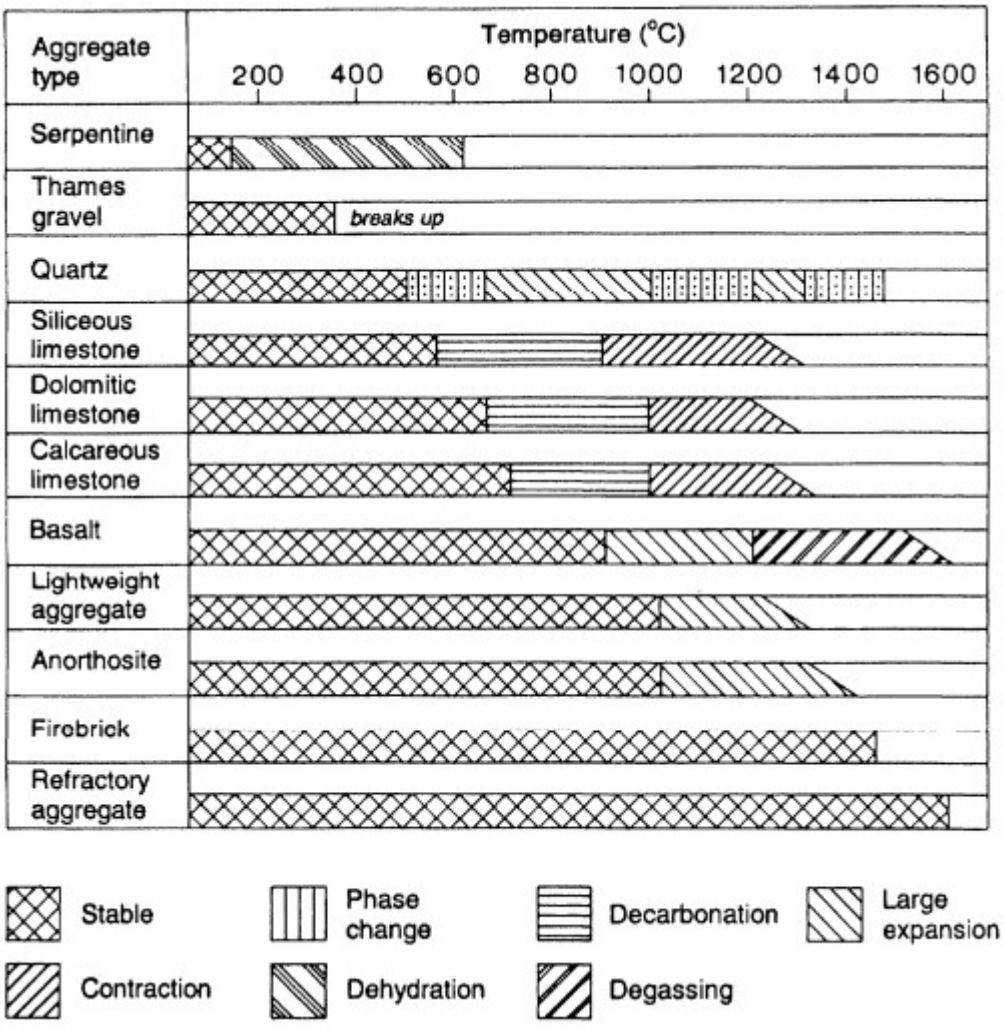

Fig. 52: Non-exhaustive examples of the large range of thermal stabilities and processes, that take place in aggregates during heating (194).

3.4 Conclusion on concrete behaviour under thermal exposure

In this chapter a comprehensive overview of individual components and phases in concrete is given, and it is evident that there are many influencing factors which have to be taken into account during the evaluation and design of concrete exposed to elevated temperatures. Behaviour of individual components might not be severe during the fire, but their mismatch behaviour is causing degradation and complete disruption of concrete. To conclude, in this chapter several significant influencing factors will be listed and marked as a benefit (+) or disadvantage (-) for concrete behaviour in elevated temperatures.

- Cement paste expands up to 250°C, and shrinks when exposed to higher temperatures.
- Most aggregates are characterised by expansion, which introduce thermal stresses in ITZ.
- Most of the aggregates are stable up to 500°C, and then the scale of deterioration is dependent on their chemical and mineral composition.
- ITZ is the weakest area in the concrete, and pronounced as the most common reason for strength properties degradation and crack location (195).
- ITZ is the most exposed area and its lower tensile strength due to more porous structure composed predominantly by larger crystals of Ettringite and calcium hydroxide.

+ Resulting from higher porosity and the presence of capillary pores in ITZ, it possibly retains less free or adsorbed water and can serve as a transportation channel for migrating water or vapor.

- Concrete with the greater maximum particle size aggregates is more susceptible to the formation of larger cracks. This finding could be connected to the coefficient of thermal expansion of aggregates (66, 196).
- Explosive spalling is more likely to occur in concrete types with reduced porosity, particularly the absence of capillary pores, such as HSC, HPC, UHPC and SCC.
- Reduced porosity and absence of capillary pores create an opportunity for high water vapour pressure build-up and more significant crack formation or spalling of concrete pieces.
- Densifying of microstructure by SCM lead to “discontinuity” of capillary pores, and additional formation of CSH gel in gel pores, which are predominantly fully saturated and release of water from gel pores and CSH interlayers is slower and can result in higher pressure development.

+ The addition of pozzolanic active SCM reduces calcium hydroxide content as it is consumed during the reaction. Such a reduction of calcium hydroxide results in degradation of cement paste at around 400°C when dehydroxylation of calcium hydroxide takes place.

+ The addition of PPF increases the amount of capillary pores (artificial capillary pores) or behaves like a network of evenly distributed cracks (182). First, the PITS serves for vapour migration, and after the melting of PPF at 130 or 150°C, larger space for moisture migration is provided (97, 174).

- Actual moisture content in concrete structure and relative humidity of surrounding ambient (tunnels approx. 75% RH) have the most influence on concrete behaviour, as the water evaporates first before all mineralogical and chemical reactions. If the relative humidity of ambient is below 50%, the free water is present predominantly in CSH interlayers, gel pores and adsorbed on walls of capillary pores. Water molecules can migrate towards the hot and cold regions without the formation of moisture clog and reducing risk of fire spalling.

+/- The water/cement or water/binder ratio has a significant influence on porous structure and properties in general. If the w/c ratio is high, more capillary pores are

formed, and concrete has a better ability to release the water, and prevent the development of high vapour pressure. Unfortunately, the strength and durability of concrete are highly reduced by high w/c ratio. If the w/c ratio is low, the denser structure is formed, and mobility of water or vapour restricted, which leads to crack formation and spalling.

- The rough surface of aggregates forms stronger ITZ, which can resist higher vapour pressure. The probability of explosive spalling could be reduced or delayed (187).
- The thermal conductivity of concrete is closely related to aggregate type and porosity. If the thermal conductivity is high, stresses are evenly distributed over the whole bulk of concrete element, and might contribute to better fire resistance. On the contrary, the low value of thermal conductivity can create areas with different actual properties and give rise to uneven thermal strengths in the concrete mass. Different rules apply if the concrete element is reinforced, then slow thermal conductivity is favourable.

Behaviour of concrete is also highly depended on the properties of elevated temperature development such as (i) length of exposure, speed of temperature gain, maximum temperature, speed of cooling, (ii) one side heating (tunnel lining), one point heating (centre of fire), full exposure (columns), (iii) rate, level and direction of loading, no loading. As can be seen, there are too many factors involved, and therefore, fire resistance evaluation, prediction and design are highly complex and sometimes unpredictable.

4 CONCRETE SPALLING IN ELEVATED TEMPERATURES

Spalling of concrete was for the first time observed and recorded in 1854 (197), and probably the first description of the spalling behaviour of concrete exposed to elevated temperatures was published by Barret (198). During those 167 years, which have passed since the first description of spalling phenomena, several theories that explain the cause and mechanism of concrete spalling were introduced. Explosive spalling was not frequently observed in the past, thanks to the higher porosity of concrete. With the introduction and use of plasticizers, the water/cement ratio was reduced and led to a reduction of the porous system. Another aspect that contributes to the reduction and modification of porous structure is the usage of supplementary cementitious materials with a high surface area. Both mentioned innovations in concrete technology contributed to the development of new types of concretes, such as self-compacting concrete (SCC), high strength concrete (HSC), high-performance concrete (HPC) and ultra-high performance concrete (UHPC). Mix design of those types of concrete is based on packing density theories, and low water content, where plasticizers and superplasticizers ensure the workability of fresh concrete.

Transformation and migration of water or vapour through the inner structure of concrete towards the heated and also cold surface of the concrete elements are the main reason of explosive spalling. The transformation of water into vapour is accompanied by pressure development, which was proven by Hinrichsmeyer et al. (199), who described in detail the pressure of water at 300°C is 8 MPa, and 17 MPa in temperature 350°C. The average strength of the cement matrix in 1990 was 5 MPa nowadays is commonly higher (152). When the vapour pressure reaches the level of flexure strength of concrete, microcracks are formed, and pressure released. If the build-up pressure is high, explosive spalling occurs. A similar theory is defined as the Boiling Liquid Expanding Vapour Explosion (BLEVE) (200), and based on the hypothesis that if the water in the pores gets to the boiling point, cement paste is exposed to high pressure which is realized by breaking of the closed pores, and a local explosion inside a structure takes place. This local explosion could be another trigger for overall fire spalling.

Another theory referring to water/vapour migration in concrete is termed “moisture clog” theory (201). Water migration in a concrete structure is caused by temperature and pressure differences when the concrete structure is exposed to elevated temperatures from one side. Water evaporates on the heated side and also migrates towards the colder non-heated surface

to even out the temperature and pressure. Migration of water toward the colder surface leads to full saturation and condensation, which results in the formation of “moisture clog”, see Fig. 53, and Fig. 54. When this moisture clog is formed, further moisture transport inwards to the colder region is slowed down or completely stops, which leads to a rapid build-up of pore pressure. When this pressure exceeds the tensile strength of concrete, spalling and explosive spalling occurs (94, 200).

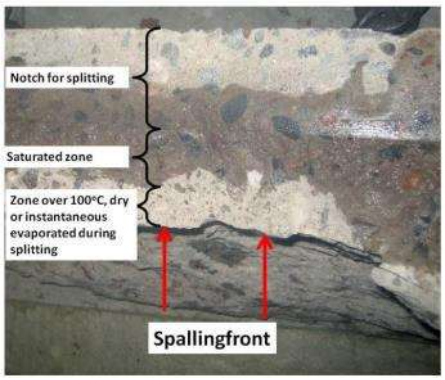

Fig. 53: The moisture zone in front of the spalling front. Visualized by splitting a 600 × 500 × 200 mm³ concrete slab during a fire test (198, 200).

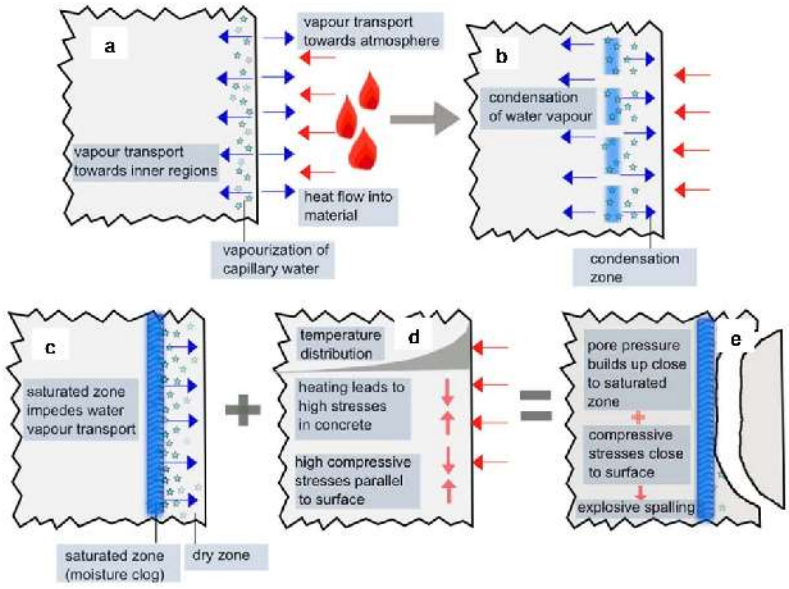

Fig. 54: Mechanism of explosive spalling – moisture clog theory (94).

Cement paste of the concrete exposed to fire is also weakened by evaporation of water from CSH gels and loss of chemically bonded water, which affects overall strength. When the vapour migrates through the porous system, forces from friction are created. The theory introduced by Waubke N. V. and Schneider U. describes explosive spalling due to friction forces from vapour flow. This theory is based on theoretical calculations assuming that all the water evaporates entirely during the exposure to high temperatures throughout the heated side (202). This theory is not verified by practice testing as the phenomenon is very hard or even impossible to monitor during real-time testing and decouple it from other actions that take place.

In general, three main elements, namely moisture, stress and cracking, are causing spalling or explosive spalling of concrete. Malhotra H.L. presented in his study an overview of main spalling theories and highlighted theories by different researches (202).

Tab. 6: Main spalling theories with subgroups according to Malhotra (200)

1) Moisture	1a) Vapour pressure
	1b) Moisture clogging
	1c) Vapour pressure enhanced by frictional resistance
2) Stress	2a) Initial compression
	2b) Initial compression + thermal stress
	2c) Initial compression + thermal stress + stress caused by frictional resistance
3) Cracking	3a) Aggregate expansion
	3b) Internal cracks
	3c) Reinforcement expansion

Tab. 7: Highlighted theories by different researchers, compilated by Malhotra (200)

Researcher	Main factors	Secondary factors
Saito (1965)	2a, 2b, 2c	1a
Harmathy (1965)	1b	-
Meyer-Ottens (1972)	1c, 2b	2c, 3c
Dougill and Sertmehmetoglu (Sertmehmetoglu,1977)	1b, 3b	2a
Akhtaruzzaman and Sullivan (1970)	1a	Dense surface layer
Gustaferro (Kordina, 1970)	1a	3a
Copier (1979)	2a, 1a	--

To conclude on the spalling of concrete, it is essential to say that the spalling of concrete weakens the structure by reduction of cross-section and, in the case of reinforced concrete, exposes steel rebars to higher heat. Furthermore, explosive spalling can complicate evacuation of involved people and the actions of a rescue team. Consequent reparation of a structure damaged by spalling could be complicated, hard to estimate, and costly.

AIM OF DISSERTATION THESIS

Fire resistance is one of the less-discussed properties of concrete, and yet crucial when it comes to closed underground structures or structures with increased fire risk level. Fire can cause extensive damages to structures, and concrete degradation and disintegration can result in a complete collapse of the structure. Problematic areas concerning behaviour of individual components in concrete exposed to elevated temperatures, such as cement paste, porous structure and aggregates, was explained in detail in the theory part of the thesis. Gained knowledge is going to be applied during the development of a new and innovative method for fire resistance of existing concrete structures based on a modification of the porous structure of the surface layer by application of heat. This method, entitled intentional heat treatment (IHT) method will serve predominantly for fire protection of existing structures with restricted space or ventilation possibilities. The main target is to describe in detail the principle of the IHT method using chemical and porous structure analysis and verification of its efficiency during large scale laboratory testing. In parallel the contribution of traditional and “new generation” air-entraining agents, and their potential to be used for the improvement of fire resistance of newly designed concrete will be developed and tested. Finally, both methods will be compared, and their efficiency evaluated.

II. EXPERIMENTAL PART

Experimental work conducted within this research was performed in different locations, the Czech Republic at the laboratory of Brno University of Technology and AdMaS center, in Germany, laboratory located at Hochschule Wismar, University of Applied Science, Technology, Business and Design, and the last location was Iceland, with the help of Reykjavik University and Innovation Center Iceland. Various test facilities were available for performing the testing, and I am very grateful for all the support I got from academic stuff and laboratory assistants at individual institutes. The experimental part is divided into 4 chapters, namely "Description of developing method," "Design of mixes and laboratory work description," "Practical development of the IHT method," and "AeA-FiResCrete under thermal load." The structure of individual chapters is graphically presented below.

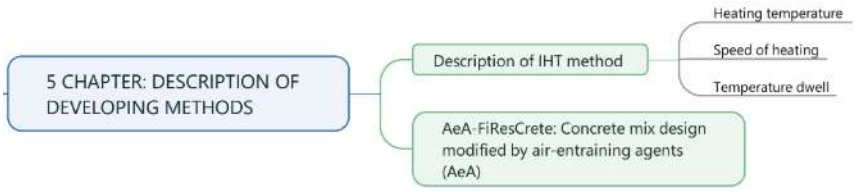

Fig. 55: Structure of 5 Chapter: Description of developing methods.

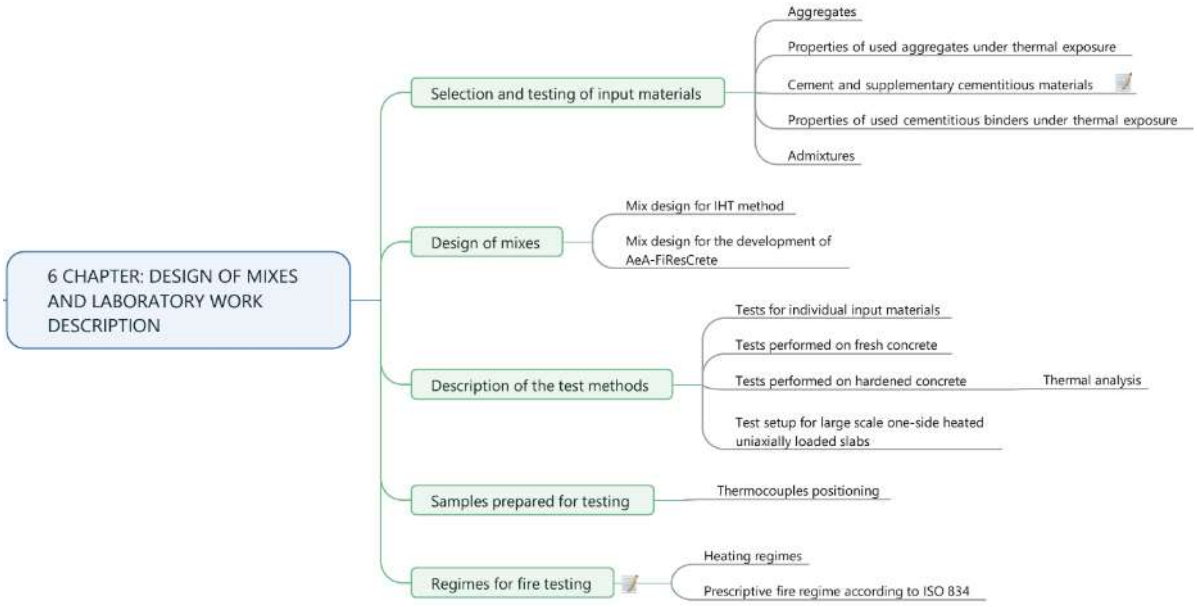

Fig. 56: Structure of 6 Chapter: Design of mixes and laboratory work description.

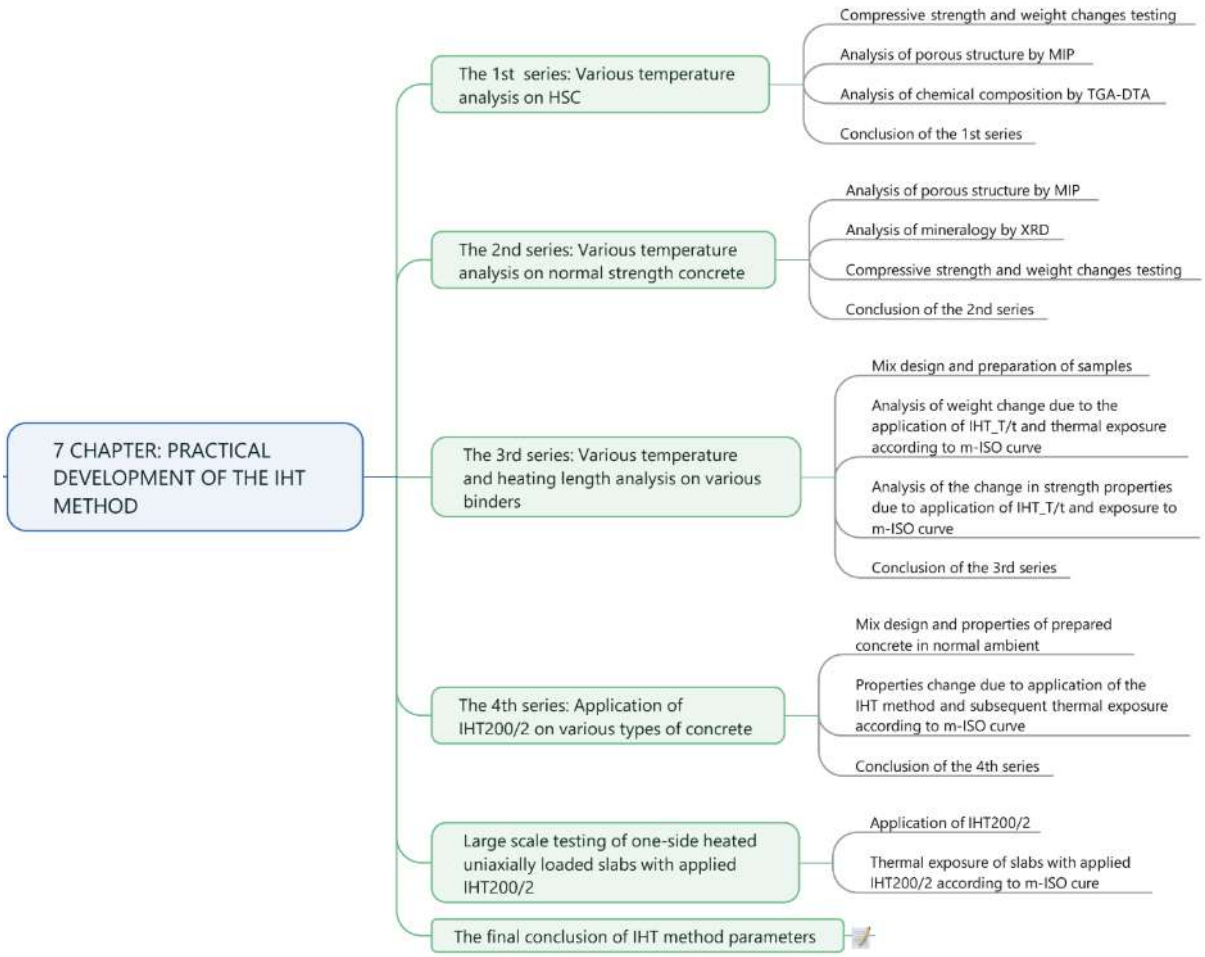

Fig. 57: Structure of 7 Chapter: Practical development of the IHT method.

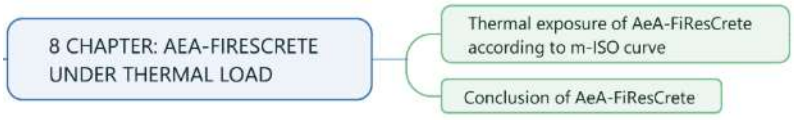

Fig. 58: Structure of 8 Chapter: AeA-FiResCrete under thermal load.

5 CHAPTER: DESCRIPTION OF DEVELOPING METHODS

In Chapter 1 will be described two methods for fire resistance of concrete structures, which are the subject of this PhD thesis. The first method and the most innovative one is focused on the modification of pores structure of the surface layer. This method is based on the idea that a suitable porous structure in the surface layer will contribute to better fire resistance of the existing concrete structure, and the acronym used throughout this thesis is IHT (Intentional Heat Treatment) method. For verification of efficiency of IHT method applicable to existing structures, other methods for fire resistance enhancement were investigated that are utilisable in new concrete structures. The second method, which is also innovative, is the usage of standard or "new generation" air-entraining agents to intentionally form an extensive pore structure, which can serve as a transporting system for migrating water and vapour. The acronym for development of concrete with AeA is AeA-FiResCrete. Both methods have an innovative aspect, but the first, IHT method, will be discussed the most, as it is a completely new approach, and results compared with AeA-FiResCrete. During PhD studies was also performed a research focused on the application of basalt micro and macro fibres as a potential solution for fire resistance enhancement, and published as scholar articles within various conferences (203–205). Results from this research are not included in PhD thesis to maintain the size in acceptable range.

5.1 Description of the IHT method

A recent situation and increased requirement on the fire safety of structures created an opportunity for development of fire protection methods for existing structures, and the rise of new protection methods. These new methods or upgraded existing methods of fire protection are either for new structures or existing structures. In case of new structures, the possible interventions for fire resistance features cover a far wider area as they can be integrated during the design process. However, in case of existing structures, many limitations and obstacles arise, and should be taken into account. A few of the parameters which which should be taken into account include the condition of an existing structure, location, surrounding ambient and climate conditions, and available space for the realisation of fire protection.

The main trigger for the development of this new method for fire protection of existing structures is extensive tunnel lining testing in Germany (206). Standards have imposed a new requirement in terms of the level of fire resistance and imposed new limits which should be met even by existing tunnel structures. Extensive tunnel lining testing took place and their conditions were reported. Testing consisted of taking core drill samples on which was performed analyses of porous structure, compressive strength testing and the degree of carbonatation was measured. Results from the testing were not always satisfactory, and therefore we focused on the development of a new method that could be applied on tunnel lining without space occupation.

The new fire protection method which is going to be described and verified within this PhD thesis is based on intentional preheating of the surface layer of the concrete structure which we expect to lead to the creation of suitable porous structure that will allow transport of water and vapour in the event of fire, and delay or entirely omit explosive spalling. Two main benefits of IHT method are (i) no requirements for space in front of the existing structure except during the application procedure, and (ii) IHT method does not cause a visual change to the existing structure, which is favourable from architectonic aspects.

The main area of application of the IHT method are locations with limited ventilation possibilities and flue gas exhaust such as tunnels and underground garages. Newly built underground structures are designed and equipped with a high-tech fire alarm and protection systems to meet the regulations, but those regulations should also be met by existing tunnels, which is more challenging and technically demanding. Fire in a closed place can have devastating consequences not only at the centre of the fire but also on surrounding structures.

Most dangerous are tunnels in big cities where there are structures above the tunnels, and if the tunnel collapses, not only people in the tunnel are endangered but also in the area above the tunnel. In the case of fire events in underground garages, the bottom part of structure and basement structures can be weakened and result in the collapse of the whole building.

As was described in chapter 3.1.5, there is a direct dependency between rising exposure temperature and porous pressure. When the pressure in the pores exceeds the tensile strength of pore walls, cracks are created. Formed cracks connect the pores in cement paste and generate an interconnected porous structure. The problem is that these cracks have a direct effect on the strength of the whole concrete element. If the cracks which are caused by extensive vapour pressure are formed slowly, and in a small scale, may not necessarily have an extensive influence on the strength and integrity of the whole element. Also, if the cracks are created only in the surface layer, the strength can remain unchanged. The creation of cracks and consequently connected porous structure could allow the transfer of a greater amount of vapour and thus prevent explosive spalling. Unfortunately, there is one more phenomenon that should be taken into account, and that is the penetration of chemical agents into the concrete structure which could accelerate degradation of concrete. Therefore, the ratio of interconnection and permeability should be carefully balanced.

One solution to create a suitable interconnected porous structure in the surface layer of the concrete element is to heat it up until the desirable porous structure is created. This layer permits vapour transfer from the concrete mass but restricts penetration of chemical agents from surrounding ambient into concrete mass. The speed of heat transfer, and respective, coefficient of thermal heat conductivity, is the decisive parameter for IHT method setup. This raises the first question for developing of the IHT method:

- At which **maximum temperature** is the best pores structure created?

The second question considers the thickness of the surface layer with a modified porous structure.

- **How long** should the thermal exposure be held to create the best performing layer in a suitable thickness?

The third and last question, which defin the parameters of IHT method is:

- **How fast** can the heating be applied to enlarge the porous structure without causing damage and still remain time efficient during the application?

There are many influencing factors which need to be taken into consideration while designing the ITH method. Factors may lead towards the variation of IHT method set up based on individual structures and conditions. To give an idea, several of them are listed below:

- Amount of the pores in a concrete structure not only in the surface layer but in the whole mass, in other words, the existing porous structure in concrete.
- Origin of aggregates, and their thermal behaviour, such as thermal expansion, thermal degradation, loss of strength, or chemical changes accompanied by volume changes.
- The average moisture content of the structure, and relative humidity of the surrounding ambient.
- Type of exposure environment and potential chemical content (chlorides from seawater in coastal areas, exhaust gasses, carbonation)
- Type of concrete structure, presence of steel rebars or any type of dispersed fibre reinforcement.

5.1.1 Heating temperature

The heating temperature should be kept in the range from 100°C to 400°C. Migration of free and physically bonded water takes place. Furthermore, chemical changes of CSH gel (formation of a crystalline form of βC_2S between 120 and 200°C) and Ettringite (release of H_2O from structure between 60 and 120°C) occurs up to 400°C. It is desirable to keep the maximum

temperature below 390°C, so the dihydroxylation of Portlandite is not initiated and possible reduction of strength of concrete prevented. The IHT method is focused on evaporation of unbonded water, which evaporates until it reaches a critical point where water and vapour are indistinguishable. The temperature at the critical point is 374°C and the pressure varies based on the applied equation range from 15,21 to 23,68 MPa (207–209).

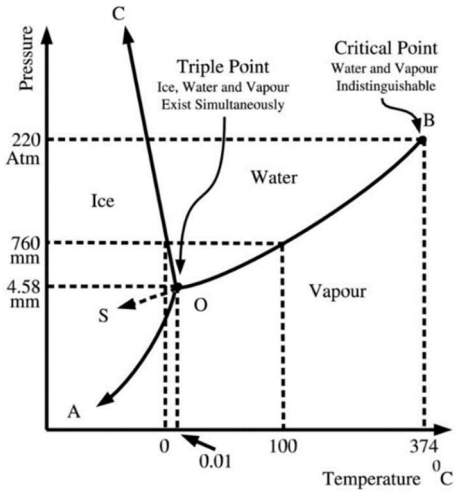

Fig. 59: Triple point of water analogy. Fine-tuned intensive variables: critical temperature T c = 0,01°C, critical pressure P c = 4.58 mm Hg.

Pressure development in cement paste was calculated according to three different theories. Based on equations from IAPWS, Tetens and Buck (207–209) and average tensile strength of cement paste an assumption can be drawn that the maximum preheating temperature cannot employ higher pressure than the tensile strength of cement paste. This statement was already verified by K. Hinrichsmeyer et al. (199). For better understanding, the vapour pressure for water as a function of temperature is displayed in Fig. 60.

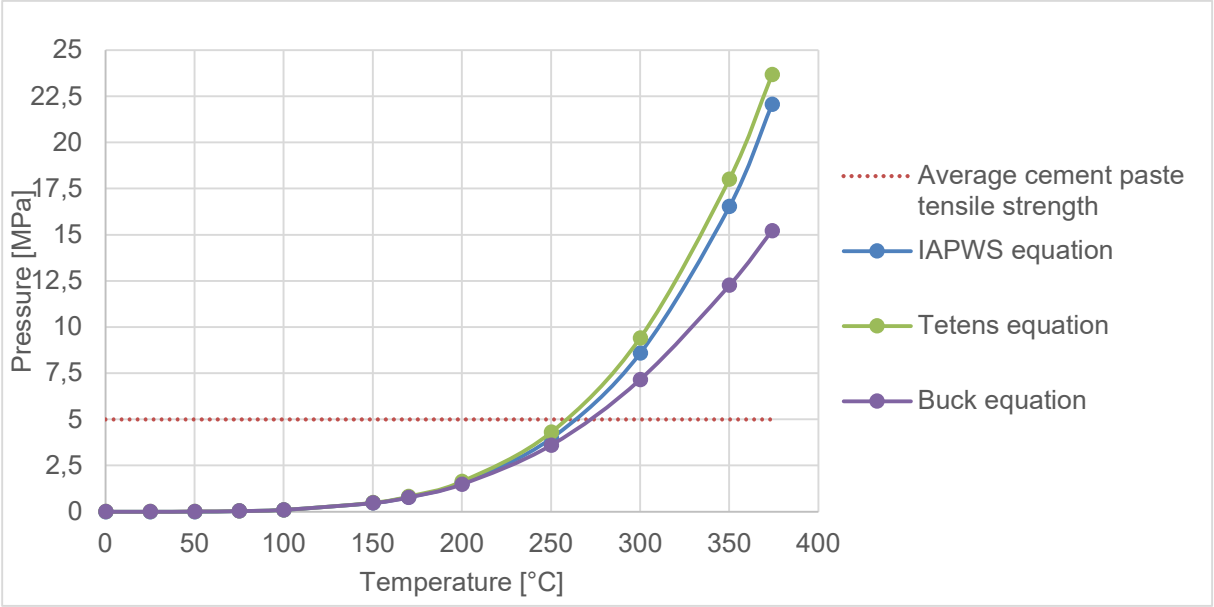

Fig. 60: Vapour pressure curves for water append by the average tensile strength of cement paste (207–209).

In detail, the area of potential heating temperatures for IHT method is in a range from 150°C to 300°C. The maximum exposure temperature is depended on the tensile strength of cement paste in concrete, therefore the higher the tensile strength of cement paste, the higher the exposure temperature that can be applied.

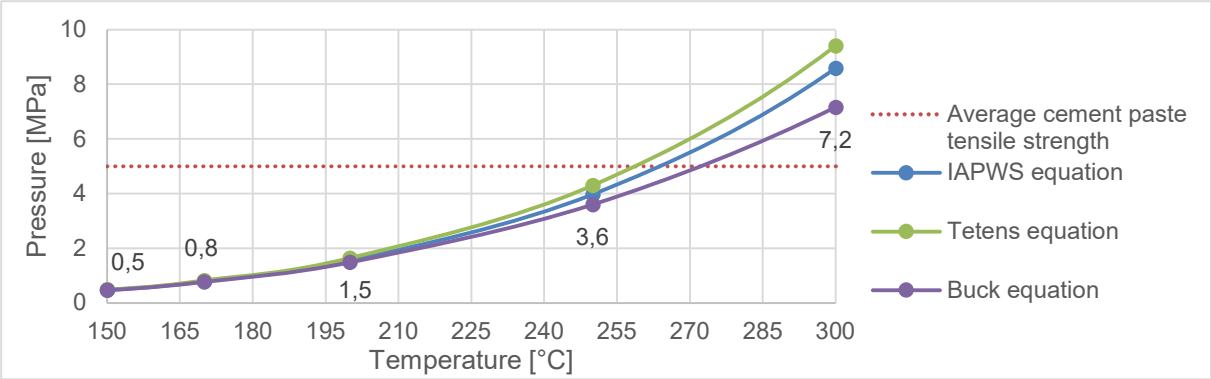

Fig. 61: Development of pressure between 150°C and 300°C.

Exposure temperature must be selected with caution to aggregate type, concrete composition (a type of cement and presence of SCM). The energetic efficiency also should not be omitted, so the IHT method can compete with other methods for fire resistance of existing structures. The impact on physical and mechanical properties is rather low as the IHT method is focused on the surface layer of concrete in tens of millimeters.

Based on described theory temperatures for preheating were selected from 150 to 450°C, and in every further development, the range was narrowed to 200 and 250°C.

5.1.2 Speed of heating

The selection of the maximum heating temperature was followed by a speed of heating determination. This parameter must be selected very carefully with respect to the moisture content of the structure. If the moisture content is higher, the larger the amount of water and vapour that will migrate from inner mass towards the surface. Too rapid migration of water vapour can cause greater cracking than is required, and the surface layer can be extensively damaged and lose resistance to penetrating chemical substances from the surrounding environment and affecting durability. On the other hand, too slow temperature rise might leave the porous structure unchanged and the efficiency of IHT method is lost.

The speed of heating can vary depending on the structure, and therefore a recommended range of heating speeds will be given. The moisture content of the concrete structure has principal influence on speed of heating and changes of porous structure. Decision making factors are moisture content, strength of the concrete and porosity of concrete. Based on reviewed literature a heating speed of 5°C/min was selected.

5.1.3 Temperature dwell

The length of preheating should be long enough to allow the preheating temperature to penetrate to sufficient depth and modify the porous system in the desired thickness. Length of heating must be balanced between a sufficient porous structure modification, and economic sufficiency to be competitive with other methods for fire resistance. The depth of heat penetration is closely connected to the coefficient of thermal conductivity of concrete. Various types of concrete are characterised by different coefficients of thermal conductivity, and thus the temperature dwell of IHT method can vary and be adjusted to individual projects.

In the following figure Fig. 62, the numerical thermal calculation of heat penetration in concrete elements, based on exposure temperature, in this case MHC fire and ISO 834 fire curve, is presented.

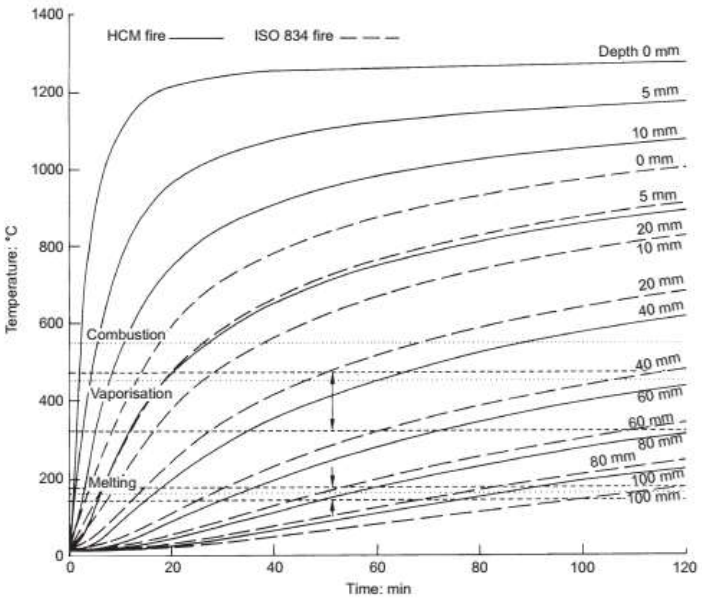

Fig. 62: Simplified non-interactive presentation of key polypropylene transformation temperatures superimposed upon the temperature fields generated in concrete when exposed on one face to HCM and ISO 8343 fires. Numerical thermal calculation carried out using the upper limit of Eurocode 24 concrete thermal conductivity. Dashed lines indicate the melting and vaporisation bands with the dotted lines indicating the peak of the transformations. Note: this representation does not show the influence of PP on the temperature fields (97).

5.2 AeA-FiResCrete: Concrete mix design modified by air-entraining agents (AeA)

AeA are primarily added to enhance freeze-thaw resistance by modification of porous structure, such as spacing factor, the specific surface area of air voids and void frequency. The pore size provided by AeA should be approximately in a range from 10 to 300 µm, as each different source states slightly different values. This pore diameter is also partly desirable for fire resistance, and can contribute to easier water and vapour migration through the cement paste in case of a fire event. The air content produced by AeA can strongly influence the compressive strength of concrete if ‘overdosed’, and therefore the number of pores contributing for better freeze-thaw resistance should be carefully balanced with other properties. Results from analysis of air voids characteristics in hardened concrete can provide useful data and help to increase understanding of concrete porous structure.

Three different types of AeA were used for the development of AeA-FiResCrete. The standard AeA is a surface-active agent that has two poles: one is hydrophobic and the other hydrophilic. The formation of pores could be easily influenced by the length of mixing and the diameter of pores varies. The second and third type of AeA are “new generation” AeA. The second type of AeA is based on chemical reaction, which forms pores in fresh concrete and the number of pores could increase during the time between mixing, casting and hardening. Formed pores are more uniform, and their amount can be more easily controlled as ‘foaming’ is not involved. The third type of AeA is polymer-based, particularly micro hollow spheres blended into the mix during the mixing process. Those micro hollow spheres have the same diameter and can be easily dispersed in fresh concrete. Their amount is stable and do not increase air content due to the mixing process. Evaluation of air content in fresh concrete could be challenging as the standard pressure method cannot fully detect microspheres, and also some difficulties were raised during the preparation of the sample for air pore system analysis in hardened concrete. During the fire testing colour charge occurred of the sample surface, which was connected to melting of the spheres.

6 CHAPTER: DESIGN OF MIXES AND LABORATORY WORK DESCRIPTION

In this chapter selection of the input materials, their individual testing and validation of their suitability will be described. Furthermore, all mix designs used within this study will be presented. As there are several groups of test performed on different concrete mixes special structuring of part 6.2 Design of mixes will be used to provide good understanding of the prepared mix series. Mix design will be followed by a list and a short description of all laboratory tests performed within experimental work. The list of the tests contains many tests performed on various types of samples, and for that reason this chapter will be concluded by description of all different samples prepared for the variety of testing employed. Special emphasis will be given to samples with incorporated thermocouples for temperature development in concrete specimens during the fire testing.

6.1 Selection and testing of input materials

The selection of materials used during the laboratory work was quite challenging as the work was carried out partly in the Czech Republic (Brno University of Technology, AdMaS), Germany (University of Rostock) and Iceland (Innovation Center Iceland, Reykjavik University). Selection of basalt aggregates was essential as basalt is the least susceptible to changes due the thermal exposure, but basalt from the Czech Republic and basalt from Iceland display incomparable properties, and therefore the comparison is stated even though basalt from the Czech Republic was not used during the development of IHT method. The last stage of IHT method verification took place in Iceland and to provide comparison to other aggregate types; granite aggregates were included in the research. Other components such as cement, supplementary cementitious materials and admixtures were matched without any significant complications.

6.1.1 Aggregates

Basalt aggregates were selected for their low coefficient of linear thermal expansion. Chemical composition of basalt can vary, as in our case basalt aggregates from Vatnsskarð quarry, Iceland, were characterised by high porosity and content of glass phase basalt (from lava pillows). Glass phase melts at lower temperatures and may interfere concrete structure. Czech basalt aggregates from Bílčice quarry are compact with low porosity and stable up to approx. 900°C. The third type of tested aggregates is granite from Norway, aggregates with low water absorption, dense structure and content of SiO_2 which is characterised by transformation of the quartz from the α to β polymorph at 573°C.

Those 3 types of aggregates were selected due to different thermal characteristics, basalt as a stable rock and granite as susceptible to thermal change at 573°C. Limestone was not available from local quarries, and therefore, we were not able to cover all the most common aggregates used in the concrete industry. Properties and characteristics of used aggregates during the research are given in Tab. 8, Tab. 9 and Fig. 63 to Fig. 66.

Tab. 8: Characteristics of rock, mineralogy and thermal properties.

	Composition - main minerals	Coefficient of thermal expansion	Thermal stability	Note
Basalt_CZ	Pyroxene, Plagioclase Feldspar	5,5-8 · 10^{-6}/°C	900°C	Dense and compact
Basalt_IS	Pyroxene, Plagioclase	5,5-9 · 10^{-6}/°C	900°C	Porous and geologically young; Glass phase

	Feldspar, glass phase basalt			starting to melt at approx. 700°C
Granite_NO	Quartz, Orthoclase Feldspar, Plagioclase Feldspar	6,5-8,5 · 10^{-6}/°C	573°C*	Transformation of quartz from α to β polymorph at 573°C (0,85% volume increase)

*Thermal stability depends on the mineralogical proportion but initiate with the transformation of quartz.

The most common properties like particle size distribution, water absorption and particle density were evaluated and further used during the mix design. Resistance to fragmentation was selected for aggregates stability at elevated temperatures.

Tab. 9: Aggregates properties

	Fraction	Water absorption 24 hours [%]	Fine particles [%]		Particle density [kg/m^3]	Resistance to fragmentation-LA test	
			Value [-]	Class		Value [-]*	Class
Basalt_CZ Bílčice	0-4 mm	0,9	7,5	f10	2971	-	LA20
	4-8 mm	0,9	0,6	f1,5	2967		
	8-16 mm	0,8	0,9	f1,5	2959		
Basalt_IS Vatnsskarð	0-8 mm	3,8	1,6	f3	2697	34	LA35
	8-22 mm	6,0	0,6	f1,5	2620		
Granite_NO Norway	0-8 mm	0,3	9	f11	2650	23	LA25
	8-16 mm	0,6	2	f4	2660		

* tested on the fraction 10-14 mm according to EN 1097-2

As mentioned earlier, characteristics of Basalt_CZ and Basalt_IS is significantly different as is visible also from density and water absorption, Fig. 63. High water absorption of Basalt_IS had to be considered in the calculations for design of mixes.

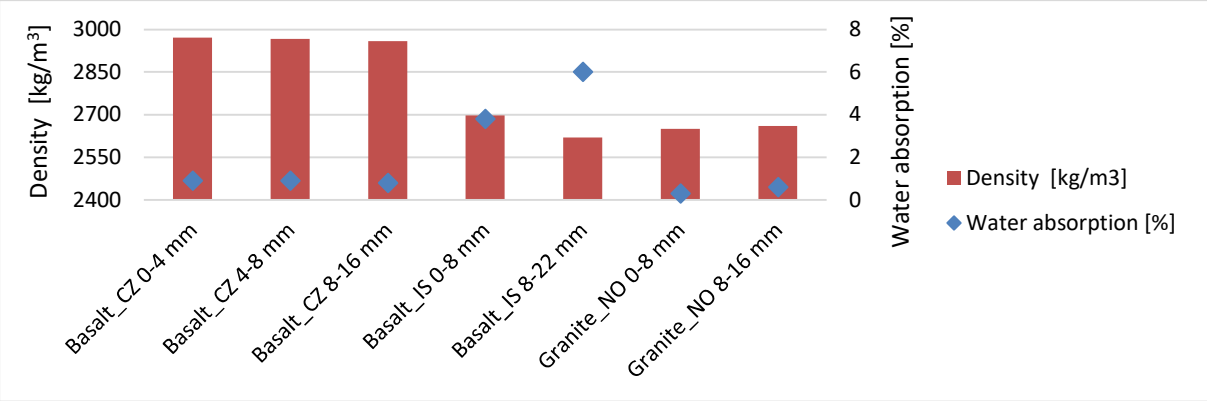

Fig. 63: Relation between density and water absorption of used aggregates.

Fraction 0-8 mm of Basalt_IS consists of 63,8% fraction 0-4 mm and in combination with coarse Basalt_IS with a high content of fraction 16-22,4 mm fresh concrete was lacking particles between 4 to 8 mm and a 'bony' mix was obtained. The design of aggregates mixes from Basalt_CZ was much easier as three fractions were available. Granite_NO contains 83% of particles 0-4 mm, which contributed to workable and "full" mix.

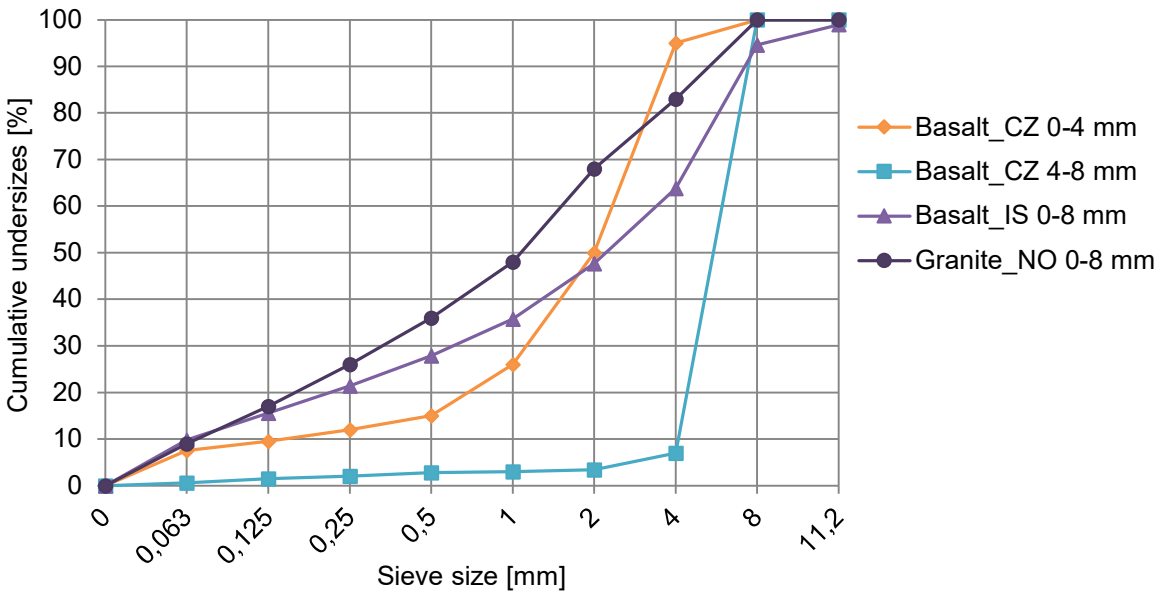

Fig. 64: Particle size distribution of fine aggregates

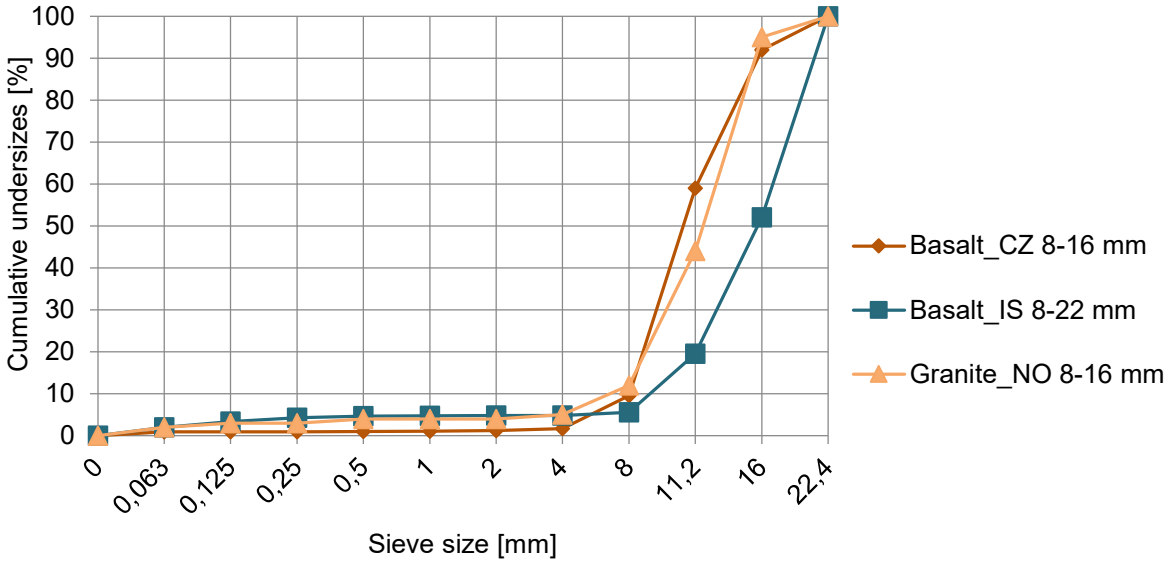

Fig. 65: Particle size distribution of coarse aggregates

All fractions of Basalt_CZ are crushed and have sharp edges, which are not favourable for fresh concrete workability. Fraction 0-8 mm Basalt_IS is from a quarry located in a glacier valley, and therefore the particles have variety of origins, including glass phase basalt (lava). As visible on the picture (f) Fig. 66, the surface of coarse aggregates is characterised by open porosity and is highly irregular. Basalt_IS had very special ability to adsorb at high amount of water on a particle surface, and even in ambient with lower relative humidity, the actual moisture content of Basalt_IS aggregates was high. The Granite_NO fraction 0-8 mm contains a lot of fines, which contributed to good workability of fresh concrete.

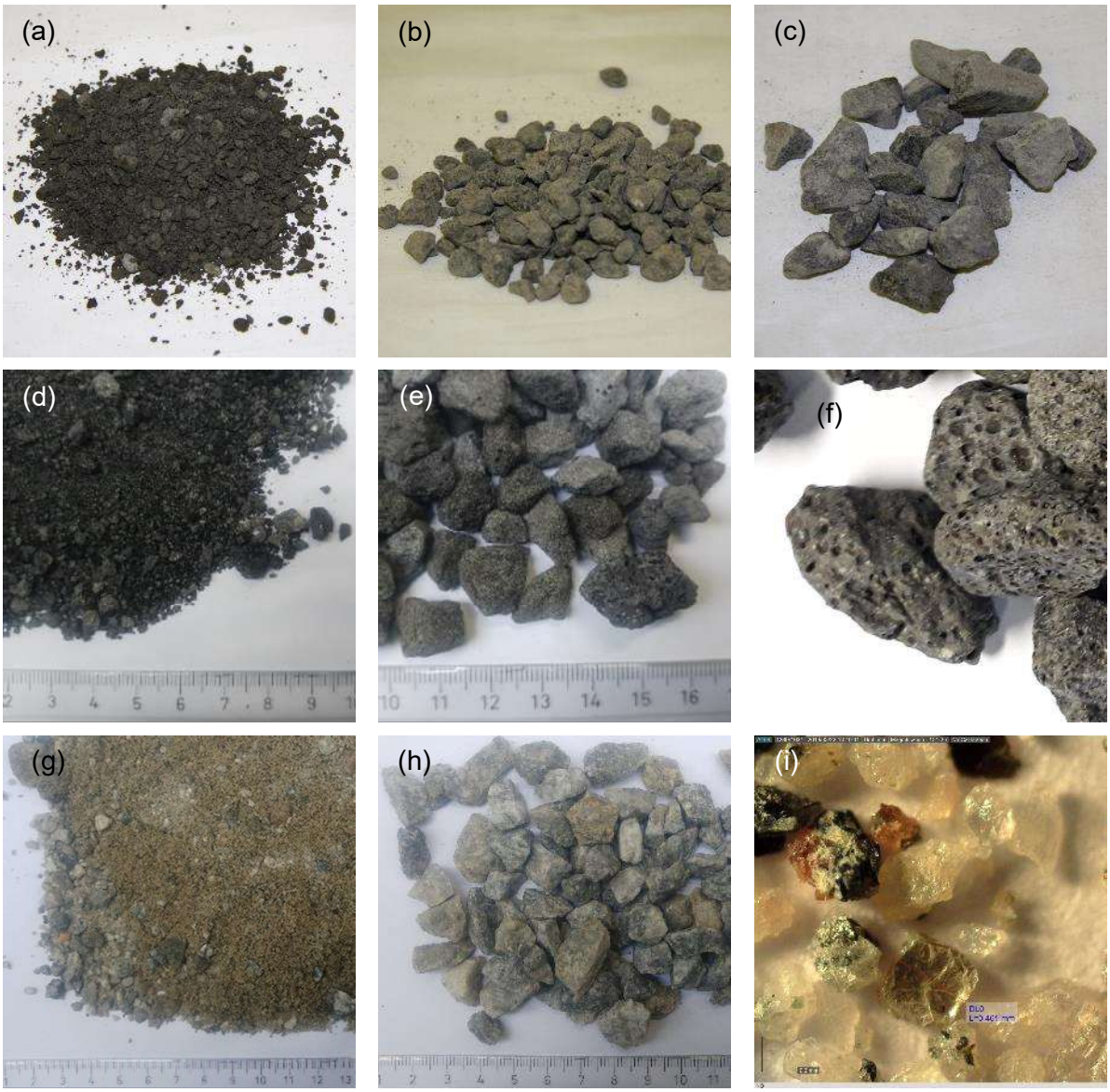

Fig. 66: Photos of individual aggregates: (a) Basalt_CZ 0-4 mm; (b) Basalt_CZ 4-8 mm; (c) Basalt_CZ 8-16 mm; (d) Basalt_IS 0-8 mm; (e) Basalt_IS 8-22 mm; (f) Basalt_IS 8-22 detail of grain surface; (g) Granite_NO 0-8 mm; (h) Granite_NO 8-16 mm; (i) Granite_NO 0-8 mm grain shape under microscope magnification 150 x.

6.1.2 Properties of used aggregates under thermal exposure

The behaviour of aggregates at high temperature was verified by heating them up to temperature 400, 800 and 1200°C with heating rate 5°C/min and natural cooling. The change of resistance to fragmentation is tested according to EN1097-2, Los-Angeles method. Basalt aggregates from quarry Vatnsskarð and granite from Norway were tested. Samples for test were prepared according to EN 1097-2; 70% fraction 10,0 - 12,5 mm and 70% of fraction 12,5 - 14,0 mm. As the requested amount (5 kg) of aggregates was prepared prior to the thermal exposure, the weight of samples was checked after heating. Additionally, beyond the resistance to fragmentation test scope, the particle size distribution of remaining material in fraction 1,6 to 14 mm was performed. Aggregates were dried in an oven at 105°C to remove free water and follow the loss of chemically bonded water, if any. Gravimetrically no change of samples weight was determined, see Tab. 10.

Resistance to fragmentation of Basalt_IS is significantly lower in comparison to Granite_NO in standard conditions (20°C). After thermal exposure to 800°C the LA value was the same for both tested aggregates type, which clearly shows the thermal degradation of Granite_NO aggregates.

Tab. 10: Results from Los Angeles test after exposure to 400, 800 and 1200°C.

Exposure temperature [°C]	Basalt_IS			Granite_NO		
	LA value	LA class	Weight loss* [%]	LA value	LA class	Weight loss* [%]
20	34	LA35	0,0	23	LA25	0,0
400	36	LA40	0,1	29	LA30	0,0
800	36	LA40	0,0	35	LA40	0,0
1200	melted			-	-	

*Weight loss of material due to thermal exposure in percentage.

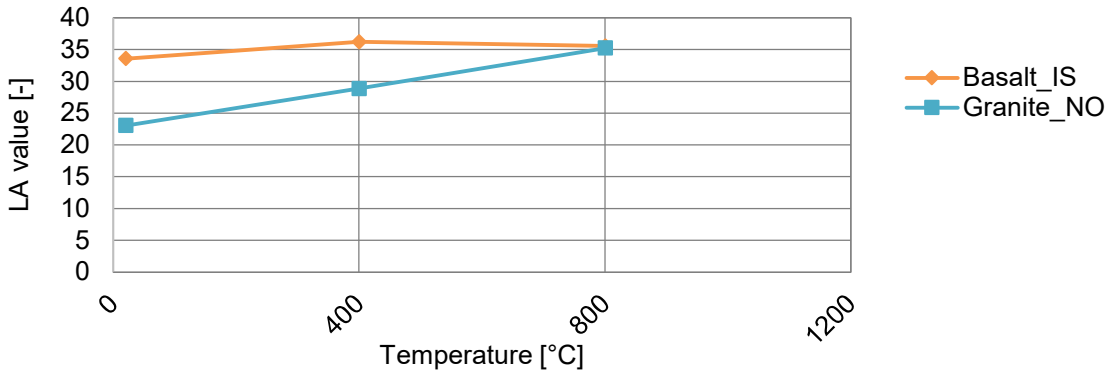

Fig. 67: Degradation of basalt and granite aggregates due to heat exposure evaluated by LA test

Basalt aggregates were stable in elevated temperatures, and the LA class was a change from LA35 to LA40, but if we have a look at values that raised from 34 to 36, the difference is only 2 compared to Granite_NO which differed by 12. The colour of basalt aggregates shifted slightly to areddish shade when exposed to 800°C. Higher exposure to 1200°C caused complete re-melting of the basalt aggregates and glass phase (lava) was formed. The change in colour to brown or red is connected to chemical changes of minerals containing iron compounds. Oxidation, rehydration and decomposition produce iron oxides characterised by the red colour.

The resistance to fragmentation of Granite was reduced by the thermal exposure as visible from the results of the LA test. The LA value was reduced by one class in every heating temperature, from LA class LA25 to LA40. More visible is a degradation of granite from the particle size distribution of remaining material in fraction 1,6 to 14 mm, see Fig. 69. The degradation is also demonstrated by colour change from grey to a reddish shade. This colour change could be explained by dehydration of amphibolite and formation of iron oxides which is a characteristic brown or red colour (210).

(a)

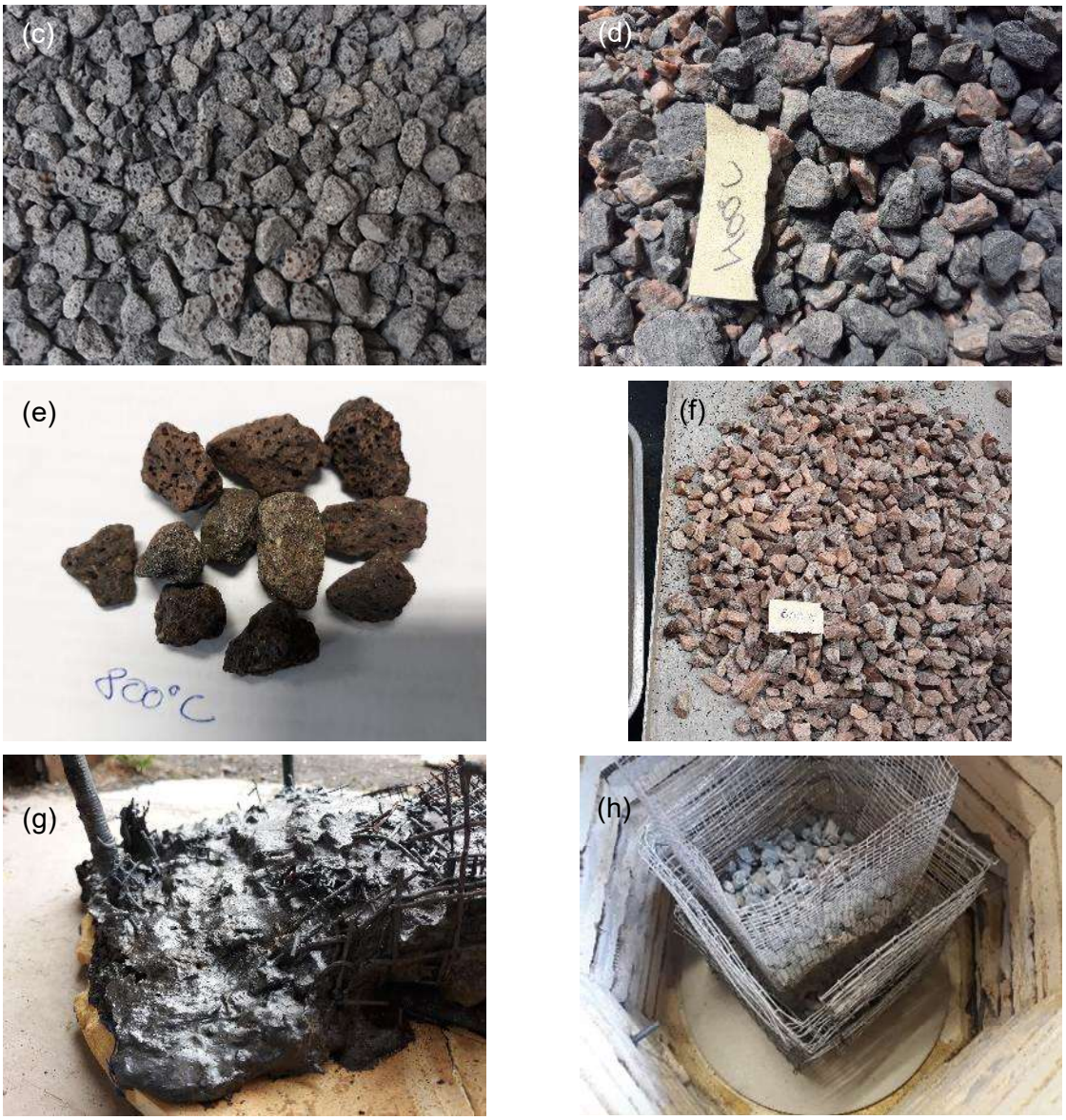

Fig. 68: Aggregates thermaly loaded for LA test: (a) Basalt_IS 20°C; (b) Granite_NO 20°C; (c) Basalt_IS 400°C; (d) Granite_NO 400°C; (e) Basalt_IS 800°C; (f) Granite_NO 800°C; (g) Basalt_IS 1200°C;(h) setup for aggregates heating

Thermal stability of tested aggregates, and their resistance to fragmentation is evident from a particle size distribution test performed on remaining material from LA testing in fraction 1,6 mm and 14 mm. The fragmentation degree of residual material from Basalt_IS sample was almost stable of all three exposure temperatures (20, 400 and 800°C exposure). There is only a slight increase when exposed to 400°C demonstrated by a higher percentage on sieve 6,3 mm, particularly by 5,0%. Exposure to 800°C did not influence resistance to fragmentation and the particle size distribution of residual material from LA test was identical to the reference Basalt_IS sample (20°C). More significant changes were observed in case of Granite_NO and its resistance to fragmentation. Exposure of Granite_NO aggregates to 400°C caused higher fragmentation and increase of particles on sieves 4,0; 5,0; 6,3; 8,0; 10,0 and 11,2 mm by 5,9% in average. Considerably higher degradation was observed after exposure of Granite_NO aggregates to 800°C, where the increase of particles on sieves 4,0; 5,0; 6,3; 8,0 mm was an average of 28%. The number of particles exposed to thermal load was the same before and after the exposure, hence all the degradation was caused by the LA test. Chemical changes in granite only weaken the strength of particles but did not cause direct fragmentation.

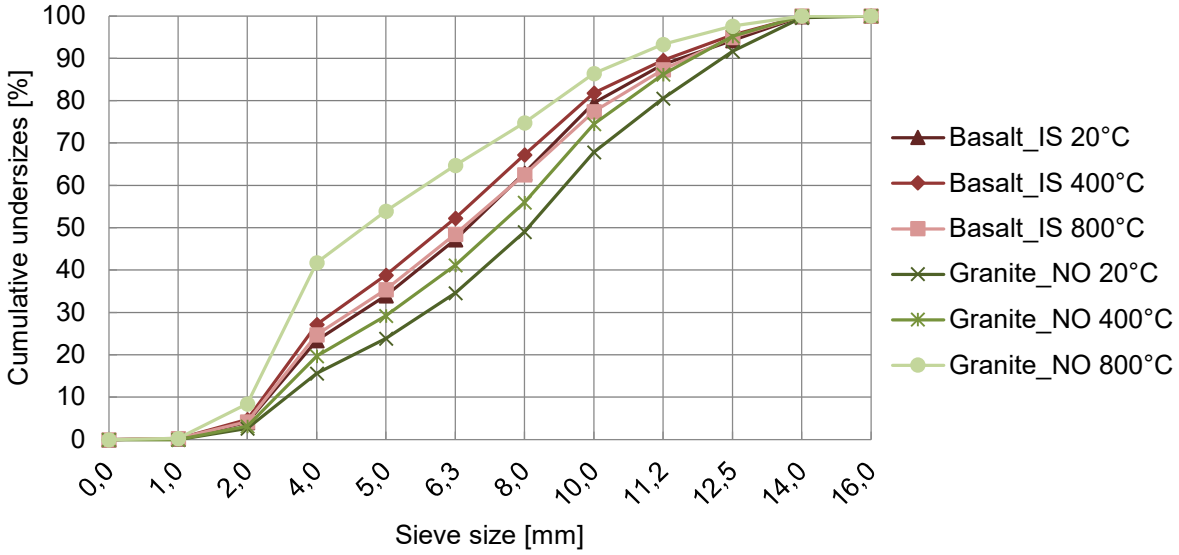

Fig. 69: Particle size distribution of 1,6 -14 mm fraction after LA test

6.1.3 Cement and supplementary cementitious materials

Throughout the whole experimental work performed for this PhD study three types of cement were used. The two most common and available cement types in Iceland were CEM I 42,5N-SR5 from Aalborg, DK and CEM II/B-M 42,5 R from Norcem, NO. During the work in the Czech Republic, cement CEM II/A-LL 42,5R was used. Those cement types were selected as their behaviour under thermal load is known from earlier performed research and the number of influencing factors within this research could be reduced. Blended CEM II/B-M 42,5 R contributes to better freeze-thaw durability and reduces development of alkali-silica reaction. As CEM II/B-M 42,5 R contains a lower amount of clinker (78% clinker, 18% fly ash and 4% limestone), it is assumed that CEM II/B-M 42,5 R performs better in elevated temperatures.

Silica fume (SF) was used as a pozzolanic reactive SCM to prepare concrete with reduced porous structure. Properties of silica fume varies based on its treatment, however most common with the concrete industry is densified silica fume. Silica fume used for laboratory work was unidentified silica fume from Elkem Iceland. Inert SCM ground basalt (basalt fines) were used to compensate the lack of fines in Basalt_IS aggregates fraction 0-8 mm. Properties of both cement types and silica fume are shown in Tab. 11 and Tab. 12.

Tab. 11: Properties of used cement

Cement type	Compressive strength		Setting time		Soundness	Density	Specific surface area
	2 days [N/mm^2]	28 days [N/mm^2]	initial	final	[mm]	[g/cm^3]	[m^2/kg]
CEM I-42,5N-SR5	15-21	54-62	-	90-150	≤ 2 mm	3,14-3,24	370
CEM II/B-M 42,5 R	31	55	140	218	1	3,00	450

*Technical data sheets for cement types are listed in the references in same order as cement types in table (211, 212).

The particle size distribution of used cement types and SCM are displayed in Fig. 70. Two curves for silica fume are presented, for milled and non-milled silica fume. As known, silica tends to agglomerate (see Fig. 71), and it is not possible to measure particle size distribution by standard methods for cement (213). Basalt fines are coarser than other powder

components, and consist of 45% fines in fraction 10 to 60 μm. Particles are sharp and have low water absorption.

Tab. 12: Properties of used supplementary cementitious material

	Bulk density		Specific density	Specific surface
	Undensified	Densified		
	[kg/m^3]	[kg/m^3]	[kg/m^3]	[m^2/kg]
Silica fume	130-430	480-720	2200	15000-30000
Basalt fines	-	-	2700	-

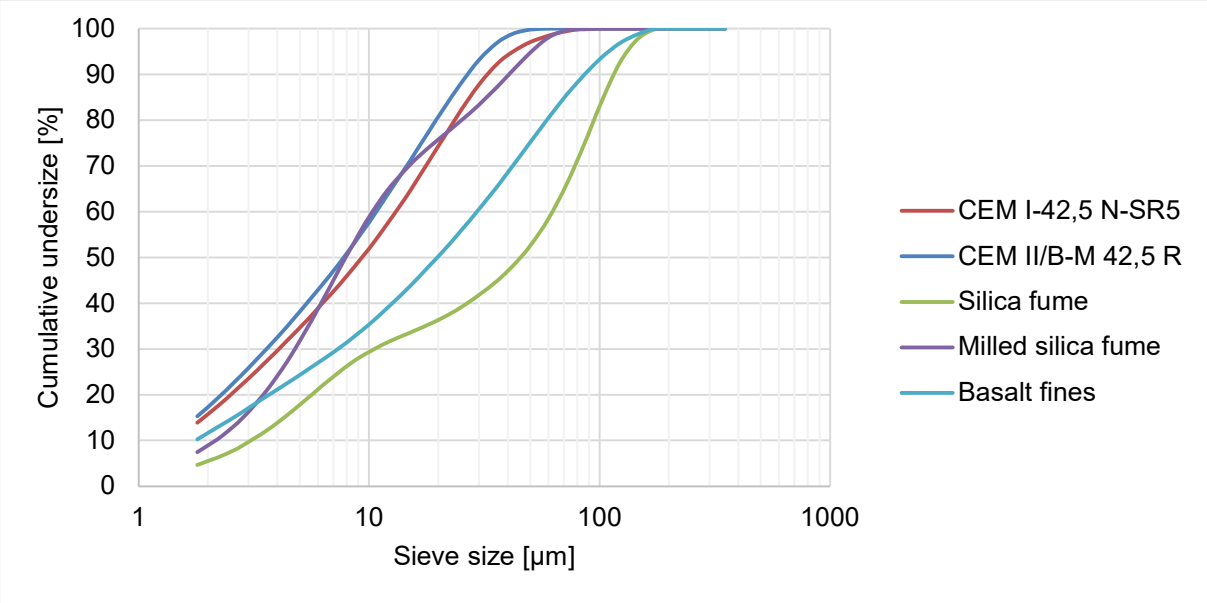

Fig. 70: Particle size distribution of cement types and SCM used during the research work.

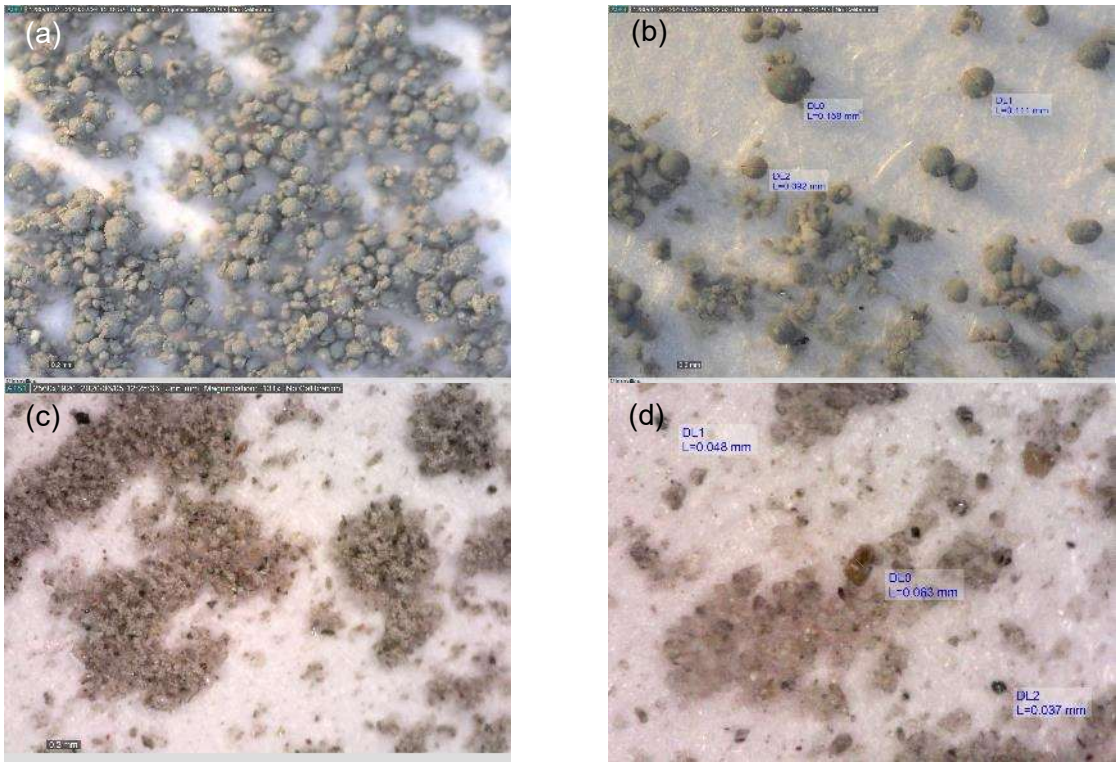

Fig. 71: Photo documentation of SCM: (a) Silica fume, magnification 130x; (b) Silica fume, magnification 226x; (c) Basalt fines, magnification 130x; (d) Basalt fines, magnification 224x.

6.1.4 Properties of used cementitious binders under thermal exposure

Throughout the development of the IHT method, three binder types were used, and 1 binder type for AeA-FiResCrete methods. The CEM I-42,5 N-SR5 served as a reference, and its behaviour under thermal load was compared to CEM II/B-M 42,5 R and CEM I 42,5 N + 25% SF. For properties testing under thermal load prisms were prepared according to EN 196-1 with standard sand. The workability of CEM I 42,5 N + 25% SF was reduced, but to maintain the same water content and other properties SP was not added. Samples were exposed to three different thermal regimes. The first and second regime was heating up to temperature 200 and 250°C temperature dwells 2 hours, heating rate 5°C/min and natural cooling, the third regime was according to modified ISO 834 fire curve with maximum temperature 1050°C. Weight loss in the case of samples from laboratory conditions (20°C) is due to free water evaporation when exposed to 50°C. The temperature for removal of free water was set to 50°C as the chemical changes start from heating to 70°C (Ettringite). Samples were dried for several days until the constant mass was not obtained, and the weight change after 1 hour does not differ more than 0,1%. Properties of samples exposed to elevated temperatures are presented in Tab. 13, Tab. 14, Tab. 15 and Fig. 72.

Tab. 13: Properties of used cementitious binders under thermal exposure – CEM I-42,5 N-SR5

CEM I-42,5 N-SR5	Density	Compressive strength		Flexure strength		Weight loss
	[kg/m^3]	[N/mm^2]	[%]	[N/mm^2]	[%]	[%]
20°C	2263	60,0	100,0	7,8	100,0	2,5
200°C	2048	65,4	109,0	7,6	98,2	7,6
250°C	2069	69,7	116,3	9,3	119,9	7,8
1050°C	2063	6,7	11,1	0,5	6,1	10,0

Tab. 14: Properties of used cementitious binders under thermal exposure – CEM II/B-M 42,5 R

CEM II/B-M 42,5 R	Density	Compressive strength		Flexure strength		Weight loss
	[kg/m^3]	[N/mm^2]	[%]	[N/mm^2]	[%]	[%]
20°C	2315	55,1	100,0	7,1	100,0	3,2
200°C	2097	65,0	118,0	6,6	93,1	7,0
250°C	2058	69,3	125,8	10,5	147,3	8,1
1050°C	2028	6,0	10,9	0,6	9,0	9,8

Tab. 15: Properties of used cementitious binders under thermal exposure – CEM I-42,5 N-SR5 + 25% SF

CEM I 42,5 N + 25% SF	Density	Compressive strength		Flexure strength		Weight loss
	[kg/m^3]	[N/mm^2]	[%]	[N/mm^2]	[%]	[%]
20°C	2186	62,4	100,0	7,8	100,0	2,1
200°C	2066	74,1	118,6	7,2	92,3	6,0
250°C	1939	52,0	83,3	5,1	65,0	9,3
1050°C	BROKEN					10,2

Based on results from weight loss and compressive strength it can be concluded that there was more free water evaporable at 50°C in CEM I-42,5 N-SR5 (CEM I) and CEM II/B-M 42,5 R (CEM II/B) mixes. Mix CEM I 42,5 N + 25% SF (CEM I+SF) bonded more water in its chemical structure which was released in a larger amount only after exposure to 250°C. If the assumption is based on the fact that all free water evaporated during the drying to 50°C, and only chemical changes of Ettringite and CSH gel took place between 20 to 200°C, it could be concluded higher content of CSH gel in CEM I. CEM II/B released the highest amount of free

water during the drying, 32,7%, and lower amount of water bonded predominantly in Ettringite and CSH gel, which evaporates between 70 to 200°C. Mix CEM I+SF consumed for hydration more water that was not released up to heating to 250°C. Between 200°C and 250°C weight was reduced by 3,3%, which is most probably connected to the release of chemically bonded water from products formed by SF, possibly dense CSH gel.

Due to the increase of temperature, additional hydration took place, and all mixes gained strength between 9,0 to 18,6%. The highest increase of compressive strength was recorded by CEM II/B, 25,8% equal to 14,2 MPa caused by an acceleration of fly ash reaction with calcium hydroxide and new formation of hydration products. Flexural strength of CEM I and CEM II/B increased due to thermal exposure to 250°C by 19,9% and 47,3%, and as connected again to additional hydration of clinker and fly ash. Flexural strength of CEM I+SF was reduced by all heating regimes, and phenomena of strength gain were recorded only in case of exposure to 200°C.

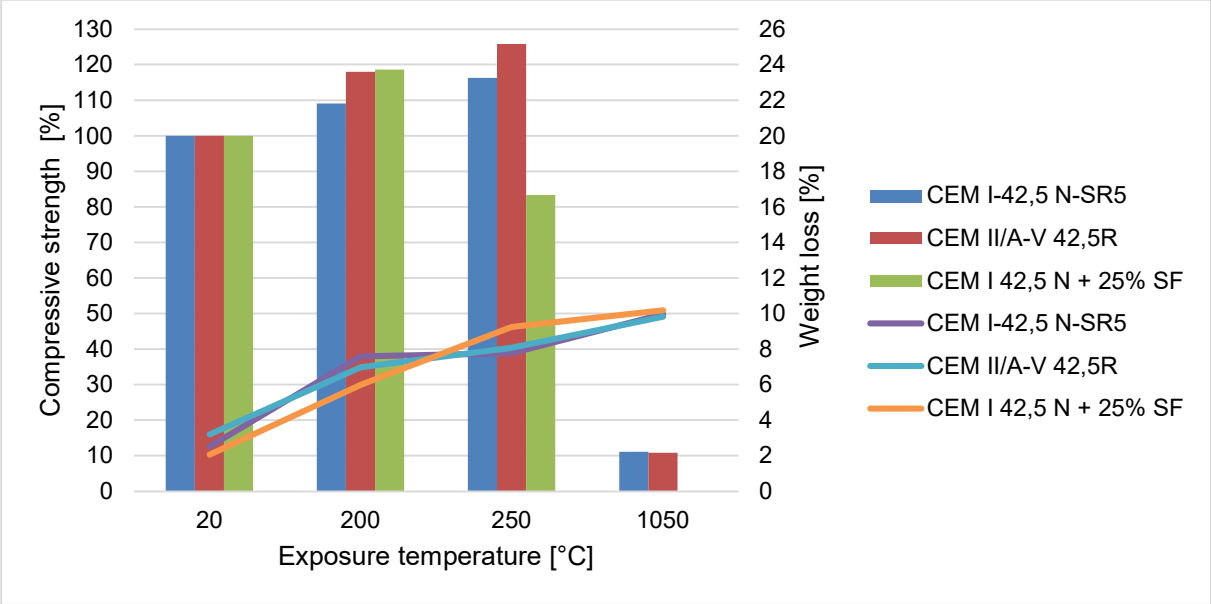

Fig. 72: Relation between compressive strength and water loss due to exposure to 200, 250 and 1050°C.

Exposure to the heating regime according to ISO 834 caused the complete disintegration of CEM I+SF samples caused by rapid water release from dense microstructure formed by silica fume. Silica fume has a high specific surface area, and spherical particles can clog gel pores resulting in dense binder. Thermal exposure with rapid temperature development leads to high pressure build-up leading to cracking and spalling of cement paste.

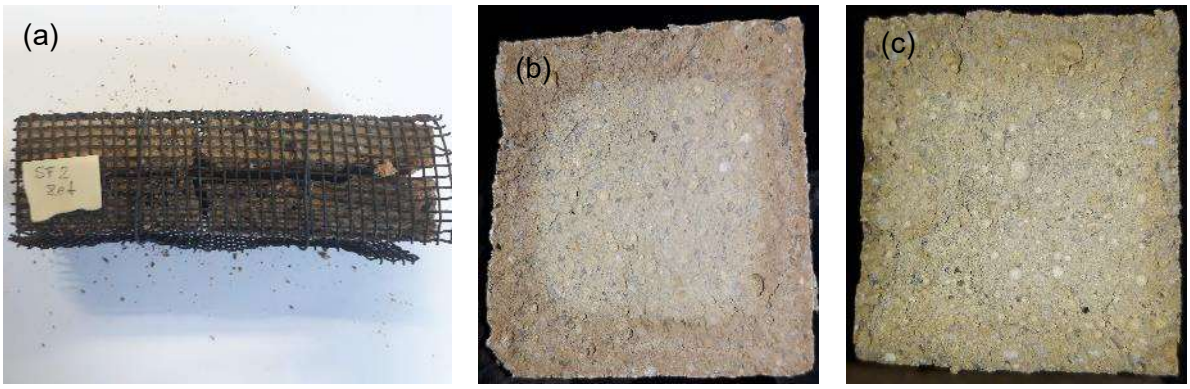

Fig. 73: Samples after thermal exposure: (a) CEM I 42,5 N + 25% SF after exposure to 1050°C; (b) Sample exposed to 1050°C and depth of heat penetration demonstrated by colour change; (c) Sample heated to 250°C, depth of heat penetration is less visible.

Standard sand is quartz sand, which is susceptible to the transformation of the quartz from the α to β polymorph at 573°C accompanied by volume change by 0,85%, also contributing to sample degradation and strength loss when exposed to ISO 834 fire regime.

6.1.5 Admixtures

Throughout the whole testing, two types of admixtures were used, namely two types of superplasticizer (SP) and three types of air-entraining agents (AeA). Work was focused on the development of IHT method, the contribution of dispersed fibres and AeA to fire resistance of concrete, and thus the influence of SP on concrete behaviour under thermal load was not investigated. The SP was exclusively used for fresh concrete properties adjustment. Both SPs are polycarboxylate (PCE) based and supplied by BASF.

Tab. 16: Properties of used superplasticizers

Producer	BASF	BASF
Name of product	MasterGlenium SKY 830*	MasterGlenium SKY 615*
Colour	Light brown liquid	Light brown liquid
Type	Polycarboxylate	Polycarboxylate
Dry content	22 ± 1,0%	19,6 ± 1,0%
Density	1040 ± 20	1050 ± 20
Chloride content	< 0,01%	< 0,01%
Equivalent Na2O	< 2,00%	< 1,00%
Dose	0,2-2,0% of cement	0,5-1,5% of cement

**Technical data sheets for SP´s are listed in references in the same order as SP´s in table* (214, 215).

Three types of AeA were used for the development of AeA-FiResCrete; standard AeA based on surface tension from BASF, and two “new generation AeA” based on the chemical reaction from Sika, and micro hollow spheres polymer-based AeA from MC-Bauchemie. Properties of all three types of AeA are presented in Tab. 17.

Tab. 17: Properties of used air-entraining agents

Producer	BASF	MC-Bauchemie	Sika
Name of product	MasterAir 11	Centrament Airpolymer	SikaControl AER-200 P
Colour	Yellowish liquid	White paste	Silver-greyish powder
Type		Elastic micro hollow spheres	Blend of calciumcarbonate and alloy powder
Dry content	10 ± 1,0%	-	-
Density	1020 ± 30	1000	1200
Chloride content	< 0,10%	< 0,10%	< 0,10%
Equivalent Na2O	< 1,00%	< 0,50%	< 1,00%
Dosage	0,02-0,1% of cement	7 kg	0,4-1,5% of cement

**Technical data sheets for AeA´s are listed in references in same order as AeA´s in table* (154, 216, 217).

Fig. 74: Photo documentation of air-entraining agents: (a) MasterAir 11; (b) Centrament Airpolymer; (c) SikaControl AER-200 P.

6.2 Design of mixes

Several different series of concrete types have been prepared and tested within this research. The main approach of mix design is to keep constant all properties besides those that are investigated, in other words, (i) various types of concrete – IHT method; (ii) various type and a dose of air-entraining agent – AeA-FiResCrete. Due to the high variability of series, involved parameters and factors, general rules for individual methods were established. The design rules are based and controlled by variable input materials, their dose, and the properties of fresh and hardened concrete. The marking system is consistent within individual series, not throughout the whole laboratory work. This section introduces only the design rules, amount of concrete series for each method and control parameters.

For processing of the mix design, the program ComPose5, developed at the Innovation Center Iceland, was used and this is able to take into account water absorption and moisture content of aggregates. Icelandic aggregates have high water absorption (see Tab. 9, Fig. 63), and it is necessary to consider this parameter during the calculation of mix proportions.

6.2.1 Mix design for IHT method

For the development of the IHT method 4 various series of concrete were prepared with an emphasis on various type of cement paste, aggregates and compressive strength to cover most common concrete types used currently and in the past 50 to 100 years. Also, fire spalling is a phenomenon more common for new types of concrete, for instance high-performance concrete or ultra-high performance concrete. Individual series will first be described in words, followed by design rules in tables for better clarity.

- IHT method 1st series: One type of high strength concrete class C65/80 with unknown mix design. Input materials were CEM II/A-LL 42,5 R, superplasticizer, and natural sand fraction 0-4 mm, coarse granite aggregates fraction 8-16 mm and 11-22 mm. Series was used for testing of exposure temperature and evaluation of modification and chemical changes of porous structure.
- IHT method 2nd series: One type of concrete in strength class C45/55 with the same mix design as used in the fourth series for IHT method development marked as 7NO. Concrete tested in this series is composed of CEM I-42,5 N-SR5, superplasticizer and Granite_NO aggregates. Series was used for evaluation of a narrowed selection of exposure temperature with various exposure length, and subsequent evaluation of porous structure modification and changes in mineralogy.
- IHT method 3rd series: The third series consists of 3 different mortars with various cement types and SCM. Samples were prepared in the same way as for standard mortar testing according to EN196-1, and the only variable is binder type: CEM I-42,5 N-SR5, CEM II/B-M 42,5 R and CEM I 42,5 N + 25% SF. The content of sand and water was kept constant. Series was used for evaluation of different exposure temperatures, different exposure length, and after application of IHT method performance in thermal load according to modified ISO 834 curve (described in 6.5.2). Based on the results from the 3rd series, the best suitable configuration of IHT method was selected.
- IHT method 4th series: The fourth series of concrete mixes consists of the same cement types as the third series, namely CEM I-42,5 N-SR5, CEM II/B-M 42,5 R and CEM I 42,5 N + 6% SF, superplasticizer, Basalt_IS and Granite_NO aggregates fraction 0-8 mm, 8-16 mm and 8-22 mm. This series was further divided into 2 groups to further evaluate (i) selected exposure temperature and exposure length, and (ii) large scale testing on one-side heated uniaxially loaded concrete slabs. Samples from both groups with applied IHT method were exposed to thermal load according to modified ISO 834 curve and compressive strength used as control parameter.

Rules for mix design of mixes for IHT method series 3 and 4 follow in Tab. 18 and Tab. 19.

Tab. 18: Mix design rules and criteria for IHT method 3rd series

IHT method 3rd series	Input material		Concrete properties			
	Type	Dose	Fresh		Hardened	
Cement	VARIABLE	CONST.	Consistency	VARIABLE	Compressive strength class	CONSTANT*
SCM	CONST.	CONST.	Air content	-	Air content	-
Aggregates	CONST.	CONST.				
w/c ratio	-	CONST.				
SP	-	-				
Fibres	-	-				
AeA	-	-				

*The property was not completely constant, but in the narrow value range, so that it could be excluded from variables.

Tab. 19: Mix design rules and criteria for IHT method 4th series

IHT method 4rd series	Input material		Concrete properties			
	Type	Dose	Fresh		Hardened	
Cement	VARIABLE	CONST.	Consistency	VARIABLE	Compressive strength class	VARIABLE
SCM	CONST.	CONST.	Air content	CONST.*	Air content	CONSTANT*
Aggregates	CONST.	CONST.				
w/c ratio	-	VARIABLE				
SP	CONST.	VARIABLE				
Fibres	-	-				
AeA	-	-				

*The property was not completely constant, but in the narrow value range, so that it could be excluded from variables.

6.2.2 Mix design for the development of AeA-FiResCrete

Three different AeA based on different technologies were used. Standard type AeA was compared to new types AeA based on chemical reaction and introduction of hollow polymer micro spheres. Due to different mechanisms of pore structure formation, it was highly challenging to keep constant air content of fresh concrete. Moreover, polymer microsphere might not be measurable with standard pressure method, and measured air content in fresh concrete could be misleading.

Tab. 20: Mix design rules and criteria for AeA-FiResCrete

AeA-FiResCrete	Input material		Concrete properties			
	Type	Dose	Fresh		Hardened	
Cement	CONST.	CONST.	Consistency	CONST.*	Compressive strength class	CONST.*
SCM	-	-	Air content	VARIABLE	Air content	VARIABLE
Aggregates	CONST.	CONST.				
w/c ratio	-	VARIABLE				
SP	CONST.	VARIABLE				
Fibres	-	-				
AeA	VARIABLE	VARIABLE				

*The property was not completely constant, but in the narrow value range, so that it could be excluded from variables.

6.3 Description of the test methods

Extensive laboratory testing was performed during the experimental work focused on the development of three different fire-resistant methods for concrete structures. Individual input tests were used for verification of (i) properties and behaviour of individual materials under thermal load; (ii) properties of fresh concrete and influence of mix design modification on fresh concrete performance; (iii) properties of hardened concrete before, during and after thermal exposure. Some tests were performed according to European EN standards, American ASTM standards or the guidelines for more advanced analyses. Other tests, for which there was no available standardised methodology, mostly fire testing, test setups and methodologies were developed with respect to previously published studies in the field of fire resistance of concrete. Fire resistance testing is highly dependent on the available equipment, and it is important to keep in mind that some tests can be performed in an extension of the equipment performance.

Tests used for individual input materials and fresh concrete properties will be described in separate chapters, 6.3.1 and 6.3.2. Tests and analyses performed on hardened concrete will be described in chapter 6.3.3 and for better understanding graphically assigned to individual methods, IHT method and AeA-FiResCrete, see Tab. 21, Tab. 22 and Tab. 23. Finally, the detailed description of fire test setup for one-side heated slabs will be given as it was used in the final stage of all three developed methods.

6.3.1 Tests for individual input materials

Those tests serve mostly for understanding the performance of individual input materials in normal ambient and elevated temperatures up to 1050°C. Sometimes it is difficult to recognise the true cause of deterioration of concrete due to thermal exposure and decoupling of individual materials is one way, to gain better understanding, and be able to include all individual factors in the final evaluation of results from laboratory testing. The most significant components of concrete are aggregates and cement paste, which also are pre-disposed to present the most significant changes due to thermal exposure, and therefore those two components are tested individually. The European standard EN12620:2013 Aggregates for concrete (218) describes all tests required for aggregates used in concrete production. The methods for testing cement are described in multi-part document EN196 (219). European standards are generalised, so there is not a direct reference to any country as EN standards from various European countries were used.

Particle size distribution

The test for geometrical properties of aggregates is described in European standard EN933-1:2012 (218). The procedure consists of washing, drying and sieving of the test sample. The amount of test sample is different for each aggregate fraction. The ventilated oven is used for drying of the sample. It is thermostatically controlled to maintain a temperature of 110 ± 5°C. Sieving is performed using a standard sieve set described in EN933-2:1996 (220), where the regulations for other sieves are also mentioned, which could be used if required.

Water absorption and density

For evaluation of water absorption and particle density EN1097-6:2013 (221) was used. The size of the sample for each fraction is described along with the different methods for the determination of water absorption of fraction 0-4 mm and bigger fractions of aggregates. Three different particle density parameters (oven-dried particle density, saturated and surface dried particle density and apparent particle density) and water absorption are determined after a soaking period of 24 h. Water absorption and particle density are crucial for Basalt_IS as those aggregates are characterised by high porosity connected to high water absorption. Water absorption of Basalt_IS is commonly over 1% and plays a major role in freeze-thaw resistance of concrete. Water absorption limits for aggregates considered as freeze-thaw resistant is less than 1%.

Fines content

The formula for fines content determination is given in EN standard EN933-1. Fines content is calculated from the difference between sample mass before and after washing on sieve 0,063 mm and material in the pan. Content of fines is also possibly obtained from dry sieving; in this case, only the material in pan passing 0,063 mm sieve is considered in the calculation. The result of fines content is expressed in %.

Resistance to fragmentation of coarse aggregate

Methods for the determination of resistance to fragmentation are described in EN1097-2:2020. The reference method, Los Angeles test, was selected, and extended by sieving of the remaining material in fraction 1,6-14 mm to gain its particle size distribution. The Los Angeles test (LA test) is conducted on a 5 000 ± 5 g sample prepared from two different fractions, 10-11,2/12,5 mm and 11,2/12,5-14 mm in ration 60:40 or 70:30. The testing drum with a predefined amount of steel balls is presented in Fig. 75 (b). After exposure of aggregates test sample to crushing in the drum, remaining material is sieved on sieve 1,6 mm, and the weight of the material with particles bigger than 1,6 mm is recorded, and use for calculation of LA value.

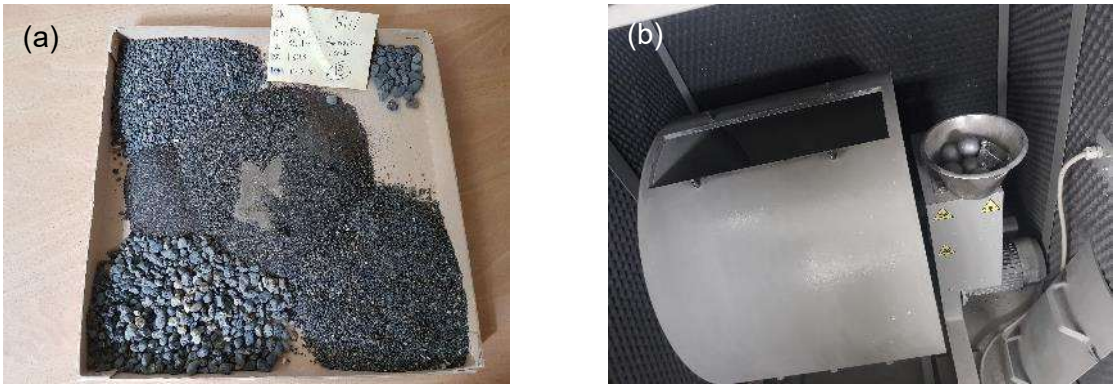

Fig. 75: Test methods for aggregates properties determination: (a) aggregate sample after particle size analysis; (b) equipment for Los Angeles test.

Preparation of cement mortar samples

Preparation of test samples, mixing procedure, casting, hardening, conditioning is described in EN196-1:2016 (222). Samples for testing of cement mortar or binder, which is prepared with partial replacement of cement by supplementary cementitious materials are composed of cement or SCM, CEN standard sand and water. The proportion by mass shall be 1 : 3 : 0,5 of cement : CEN standard sand : water, with w/c ratio 0,5. Each batch for three test samples shell consists of 450 ± 2 g of cement, 1 350 ± 5 g of CEN standard sand and 225 ± 1 g of water. Replacement of cement by SCM should be made by weight if the density of both materials is the same. If the density of cement and SCMs differs significantly, replacement by volume is recommended. Mortar is mixed according to prescribed procedure and then cast in the moulds with dimensions 40 × 40 × 160 mm. After hardening in moulds samples are stored in water at 20 ± 1°C until the determination of strength is carried out.

Density of cement mortar

The determination of cement mortar density was calculated from dimension measurement and weight of the hardened sample. As the weight of samples was used for determination of water loss due to thermal exposure, reference weight was recorded on samples in saturated surface dry conditions. Weight of samples in dry condition was recorded after drying in the oven with a thermostatically controlled temperature 50°C. Those samples were referred to as samples with 0% content of free water. Weight recorded after thermal exposure was specified by maximum exposure temperature.

Flexural and compressive strength

Determination of strength properties of cement mortar was performed according to EN196-1:2016 (222). Measurement of sample dimension and weight took place before the flexural strength test. The loading rate during the test was 50 ± 10 N/s. For compressive strength determination with the loading rate 2 400 ± 200 N/s two halves of specimen broken during the flexural strength testing were used. The test results are calculated with the use of formulas given in EN196-1:2016, and expressed as the arithmetic means of three samples in case of flexural strength and six samples for compressive strength and expressed to the nearest 0,1 N/mm^2.

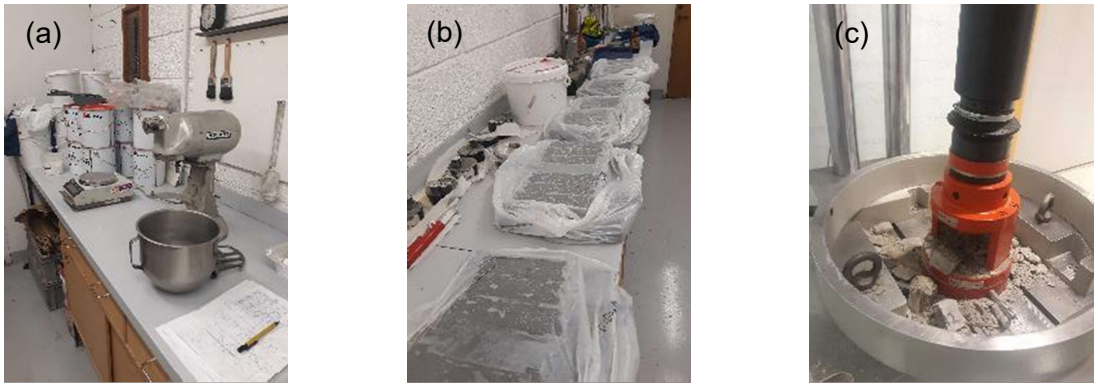

Fig. 76: Test methods for cementitious binder properties determination: (a) mixing equipment for cement mortar samples; (b) hardening of samples between casting and demoulding; (c) compressive strength testing equipment.

6.3.2 Tests performed on fresh concrete

All concrete types prepared during this research, from both approaches, namely IHT method development (2nd, 3rd and 4th series) and AeA-FiResCrete, were tested in a fresh state. As laboratory work took place in several different locations, various mixers were used, but tests for consistency, air content and density were always performed according to EN standards stated in EN206:2013+A1:2016 (223).

Consistency by slump test

Consistency of fresh concrete was tested according to EN12350-2:2019 (224). The slump flow test is the most common test for consistency determination. A test cone is placed on a flat, levelled and moist surface and filled in three layers, where each layer is compacted by 25 pokes with a stick. When the filling is completed, the cone is lifted, and the difference between height of the cone and highest point of concrete is measured and expressed to the nearest 10 mm. If the value exceeds 220 mm, the flow table test shall be considered.

Density

The density of fresh concrete is measured according to EN12350-6:2019 (225). A bucket for air content pressure test with a known volume, 8 l, and weight was used. Filling of the bucket followed the procedure described in EN12350-6:2019 and EN12350-7:2019, three layers, with compacting of each by 25 pokes with a stick. After filling and leveling of the surface, the weight of bucket with concrete is recorded. The density of fresh concrete is calculated and expressed to the nearest 10 kg/m^3.

Air Content pressure test

Air content in fresh concrete is measured according to EN12350-7:2019 (226). A bucket for air content measurement is filled in three layers, with compacting of each by 25 pokes with a stick. After the removal of excessive concrete, the top part of the bucket is placed, and test performed. Content of air in fresh concrete is expressed in % to the nearest 0,1%.

Preparation of samples

Preparation of individual samples took place after the performance of fresh concrete testing, and it was carried out according to EN12350-1:2019 (227). Compacting of samples was done either by compacting of three layers with steel stick by 15 pokes, or compacting on a vibration table. After filling up the mould with concrete, samples were covered with plastic foil, and left to harden for 24 hours. Samples were removed from moulds after 24 hours and moved to the climate chamber with 20 ± 1°C and 100% relative humidity, where they remained until the hardened concrete testing.

Fig. 77: Test methods for fresh concrete properties determination: (a) concrete mixer Gustav Eirich; (b) slump test; (c) equipment for air content pressure test.

6.3.3 Tests performed on hardened concrete

All concrete types prepared during this research, from both approaches, namely IHT method development (1st, 2nd, 3rd and 4th series) and AeA-FiResCrete, were tested in a hardened state. As laboratory work took place in several different locations, various tests were performed on various mixers. Standardised tests were performed according to test procedures stated in EN206:2013+A1:2016 (223), according to ASTM, and guidelines for the test procedure. The new test setup was developed for one-side thermally loaded concrete slabs with uniaxial loading.

Measuring of samples

All samples prepared for standardised tests, which are listed among the others for fresh concrete in EN206:2013+A1:2016 were prepared in conformity to EN12390-1:2012 (228). The volume was determined by measuring of real dimensions of samples.

Density and water absorption

In EN standard EN12390-7:2019 (229) three different methods for volume determination are presented, and throughout this entire work, the measuring of real dimensions of samples was used. Water absorption was determined by drying the sample in an oven with a thermostatically controlled temperature 50°C and measuring their weight. Those samples were referred to as samples with 0% content of free water. Weight recorded after thermal exposure was specified by maximum exposure temperature. Density is expressed in kg/m^3 to nearest 10 kg/m^3, and water absorption in % to the nearest 0,1%.

Compressive strength

Compressive strength is performed according to EN12390-3:2019 (230) on standardised samples described in EN12390-1:2012 unless the size of sample was changed for thermal exposure testing. Samples were loaded perpendicularly to compacting direction by rate 0,6 ± 0,2 MPa/s (N/mm^2·s). The maximal recorded load in kN was used for calculation of compressive strength expressed in MPa (N/mm^2) to the nearest 0,1 MPa (N/mm^2).

Air void characteristics

For determination of air void characteristics in hardened concrete two different methods were used. The first method followed ASTM C457/C457M (232), Procedure B: Modified Point-count method, and was used during laboratory work at Innovation Center Iceland. The second method followed EN480-11:2005 (233) and was used during the laboratory work at Brno University of Technology. The result after processing of raw data are used for calculation of Spacing factor (L) related to the maximum distance of any point in the cement paste from the periphery of an air void, measured through the cement paste, units are mm; Specific surface of air void system (α) representing the total surface area of the air voids divided by their volume, and units are mm^{-1}; Total air content (A) expressed as a percentage by volume; Paste content which is the proportion of the total volume of the concrete that is hardened cement paste, expressed as a percentage by volume.

Freeze-thaw resistance

Determination of freeze-thaw resistance was performed according to CEN/TS 12390-9:2016 (234). Preparation of samples cut from cubes with dimensions 150×150×150 mm followed the procedure described in the standard, and sample exposure to time-temperature cycles initiated. Scaled material from samples surface was collected after 7, 14, 28, 42 and 56 cycles. In total, the test takes approximately 90 days. Results are expressed as the mass of scaled material related to the surface area after the n-th cycle in kg/m^2. In the test report, visual assessment of the sample before and after the testing shell also be mentioned.

Thermal analysis

Modern devices commonly combine differential thermal analysis and thermogravimetric analysis, and monitoring temperature and weight of test and inert specimen over the test period. Several phenomena contribute to temperature and weight differences between test and inert specimens such as recrystallization, melting, boiling, oxidation, chemical decomposition or dehydration, which are accompanied by weight changes. Exothermic or endothermic reactions could occur. The output of the measurement is the TGA-DTA diagram with temperature and weight changes of test specimens. The sample for thermal analysis is in powder form, and amount is about 0,065 to 0,1 g.

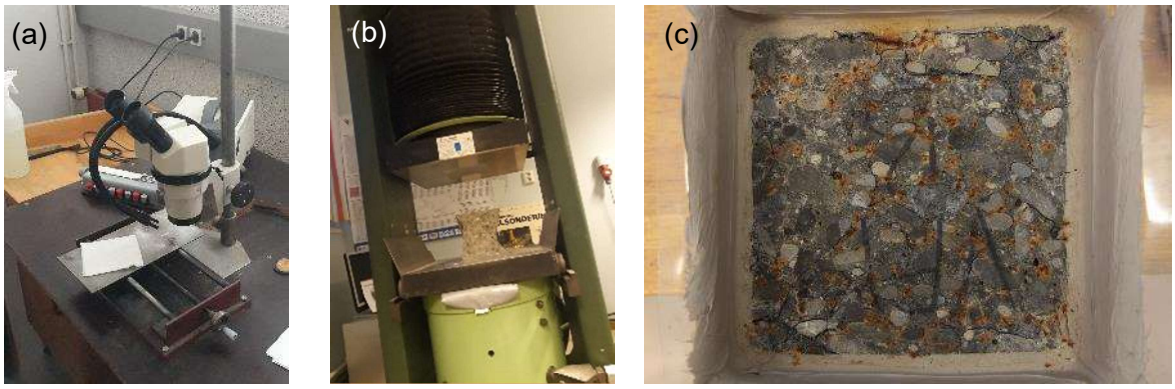

Fig. 78: Standardised test methods for hardened concrete properties determination: (a) test setup for air void characteristics determined according to ASTM C457/C457M; (b) compressive strength testing device; (c) sample after carrying out freeze-thaw resistance test.

Mercury intrusion porosimetry

Mercury intrusion porosimetry (MIP) is a powerful technique utilized for the evaluation of porosity, pore size distribution, and pore volume (among other factors) to characterize a wide variety of solid and powder materials. The instrument, known as a porosimeter, employs a pressurized chamber to force mercury to intrude into the voids in a porous substrate. As pressure is applied, mercury fills the larger pores first. As pressure increases, the filling proceeds to smaller and smaller pores. Both the inter-particle pores (between the individual

particles) and the intra-particle pores (within the particle itself) can be characterized using this technique (235). Analysis is suitable for porous structure in a range from 10 nm to 100 μm.

X-ray diffraction analysis

X-ray diffraction analysis (XRD) is suitable for crystalline materials. This test method is performed by directing an X-ray beam at a sample and measuring the scattered intensity as a function of the outgoing direction (235). Despite XRD analysis being able to provide quantitative information about the tested powder sample, the main information provided is qualitative, and therefore it is highly essential to combine it with thermal analyses.

Visual evaluation by standard camera and optical microscope

Photo documentation is essential, and many details could be recognised with the naked eye, such as crack formation, discolouration or disintegration of the sample. For more detail a visual analysis with an optical microscope, Dino-Lite digital optical microscope, with magnification up to 225 x was used.

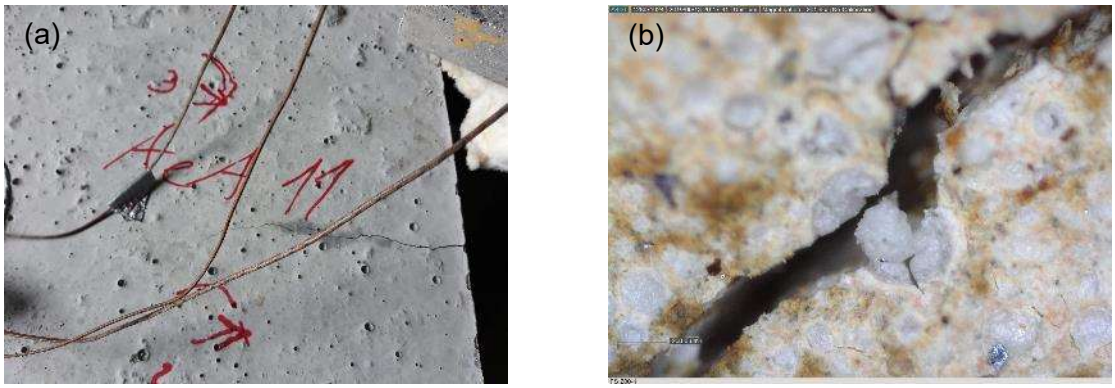

Fig. 79: Photo documentation: (a) Slab after thermal exposure; (b) Detail of crack on the heated surface, magnification 200 x.

6.3.4 Test setup for large scale one-side heated uniaxially loaded slabs

For one-side heating of test slabs an electric oven with an opening from the top was used. The oven was adjusted to a one-side heating test by removal of the top lid and safety sensor for lid opening control. The support frame was built with height-adjustable feet to eliminate the overloading of the oven itself. The test slab weight was approximately 55 kg. The loading frame for the sample was made out of two steel profile HEB 100 fixed together on both ends by two threaded rods, as displayed in Fig. 80 a) and d). Steel profiles HEB 100 are longer than the support frame and made to lean on four points of the support frame. Loading of samples is provided by the pre-stressing of the threaded rods in the horizontal direction, as illustrated by arrows in Fig. 80 a). The steel net and high temperature resistant insolation wool was placed around the rim to prevent heat loss and protect the inner structure of the oven, see Fig. 80 b).

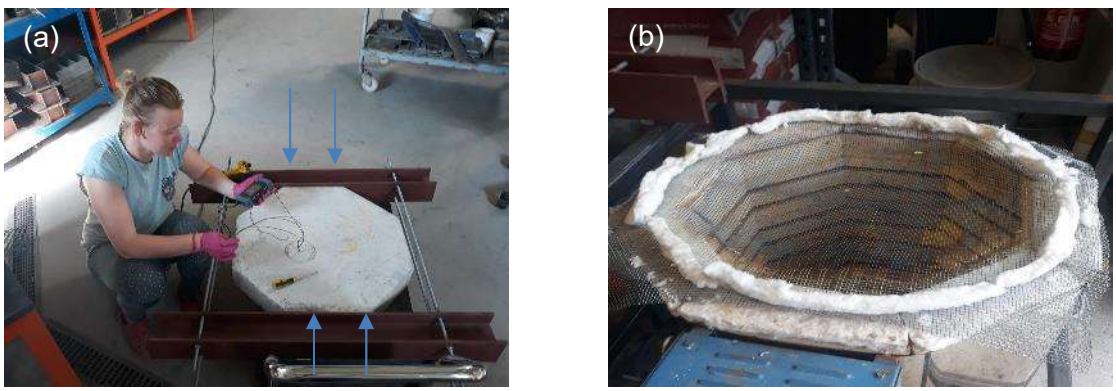

Fig. 80: Test setup for large scale one-side heated uniaxially loaded slabs: a) Uniaxial loading steel profile HEB 100 with prestressed treaded rods, assembling thermocouples and plugging in thermometer log; b) Protection net to prevent damage of the oven by explosive spalling and high temperature insolation wool; c) Load bearing frame serves as a support for loading steel profile HEB 100 in order to prevent overloading of the oven; d) Testing slab placed on load-bearing frame and connected to thermal log.

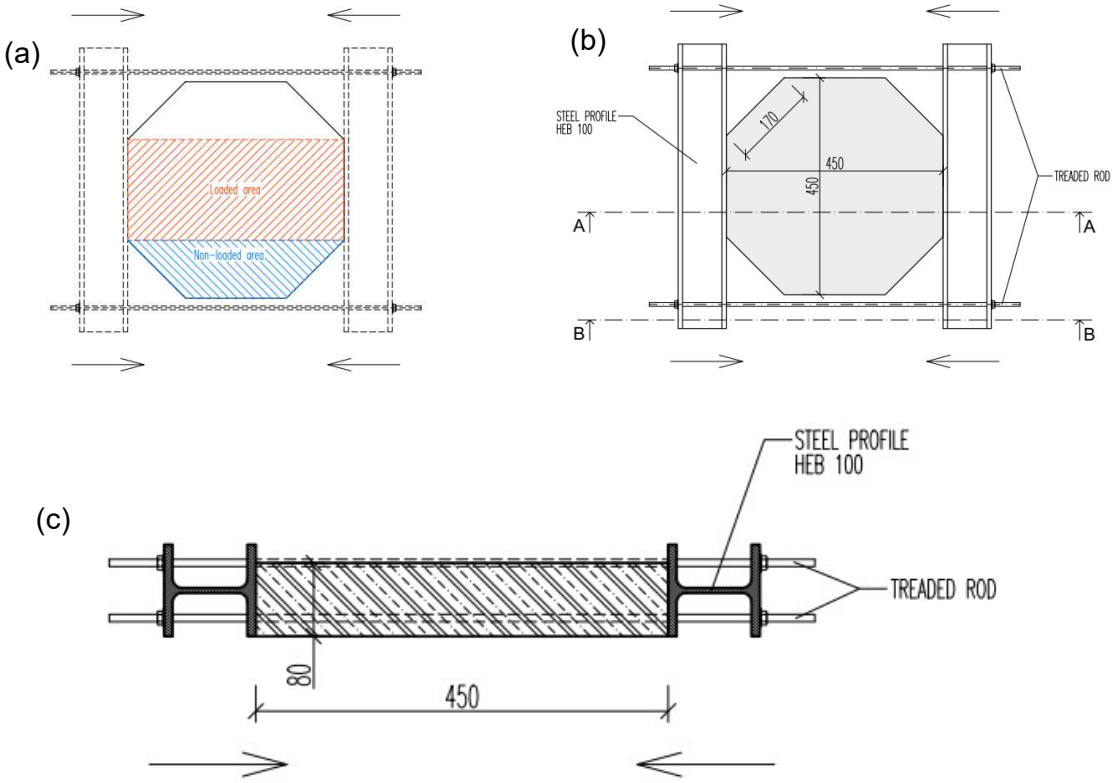

Fig. 81: Schematic drowing of the test slab: (a) The uni-axial loading is applied in central area due to the shape of tested slabs; (b) Dimensions of the test slab; (c) Placement of steel profile HEB 100 and prestressing treaded rods.

Measured parameters during the test are temperature, moisture and crack width during and after fire test. A thermocouple probe monitored the temperature in the oven through the ventilation opening, which was plugged with high temperature resistance wool.

Temperature and moisture measurements

Measurements of temperature development in one-side heated slabs were recorded during the test by integrated thermocouples. As thermocouples were placed in depths 20, 40 and 60 mm, it is possible to calculate the thermal gradient in given depths, which can provide highly useable results. Even the thermal loading of individual slabs was performed in exactly the same manner, temperature development in the oven was slightly different, and therefore it could be misleading to directly compare obtained temperature curves from integrated

thermocouples. Details of installation of thermocouples in the samples is described in section 6.4.1.

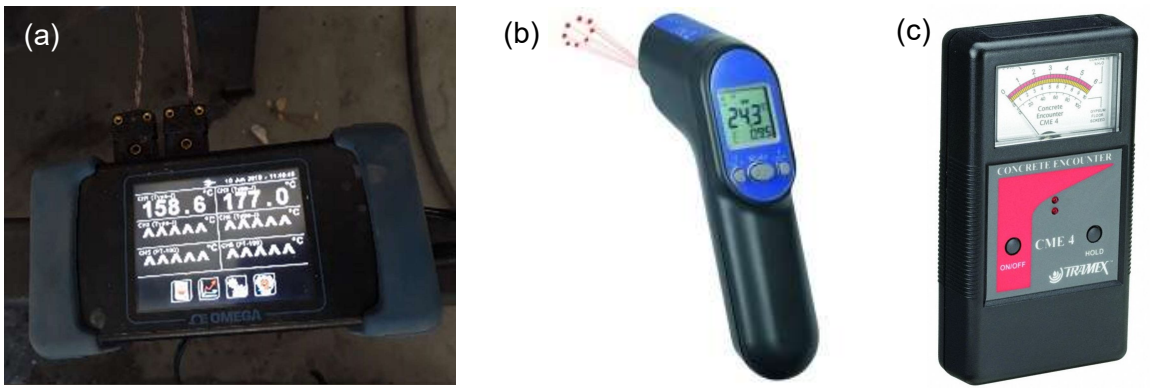

Fig. 82: Equipment for recording temperature and moisture: (a) Omega temperature logger; (b) laser infrared thermometer; (c) Tramex CME4 surface contact moisture-meter.

Crack width and location analysis

Formed cracks on the sides and non-heated surface are measured with a crack width meter during and after heating on all samples with the naked eye or with a microscope. The program used for the Dino-Lite microscope provides functions for measuring distance, area, diameter and other parameters. Even the thermal loading of individual slabs was performed in exactly the same manner, temperature development in the oven was slightly different and imposed some extra processing on the gained data.

Assignment of performed tests to develop methods

The number of performed tests is rather high, and to make whole testing and method development more understandable, individual tests were assigned to individual methods. The system is presented in Tab. 21 and Tab. 22 for IHT method and in Tab. 23 for Fib-FiResCrete and AeA-FiResCrete.

Tab. 21: Test performed in IHT method - 1st series and IHT method - 2nd series

Test	IHT method - 1st series			IHT method - 2nd series		
	Before	During	After	Before	During	After
Measuring of samples	×	-	×	×	-	×
Density	×	-	×	×	-	×
Weight loss	-	-	×	-	-	-
Compressive strength	×	-	×	×	-	×
Tensile splitting strength	-	-	-	-	-	-
Freeze-thaw resistance	-	-	-	-	-	-
Air void system analysis	-	-	-	×	-	-
Differential thermal analysis	×	-	×	-	-	-
Mercury intrusion porosimetry	×	-	×	×	-	×
X-ray diffraction analysis	-	-	-	×	-	×
Visual evaluation	×	-	×	×	-	×
Temperature data logging	-	-	-	-	-	-
Moisture data logging	-	-	-	-	-	-
Crack width analysis	-	-	-	-	-	-

Tab. 22: Test performed in IHT method - 3rd series and IHT method - 4th series

Test	IHT method - 3rd series			IHT method - 4th series		
	Before	During	After	Before	During	After
Measuring of samples	×	-	×	×	-	×
Density	×	-	×	×	-	×
Weight loss	-	-	-	-	-	-
Compressive strength	×	-	×	×	-	×
Flexural strength	×	-	×	-	-	-
Tensile splitting strength	-	-	-	-	-	-
Freeze-thaw resistance	-	-	-	-	-	-
Air void system analysis	-	-	-	×	-	-
Differential thermal analysis	-	-	-	-	-	-
Mercury intrusion porosimetry	-	-	-	-	-	-
X-ray diffraction analysis	-	-	-	-	-	-
Visual evaluation	×	-	×	×	-	×
Temperature data logging	-	×	-	-	×	-
Moisture data logging	-	-	-	×	×	×
Crack width analysis	-	-	-	×	×	×

Tab. 23: Test performed in AeA-FiResCrete

Test	AeA-FiResCrete		
	Before	During	After
Measuring of samples	×	-	×
Density	×		×
Weight loss	×		×
Compressive strength	×	-	×
Tensile splitting strength	-	-	-
Freeze-thaw resistance	×	-	-
Air void system analysis	×	-	-
Differential thermal analysis	-	-	-
Mercury intrusion porosimetry	-	-	-
X-ray diffraction analysis	-	-	-
Visual evaluation	×	-	×
Temperature data logging	-	×	-
Moisture data logging	×	×	×
Crack width analysis	×	×	×

6.4 Samples prepared for testing

Samples were produces in various shapes and dimensions. Some samples were prepared to fulfil standard testing requirements, and some in size to fit testing equipment. For better comprehension, a list of all prepared samples, their dimensions and the test method they are for, are presented in

Tab. 24.

Compressive strength was used as a main parameter for IHT method development, and thus various shapes and dimensions of samples were used.

Tab. 24: Overview of all prepared and tested samples

Test	Type of sample	Parameters				
		a	b	c/h	Ø	m
		[mm]	[mm]	[mm]	[mm]	[g]
Density	All samples	-	-	-	-	-
Compressive strength	cylinder	-	-	200	100	-
	cylindre	-	-	300	150	-
	cube	150	150	150	-	-
	cubes	100	100	100	-	-
	1/2 prism	40	40	160	-	-
Flexural strength	prism	40	40	160	-	-
Tensile splitting strength	cylinder	-	-	300	150	-
Freeze-thaw resistance	sample	50	150	150	-	-
Air void system analysis	sample	50	150	150	-	-
Differential thermal analysis	powder	-	-	-	-	50
Mercury intrusion porosimetry	small piece	10	10	10	-	-
X-ray diffraction analysis	powder	-	-	-	-	10
Visual evaluation	all samples	-	-	-	-	-
Temperature data logging	slab - prism with octagonal base	-	-	80	450	-
Moisture data logging	slab - prism with octagonal base	-	-	80	450	-
Crack width analysis	all samples	-	-	-	-	-

To be able to record temperature development during the fire tests, thermocouples type K were placed in exact depths and positions during casting. As it is rather difficult to record temperature and heat spread during the fire testing, the maximum temperature in the concrete samples was also verified by DTA analysis, which can detect the amount of chemical components. As those components are created under a certain temperature, the maximum temperature reached in the concrete elements can be estimated.

6.4.1 Thermocouples positioning

Temperature penetration in one-side heated slabs was recorded by a specially design ‘thermocouple tree’, see Fig. 83. The thermocouple tree was always placed in the centre of the slab, and the correct level was ensured by the placement of a plastic disc on the top of the slab. The plastic disc was adjusted to the cable tie sign at 60 mm from the bottom detection point. Each cable was marked, so the measurement in individual depths could be followed.

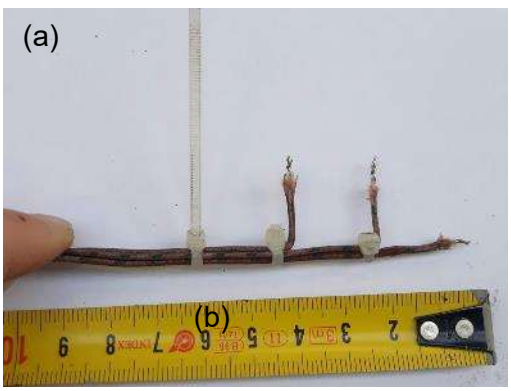

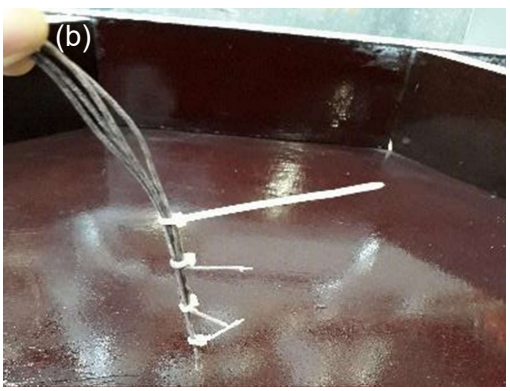

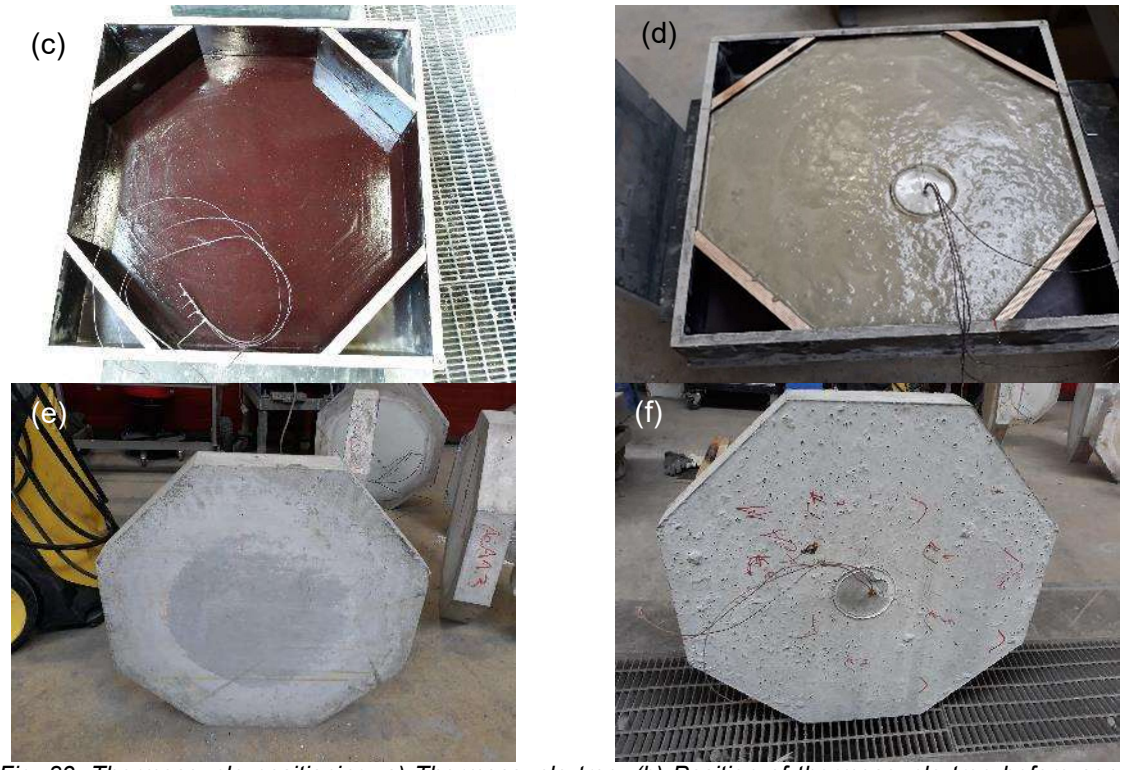

Fig. 83: Thermocouple positioning: a) Thermocouple tree; (b) Position of thermocouple tree before concrete pouring; (c) Mould for casting of the slab; (d) Mould with fresh concrete and placed thermocouple tree; (e) Heated side of the slab; (f) Top surface of the slab with integrated thermocouple tree.

After casting, the test slabs were demoulded after one day and stored in a climate chamber with standard curing conditions 20±1°C and 100% RH for 27 days. Slabs were removed from the curing chamber at the age of 28 day, and place in a laboratory, where they were kept for approximately 12 months until the fire testing took place. The requirement for the slabs was moisture content under 3% measured by surface moisturemeter.

6.5 Regimes for fire testing

Samples were tested either according to the heating regime with defined temperature ramp, maximum temperature and dwell, and cooling, or according to standardised time-temperature ISO 834 curve. Several types of heating regimes were used for the IHT method development. All fire tests were performed in an electric oven, which is highly suitable for defined heating regimes, but has certain limitations when it comes to rapid heat development required by ISO 834. The electrical oven is temperature controlled but for better accuracy, one or two high temperature probes were placed inside the oven in different locations. Overheating or evening of temperature growth could include temperature difference up to 20°C and variation between area on the top or bottom of the oven could also vary based on the sample quantity, Fig. 84.

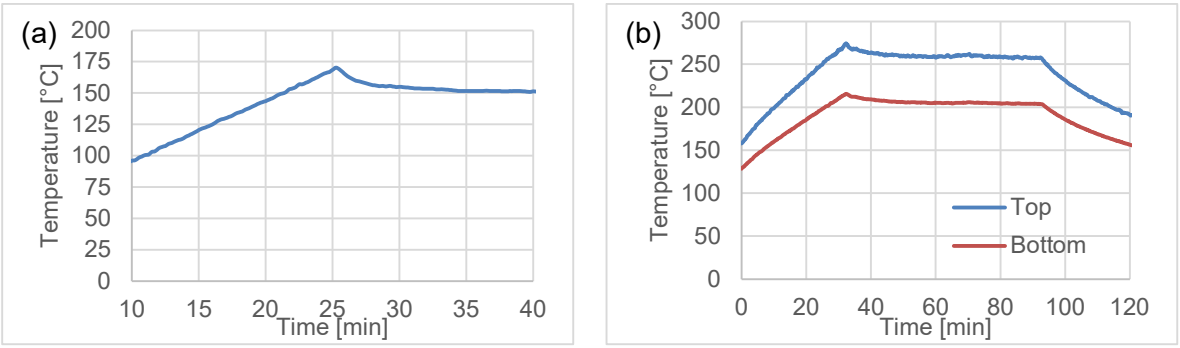

Fig. 84: Imperfection of electrical oven used for experiments: (a) Overheating at start of temperature dwell; (b) difference between temperature measured at the top or bottom area of the oven.

6.5.1 Heating regimes

Heating regimes were used for the analysis of individual phenomena, that are related to specific exposure temperature. Processes such as water evaporation accompanied by water migration, crack formation or even spalling of surface layer, chemical changes coupled with volume changes, and mutual influence of all those factors on the concrete element. Heating regimes used in this research had all the same heating ramp 5°C/min (300°C/hour) and natural cooling. The length of the exposure to maximum selected temperature, so-called temperature dwell, was 60, 120 or 240 minutes (1, 2 or 4 hours).

The development of IHT method consists of several series. In 1st series, which was performed at Rostock University in Germany, maximum exposure temperatures 150, 250, 350 and 450°C were used. Maximum exposure temperatures in the 2nd series were set for 150, 200 and 250°C, and in the 3rd series and 4th series exposure temperatures 200 and 250°C with temperature dwell 60 or 120 min were used.

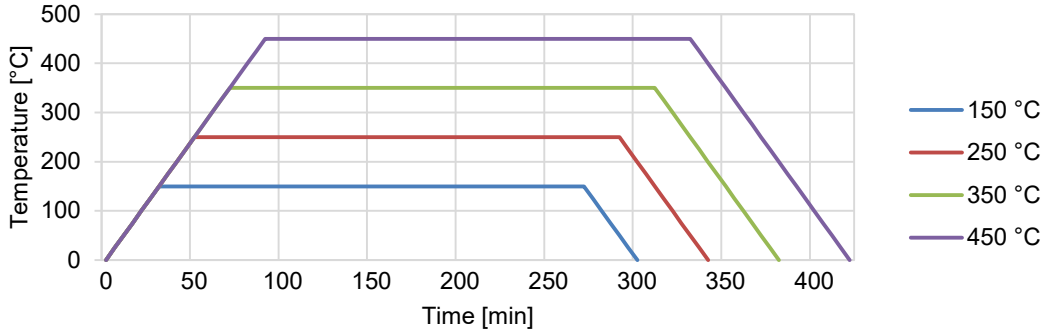

Fig. 85: Heating regimes for development of IHT method 1st series, maximum exposure temperatures 150, 250, 350 and 450°C.

6.5.2 Prescriptive fire regime according to ISO 834

The selected regime for fire testing of concrete was the most common time-temperature curve ISO 834, which has rapid development of temperature in the beginning, approx. 570°C in the first 5 minutes. This rapid heat development was not possible to obtain with available equipment, and therefore samples for fire testing were loaded in the fastes possible rate which the electric oven could develop, see Fig. 86. The attempt was to program the oven according to ISO 834, as visible in Fig. 86, but even with the oven lid it was not possible to follow the desired heating regime. When the lid was replaced with the test slab, temperature gain becomes even slowlier, and therefore the term 'modified ISO 834' (m-ISO curve) will be used throughout this work when referring to the heating regime.

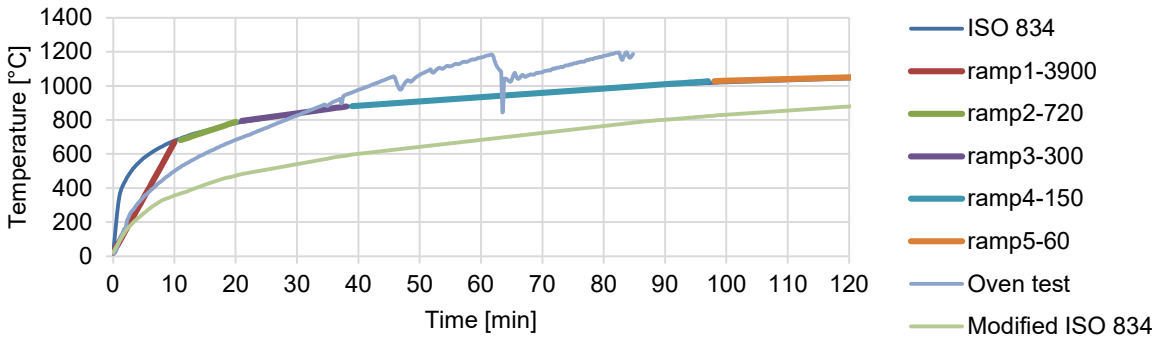

Fig. 86: Modelling of ISO 834 for electric oven set up, test of the oven with a lid, modified ISO 834 with testing slab instead of lid.

Fire testing, according to the m-ISO cure, was performed on smaller samples where they were placed in the oven in a special frame, so they were heated evenly from all sides. The

large-scale testing of uniaxially loaded slabs placed on the top of the oven and heated from one side was also the following m-ISO curve. Volume, presence of samples in the oven, and overall setup strongly influence the heat development, and therefore, fire tests of slabs and samples placed inside the oven were not combined. Each test was performed separately and the number of samples in the oven regulated.

7 CHAPTER: PRACTICAL DEVELOPMENT OF THE IHT METHOD

The development of the IHT method started in Germany under the supervision of Ulrich Diederichs. The main parameters to be defined throughout this testing are the speed of heating, maximum temperature, and length of exposure to designed preheating temperature. The intentional heat treatment (IHT) of the surface layer is supposed to modify the porous structure in surface layer, which is predominantly composed of cement paste and fine aggregates. Concrete is non-homogenous material, and thermal exposure of various sample sizes and concrete types can result in different performance, it is highly challenging to define one setting for the IHT method applicable to all element shapes and concrete types. This work attempts to verify if our innovative method might improve fire resistance. The database of setting and adjustment for individual concrete types could be subject to the further development of the IHT method.

Development of the IHT method was divided into 4 individual parts, namely "1st series: Various temperature analysis on HSC", "2nd series: Various temperature analysis on normal strength concrete", "3rd series: Various temperature and heating length analysis on mortar prisms" and "4th series: Application of IHT200/2 on various types of concrete". The outcome of the 3th series will be exact parameters of the IHT method, which will be applied and verified on various samples in the 4th series and in large scale testing of one-side heated, uniaxially loaded slabs. The same test slabs will be prepared with concrete from the other method, which is being investigated, AeA-FiResCrete, to validate effectiveness of both methods.

The marking system used during the development of the IHT method will be IHT exposure temperature/duration of exposure to selected temperature, an example would be IHT200/2. If it will be referred in general to application of IHT method, the abbreviation IHT_T/t will be used. Structure of data will be the same throughout both methods under development (i) description of action; (ii) mixes; (iii) fresh concrete properties; (iv) hardened concrete properties; (v) fire testing; (vi) conclusion on further developing method.

7.1 The 1st series: Various temperature analysis on HSC

Activities in this chapter were the first attempt to verify the assumption that the intentional heating of the concrete element would modify the porous structure of the surface layer beneficially for fire resistance. In total, 4 cubes with an edge of 150 mm were available for the 1st series of IHT method development. Test specimens for thermal treatment were prepared by the cutting of a cube with an edge of 150 mm into 4 samples with an edge of approximately 73 mm using circular saw. Mix design such as cement dose, w/c ratio, and aggregates proportion is not known, but the input materials are known. Cement CEM II/A-LL 42,5R, granite aggregates, superplasticizer, and water were used as input materials. Samples were older than one year.

Conditioning of samples prior to the thermal exposure testing consisted of 7 days water-storage and 21 days at laboratory ambient (23°C and 50% RH). Reference samples were tested without any thermal exposure. The rest of the samples were exposed to heating regimes with maximum temperature 150, 250, 350 and 450°C. The temperature rise was 5°C/min (300°C/hour), and temperature dwell at maximum exposure temperature was held for 4 hours, followed by natural cooling back to ambient temperature, see Fig. 85. The speed of heating

was selected based on the reviewed literature, and the length of the heating 4 hours was used to gain penetration of the maximum temperature in the whole mass of tested samples. If the exposure temperature had fail to penetrate the whole mass, the results of compressive strength might not be representative for the given exposure temperature. The total length of the IHT method will play significant role for industrial use, and the speed of reaching maximum temperature and its duration is critical.

Half of the thermally loaded samples were directly tested, and the second half were submerged in water for 28 days. Water storage (WS) after IHT_T/t is meant to represent relative humidity to which the concrete structure with IHT_T/t would be exposed in reality. The same tests were performed before thermal treatment, after IHT_T/t, and after IHT_T/t&WS. Monitored properties were weight, compressive strength, porous structure analysed by mercury intrusion porosimetry method (MIP), and identification and quantification of chemical composition by thermal analysis (TGA-DTA). Samples for MIP and TGA-DTA were obtained after compressive strength testing from the surface layer, which is the main objective of the investigation. Furthermore, it is important to mention that the surface layer is predominantly constituted by cement paste and a fine fraction of aggregates, and thus the results of MIP and DTA were evaluated as if they were performed on cement mortar sample. Analysed data are presented in the following sections 7.1.1, 7.1.2, 7.1.3.

7.1.1 Compressive strength and weight changes testing

Changes of samples due to thermal expansion were controlled by weight change. Density or volume changes were not considered relevant as the samples were cut from a bigger sample, and dimensions accuracy was ± 5%. The sample size used for compressive strength is not a standard size (73×73×73 mm), and therefore the samples were compared only within this series and not to any other shape or size samples from other series. The abbreviations used throughout the result dissemination are laboratory condition curing (LAB), application of various configurations of IHT method (IHT_T/t) and water storage (WS).

Weight change was increasing along with the rising exposure temperature. As samples were kept in laboratory conditions prior to the testing, the share of free water evaporation is significant. The release of chemically bonded water of all exposure temperatures starts at 70°C by recrystallisation of Ettringite and CSH gel (in parallel with release of water molecules from interlayer), and the only difference is IHT450/4 with exposure temperature 450°C, where in addition $Ca(OH)_2$ dehydrates. The degree of weight regains due to water storage almost reached the laboratory condition before the thermal testing in the cases of IHT350/4 and IHT450/4 exposure temperature, as can be seen in Fig. 87.

Tab. 25: Data from weight change testing due to IHT_T/t and IHT_T/t&WS.

Marking of sample	Exposure temperature [°C]	Measured weight [g]			Weight change [%]		
		LAB	After IHT_T/t	After TE IHT_T/t&WS	After IHT_T/t	After IHT_T/t&WS	From IHT_T/t to IHT_T/t&WS
IHT150/4	150*	891	851	883	4,5	0,9	3,6
IHT250/4	250	1863	1755	1850	5,8	0,7	5,1
IHT350/4	350	1974	1846	1968	6,5	0,3	6,2
IHT450/4	450	1920	1795	1917	6,5	0,2	6,4

*Due to a limited amount of test samples exposed to temperature 150°C, only one cube, while to other temperatures two cubes.

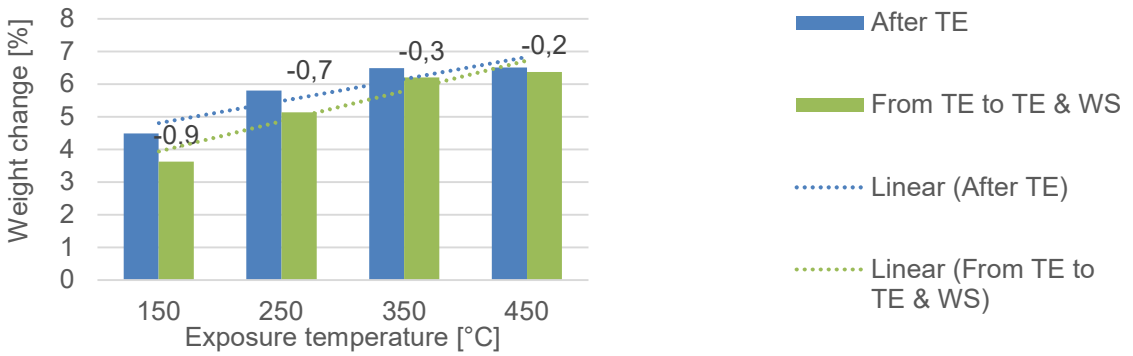

Fig. 87: Graphical representation of results of the weight change due to IHT_T/t and IHT_T/t&WS.

Results from compressive strength testing are presented in Tab. 26 and graphically in Fig. 88. Compressive strength was reduced by thermal exposure, which is most likely caused by the formation of micro-cracks as a result of free water evaporation and chemical changes of Ettringite, CSH gels, and eventually $Ca(OH)_2$ in the case of IHT450/4. Additional hydration of unreacted cement grains in connection to elevated temperature was not recorded as in the research work of Morsy (139). Water storage for 28 days caused further compressive strength reduction of all samples, besides the IHT450/4, where a gain of strength by 22,3% was recorded. Regain of strength due to water storage might be caused by re-formation of Ettringite from the reaction of water with Bassanite and/or γ-anhydrite (113, 236), and additional formation of CSH gel (118, 237). New compounds were formed in pores with diameter from 0,03 to 1 µm as detected by intrusion mercury porosimetry (MIP) and thermal diffraction analysis (DTA), as shown in detail later.

Tab. 26: Results from compressive strength testing and changes due to IHT_T/t and IHT_T/t&WS.

Sample	Compressive strength [N/mm²]		Strength change [%]		
	After IHT_T/t	After IHT_T/t&WS	Due to IHT_T/t	Due to IHT_T/t&WS	Due to IHT_T/t&WS from Ref.
Ref	84,9	84,9	-	-	-
IHT150/4	78,1	61,8	-8,0	-19,2	-27,3
IHT250/4	80,7	53,1	-5,0	-32,5	-37,5
IHT350/4	74,4	58,7	-12,4	-18,4	-30,8
IHT450/4	49,8	68,7	-41,4	+22,3	-19,1

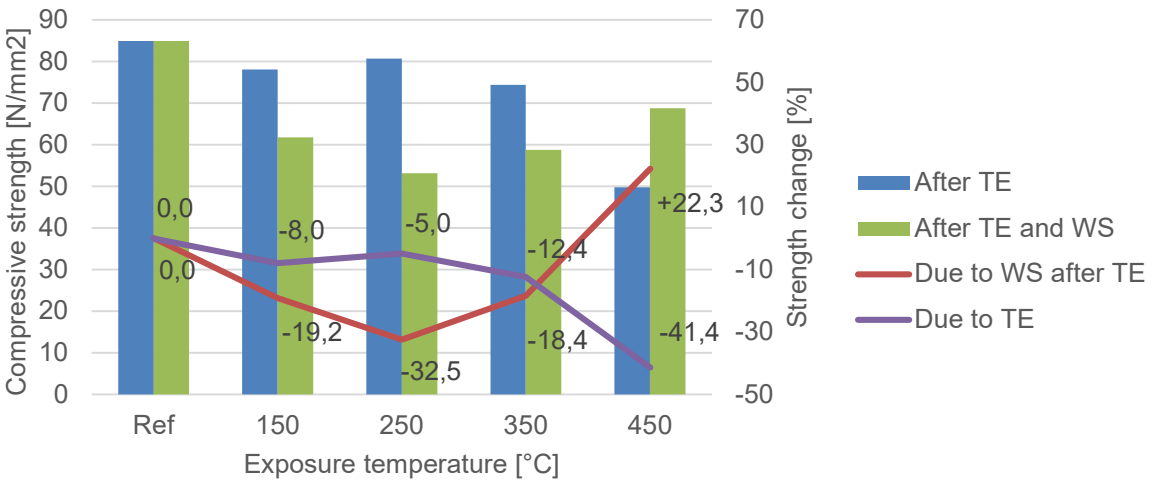

Fig. 88: Graphical presentation of results from compressive strength testing.

The compressive strength reduction of IHT150/4 and IHT250/4 was not significant, but rapidly increased by WS. This fact is crucial, and therefore, it is essential to apply the IHT_T/t only on a thin surface layer where the strength loss would not influence the overall mechanical properties of a concrete element or the entire structure. The fact that in the saturated state in RH higher than 85%, exposure of samples to 100% RH (fully submerged in water) is rather severe as common relative humidity in tunnels is 75% (96). Distribution of water to the inner structure by capillary pore can cause the extensive formation of new compounds and contribute to microcracking due to crystal growth.

Another factor influencing the strength development due to TE and WS is the used cement, CEM II/A-LL 42,5R, which contains limestone fines in dose 6 to 20%. Limestone powder is fine and forms dense structure of cement paste and can additionally hydrate after contact with water and $Ca(OH)_2$ (238, 239). Other influencing factors such as the origin of aggregates, granite, can be neglected as changes of granite starts at 537°C by the transformation of quartz, and tested IHT exposure temperature was maximally 450°C.

7.1.2 Analysis of porous structure by MIP

Porous structure is a decisive factor for fire resistance, and its detailed analyses are essential. Mercury intrusion porosimetry can analyse pores in the range from 10 nm to 100 µm, which is a suitable range for fire resistance evaluation. However, there are researchers who disagree with the principle of MIP as it uses high pressure for filling up the pores by Hg. Pressure up to 0,13 MPa is used to detect larger pores in a range from 60 to 100 µm, and higher pressure, up to 200 MPa, for detection of smaller pores down to 10 nm. Inaccuracy can occur by breaking the pore walls and filling the close pores by applying greater pressure than needed. Despite this phenomenon, the results obtained by MIP correlate well with DTA and strength testing presented in the 1st series.

Results from MIP were processed for individual exposure temperatures, water storage, and pore size. Pores were divided into five groups; gel pore <0,03 µm; capillary pores in three segments, 0,03 to 0,1 µm; 0,1 to 1 µm and 1 µm to 30 µm. One of the reviewed articles states the overlap of gel pores and capillary pores in the area between 0,03 and 0,08 µm, which is fairly understandable. The bigger macropores belong to the last group with a diameter greater than 30 µm. Several approaches could be used to analyse the raw data from MIP testing, and therefore two methods were selected (i) data were processed as a share of total measured porosity, and (ii) as a share in 100% in accordance with total porosity. The first method is more suitable for comparison of results between samples after IHT_T/t and samples after IHT_T/t&WS, see Fig. 89. Processed data are not significantly different, but their comparison could bring up some details, which would be otherwise overlooked. An obvious example is the content of macro capillary pores in a range from 1 to 30 µm, where the amount remains the same if the method (i) is applied. Processing the data by (ii) methods shows that sample after IHT_T/t&WS contains 17,4% more macro capillary pores than sample after IHT_T/t, see Fig. 89.

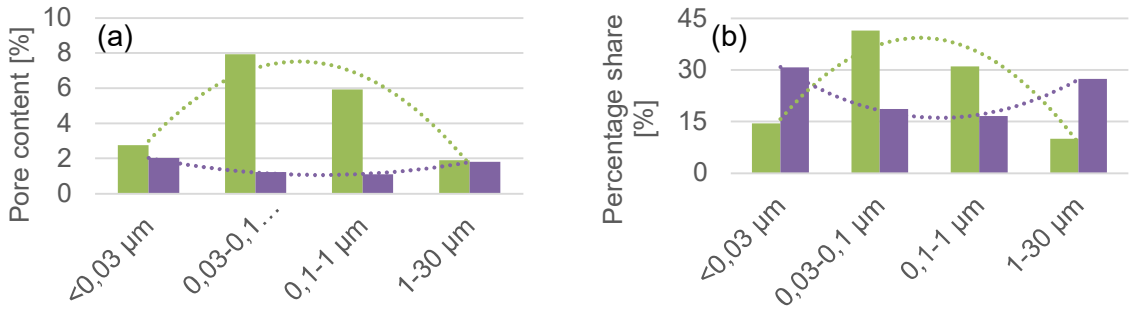

Fig. 89: Comparison of different processing of the same data from MIP of sample IHT450/4 and IHT450/4 & WS. (a) Realistic pores content connected to total measured porosity; (b) calculated share of individual pores connected to 100% equal to total porosity.

The total porosity of samples after IHT_T/t is higher than the porosity of the Ref sample and IHT_T/t&WS samples, see Fig. 90. The porosity of samples IHT150/4 slightly lowered porosity, which signifies greater bonding of water in new chemical products.

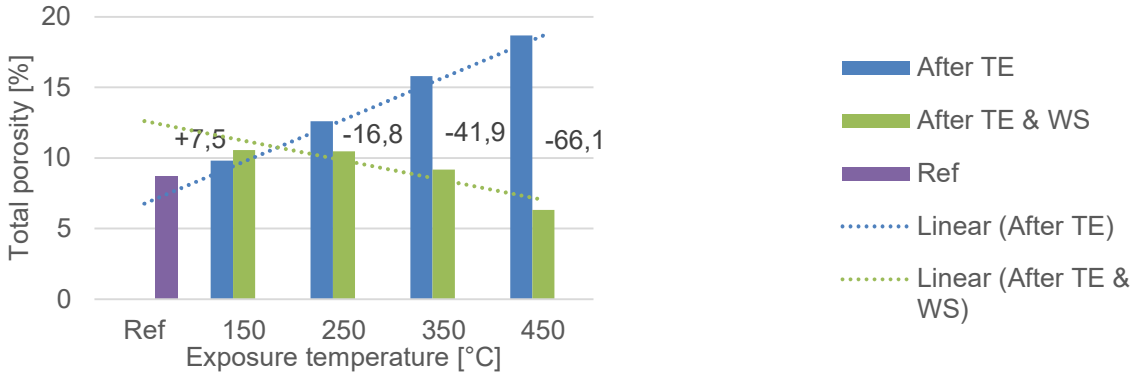

Fig. 90: Total porosity of Ref sample, samples after IHT_T/t and samples after IHT_T/t&WS.

Calculation of individual pore size share in total porosity is processed in connection to the total porosity of individual samples, Tab. 27, and as total porosity equals 100%, Tab. 28. The sum in Tab. 28 is slightly lower than 100% due to data processing.

Tab. 27: Results processed as the total porosity is equal to the measured value.

Pore diameter	Ref	IHT 150/4	IHT 150/4& WS	IHT 250/4	IHT 250/4& WS	IHT 150/4	IHT 350/4& WS	IHT 450/4	IHT 450/4& WS
Gel <0,03 µm	5,54	0,74	2,69	2,25	3,12	3,17	4,51	2,76	2,03
Cap 0,03-0,1 µm	1,50	5,93	5,90	6,01	4,92	6,80	2,45	7,92	1,23
Cap 0,1-1 µm	0,96	2,01	0,90	3,12	1,08	4,73	1,12	5,93	1,10
Cap 1-30 µm	0,66	1,02	0,97	1,10	1,30	0,93	1,03	1,91	1,81
Macro > 30 µm	0,06	0,12	0,09	0,11	0,06	0,17	0,05	0,15	0,17
Sum	8,71	9,81	10,54	12,59	10,47	15,79	9,17	18,67	6,33

The porosity of Ref sample without exposure to elevated temperature is characterised by a high content of gel pores, 62,3% of total porosity, with a diameter below 0,03 µm. Tested concrete was HSC with a dense porous structure thanks to fine ground limestone powder in the cement used. The measured content of capillary pores is very low, which contributes to higher compressive strength and durability, but increases the risk of fire spalling in case of fire exposure.

Tab. 28: Results processed as the total porosity is equal to 100%.

Pore diameter	Ref	IHT 150/4	IHT 150/4& WS	IHT 250/4	IHT 250/4& WS	IHT 150/4	IHT 350/4& WS	IHT 450/4	IHT 450/4& WS
Gel <0,03 µm	62,3	7,4	25,0	17,5	29,1	19,7	48,0	14,4	30,8
Cap 0,03-0,1 µm	16,8	59,4	54,8	46,8	45,8	42,3	26,1	41,5	18,7
Cap 0,1-1 µm	10,8	20,2	8,4	24,3	10,0	29,4	11,9	31,1	16,7
Cap 1-30 µm	7,4	10,2	9,0	8,6	12,1	5,8	10,9	10,0	27,4
Macro > 30 µm	0,7	1,2	0,8	0,9	0,6	1,0	0,6	0,8	2,6
Sum	98,0	98,4	98,0	98,1	97,6	98,3	97,5	97,7	96,1

Detail analyses of data obtained from MIP showed increasing content of pores with diameter from 0,03 μm to 0,1 μm and 0,1 μm to 1 μm due to rising exposure temperature. This fact also correlates with total measured porosity and decrease the presence of Ettirngite and CSH gel detected by DTA-TGA. Total porosity, and especially capillary pores in the same range, from 0,03 μm to 0,1 μm and 0,1 μm to 1 μm, were reduced by WS in almost all cases. The change of total porosity in the sample IHT150/4 increased by 7,5%, which is a negligible change and is something that can be discussed. Other samples IHT250/4, IHT350/4, IHT450/4 recorded a reduction in porosity by 16,8%, 41,9% and 66,1%. The reduction of porosity resulting from the WS might not be suitable for the IHT_T/t and negatively influence its performance ability.

Another proof of the formation of new hydration products such as Ettringite and CSH gel can be an increase of gel pores, which are an indispensable part of CSH gel formation. Increase of gel pores with a diameter under 0,03 μm was not recorded in the case of the sample IHT450/4, which might be caused by the formation of denser CSH gel or other products thanks to additional free lime (CaO) from the decomposition of $Ca(OH)_2$ initiated at 390°C. Used cement contains fine ground limestone powder, which could have reacted with water and other compounds, and formed a new product with porosity undetectable by MIP. The presence of denser CSH gel could also explain the regain of strength after WS of samples IHT450/4.

The number of capillary pores with dimension 1 to 30 μm remain unchanged after WS, which is beneficial in connection to the durability and strength of concrete (150). Additional hydration products, predominantly CSH gel and Ettringite, might form in the smaller pores located in the walls of pores with diameter 1 to 30 μm, as the water in those pores is commonly adsorbed to the surface and the pore remains empty. Preserved pores of this diameter are favourable for the improvement of freeze-thaw resistance (147).

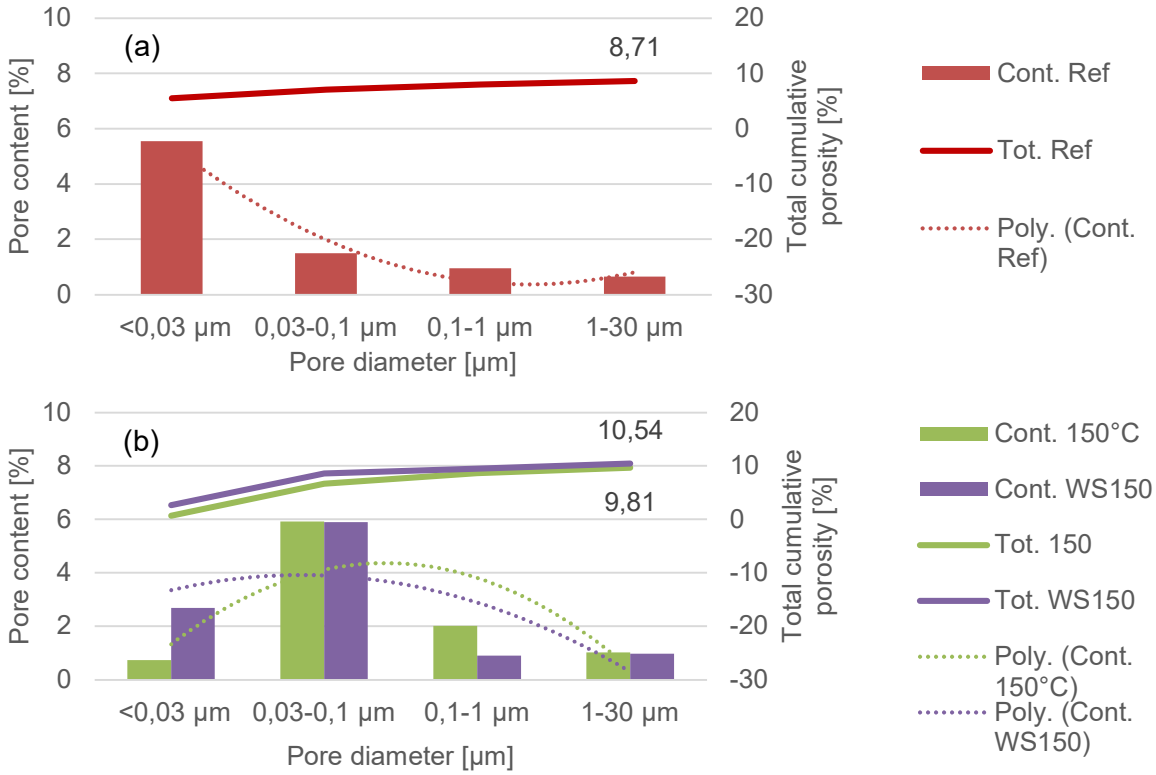

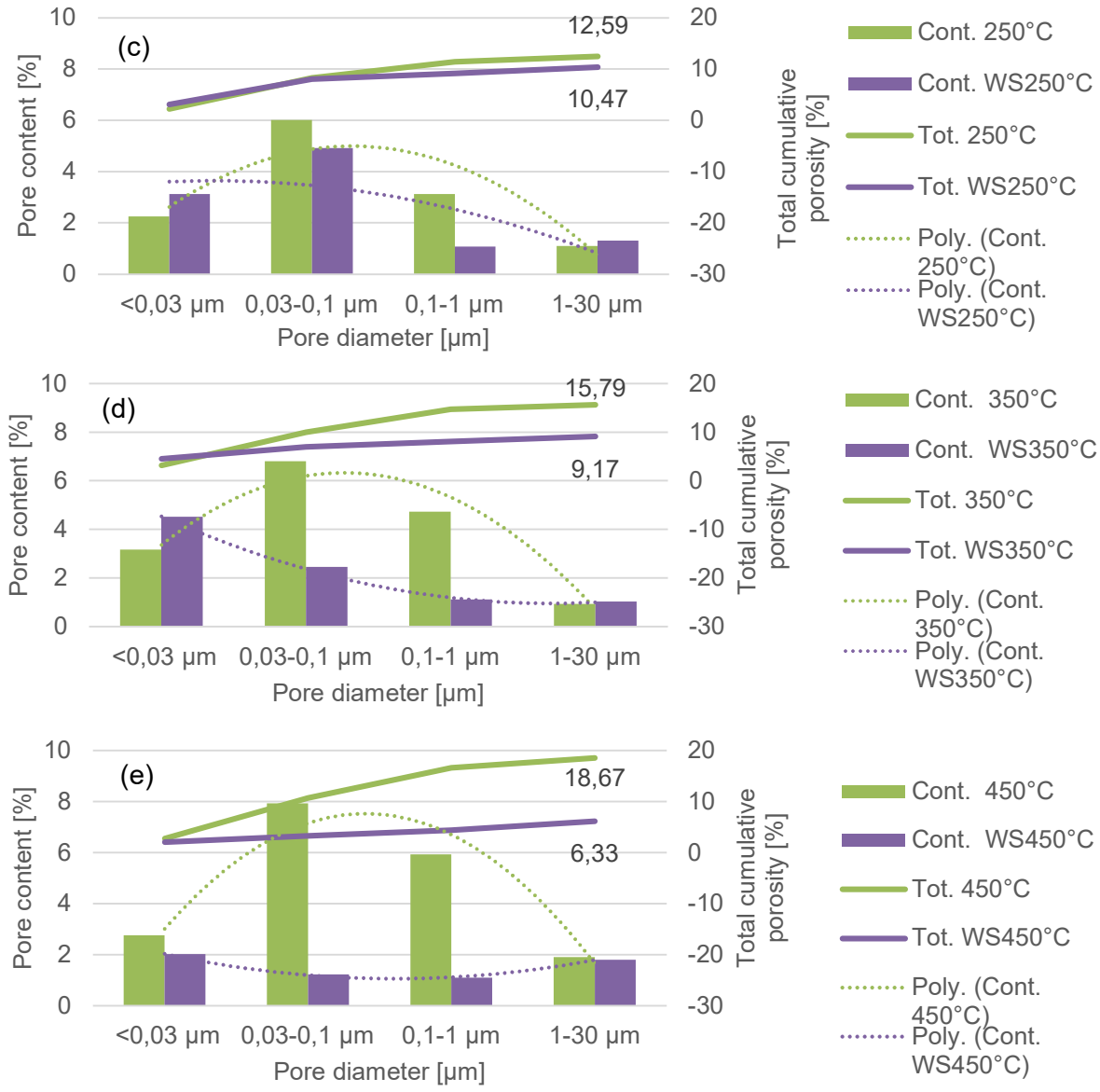

Fig. 91: Results from MIP of individual pore size share correlated to total measured porosity. Figure combines pore content and total cumulative pore content of individual exposure temperatures (a) Ref with no heating; (b) 150°C; (c) 250°C; (d) 350°C; (e) 450°C and samples after IHT_T/t&WS.

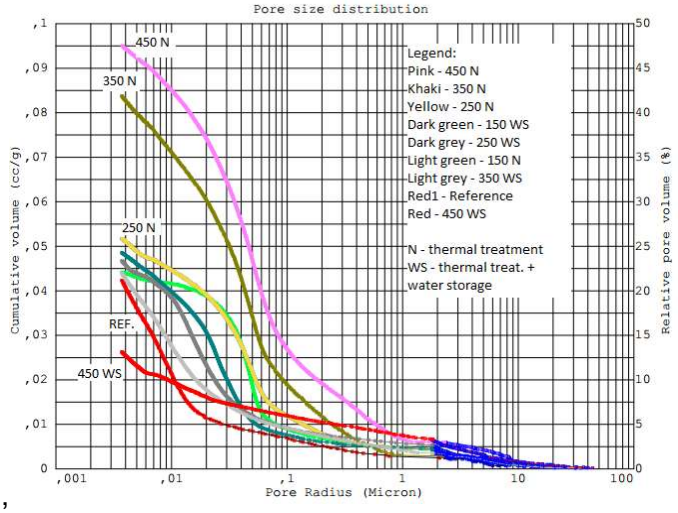

Fig. 92: Pore size distribution of tested samples in the 1st series of IHT method.

The content of macropores greater than 30 μm was minimal, between 0,6 and 2,6% out of 100%, and was not pointing in any direction, see Fig. 92. Thus, it was not incorporated in the data presented in Fig. 91.

7.1.3 Analysis of chemical composition by TGA-DTA

Thermal analyses are entirely appropriate for the study of chemical compound changes due to thermal exposure and subsequent WS. Samples are vacuum dried at temperature 20°C and pressure 1/100 torr for 24 hours before the testing. The vacuum drying removes most of the free water, and water present in CSH interlayers might not be entirely gone, which would explain higher weight change from 20 to 70°C during the TGA-DTA test in case of IHT_T/t&WS samples. The highest exposure temperature was 450°C, and therefore, reactions up to that temperature will be investigated. Reactions between 20 and 450°C are (i) evaporation of remaining free or physically bonded water between 20 and 70°C; (ii) dehydration of Ettringite with hydration products water, Bassanite and γ-anhydrite between 70 and 120°C; (iii) dehydration of CSH gel with hydration products water and β-C_2S (Larnite) between 120 and 200°C; (iv) continuous hydration of CSH gel and C_2AS with hydration products water, β-C2S (Larnite) and Gehlenite (118) between 200 and 390°C; (v) dehydroxylation of $Ca(OH)_2$ with hydration products water and CaO (lime) between 390 and 475°C. It must be taken into consideration that processes are overlapping, and it is not fully possible to totally decouple them, therefore presented temperature ranges were set for processing the results at way that they are comparable to each other. Detailed description of chemical changes of cement paste is described in the theory section 3.1 Cement matrix. Origin of aggregates does not influence the development of the IHT method, and data gained by TGA-DTA up to 450°C, as all types of rock are susceptible to changes in higher exposure temperature than tested IHT exposure temperature.

Measured weight loss during the TGA-DTA analysis was higher in the case of Ref sample and samples after TE & WS, while weight loss of TE samples was decreasing with increasing exposure temperature. Results from TGA-DTA confirm the presumption that all earlier described processes are based on the release of chemically bonded water and its evaporation. Increasing weight loss of IHT_T/t&WS samples follows the theory that exposure to high RH initiates rehydration and formation of new or recovered hydration products, and data in Fig. 93 corresponds with results presented in Fig. 87 and Fig. 90.

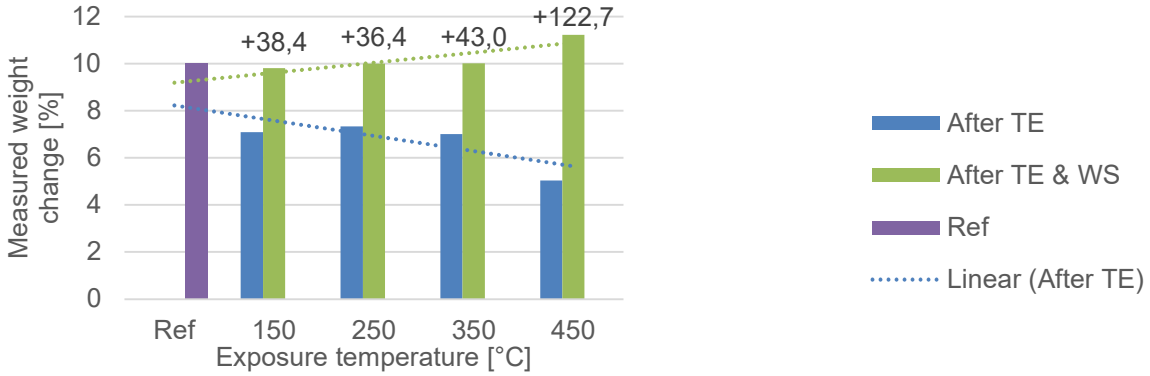

Fig. 93: Results of TGA analysis of Ref sample, samples after TE and samples after TE & WS.

Calculation of individual compounds share in total weight loss is processed in connection to a total weight loss of individual samples, Tab. 29, and as a total weight loss equal to 100% in Tab. 30.

Individual chemical compounds are dehydrated and changing their crystal structure or transform from the amorphous phase into the crystalline phase. Evaporation of water, most probably physically bonded in CSH globules between interlayers, was more significant in the case of samples IHT_T/t&WS. Weight change of the Ref sample and IHT450/4&WS differed only by 1,9%, which points towards the high recovery of sample IHT450/WS.

Tab. 29: Results processed as the total weight reduction is equal to the measured value.

Sample	H_2O	Ettringite	CSH	CSH/ C_2AS	$Ca(OH)_2$	Granite/ Larnite (β-C_2S)	$CaCO_3$	Other reactions	Total
	20-70	70-120	120-200	200-390	390-476	500-700	750-800		
Ref	1,38	3,05	1,32	0,49	0,72	2,33	0,18	0,55	10,02
IHT150/4	0,29	0,55	0,96	2,10	0,83	1,88	0,12	0,35	7,08
IHT150/4&WS	1,40	1,67	1,10	1,86	0,93	2,06	0,14	0,63	9,80
IHT250/4	0,48	0,59	0,56	1,53	1,27	2,22	0,18	0,50	7,33
IHT250/4&WT	0,99	1,59	0,93	1,88	1,01	2,46	0,13	1,01	10,00
IHT350/4	0,16	0,64	0,59	0,93	1,15	2,44	0,25	0,85	7,00
IHT350/4&WS	0,88	2,52	1,30	1,06	0,79	2,45	0,15	0,88	10,01
IHT450/4	0,19	0,33	0,31	0,39	0,74	2,08	0,08	0,91	5,04
IHT450/4&WT	1,56	3,40	1,44	1,24	0,63	1,93	0,19	0,83	11,22

Tab. 30: Results processed as the total weight reduction is equal to 100%.

Sample	H_2O	Ettringite	CSH	CSH/ C_2AS	$Ca(OH)_2$	Granite/ Larnite (β-C_2S)	$CaCO_3$	Other reactions	Total
	20-70	70-120	120-200	200-390	390-476	500-700	750-800		
Ref	13,7	30,5	13,2	4,8	7,2	23,3	1,8	5,5	10,0
IHT150/4	4,1	7,7	13,5	29,7	11,7	26,6	1,7	5,0	7,1
IHT150/4&WS	14,3	17,1	11,2	19,0	9,5	21,1	1,4	6,4	9,8
IHT250/4	6,6	8,0	7,6	20,9	17,3	30,3	2,5	6,9	7,3
IHT250/4&WT	9,9	15,9	9,3	18,8	10,1	24,6	1,3	10,1	10,0
IHT350/4	2,3	9,1	8,4	13,2	16,4	34,8	3,6	12,2	7,0
IHT350/4&WS	8,7	25,1	13,0	10,6	7,9	24,5	1,5	8,8	10,0
IHT450/4	3,8	6,6	6,2	7,7	14,6	41,4	1,6	18,0	5,0
IHT450/4&WT	13,9	30,3	12,9	11,1	5,6	17,2	1,7	7,4	11,2

During the dehydration process of Ettringite, crystal cross-section 2-4 μm and length 20-30 μm, are released water molecules (240), and Bassanite with crystal size around 0,1 μm and γ-Anhydrite, which is structured by Bassanite needles agglomeration, are formed (241, 242). Subsequent contact of Bassanite and γ-Anhydrite with water causes rehydration and formation of Ettringite or Gypsum characterised by larger crystals, which can form either in pores or causes damage to the microstructure. The content of Ettringite was reduced by thermal exposure as all temperatures were higher than 120°C at which the decomposition of Ettringite terminates. The amount of Ettringite or other calcium sulphate compounds increases rapidly with the WS and previous TE. Crystals were probably formed in the larger macropores non-detectable by MIP, and in capillary pores with diameter from 0,1 to 1 μm. Formation of calcium sulphate compounds such as gypsum or anhydrite in capillary pores with diameter 0,1 to 1 μm, thus limited space, could result in either formation of smaller crystals or destruction of microstructure.

Dehydration of CSH gel results in the formation of β-C_2S with crystal size approx. 0,09 μm. Rehydration of β-C_2S and additional hydration of nonahydrate cement grains can be formed

in both capillary pores with diameter from 0,03 µm to 0,1 µm or 0,1 µm to 1 µm. The structure of CSH gel is amorphous, and its size range from 0,001 µm to 0,1 µm based on chain length or globule size (96, 116). As the content of CSH gel is around 60% of cement paste, its rehydration and additional formation play an important role in the mechanical properties of concrete and porous structure form. From the results increase of CSH and C_2AS content in samples IHT150/4 and IHT250/4 is visible, which is only slightly changed due to WS. This finding corresponds to the increase of gel pores under 0,03 µm after WS, and almost unchanged capillary pore structure created by IHT150/4 and IHT250/4. In the case of IHT250/4 the capillary pores were slightly reduced but not dramatically if compared to IHT350/4 and IHT450/4.

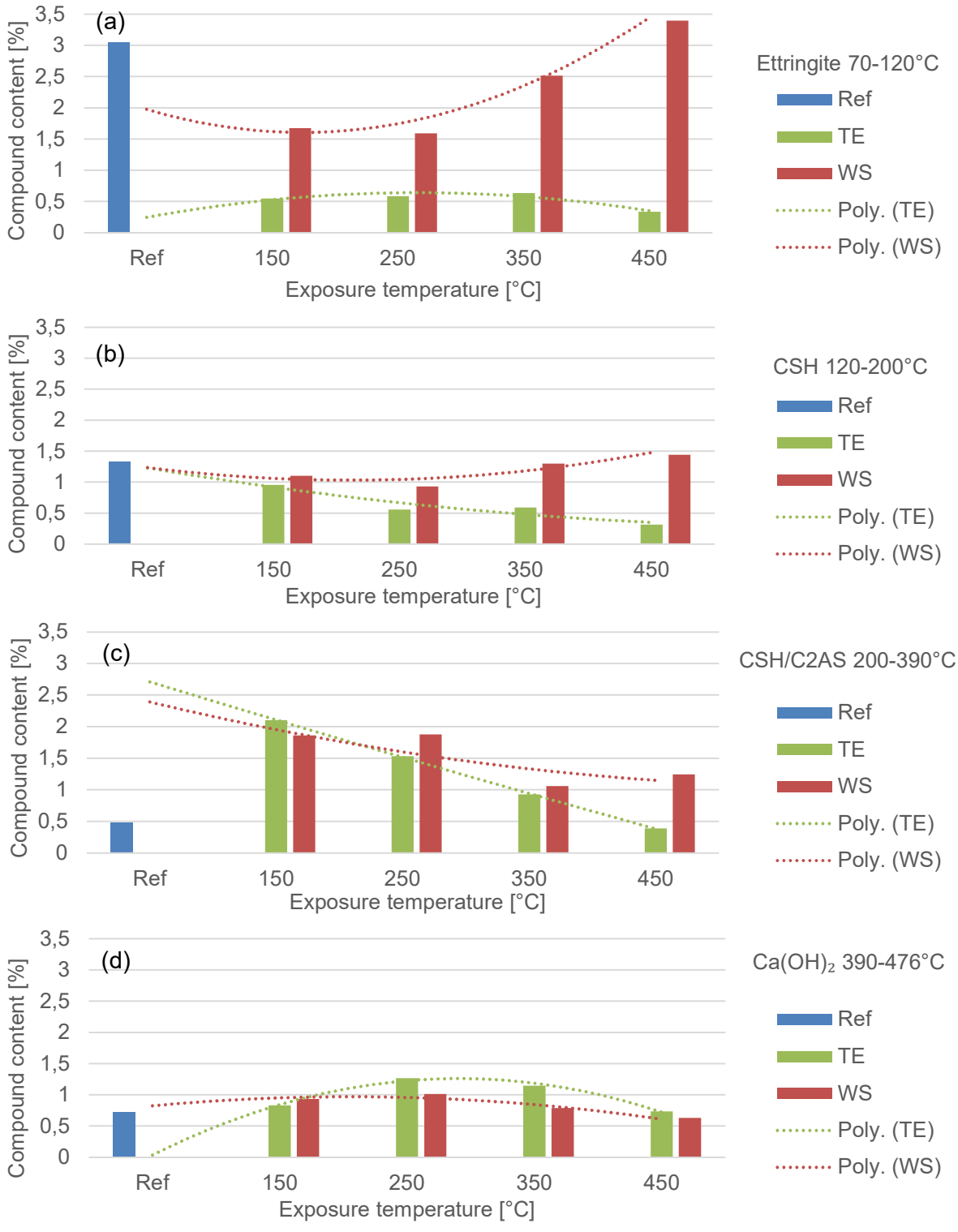

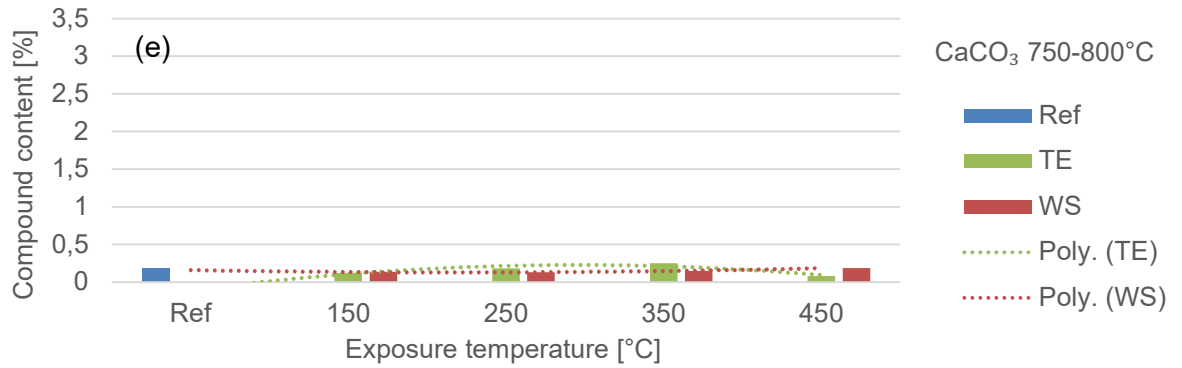

Fig. 94: Results from TGA-DTA of individual chemical compounds share correlated to total measured weight loss. (a) Ettringite 70-120°C; (b) CSH 120-200°C; (c) CSH/C2AS 200-390°C; (d) Ca(OH)2 390-475°C; (e) CaCO3 750-800°C of samples after TE and TE & WS.

Detected content of $Ca(OH)_2$ was higher in the case of heated samples than in water stored samples, which might be caused by its consumption for chemical reactions connected to hydration of limestone powder from used cement. The content of $CaCO_3$ was very low in comparison to other compounds, and no reasonable statement can be made.

7.1.4 Conclusion of the 1st series

The decrease of compressive strength due to water storage in the case of samples IHT150/4, IHT250/4 and IHT350/4 is unexpected as literature sources frequently reveal regain of strength thanks to exposure to temperatures up to 200°C. Also, results from the 3rd series showed strength gain due to thermal exposure up to 250°C in some cases. One of the possible explanations of strength loss is the extensive formation of new, large crystals, which cause severe damage to cement paste microstructure. Such damage and formation of interconnected micro- and macro- cracks was not possible to detect by MIP, and other methods for porous structure analysis should be used.

Visual inspection of samples did not detect any extensive formation of macrocracks or spalling of the surface layer, which is normally caused by a rapid heating ratio. Heating speed 5°C/min (300°C/hour) seems reasonable and efficient in the case of industrial upscale of the IHT method.

The selected length of the exposure to maximum temperature was 4 hours, which is not economically efficient and will not be viable on a industrial scale. In this phase, the length of exposure to maximum temperature was meant to evenly heat the whole sample, and to gain representative results for compressive strength testing. Maximum exposure temperatures (150, 250, 350 and 450°C) and subsequent exposure to high relative humidity (represented by water storage for 28 days), caused a reduction of compressive strength. The only exception was partial recovery of compressive strength of sample IHT450/4&WS due to the extensive formation of new hydration products. Regain of denser microstructure was confirmed by results from MIP and TGA-DTA. The length of thermal exposure to maximum heating temperature will be reduced to 2 hours as the aim is to modify porosity in the surface layer, not in the whole mass of the concrete element.

The Ref sample, which was not exposed to elevated temperature, contained a large share of gel pores under 0,03 μm, and a low number of capillary pores, which was inversed by exposure to all test temperatures. The content of capillary pores increased, and number of gel pores reduced. Selected exposure temperatures changed porosity of concrete and, in all cases, increased the number of capillary pores. However, porosity was further modified in the case of IHT350/4&WS and IHT450/4&WS where exposure to high humidity was simulated by water storage of samples for 28 days. Exposure to high humidity caused the formation of hydration products in shaped capillary pores with a diameter from 0,03 to 1 μm. The porosity of samples IHT150/4 and IHT250/4 was positively extended by IHT_T/t, and only slightly modified by consequent water storage, which is substantial for the IHT method. Further

development of the IHT method will be focused on exposure temperatures between 150°C and 250°C.

7.2 The 2nd series: Various temperature analysis on normal strength concrete

The 2nd series will be focused on a narrower range of exposure temperatures, particularly 150°C, 200°C and 250°C. The length of the exposure is reduced to 2 hours, but the speed of heating (5°C/min) and natural cooling remains the same. The total length of various IHT method configurations, concerning heating ramp, temperature dwell and cooling, is presented in Tab. 31.

Tab. 31: Duration of various configurations of the IHT method.

Marking of sample	Exposure temperature [°C]	Heating ramp duration [min]	Temperature dwell [min]	Natural cooling [min]	Total duration of IHT_T/t	
					[min]	[hours]
IHT150/2	150	30	120	70	220	3,7
IHT200/2	200	40	120	90	250	4,2
IHT250/2	250	50	120	170	340	5,7

The duration of natural cooling was relatively long, which can be explained by closed ambient for application of the IHT method, see Fig. 95. For the development of the IHT method an electric oven was used, which was kept closed during natural cooling. The speed of cooling can have a significant impact on the concrete element, as will be shown in the case of large-scale testing of slabs. The option of shortening the cooling period by opening the oven or lifting test slabs was not considered but might be a relevant task for further development of the IHT method.

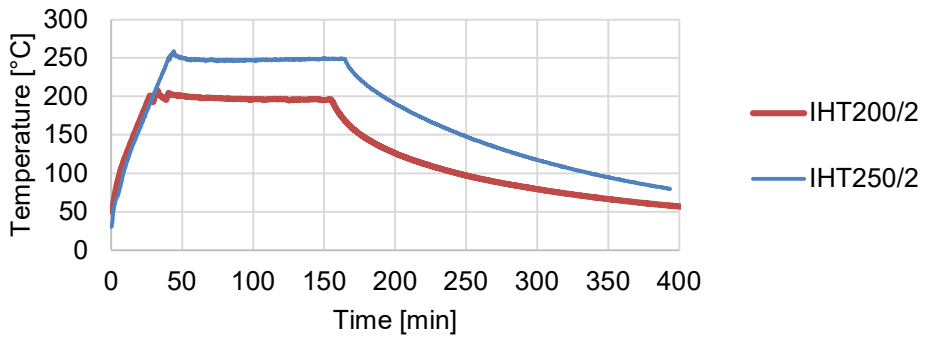

Fig. 95: Temperature recorded during the application of the IHT method, particularly IHT200/2 and IHT150/2.

Tab. 32:Mix design of concrete 7NO used for IHT development in the 2nd series.

Name	Aggregates		Cement		Admixtures		Water	
	Fraction	Dose [%]	Type	Dose [kg]	Type	Dose [% of m_c]	w/c ratio	[l]
7NO	0-8 mm Granite_NO	62	CEM I 42.5N-SR5	340	MasterGlenium SKY 830	1,5	0,32	109
	8-16 mm Granite_NO	38						

Concrete prepared for the 2nd series is normal strength concrete belonging to strength class C60/75 made of Granite aggregates from Norway (Granite_NO), cement CEM I 42,5N-SR5 from Aalborg cement Denmark, water and superplasticizer Master Glenium Sky 830 from

BASF. The mix design of the tested mix is presented in Tab. 32, and marked 7NO as it is further tested in the 4th series and large-scale testing.

Properties of fresh concrete and selected hardened concrete properties are given in Tab. 33, and the other characteristics of hardened concrete, such as air void system analysis and freeze-thaw resistance will be listed in section 7.4, Tab. 40.

Tab. 33: Fresh and hardened concrete properties of mix 7NO.

Name	Fresh concrete				Hardened concrete			
	Slump test [mm]	Slump flow [mm]	Air content [%]	Density [kg/m3]	Density [kg/m^3]	Compressive strength [MPa] 3 days	28 days	90 days
7NO	210	600	1,8	2526	2460	52,3	66,8	68,5

The main focus of this series, the 2nd series, is a detail analysis of porous microstructure by mercury intrusion porosimetry (MIP) and mineralogy by X-ray powder diffraction (XRD). Data obtain from MIP are analysed in the same manner as data from MIP in section 7.1.2, the 1st series of IHT method development. X-ray powder diffractograms were processed in Match! software from Cristal Impact (243). Weight loss and strength changes due to the application of IHT_T/t were also measured and processed. Finally, the decision of IHT method effectiveness on normal strength concrete will be discussed in detail, and optimal configuration of IHT method with a further step is suggested.

7.2.1 Analysis of porous structure by MIP

The same method for porous structure evaluation was used to gain data, that are comparable to IHT method development in the 1st series. The total porosity of 7NO was low, as recorded during the measurement of fresh (1,8%) and hardened (2,3%- tested according to ASTM C457/C457M) concrete. Even the measured air content was low, the higher content of capillary pores was presumably expected as no SCM was used to additionally hydrate in capillary pores and seal them. The w/c ratio was rather low (w/c ratio 0,32), and the share of unhydrated cement grains might be higher and contribute to additional hydration.

For porosity analysis by MIP cubes with an edge of approx. 7 mm, by cutting from a larger sample, were prepared. The samples were stored for about 90 days in a climate chamber with 20°C and 100% RH prior to the application of IHT method. Results of MIP are given in Fig. 96, Fig. 97 and Tab. 34.

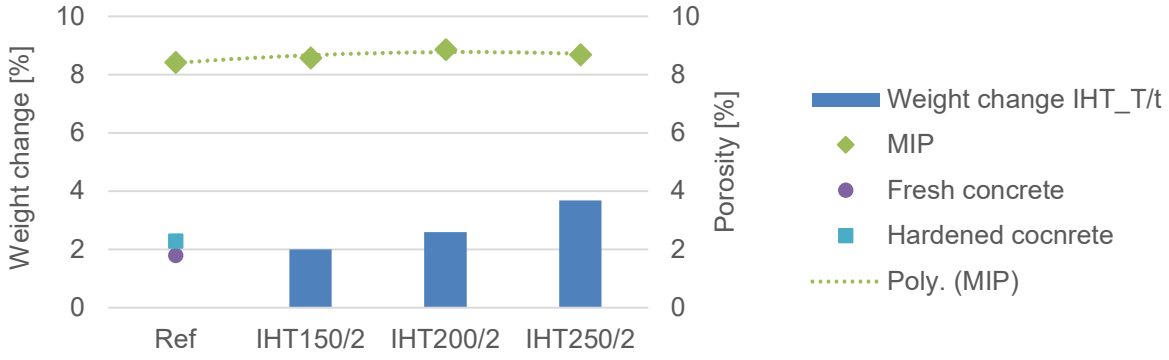

Fig. 96: Weight and porosity change due to the application of various configurations of the IHT method.

The weight of samples with IHT_T/t was reduced due to the evaporation of free, physically and partly chemically bonded water. The total porosity of samples with applied IHT_T/t slightly increased. Evaporation of residual water from CSH gel interlayers, and also their partial recrystallisation caused a reduction of pores by 2,2% in average, and extend the content of capillary pores.

Tab. 34: Results of MIP processed as total porosity is equal to 100%.

Pore diameter [µm]	Ref	IHT150/2	IHT200/2	IHT250/2
Gel <0,03	13,5	13,6	11,0	9,5
Cap 0,03-0,1	58,0	58,1	62,7	53,3
Cap 0,1-1	17,7	19,9	15,9	27,5
Cap 1-30	8,1	5,3	7,5	7,1
Macro > 30	2,6	3,0	2,9	2,6
Sum	100,0	100,0	100,0	100,0
Total porosity	8,43	8,58	8,86	8,69

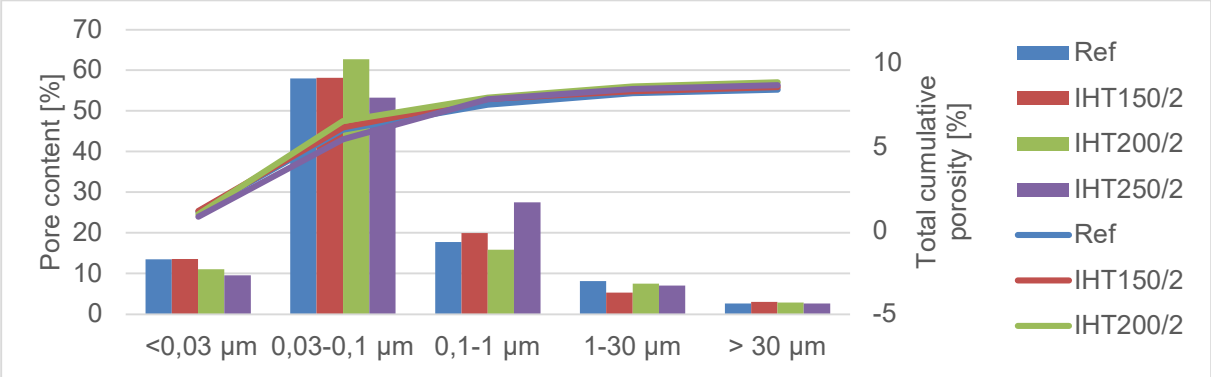

Fig. 97: Graphical presentation of results processed as the total porosity is equal to 100%, presented in Tab. 34.

The trend of higher formation of capillary pores with diameter between 0,03 and 0,1 µm in sample IHT200/2, while exposure to 250°C contributed to the greater formation of larger capillary pores with diameter 0,1 to 1 µm, is the same as in the 1st series IHT development. This might be due to the continuous crystallisation of CSH gel and recrystallisation of other hydration products. The effectiveness of the IHT method is not as significant as in the case of HSC, and therefore XRD was selected to detect recrystallisation of cementitious minerals.

7.2.2 Analysis of mineralogy by XRD

The mineralogy of concrete 7NO without and with the application of various configuration of the IHT method was analysed by XRD. The focus on chemical composition changes in a temperature range from 70°C to 250°C was selected as 250°C was the maximum exposure temperature IHT method. Concrete 7NO with Granite aggregates, commonly composed of Quartz, Mika and K-feldspar, were significantly influencing the automatic phase identification. As the detection of minerals with predominant content was not our intention, wanted minerals were pre-set in Match! software and analysed. The peak area belonging to the detected minerals was in the range from 0,63 to 1,26% of the total detected phases (Quartz, Mica and K-feldspar represented 4,4% of peak area). The content is very low, but the uniform pre-set of detected minerals allowed the detection of the differences between tested samples. Moreover, a limited quantity of detected minerals might be caused by the amorphous CSH gel phase, which cannot be detected by XRD and constitute approx. 60% of cement paste.

Configuration of March! software contained minerals before and after their crystalline structure change due to thermal exposure, (i) dehydration of **Ettringite** with hydration product **Bassanite** between 70 and 120°C; (ii) crystalline phase of CSH gel – **Tobermorite** with hydration product **β-C_2S (Larnite)** between 120 and 200°C; (iii) partial dehydration of **Brownmillerite** and formation of **Gehlenite**. Formation and recrystallisation of other phases are not excluded but the selected 6 minerals are considered as the most significant ones. Content of those 6 minerals was considered as 100%, and results of XRD analyses are presented in Tab. 35 and Fig. 98.

Tab. 35: Results from analyses of X-ray powder diffractogram by Match! software.

Mineral	Transformation temperature [°C]	Produced mineral	Ref [%]	IHT150/2 [%]	IHT200/2 [%]	IHT250/2 [%]
Ettringite	70-120	Bassanite	33	19,2	19,8	22,6
			0,2	0,4	1,6	1,7
Tobermorite crystal structure of CSH gel	120-200/ 200-390	Larnite (β-C2S)	26,6	17,9	15,6	15,6
			2,3	29,9	33,1	33,1
Brownmillerite (C_2AS)	approx. 200-390	Gehlenite	30,8	20,5	18,3	21
			7,1	12	11,7	6
Total amount			100	99,9	100,1	100

The Ref sample had a higher content of Ettringite, Tobermorite and Brownmillerite as expected, and the quantity was reduced due to the application of the IHT method. Crystallisation of amorphous CSH gel is signified by a rapid increase of Larnite, from 2,3% to 29,9-33,1-33,1 respectively. Formed crystals of Larnite probably creates more porous microstructure than CSH gel, which correlates with the results from MIP. Furthermore, formed crystals might be stronger, which would partly explain the compressive strength gain.

The selected technique for evaluation of diffractograms is not representative for the samples as a unit, as the main purpose was a comparison of the Ref sample without application of IHT method, and samples IHT150/2, IHT 200/2 and IHT250/2.

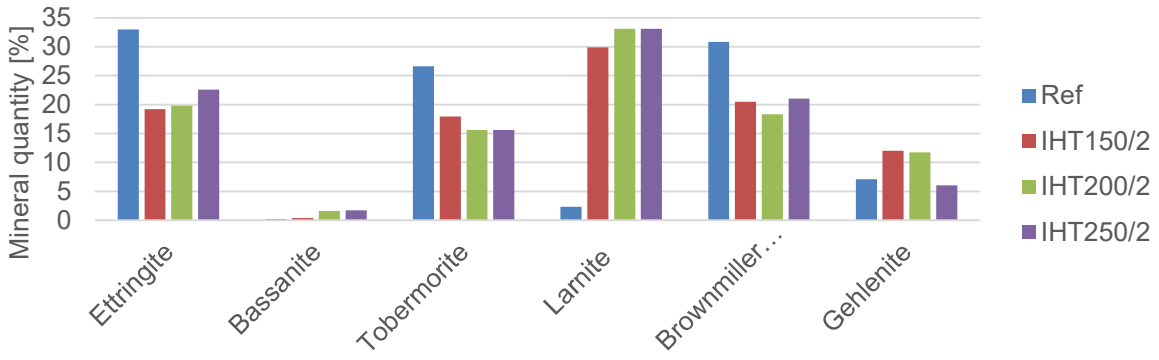

Fig. 98: Graphical presentation of results from XRD analyses.

7.2.3 Compressive strength and weight changes testing

The influence of the IHT method on the most significant property of concrete, compressive strength, was measured on cubes with edge 100 mm. From results presented in Fig. 99 an increase of strength by 0,7%, 3,2% and 5,9% respectively is visible for all configurations of the IHT method. Strength improvement is not significant but indicates that none of the tested IHT_T/t configuration have a negative impact on compressive strength.

The increase of strength could be due to additional hydration of remaining non-hydrated cement grains caused by exposure to elevated temperature in the range from 150°C to 250°C. Concrete 7NO had lower w/c ratio, which could lead to uncompleted hydration of all cement grains, and due to thermal exposure, water released from CSH gel interlayers and free water migration could serve for additional hydration of those cement grains. Supplementary analysis of Ref and IHT_T/t treated samples by TGA-DTA would be suitable for verification of additional formation of CSH gel due to thermal exposure.

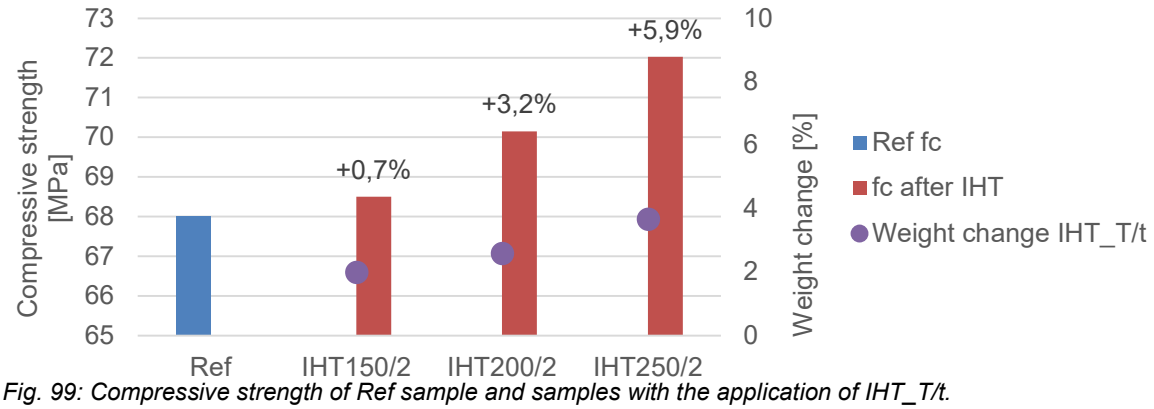

Fig. 99: Compressive strength of Ref sample and samples with the application of IHT_T/t.

The formation of Larnite with stronger crystal structure than CSH gel, and certainly higher porosity demonstrated by change of pore diameter, its higher detected content, and overall gain of compressive strength. Also, recrystallisation of Ettringite could influence the strength of cement paste as Ettringite crystals are large (diameter 1,5-5 μm and length 20,30 μm) in comparison to Bassanite and γ-anhydrite which might form denser and stronger, but still porous, microstructure.

7.2.4 Conclusion of the 2nd series

Testing of normal strength concrete showed a less significant change of porous microstructure due to the application of three different configurations of the IHT method, namely IHT150/2, IHT200/2 and IHT250/2. Content of capillary pores slightly increases in the case of samples IHT200/2 and IHT250/2, while IHT150/2 remains almost unchanged. The IHT method modifies the pores up to diameter 30 μm, and its influence on freeze-thaw resistance is not chnaged as suitable pore diameter for freeze-thaw resistance is between 10 to 100 μm. It seems that a negligible overlap of pore diameter suitable for fire resistance and freeze-thaw resistance, 10-30 μ, does not play a significant role.

The duration of thermal exposure to individual maximum temperatures seems appropriate as the porous structure of the surface layer was modified, but the strength of the sample has not decreased. Evaluation of the depth penetration of IHT_T/t is challenging as the installation of a thermocouple close to the surface might locally increase heat spread and produce unreliable results.

The length of the IHT method is relatively long, thanks to natural cooling. It would be suitable to investigate this area further if faster cooling can be performed and not cause an increase of microcracks formation or other defects of surface layer microstructure. Slow cooling is essential as samples remained in closed test oven after the application of the IHT method. Opening of the oven would accelerate the cooling and reduce the length of the cooling phase, but due to safety features it was not possible to open the oven directly after temperature dwell.

Exposure temperature 200°C and 250°C showed promising results, and 2 hours of thermal exposure also seems favourable.

7.3 The 3rd series: Various temperature and heating length analysis on various binders

The 3rd series will be focused on two main parameters. The first one is a further development of the IHT method, particularly the length of thermal exposure, which will be set to 1 and 2 hours. The heating ramp (5°C/min) and natural cooling remain unchanged. The maximum exposure temperature was selected based on results from the 2nd series, 200°C and 250°C. Tested configurations of the IHT method will be IHT200/1, IHT200/2, IHT250/1 and IHT250/2. The second approach in this series is the evaluation of various types of binders and their performance in elevated temperatures with and without applied IHT method.

The influence of the IHT method on various binders will be controlled by testing of weight change, flexural and compressive strength, and visual evaluation of cracks and discolouration using an optical microscope. Listed properties will be tested on the Ref sample without any thermal treatment with a known content of free water evaporable at temperature 50°C, and in samples with applied IHT method. Finally, all samples (Ref and 4 various IHT_T/t) will be exposed to the heating regime according to the modified ISO 834 curve (m-ISO) described in Fig. 86 and Fig. 101(b). Some samples were fragmented completely due to thermal exposure according to m-ISO, and it was not possible to perform testing on them, see Fig. 100.

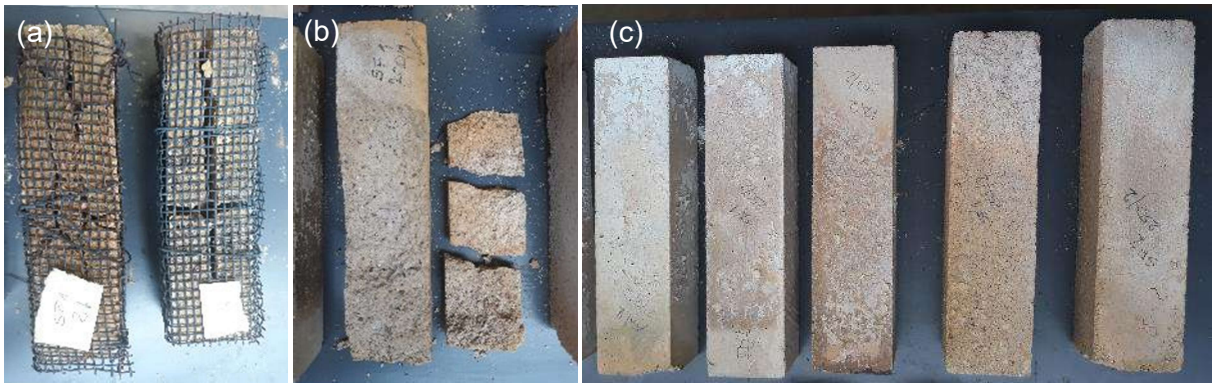

Fig. 100: Test samples after thermal exposure according to m-ISO curve: (a) Completely fragmented samples - CEM+SF; (b) Partly damaged sample - CEM+SF; (c) Samples without fragmentation or other significant damage.

The 3rd series will be structured into four parts starting with (i) description of binder composition and sample preparation; (ii) evaluation of weight changes due to application of IHT_T/t and exposure to modified ISO 834 curve; (iii) evaluation of flexural and compressive strength changes due to application of IHT_T/t and exposure to modified ISO 834 curve; (iv) conclusion of the 3rd series.

7.3.1 Mix design and preparation of samples

Three different types of binders were prepared, specifically binder with CEM I-42,5 N-SR5 from Aalborg cement Denmark, CEM II/B-M 42,5R (sold as a Standard FA-sement in Iceland) from Norcem Norway, and CEM I-42,5 N-SR5 with 25% replacement of cement by silica fume (SF). Replacement ratio is in conformity to EN 450-1 (244) The properties and whole preparation of test samples followed the standard procedure for mortar testing, according to EN 196-1 (222) . All used input materials were kept constant, and the replacement by SF was arranged by weight, and that caused a reduction of workability of mix CEM+SF. The water content, particularly w/c ratio was kept constant, and no workability improving agent (superplasticiser) was added, so it is possible to follow the water change due to IHT_T/t and thermal exposure according to m-ISO curve. Mix design of prepared mortar is presented in Tab. 36, and the amount is related to the preparation of one three-prism mould.

Tab. 36: Mix design of tested binders.

Name	Cement		SCM		Aggregates		Water	
	Name	Dose [g]	Name	Dose [g]	Name	Dose [g]	w/c ratio	Dose [g]
CEM	CEM I-42,5 N-SR5	450	Silica fume	0	CEN stand. sand	1350	0,5	225
FA	CEM II/B-M 42,5 R	450		0	CEN stand. sand	1350	0,5	225
CEM+ SF	CEM I-42,5 N-SR5	337,5		112,5	CEN stand. sand	1350	0,5	225

Prepared mortars were cast in prisms with dimensions 40×40×160 mm and cured for 28 days in a climate chamber with 20°C and 100% RH. After curing for 28 days samples were

placed in laboratory ambient for another 5 days prior to the application of IHT method and thermal exposure according to m-ISO. The moisture content of samples kept in laboratory ambient was measured on Ref samples by drying to 50°C until the weight change of two consecutive measurements after 1 hour, did not differ by more than 0,1%. The drying temperature of 50°C was selected to prevent any initiation of physically or chemically bonded water removal. Two thermocouple probes were used for the temperature monitoring in the top and bottom of the electric oven. Samples were wrapped in the steel net with opening 10 mm during the thermal exposure according to m-ISO curve with the purpose of protecting the oven in case of explosive spalling of tested samples. Samples were placed in the oven in such a way that they can be fully exposed to the requested temperature during all thermal loading tests. Thermal exposure regimes, IHT_T/t and m-ISO curve, are presented in Fig. 101.

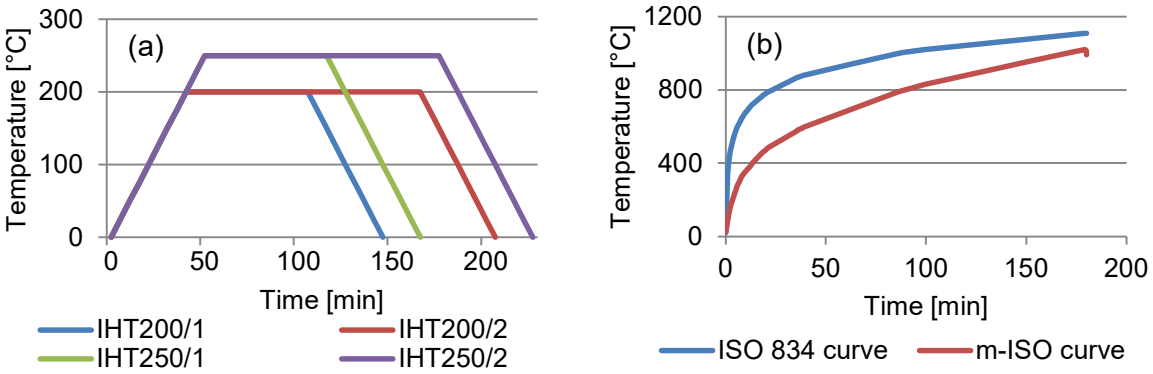

Fig. 101: Thermal exposure regimes used in the 3rd series: (a) IHT_T/t; (b) M-ISO curve.

7.3.2 Analysis of weight change due to the application of IHT_T/t and thermal exposure according to m-ISO curve

Samples were weighed before application of IHT_T/t, after application of IHT_T/t and after thermal exposure according to m-ISO. The reference sample was measured in laboratory conditions and moisture content was measured by drying to 50°C. Samples with applied IHT_T/t were kept in 0% RH chamber where they cooled down to ambient temperature prior to thermal exposure according to m-ISO. The weight changes measured during the application of individual IHT_T/t were recorded before IHT_T/t and before thermal exposure, according to m-ISO. The weight changes due to application of IHT_T/t was expressed as a percentage of total measured weight loss (=100%). Results are given in Tab. 37 and graphically processed Fig. 103, Fig. 104 and Fig. 105.

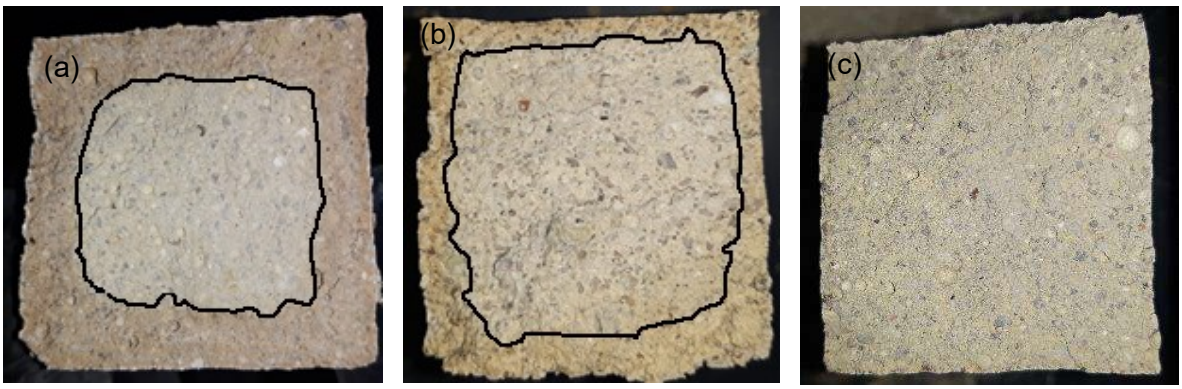

Fig. 102: Photo documentation of samples after thermal exposure according to m-ISO: (a) Ref sample; (b) IHT200/1; (c) IHT200/2

Tab. 37: Results of the weight changes due to application of IHT_T/t and thermal exposure according to m-ISO curve.

Binder type	IHT_T/t configuration	IHT_T/t		m-ISO	
		Measured	Share in 100%	Measured	Share in 100%
CEM	Ref*	4,61*	46,2*	9,98	100,0
	IHT200-1	5,42	51,2	10,58	100,1
	IHT200-2	6,64	62,4	10,64	100,0
	IHT250-1	6,62	62,9	10,53	100,0
	IHT250-2	7,32	65,7	11,14	100,0
FA	Ref	5,13*	52,2	9,83	100,0
	IHT200-1	5,7	52,4	10,88	100,0
	IHT200-2	6,56	64,4	10,19	100,0
	IHT250-1	7,03	65,2	10,78	100,0
	IHT250-2	7,75	68,7	11,28	100,1
CEM+SF	Ref	3,7*	36,3	10,18	100,0
	IHT200-1	5,63	50,7	11,1	100,1
	IHT200-2	6,67	59,9	11,14	100,0
	IHT250-1	7,52	67,2	11,19	100,0
	IHT250-2	9,23	76,2	12,12	100,0

*Ref sample is without application of IHT_T/t, and the weight loss is equal to free water content evaporable up to 50°C.

Application of IHT200/2 and IHT250/1 released the same amount of water in the cases of CEM and FA, that could be explained by the same depth of IHT penetration with different speed driven by maximum exposure temperature for individual IHT_T/t configurations. The samples without IHT_T/t were discoloured on the surface area, Fig. 102(a) while the discolouration was weakened with an increase of heating duration length and maximum exposure temperature, Fig. 102(b) and (c).

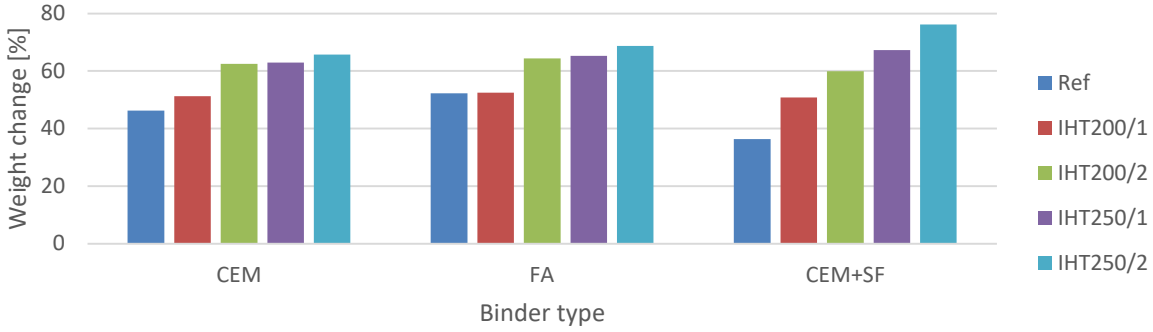

Fig. 103: Graphical presentation of the weight change due to application of IHT_T/t expressed as a percentage of the total weight loss due to exposure to m-ISO. The weight loss of Ref sample is the value of moisture content measured by drying to 50°C.

The higher temperature might cause the creation of higher pore pressure and increase microcrack formation, which is not desirable. The release of water in the case of IHT250/2 for all three tested binders is relatively high, 65,7%, 68,7% and 76,2%, and might also modify pores with a diameter higher than 30 μm and influence freeze-thaw resistance and durability of the concrete. Furthermore, IHT250/2 will be not energy efficient in real conditions due to long exposure and higher temperature requirements. The difference between moisture content (free water content) of Ref sample and IHT200/1 is indicative of the amount of water used for hydration, where in case of FA a higher amount of free water is in the structure, while SF consumed most of the mixing water for pozzolanic reaction with $Ca(OH)_2$ and created a more significant amount of CSH gel. Amorphous CSH gel crystallises under exposure to

temperatures higher than 120°C, and releases a larger quantity of chemically bonded water which migrates through dense microstructure. Migration of released chemically bonded water might cause microcracking and negatively impact strength properties of mortars or concrete with SF.

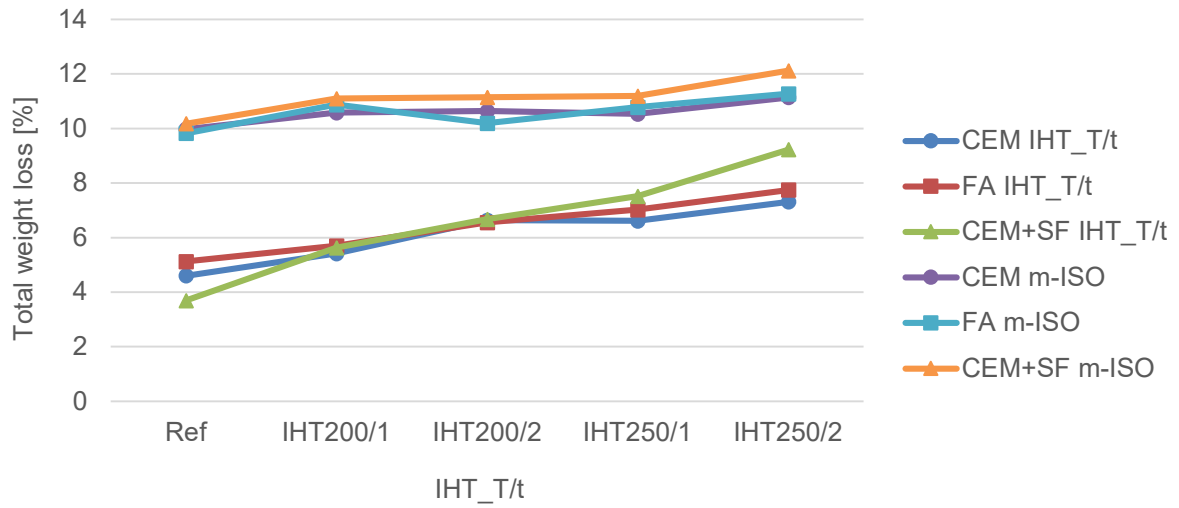

Fig. 104: Graphical presentation of the total weight loss due to application of IHT_T/t and consequent thermal exposure according to m-ISO curve. The weight loss of Ref sample is the value of moisture content measured by drying to 50°C.

The weight loss due to thermal exposure according to m-ISO curve was very high in all cases if we consider that mixing water constitutes 11% of input materials by weight. The amount of released water due to thermal exposure according to m-ISO curve was higher in the cases of all samples with applied IHT_T/t. This could be caused by faster penetration of exposure temperature in the test sample, and the release of chemically bonded water is completed to the higher extend.

The higher heating speed might cause local overheating of the concrete structure and lead to creation of excessive thermal stresses due to uneven heat spread. On the other hand, faster heat transition through the concrete mass might cause faster heating of steel rebars in the case of reinforced concrete elements.

7.3.3 Analysis of the change in strength properties due to application of IHT_T/t and exposure to m-ISO curve

Flexural and compressive strength were tested on prisms with dimensions 40×40×160 mm. Samples for strength evaluation after IHT_T/t were weighed directly after cooling down and again directly before strength testing. Those samples were not kept in a “dry chamber” at once for further thermal exposure according to m-ISO curve, and a regain of weight in the range from 0,03 to 0,31% was observed. Natural moisture uptake from surrounding ambient was higher in the case of IHT250/t, 0,24% and 0,31%, and was probably caused by the recovery of CSH gel by uptake of water molecules in CSH interlayers. Four out of the 10 CEM+SF samples broke during the thermal exposure according to m-ISO curve.

A significant increase of strength due to application of IHT_T/t to CEM and FA binder types was recorded, while the strength was reduced when the CEM+SF was exposed to IHT250/1 and IHT250/2. The most significant increase of strength, up to 25,8% was measured in the case of FA sample exposed to IHT250/2. Fly ash is less reactive pozzolanic SCM the reactivity of which could be enhanced by exposure to elevated temperature, which happened during the application of IHT_T/t. The compressive strength of CEM samples was also improved most likely by additional hydration of non-hydrated cement grains and crystal formation of Larnite or recrystallisation of other minerals as explained in the 2nd series of IHT method development.

Tab. 38: Results of the change in compressive strength due to application of IHT_T/t and thermal exposure according to m-ISO curve.

Binder type	Ref/IHT_T/t	Compressive strength IHT_T/t		Compressive strength m-ISO	
		[MPa]	Change due to IHT_T/t [%]	[MPa]	Change due to IHT_T/t [%]
CEM	Ref	60,0	100,0	6,7	11,1
	IHT200/1	62,9	104,8	5,1	8,5
	IHT200/2	65,4	109,0	4,6	7,7
	IHT250/1	71,8	119,8	5,6	9,4
	IHT250/2	69,7	116,3	5,6	9,3
FA	Ref	55,1	100,0	6,0	10,9
	IHT200/1	59,2	107,4	4,9	8,9
	IHT200/2	65,0	118,0	6,4	11,7
	IHT250/1	66,1	120,0	6,7	12,1
	IHT250/2	69,3	125,8	6,5	11,8
CEM +SF	Ref	62,4	100,0	0*	0*
	IHT200/1	64,5	103,2	5,31**	8,5**
	IHT200/2	74,1	118,6	5,9	9,5
	IHT250/1	56,5	90,4	5,97**	9,6**
	IHT250/2	52,0	83,3	4,5	7,1

*Two samples were broken; **One sample was broken.

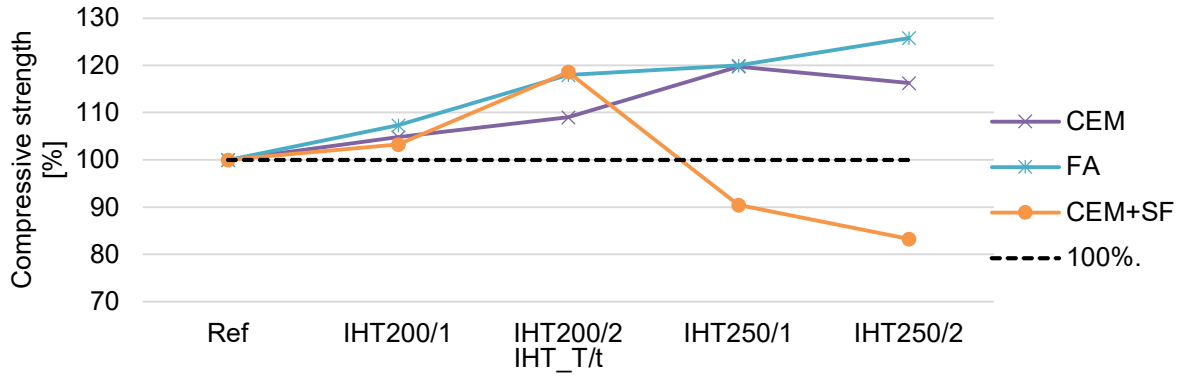

Fig. 105: Graphical presentation of the compressive strength change due to application of IHT_T/t expressed as a percentage change in relation to Ref sample.

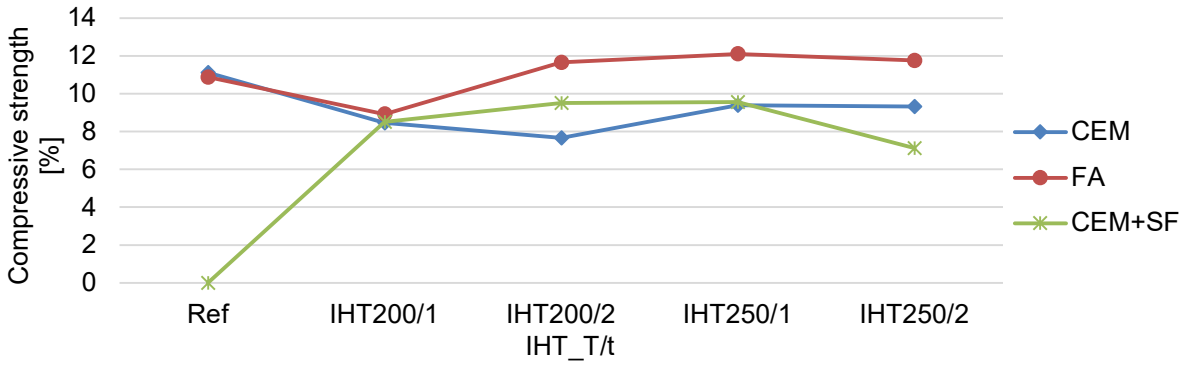

Fig. 106: Graphical presentation of the change in compressive strength due to application of IHT_T/t and thermal exposure according to m-ISO heating regime expressed as a percentage change in relation to Ref sample without thermal exposure according to m-ISO heating regime.

Properties of a binder with 25% replacement of cement by silica fume also gain strength due to exposure to elevated temperature, but only when exposed up to 200°C, specifically compressive strength gain 3,2% and 18,6% were observed. Any further rise of temperature had a contrary effect. Observed microcracks resulted from extensive evaporation of chemically bonded water, which had difficulties in migration through the dense mass.

Tab. 39: Results of the flexural strength change due to application of IHT_T/t and exposure to m-ISO.

Binder type	Ref/IHT_T/t	Flexural strength IHT_T/t		Flexural strength m-ISO	
		[MPa]	Change due to IHT_T/t [%]	[MPa]	Change due to IHT_T/t [%]
CEM	Ref	7,8	100,0	0,5	6,1
	IHT200/1	7,9	101,4	0,4	5,4
	IHT200/2	7,6	98,2	0,4	5,2
	IHT250/1	8,2	105,3	0,5	5,8
	IHT250/2	9,3	119,9	0,4	5,4
FA	Ref	7,1	100,0	0,6	9,0
	IHT200/1	6,9	96,9	0,5	6,9
	IHT200/2	6,6	93,1	0,6	8,3
	IHT250/1	7,2	101,5	0,6	8,3
	IHT250/2	10,5	147,3	0,6	8,2
CEM+SF	Ref	7,8	100,0	0*	0*
	IHT200/1	7,1	90,8	0,3**	4,0**
	IHT200/2	7,2	92,3	0,4	4,9
	IHT250/1	6,2	79,5	0,3**	3,8**
	IHT250/2	5,1	65,0	0,3	3,8

*Two samples were broken; **One sample was broken.

All CEM+SF samples without application of IHT_T/t broke, and, in addition slide improvement of properties in the case of FA samples with an application of ISO200/2 and ISO250/2 was observed. Compressive strength of CEM samples reduced in the case of all IHT_T/t configurations.

The flexural strength of CEM and FA remain stable after application of IHT_T/t with the exception of IHT250/2 where increases by 19,9% and 47,3% respectively were measured. Contrarily, the same strength reduction as in the case of compressive strength was observed with CEM+SF samples after application of IHT250/1 and IHT250/2. Strength loss is associated with release of chemically bonded water and its migration through dense microstructure and microcrack formation. Measured flexural strength of samples before and after IHT_T/t have changed within acceptable area as the pressure (tensile forces from vapour expansion) connected to exposure temperature are 2,1 MPa for 200°C and 3,6 MPa in the case of 250°C, see Fig. 61. Photo documentation of samples deterioration due to thermal exposure according to m-ISO curve is attached as Annex 1.

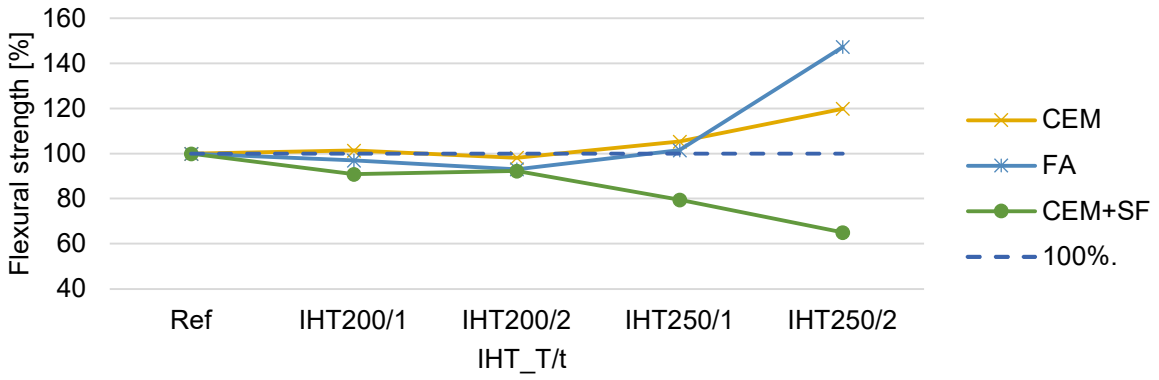

Fig. 107: Graphical presentation of the compressive strength change due to application of IHT_T/t expressed as a percentage change in relation to Ref sample.

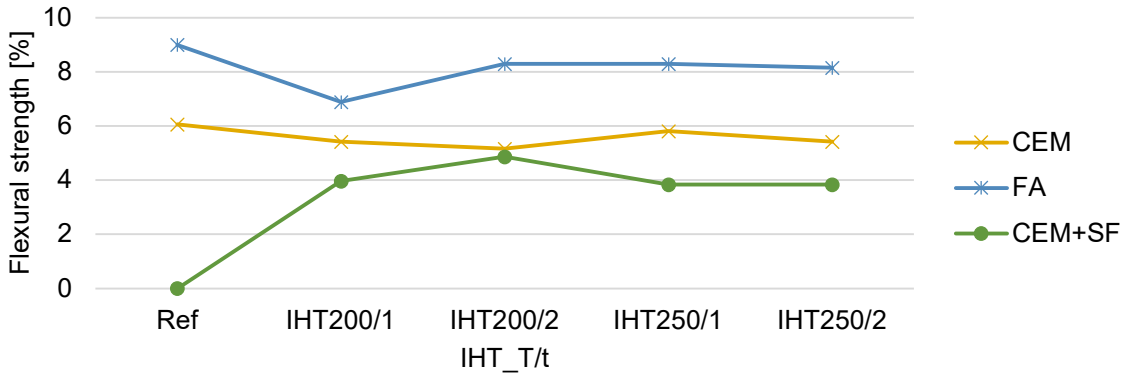

Fig. 108: Graphical presentation of the compressive strength change due to application of IHT_T/t and thermal exposure according to m-ISO heating regime expressed as a percentage change in relation to Ref sample without thermal exposure according to m-ISO curve.

The IHT method seems to have a positive impact on CEM+SF samples, otherwise the effect is not significant on flexural strength. Remaining flexural strength ranged between 9% and 3,8% (0,6 and 0,3 MPa) for all samples, which might not be the most suitable parameter for evaluation of IHT method effectiveness.

7.3.4 Conclusion of the 3rd series

Four different configurations of IHT method, namely IHT200/1, IHT200/2, IHT250/1 and IHT250/2, were applied on three different binder types, namely CEM I-42,5 N-SR5, CEM II/B-M 42,5R (sold as Standard FA-sement in Iceland) and CEM I-42,5 N-SR5 with 25% replacement of cement by silica fume (SF). Treatment of samples by the IHT method was followed by thermal exposure according to the modified ISO 834 curve. The change of strength properties, and weight loss was measured and analysed.

Application of IHT_T/t increased compressive strength up to 25,8% and flexural strength up to 47,3% in the case of all binders and IHT method configurations. The only exception were samples CEM+SF with applied IHT250/1 and IHT250/2, where compressive strength decreased by 16,7% and flexural strength by 35%. The strength loss was caused by microcracks and extensive evaporation of chemically bonded water, which had difficulties in migration through the dense mass of CEM+SF when exposed to 250°C.

Generally, the loss of flexural and compressive strength due to exposure to m-ISO thermal regime was extremely high, and besides the binder type, the influence of used aggregates must be taken into consideration. The CEN standard sand is pure quartz sand which is susceptible to recrystallisation at 573°C accompanied by volume increase of 0,85%. As the samples were exposed to a maximum temperature of 1050°C, recrystallisation of quartz took place and had a significant impact on the strength properties of tested binders. Additional testing with more thermally stable aggregates would be recommended.

The IHT200/2 and IHT250/1 had the same weight loss, which could signify the same penetration depth of IHT method with different speed. As was mentioned in the description of the IHT method, the variation could be needed for different types of binders or aggregates. Results from the 3rd series showed that the influence of the IHT method on CEM is not sufficiently contributing to preservation of the strength, but FA and CEM+SF binders registered an increase of strength, and, indeed, complete fragmentation of CEM+SF samples was eliminated.

Based on the results from this chapter it was decided that final configuration of IHT for testing of various concrete types and large-scale testing of slabs will be performed with IHT200/2. The temperature gradient of IHT200/2 is lower thanks to lower maximum exposure temperature, and it is known that the cement binder expands up to 200°C, while in higher temperatures it shrinks. This fact is also useful for the selection of maximal IHT method exposure temperature 200°C.

7.4 The 4th series: Application of IHT200/2 on various types of concrete

The 4th and the final series of the IHT method development is going to verify the selected configuration of the IHT method based on obtained results throughout the 1st, 2nd and 3rd series. The final configuration of the IHT method, which is going to be used within the following testing, is temperature ramp 5°C/min (300°C/hour), exposure temperature 200°C held for 2 hours and finished by natural cooling – IHT200/2. From the results of the 3rd series, more significant impact of IHT200/2 on mortar with blended cement or concrete with supplementary cementitious materials was observed than its effect on mortar prepared exclusively with Portland cement. This series is going to be tested concrete, where the cement paste constitutes only about 30 to 35%, and results might be different from the results of mortar thermal exposure testing.

Four concrete mixes were prepared, and their behaviour with and without applied IHT200/2 were tested under thermal load according to m-ISO curve. The variables of concrete mixes were (i) binder type Portland cement, blended cement and addition of SCM, and (ii) aggregate type. The shape and size of the samples exposed to thermal load is also an important parameter, and therefore two different sample sizes, a cube with an edge of 50 mm and a cube with an edge of 100 mm will be tested. The last part is focused on IHT200/2 efficiency verification and consists of large-scale testing of one-side heated uniaxially-loaded slabs exposed according to m-ISO curve. The depth of the IHT200/2 was recorded during the large-scale testing using inbuild thermocouples in test slabs.

7.4.1 Mix design and properties of prepared concrete in normal ambient

In total four concrete mixes were prepared. Three with Basalt_IS aggregates and various binders: 4CEM with CEM I-42,5 N-SR5 from Aalborg cement Denmark; 5FA with CEM II/B-M 42,5R (sold as a Standard FA-sement in Iceland) from Norcem Norway; 6SF with CEM I-42,5 N-SR5 with 6% replacement of cement by silica fume (SF). The fourth concrete, 7NO, contains CEM I-42,5 N-SR5 from Aalborg cement Denmark and Granite_NO aggregates.

Basalt_IS aggregates from Vatnsskarð quarry, Iceland, are stable in high temperatures but have very high porosity closely connected with water absorption, fraction 0-8 mm 3,8%, and fraction 8-22 mm 6,0%. Such a high water absorption is disadvantageous for properties of fresh concrete, especially workability, which gets easily reduced by sharp and angular particles with a high surface area. The high w/c ratio and addition of fine fraction under 0,125 mm was needed to compensate unfavourable characteristics of the Basalt_IS aggregates. The last mix, 7NO, had significantly better properties due to dense Granite_NO aggregates with a sufficient amount of fines, which provide good workability. The consistency of fresh concrete was adjusted by the addition of plasticizer and monitoring of moisture content in Basalt_IS aggregates over the whole period of concrete preparation. The dose of mixing water, added directly to a mixer, was combined with an actual moisture content of aggregates, in order to correctly maintain w/c ratio. In other words, w/c ratio would be significantly higher if the actual moisture content of aggregates is not integrated into the mix design. For calculation of the mix design ComPose software developed in Iceland was use. The general rules for mix design are given in chapter 6.2.1, where constants and variables are specified with the aim to obtain comparable mixes. Detail mix design is given in Annex 2. The pre-set mixing procedure was developed to eliminate additional influencing factors, i.e., more variables involved.

Fresh concrete properties, such as workability measured by a slump, density and air content were tested, and results are given in Tab. 40, along with properties of hardened concrete. Workability was significantly influenced by the shape and fines content in aggregates, and recorded lower in case of mixes with Basalt_IS aggregates. Granite_NO used in mix 7NO contains 9% of fines and performed better in fresh concrete. The air content of mixes was kept low with the aim of dense microstructure formation, which would be susceptible to spalling during the thermal exposure. Measured air in fresh concrete was between 1,60 and 3%, which

is extremely low when high open porosity of Basalt_IS aggregates is considered. The density difference between fresh and hardened concrete was most significant in the case of mix 5FA and caused by a lower degree of hydration product formation as a result of the presence of fly ash, which reacts with significant delay. The w/c ratio of mix 7NO was 0,32, lower than in other mixes, which is causing slow and uncomplete hydration of cement.

Tab. 40: Properties of mixes 4CEM, 5FA, 6SF and 7NO tested in the 4th series of the IHT method development.

Name	Fresh concrete		Hardened concrete						
	Slump test	Air content	Density	Compressive strength [MPa]		Air void characteristics			F-T res*
	[mm]	[%]	[kg/m^3]	28 days	90 days	α [mm^{-1}]	A [vol.%]	L [mm]	56 cyc. [kg/m^2]
4CEM	70	3,0	2460	55,7	61,6	10	3,0	0,68	4,65
5FA	130	1,6	2476	48,6	56,7	6	2,1	1,24	7,00
6SF	120	2,8	2455	65,0	68,0	13	0,9	0,84	5,23
7NO	210	1,8	2460	66,8	68,5	20	2,3	0,39	0,08

*The amount of scaled material after exposure to 56 freeze-thaw cycles.

Compressive strength was tested on cylinders with diameter 100 mm and height 200 mm after 28 and 90 days. The same dose of cement, 340 kg per m^3, was used for all mixes 4CEM, 5AF and 7NO, while mix 6SF contained 320 kg of cement + 20 kg of SF. The development of compressive strength of 5FA was slower, but after 90 days was already comparable to mix 4CEM. Granite_NO aggregates and low w/c ratio contributed to the high strength of mix 7NO, such as silica fume in the case of mix 6SF with Basalt_IS aggregates. All results of the strength and air content of individual mixes are given in Tab. 40 and Fig. 109.

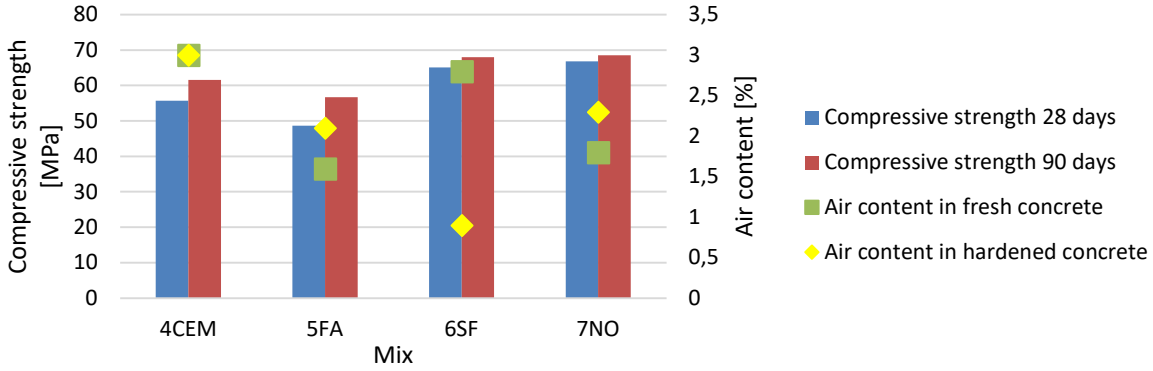

Fig. 109: Graphical presentation of relation between compressive strength after 28 and 90 days, and air content measured in a fresh and hardened state.

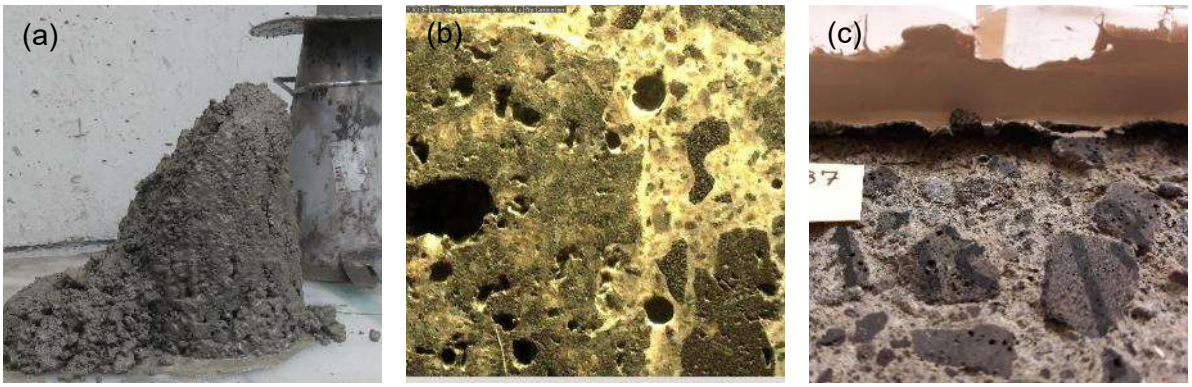

Fig. 110: Photo documentation of concrete prepared in the 4th series: (a) slump flow test of mix 4CEM; (b) porous structure of mix 5FA and (c) Scaled surface of 6SF sample after freeze-thaw resistance test.

The porous structure of hardened concrete was analysed according to ASTM C457/C457M (232), which showed much better air void characteristics of the mix 7NO than all three mixes

with Basalt_IS aggregates. Air content in hardened concrete was significantly lower in the case of 6SF due to silica fume, which filled capillary pores and densified the microstructure. Air void characteristics of mix 7NO indicate a denser network of pores with smaller diameter, which also contributes to adequate frost resistance. In general, Icelandic aggregates perform poorly when it comes to frost resistance, and combination with low air content resulted in very low freeze-thaw durability, even in the case of silica fume addition, which commonly improves freeze-thaw resistance of concrete. Fresh concrete, porous structure, and sample after completion of freeze-thaw resistance test are pictured in Fig. 110. Based on the mix design and properties of fresh and hardened concrete in normal ambient higher fire resistance could be expected of samples with a larger porous structure, 4CEM and 7NO.

7.4.2 Properties change due to application of the IHT method and subsequent thermal exposure according to m-ISO curve

The final configuration of the IHT method, IHT200/2 will be applied on cubes with an edge of 50 mm cut from cubes with an edge of 150 mm, and on cubes with an edge of 100 mm cast individually. Measured parameters are (i) weight change due to application of IHT200/2 and consequent thermal exposure according to m-ISO curve, and (ii) compressive strength reduction due to thermal exposure according to m-ISO curve. The change of compressive strength due to the application of IHT200/2 was not evaluated as the number of samples was limited, and no significant compressive strength loss due to the application of IHT200/2 was recorded in the previous series. Data obtained during the testing are presented in Tab. 41 and Fig. 111 to Fig. 113.

Tab. 41: Data and results from testing of concrete mixes after application of IHT200/2 and thermal exposure according to m-ISO curve.

Name	Ref/ IHT_T/t	Edge of cube [mm]	Weight loss			Compressive strength	
			IHT_T/t [%]	Share of IHT_T/t on total m-ISO [%]	Total m-ISO	Measured [MPa]	Remaining after m-ISO [%]
4CEM	Ref	50	-	-	-	66,4	100,0
		100	-	-	-	61,6	100,0
	Ref_m-ISO	50	-	-	6,64	19,5	31,7
		100	-	-	5,40	16,9	27,5
	IHT200/2*	50	3,99	53,41	7,47	18,4	29,9
		100	2,00	37,74	5,30	15,0	24,4
5FA	Ref	50	-	-	-	55,4	100,0
		100	-	-	-	56,7	100,0
	Ref_m-ISO	50	-	-	7,85	15,3	28,3
		100	-	-	5,7	19,8	35,8
	IHT200/2*	50	4,86	57,79	8,41	15,7	29,0
		100	2,10	35,00	6,00	20,9	36,9
6SF	Ref	50	-	-	-	68,0	100,0
		100	-	-	-	65,4	100,0
	Ref_m-ISO	50	-	-	7,32	20,2	29,6
		100	-	-	6,90	18,3	28,0
	IHT200/2*	50	3,05	50,50	6,04	21,5	31,7
		100	2,30	35,38	6,50	21,6	33,0
7NO	Ref	50	-	-	-	68,5	100,0
		100	-	-	-	68,5	100,0
	Ref_m-ISO	50	-	-	7,34	6,2	9,1
		100	-	-	6,50	9,6	14,0

	IHT200/2*	50	2,89	44,74	6,46	7,4	10,9
		100	2,30	34,85	6,60	9,2	13,5

*Sample with applied IHT200/2 and subsequently exposed according to m-ISO.

Total weight loss due to application of IHT200/2 was significantly higher for samples 4CEM and 5FA with an edge of 50 mm (abbreviation 50), 3,99% and 4,86%, while mixes 6SF and 7NO weight loss was 3,05% and 2,89 respectively, which was still higher than in the case of all samples with an edge of 100 mm (abbreviation 100). As mentioned earlier, samples 50 were cut from the bigger sample, and the cut surface is characterised by higher porosity than "casted surface" composed predominantly by cement paste. The most significant weight loss was recorded with mix 5FA and was caused by the greater volume of free or adsorbed water in the porous structure, that was not chemically bonded into hydration products. The additional reaction of FA is standardly delayed, and it is possible that the reaction still had not fully terminated as thermal exposure testing took place approx. 7 months after casting. The higher weight loss in the cases of mix 6SF Ref and 7NO Ref might be caused by the greater interconnection of a porous structure by extensive microcrack formation. Denser microstructure or lower total moisture content could explain lower weight loss of 4CEM sample 100 and 5FA sample 100 in comparison to mix 6SF and 7NO, where the weight loss of 100 was similar to samples 50.

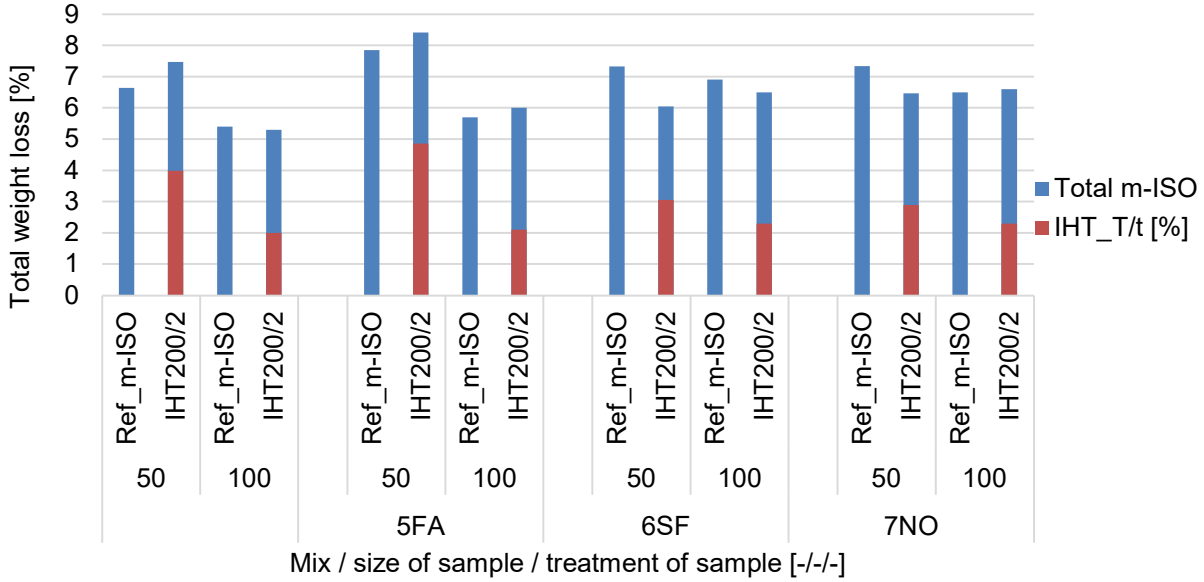

Fig. 111: Weight loss of tested mixes after application of IHT200/2 and consequently thermally loaded according to m-ISO curve.

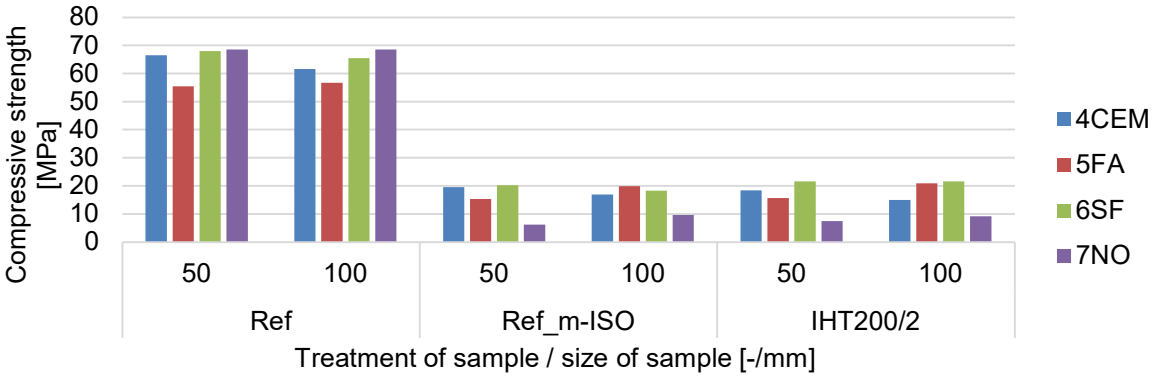

Fig. 112: Compressive strength of reference samples with and without thermal exposure according to m-ISO curve (Ref, Ref_m-ISO), and samples after IHT200/2 application and consequent thermal exposure according to m-ISO curve (IHT200/2).

Overall reduction of strength by thermal exposure according to m-ISO curve was approx. by 69,5% for mixes with Basalt_IS aggregates and 88,1% when Granite_NO was used, see Fig. 112. Explosive spalling or disintegration of samples was not recorded, only the formation of the denser or thinner network of cracks on the surface of samples was observed. Basalt rock is characterised by low thermal expansion coefficient, and even the porosity of the Basalt_IS aggregates was higher but, they still performed much better than Granite_NO.

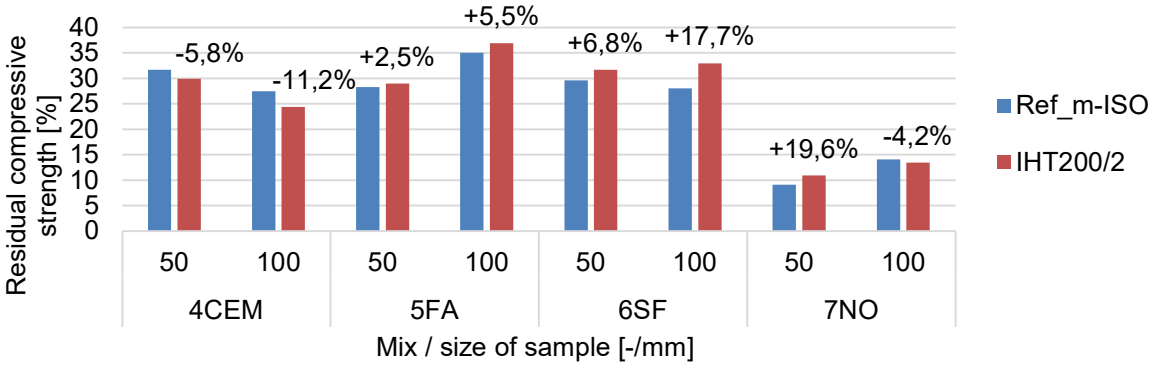

Fig. 113: The compressive strength reduction due to thermal exposure according to m-ISO curve expressed as a percentage of Ref samples without thermal exposure, and the difference between samples with and without application of IHT200/2.

The application of IHT200/2 improved compressive strength in the cases of all samples 5FA and 6SF regardless of the shape, but lower compressive strength was measured in the case of 4CEM. Samples 7NO preserved more strength when a smaller sample, 50, was tested.

7.4.3 Conclusion of the 4th series

Prepared concrete mixes with various binders and aggregates types were intentionally designed with low air content and comparable properties to each other. Properties in a fresh and hardened state were evaluated prior to the application of IHT200/2 and subsequent thermal exposure according to m-ISO curve. Monitored parameters were weight loss and reduction in compressive strength.

Size of the samples and its origin (cut or individually cast) is more significant in the case of mixes 4CEM and 5FA and may be a result of lower heat transfer in concrete, reduced depth of heat penetration, and lower water release from a structure. There was no significant influence of shape and origin on weight loss in the case of the other two tested mixes, 6SF and 7NO, which might be positive when applied in industrial scale on whole structural elements.

Application of IHT200/2 increased residual compressive strength up to 17,7% in case of mix 6SF sample 100, and the difference between residual strength of mix 7NO sample 50 with and without application of IHT200/2 was 19,6%. However, the sample 100 of mix 7NO recorded impairment due to application of IHT200/2 as the influence of Granite_NO aggregates expansion was greater than modification of porous structure in cement paste. Slide improvement was also recorded in the case of mix 5FA by 2,5 and 5,5%. The only mix where the residual strength was higher without application of IHT200/2 was 4CEM, and results from the 3rd series were confirmed.

Visual evaluation of samples proved a less dense network of wider microcracks on the surface of all samples, which might be positive in case of reparation of structures affected by the fire.

The strength improvement in case of mix with silica fume is crucial as it is known that concrete with denser microstructure formed by additional hydration is more susceptible to spalling than concrete with traditional Portland cement and higher w/c ratio. The reduction of the total weight of samples with applied IHT200/2 can be closely connected to the extent of microcrack formation in the whole mass of samples confirmed by lower strength loss of non-

treated samples. The S/C ratio is lower for blended types of cement and concrete with SCM, which is supposed to contribute to a lower quantity of released water, but the dense microstructure seems to play a more significant role when it comes to the fire resistance of concrete.

7.5 Large scale testing of one-side heated uniaxially loaded slabs with applied IHT200/2

Testing of various concrete types with applied IHT200/2 under thermal load according to m-ISO curve was performed on one-side heated uniaxially loaded slabs. The same binder types as in the 4th series but with basalt or granite aggregates, 4CEM, 5FA, 6SF and 7NO were prepared. Slabs thickness was 80±5 mm with exposure area 0,148 m^2. Slabs were placed in the oven, and the rim was insolated by fire resistance fibre insolation to prevent the escape of heat around the test slab. Detailed description of slabs themselves, method of loading and placement of thermocouples are in chapter 6.3.4, and graphically in Fig. 80 and Fig. 81. Thermocouples were monitoring temperature development at depths of 0, 20, 40 and 60 mm from the heated surface. Set up was inspired by experimental work presented during the 5th International RILEM Workshop on Concrete Spalling due to Fire Exposure, Borås, Sweden.

Test slabs were stored in wet storage for 28 days after casting, and then moved into a laboratory where they aged for about 6 months, to reduce the moisture content approx. to 3% as recommended in EN 1992-1-2: 2004 Eurocode 2: Design of concrete structures - Part 1-2: General rules - Structural fire design (6). Actual moisture content was monitored by the surface moisture-meter Tramex CME4 every 2 weeks. Test slabs were weighed prior to the application of IHT200/2 and subsequently loaded and placed on the test frame. After the application of IHT200/2 cracks, discolouration, and weight loss of slabs were inspected. Thermal exposure, according to m-ISO curve, was performed within 72 hours after the IHT200/2 application, the load level was unknown. After reaching the requested maximum temperature 1050°C, the oven was switched off and the test slab remained placed on the oven with applied uniaxial loading during the whole cooling period.

The moisture content was measured before and after application of IHT200/2, and again before, during and after thermal exposure according to m-ISO curve. During the thermal exposure, according to m-ISO curve, the surface temperature on the top and sides was recorded by laser temperature-meter, as well as crack formation on the top and sides of the sample. Finally, overall monitoring of phenomena such as explosive spalling, moisture release from cold surface, and discoloration or shape changes of the slab were carefully observed during the whole exposure period.

Results of weight changes, moisture, temperature and crack development after IHT200/2 and thermal exposure according to m-ISO curve will be presented and discussed. Diagrams of heat spread during IHT200/2 and exposure according to m-ISO curve will be given in two separate diagrams for all four slabs, and individually processed diagrams are attached as Annex 3. It is important to mention, the limitation of equipment for testing of thermal exposure up to temperature 1050°C with an electric oven designed for cauterisation of potteries, and which does not have any protection features against explosive spalling of concrete. Based on this fact, it was decided to perform slab testing only of slabs with applied IHT200/2, where the probability of explosive spalling was predicted to be lower.

7.5.1 Application of IHT200/2

The weight loss due to application of IHT200/2 was low, from 0% in the case of 5FA up to 0,17% in the case of 7NO. A small overheat was recorded between the heating ramp and establishment of heating temperature, but exposure temperature 200°C was stabilised within 15 minutes. During the application, cracks on the side of slab 7NO appeared. A lower heating rate shall be selected to prevent crack formation during IHT method application. Another option is also lower exposure temperature, but that would influence the length and efficiency of lower

heating rate shall be selected IHT method. The maximum temperature gradient (Tg) was similar for all concrete mixes, see Tab. 42, and individual Tg calculated between 0 to 20 mm, 20 to 40 mm and 40 to 60 mm are presented in Fig. 114, and in detail in Annex 3.

Tab. 42: Parameters of tested slabs.

	Thickness of slab [mm]	Weight of slab before IHT200/2 [kg]	Heated area [m^2]	Weight loss due to IHT200/2 [%]	Max. Tg [*10^3 °C/m]
4CEM	79,0	55,45	0,148	0,09	7,63
5FA	81,0	56,35	0,148	0,00	8,05
6SF	81,0	57,2	0,148	0,09	8,72
7NO	80,0	57,45	0,148	0,17	8,28

The Tg in the first 20 mm from the heated surface was increasing rapidly during the whole heating ramp period up to 200°C and reached values from 7,63 to 8,72*10^3 °C/m. During the temperature dwell Tg was gradually decreasing until the end of the temperature dwell and subsequently Tg was dropping rapidly. The same trend, but with the maximum Tg between 0,8 to 1,0 *10^3 °C/m was observed in depths between 20 to 40 mm, and even lower between 40 to 60 mm which is favourable for IHT method as it is meant to be applied only up to a depth of 50 mm (standard thickness of a cover layer of steel rebars). The gradual decrease of Tg between 0 and 20 mm during the temperature dwell is resolute for efficiency (length and depth of application).

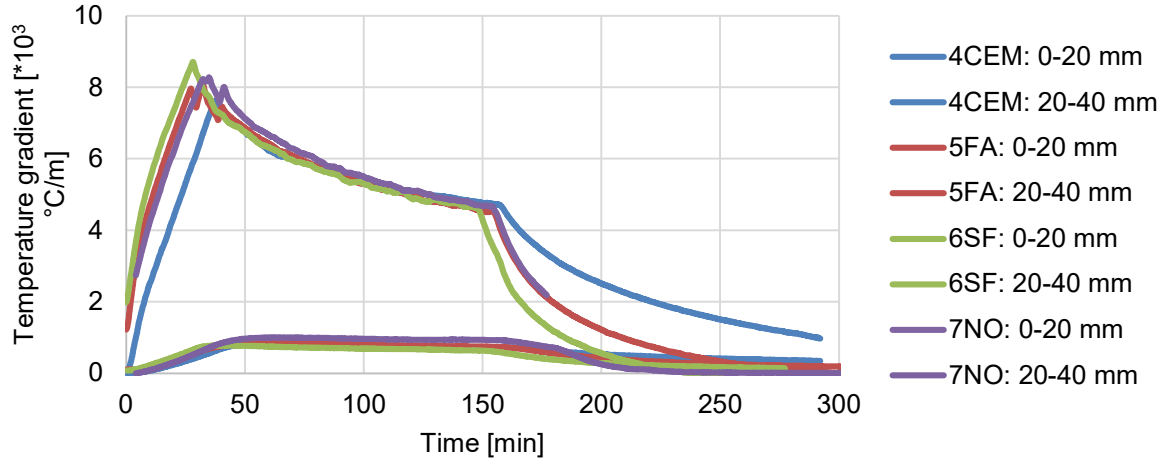

Fig. 114: The development of thermal gradient in slabs during the application of the IHT200/2.

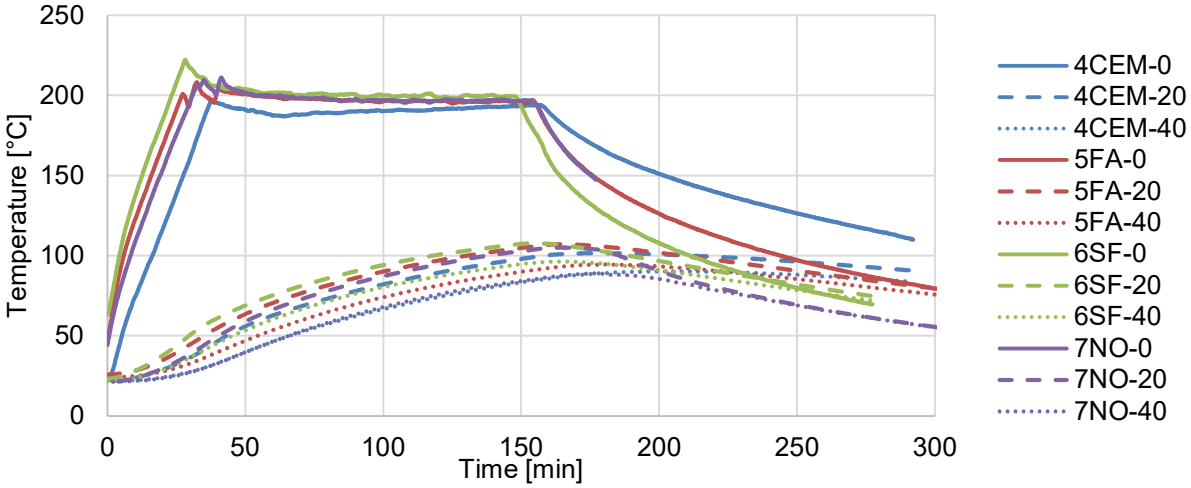

Fig. 115: Exposure temperature measured during the application of IHT200/2.

Within individual slabs, the heat spread differed due to concrete type, its porosity and moisture content, both connected to coefficient of thermal conductivity, but was not crucial during the application of IHT200/2. Based on all processes which arise during the thermal exposure of concrete, a temperature of 120°C was selected as decisive for IHT zone and temperature 95°C for IHT transition zone. In other words, the thickness of the IHT method is defined by a temperature higher than 95°C, as showed schematically in Fig. 116, and exact calculation for 6SF in Fig. 117.

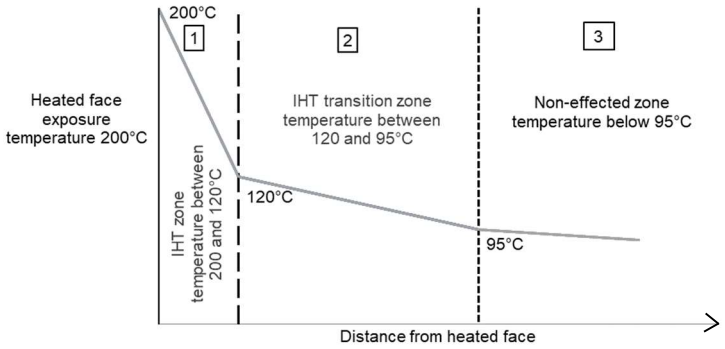

Fig. 116: Graphical presentation of the IHT method zones. Zone 1: Evaporation of free and mechanically bonded water from pores and CSH interlayers, and release of chemically bonded water from Ettringite and CSH gel; Zone 2: Evaporation of free and mechanically bonded water from pores and CSH interlayers; Zone 3: Evaporation of free water formed pores in limited amount and low speed.

Processes which are taking place between 200°C and 120°C are (i) modification of CSH gel and predominant formation of Larnite, with the highest intensity between 120°C and 200°C; (ii) recrystallisation of Ettringite between 70°C and 120°C, and (iii) evaporation of free, surface adsorbed (physically bonded by van der Waals forces), and chemically bonded water. The highest ratio of free water evaporation is between 95 and 105°C (84), which is extending the thickness of the affected area and is called a transition zone between non-treated concrete and IHT method. In this transition IHT zone, defined by minimum exposure temperature 95°C, is a partly reduced amount of free, adsorbed and chemically bonded water from Ettringite.

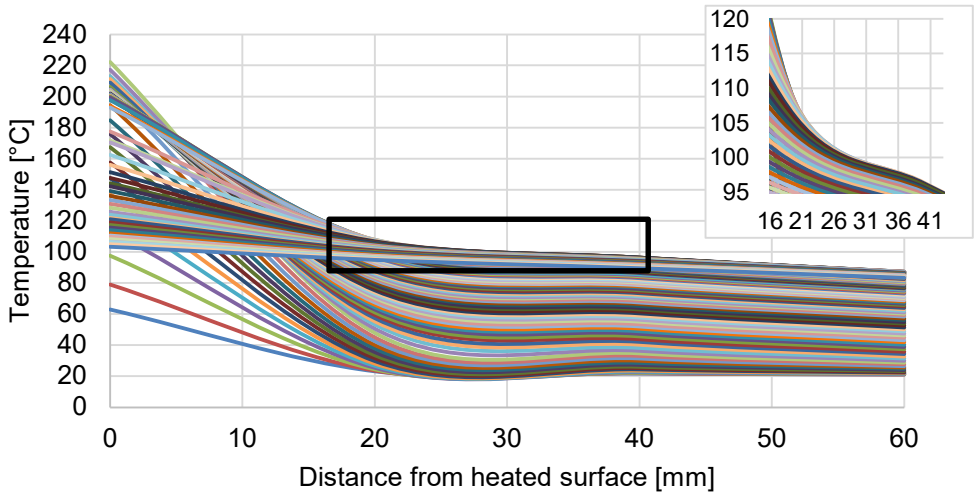

Fig. 117: Heat penetration: dependency of temperature and distance from the heated surface – detail of IHT transition zone, sample 6SF.

Cooling to ambient temperature does not have an influence on the IHT method; the only parameter to be considered is the length of cooling for the total IHT_T/t application length determination. Cooling to ambient temperature is much longer, but the decisive temperature is 95°C, which is selected as conclusive temperature for the establishment of the IHT transition zone.

Tab. 43: Parameters for IHT zone and IHT transition zone for tested concrete types.

	IHT zone: Target temp. 120°C				IHT transition zone: Target temp. 95°C				Total IHT
	Surface temp. [°C]	Width [mm]	Time [min]	Tg [*10^3 °C/m]	Surface temp. [°C]	Width [mm]	Time [min]	Tg [*10^3 °C/m]	[mm]
4CEM	193,1	14,5	158	5,04	147,5	11,0	206	2,06	25,5
5FA	196,5	15,5	154	4,94	140,6	23,0	184	1,18	38,5
6SF	199,3	16,0	148	4,96	142,8	27,0	168	1,11	43,0
7NO	197,1	15,5	154	4,97	146,0	13,5	178	1,76	29,0

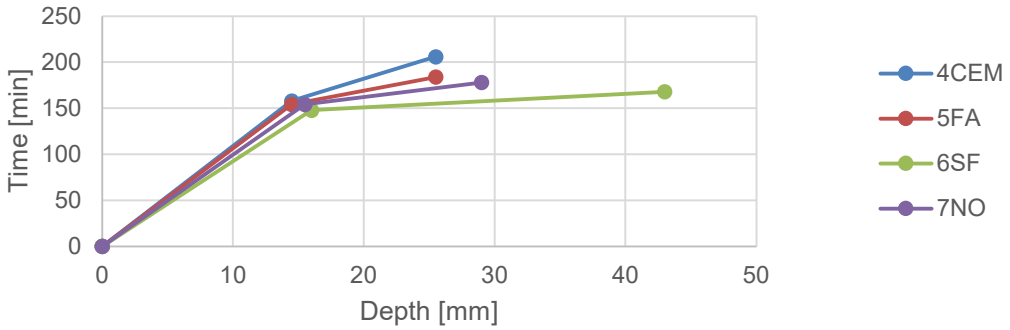

Fig. 118: Dept of IHT200/2 penetration and IHT transition zone.

Application of IHT200/2 did not cause any damage to all mixes with Basalt_IS aggregates – 4CEM, 5FA and 6SF. Cracks with a width of 0,4 mm formed on the non-loaded sides of slab 7NO with Granite_NO aggregates, during the application of IHT200/2. Cracks were forming during the heating period, and therefore it is assumed that temperature gradient (8,28*10^3 °C/m) is too high and by a selection of slower heating regime, or reduction of maximum temperature, crack formation could be prevented. The temperature gradient of all slabs was up to 8,72*10^3 °C/m, and the depth of IHT200/2 penetration from 14,5 to 16 mm (6SF). The width of the IHT transition zone was between 11,0 and 27,0 mm, and is dependent on the speed of cooling and related to penetration depth of temperatures between 120 and 95°C, below 95°C is concrete considered non-effected by the IHT method, see **Error! Reference source not found.**. Total thickness of IHT method is between 25,5 and 43,0 mm.

7.5.2 Thermal exposure of slabs with applied IHT200/2 according to m-ISO cure

Exposure of one-side heated, uniaxially loaded slabs was performed approx. 48 hours after the application of IHT200/2. The behaviour of individual slabs, 4CEM, 5FA, 6SF and 7NO was slightly different, but overall results from testing were comparable and followed the same trend, no explosive spalling and formation of one larger crack during the cooling period. The only expectation was slab 6S with silica fume, which contributed to formation of network of cracks with width up to 0,6 mm. Temperature development in individual test slabs is presented in Annex 3, and it could be concluded that 6SF has the highest thermal conductivity, which is also confirmed by Tg.

Fourier´s law explains temperature gradient relation to thermal conductivity, which is essential for research connected to fire resistance of concrete. Measurements of temperature in depths 20, 40 and 60 mm from the heated surface provided valuable data for evaluation of moisture migration through the test slab. As the cold surface of the slab was not isolated, moisture could freely migrate in all directions and evaporate from all surfaces (heated and non-heated). From Fig. 119 areas are visible where Tg is constant which signifies moisture migration towards a non-heated surface. This phenomenon was observed in the case of all samples and varies based on the coefficient of thermal expansion, moisture content and porous structure of given concrete.

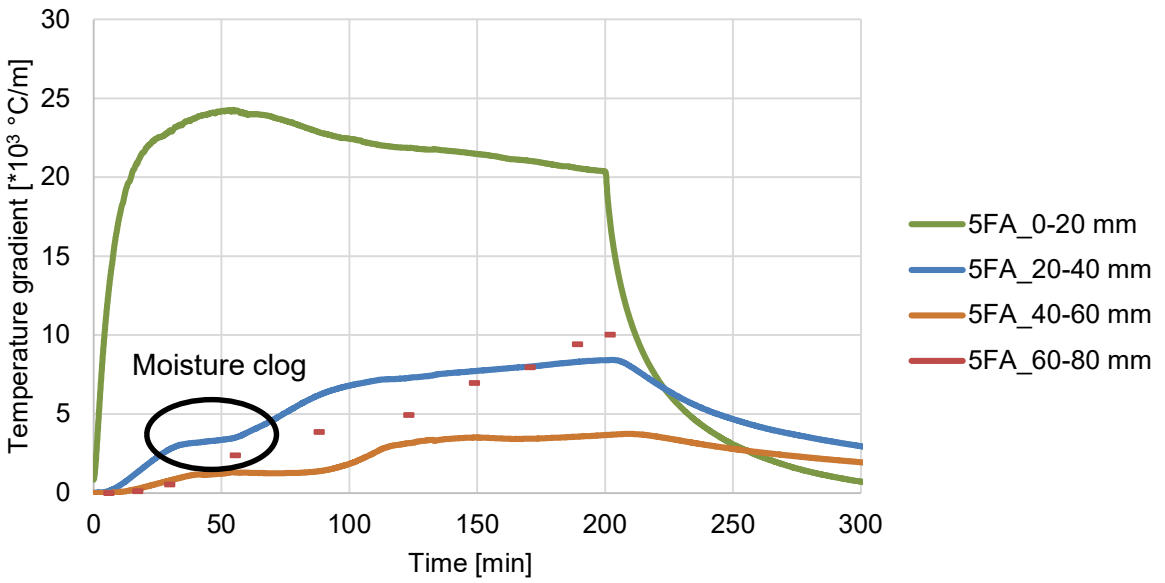

Fig. 119: Temperature gradient development of sample 5FA during the thermal exposure according to m-ISO curve.

Moisture migration and its evaporation from the non-heated surface was also verified by moisture measurements performed during the thermal exposure according to m-ISO curve on top and sides of individual slabs. As an example moisture development of sample 5FA, Fig. 120, is presented where the release of moisture was continual and has not reached high values as recorded during the testing of AeA-FiResCrete (Fig. 128).

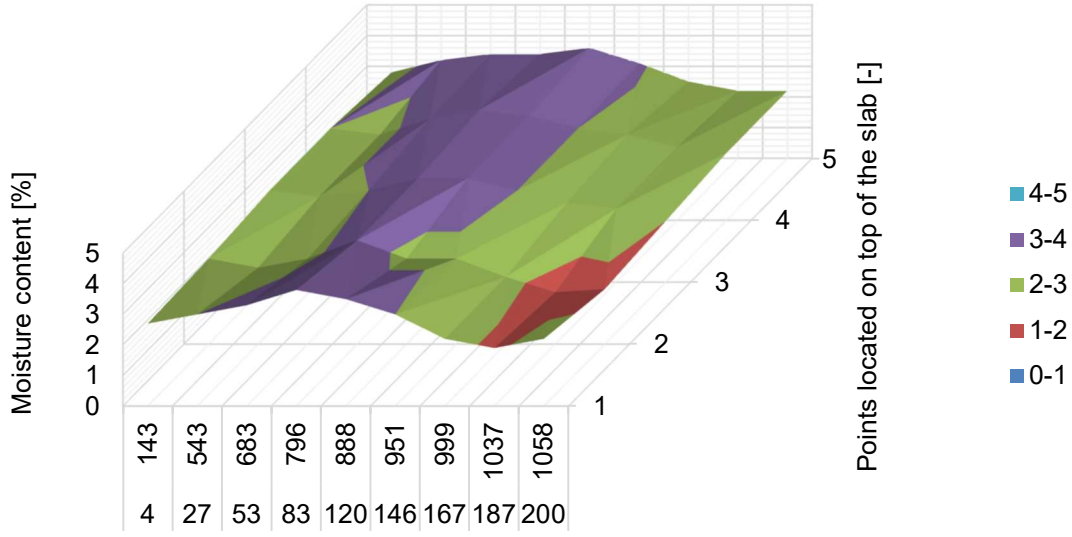

Fig. 120: Moisture development on the top surface of slab 5FA with applied IHT200/2 during thermal exposure according to m-ISO curve.

The most significant damages were recorded in the case of 7NO and 6SF. The cracks which were formed during the thermal exposure on slab 6SF have not closed as in the case of other tested samples and remain open. The release of vapour from slab 7NO was significant, and the width of a single crack during cooling was the biggest, see Fig. 121.

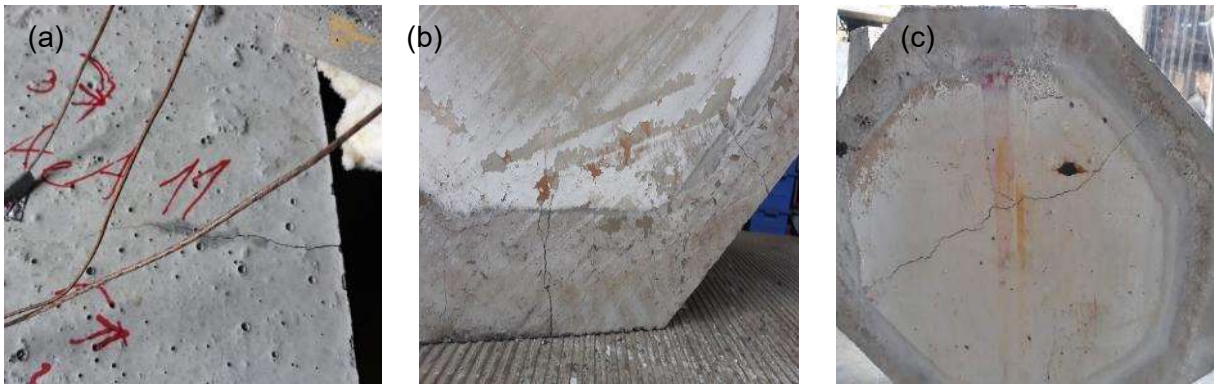

Fig. 121: Photo documentation of sample 7NO and 6SF during and after thermal exposure. (a) Moisture evaporation during heating period; (b) Cracks on the edges after cooling; (c) one crack formed during cooling across the whole slab in the direction of loading.

7.6 The final conclusion of IHT method parameters

The efficiency of the IHT method is based on three main parameters, speed of heating, maximum exposure temperature and length of thermal exposure.

The maximum rate of the heating should not cause cracking of surface and extensive microcrack formation. The speed of heating is closely connected to a temperature gradient, which can serve as a monitoring parameter for the selection of the heating speed. The IHT200/2 with the maximum temperature gradient $8{,}72*10^3$ °C/m showed satisfactory results besides the concrete mix with Granite_NO aggregates where the slower heating rate with a lowered temperature gradient would be recommended.

It is beneficial to keep the maximum exposure temperature under 200°C due to thermal volume changes of cement paste and degradation due to recrystallisation of chemical compounds in the cement paste. The IHT200/2 achieved a depth of IHT penetration between 14,5 to 16,0 mm in the case of all tested concrete types, and the cracks formed during the heating of 7NO stabilised and have not expanded further. The thickness of the IHT zone and IHT transition zone is predominantly depended on the coefficient of thermal conductivity and moisture content of concrete. However, as those parameters are changing based on exposure temperature, it is not convenient to set them as reference parameters for the configuration of individual IHT method parameters for various concrete types.

The length of the application of the IHT method is decisive for its efficiency and thickness of the surface layer modified by the IHT method. The penetration of heat is decreasing over the exposure time, and with longer exposure time, the method is becoming less efficient. The temperature gradient showed a decreasing tendency, and therefore the exposure length 2 hours seems to be the most effective. The thickness of the IHT zone, and the IHT transition zone cannot be wider than the cover layer due to the overheating of steel rebars, which was achieved. Furthermore, the IHT method does not have any impact on bearing capacity and durability of the existing structure.

The results of all four series are consistent and would serve for the development of a mathematical model for configuration of the IHT method and its design for various concrete types. Furthermore, all four series adjoin each other and confirm the final configuration and mechanism of the IHT method. During the development of the IHT method more influencing factors than expected was identified and the extension of the development was enormous. Due to this fact, the detailed investigation of the other two methods was reduced and served only for comparison to the IHT method and its verification.

Moisture content and porous content influencing the heat transfer in concrete, and penetration of heat is lower with denser porous structure. Higher moisture content contributes to higher conductivity, but when more pores are present, conductivity is reduced despite higher

moisture content in the pores. Also, higher porosity is commonly characterised by higher moisture content and when the moisture evaporates, the heat conductivity is changed. Thanks to the higher conductivity of dense structure with silica fume, heat transfer during the application of the IHT method is faster, and thickness of the IHT transition zone is bigger, but still within the limits of the cover layer, which is commonly 50 mm. This phenomenon is highly beneficial for extension of drying zone, and a significant reduction of pressure development and formation of moisture clog. Graphical explanation of the IHT method principle by temperature (T), vapour pressure (p_v) and moisture content (w) changes in relation to time during the thermal exposure as described in Fig. 122**Error! Reference source not found.**.

The Dry zone (DZ) and Vapour zone (VZ) are wider in the case of normal strength concrete while high strength concrete, such as high-performance or ultra-high performance concrete has thinner VZ closer to the heated surface. As moisture clog and rise of vapour pressure is concentrated in thin area, explosive spalling could occur. The application of IHT method extends the VZ and remains closer to the heated surface as in the case of high-performance concrete, which provides easier migration of moisture with lower vapour pressure as the release takes place in a larger area (wider vapour zone).

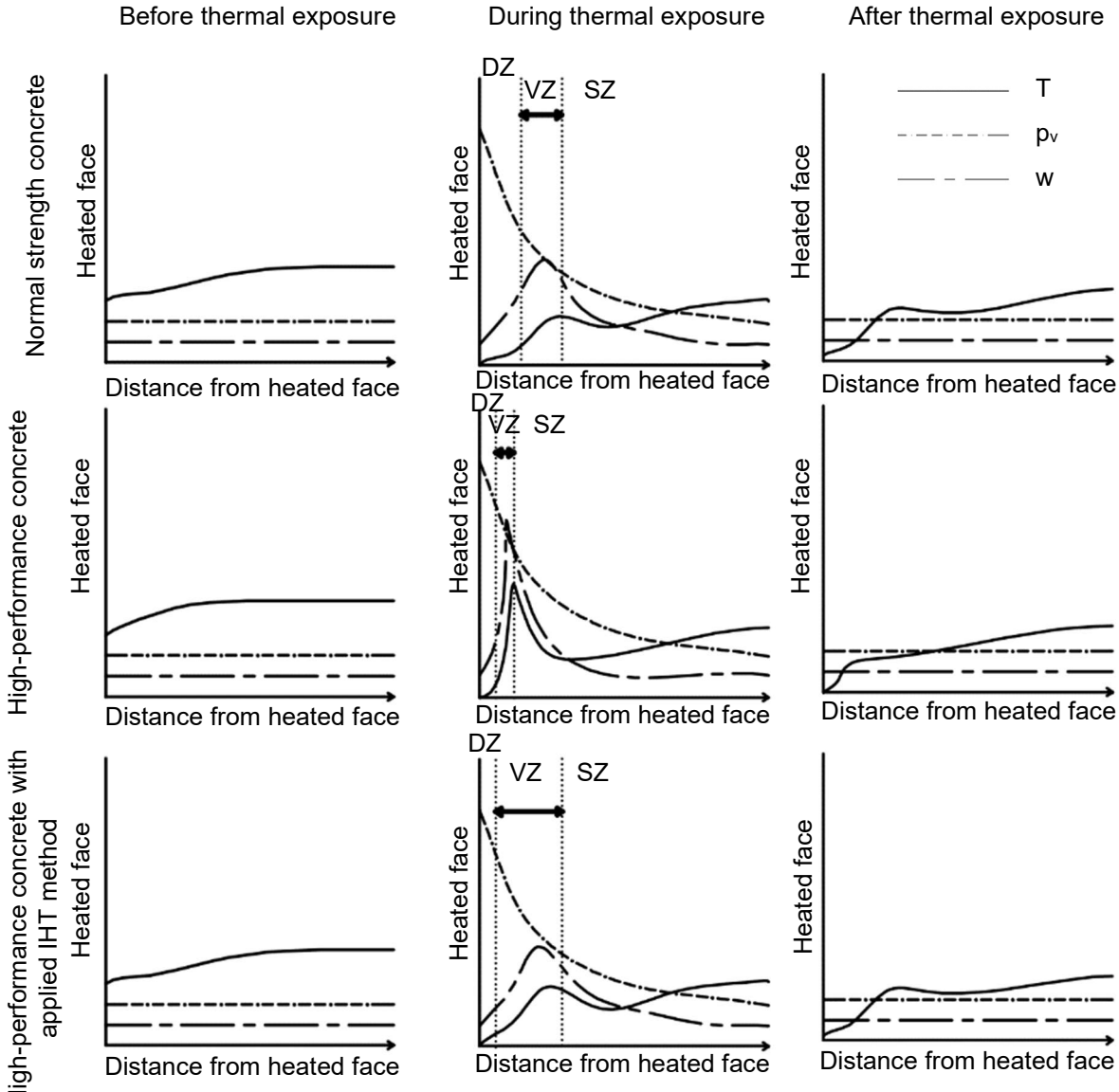

Fig. 122: Graphical explanation of IHT method principle. The thickness change of dry zone and extension of vapour zone thanks to application of the IHT method. Abbreviations: Dry zone (DZ); Vapour zone/Drying zone (VZ); Saturated zone/Moist concrete (SZ); Temperature (T); Vapour pressure (p_v); Moisture content (w).

In comparison to polypropylene fibres (PPF) IHT method is active since the first moment of a fire event, while PP fibres contribute in a bigger share to fire resistance after their melting, which could be from 150 to 170°C depending on their individual characteristics. Prior to the melt of PPF, the vapour escape channels are only in porous ITZ around the fibres - PITS principle (97).

The technique for application of the IHT method on existing structures would be executed by truck with hydraulic arms finished with radiator boards in the shape of the surface prepared for treatment. A truck would move according to the configuration of IHT_T/t. The speed of the truck will define the heat ramp (indirect radiation from sides of main heat panel), maximum exposure temperature (adjustable on the radiator), and length of exposure to requested maximum exposure temperature will be again defined by the speed of the truck. The cooling phase will depend on overall conditions in the tunnel, and its duration can be eventually regulated by some shielding located next to the radiator for extension of the cooling phase. An example of the truck for the application of the IHT method is shown in Fig. 123.

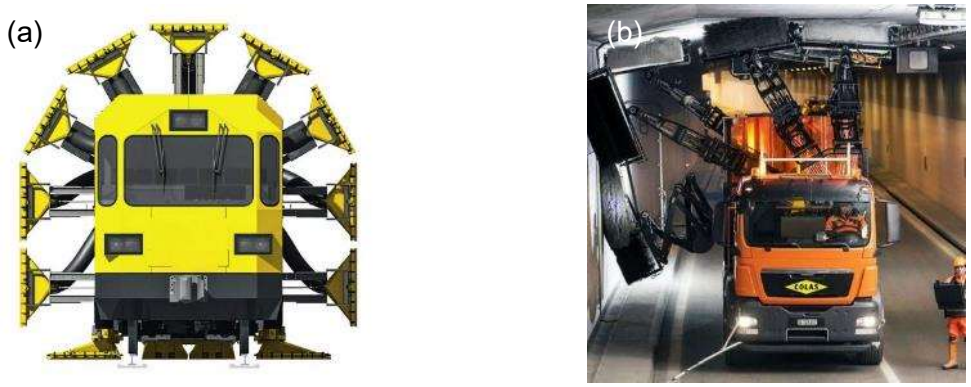

Fig. 123: Example of truck for application of IHT method: (a) for train tunnels; (b) for road tunnels.

Newly developed IHT method for enhancement of fire resistance might be innovatively used also for the treatment of industrial floors in fabric with high temperature production processes.

8 CHAPTER: AEA-FIRESCRETE UNDER THERMAL LOAD

Experimental work focused on the behaviour of concrete with the addition of traditional and new generation AeA exposed to elevated temperatures consists of 4 mixes. Structure of data is the same as in previous sections (i) description of action; (ii) mix design; (iii) fresh concrete properties; (iv) hardened concrete properties; (v) fire testing; (vi) conclusion on fire resistance of AeA-FiResCrete. The assumption that higher air content in concrete contributes to fire resistance will be verified. Data from fire testing consists of small-scale testing on cubes with an edge 100 mm and large-scale test of one-side heated, uniaxially loaded slabs.

Concrete with the same aggregates type (Basalt_IS), cement, relatively same w/c ratio and a dose of superplasticizer. Workability and air content varied significantly, see Tab. 44. New generation AeAs have different dosing as they are in solid, not liquid form, and the optimal dose was verified before final fire resistance testing. Detailed description of individual AeA is in chapter 3.1.4 and 6.1.5. Traditional pressure methods for evaluation of air content in fresh is not fully suitable for air in the form of polymer microspheres, and chemically formed air, which can evolve during the solidification of fresh concrete.

Results from air void characteristics correlate with freeze-thaw resistance in the case of all tested samples, 1AeA-N and 3AeA-Si had sufficient air content, which contributed to low scaling during the freeze-thaw testing, while the other two samples had low air content in hardened concrete and failed freeze-thaw resistance testing. Sample 2AeA-MC with polymer microspheres showed rather suitable air content in the fresh state (4,0%), but it is a matter for discussable weather the measured air contains polymer microspheres or not. Freeze-thaw

resistance was insufficient and explained by poor air void distribution and total air content in hardened concrete, which also resulted in unsatisfactory performance under thermal load.

Tab. 44: Properties of four AeA-FiResCrete mixes in the fresh and hardened state.

Name	Fresh concrete		Hardened concrete						
	Slump test	Air content	Density	Compressive strength [MPa]		Air void characteristics			F-T res*
	[mm]	[%]	[kg/m^3]	28 days	90 days	α [mm^{-1}]	A [vol.%]	L [mm]	56 cyc. [kg/m^2]
1AeA-N	110	9,6	2342	49,9	54,3	22	8,4	0,11	0,05
2AeA-MC	210	4	2430	48,3	53,5	21	2,9	0,3	0,76
3AeA-Si	50	5,1	2433	55,3	62,6	23	4,8	0,21	0,23
4CEM	70	3,0	2570	55,7	61,6	10	3,0	0,68	4,65

*The amount of scaled material after exposure to 56 freeze-thaw cycles.

The cause of insufficient freeze-thaw resistance in the case of 2AeA-MC might also be due to incomplete dispersion of polymer microspheres during the mixing process. The high content of air (8,4%) in mix 1AeA-N ensured good freeze-thaw resistance, but the reduction of compressive strength by 16 MPa in comparison to 4CEM (same mix without AeA) is inappropriate.

8.1 Thermal exposure of AeA-FiResCrete according to m-ISO curve

Fire resistance of AeA-FiResCrete mixes was at first tested on cubes with an edge of 100 mm and loss of compressive strength along with weight loss recorded, see Tab. 45 and Fig. 124. Concrete mix 1AeA-N, which performed the best in freeze-thaw resistance test, had the highest strength loss due to thermal exposure according to m-ISO curve. Both new generation AeA performed slightly better than traditional AeA (1AeA-N), but remaining strength was lower or equal to samples treated with IHT method. The dependency of the high content of air in hardened concrete on remaining compressive strength after thermal exposure was unclear, especially when sample 3AeA-Si is compared to 4CEM with low air content and extremely poor freeze-thaw resistance.

Tab. 45: Results from thermal exposure of AeA-FiResCrete samples according to m-ISO curve.

Concrete type	Ref/IHT_T/t	Weight loss m-ISO [%]	Density [kg/m^3]	Compressive strength m-ISO	
				[MPa]	Remaining f_c after m-ISO [%]
1AeA-N	Ref		2220	62,5	-
	m-ISO	5,6	2119	13,5	21,6
2AeA-MC	Ref		2309	56,0	-
	m-ISO	5,9	2186	13,2	23,5
3AeA-Si	Ref		2326	59,1	-
	m-ISO	5,7	2202	16,1	27,2
4CEM	Ref		2466	61,6	-
	m-ISO	5,4	2212	16,9	27,5

Weight loss of 2AeA-MC was the highest due to melting and subsequent evaporation of polymer microspheres, which was also proven by the discolouration of the test sample. In

general, the loss of strength as a result of thermal exposure is too extensive, in the range of 79,4 to 72,5%, and reparation of such a damaged concrete would be an impossible task as the whole section of an effected element must be changed.

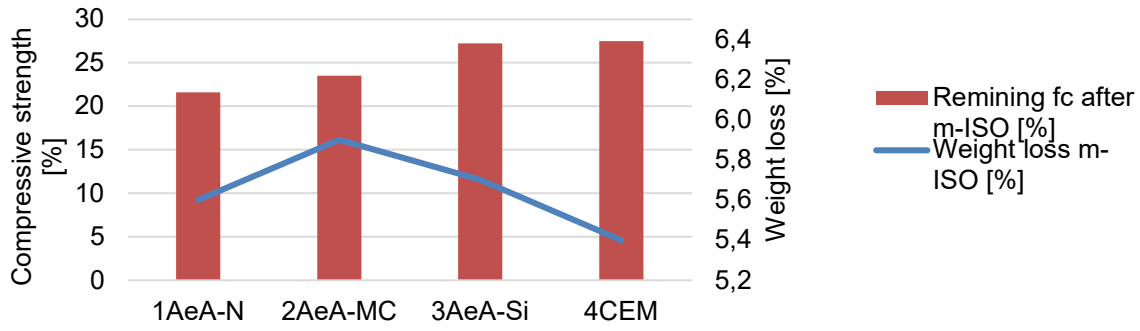

Fig. 124: Graphical presentation of remaining strength and weight loss due to thermal exposure of AeA-FiResCrete samples according to m-ISO curve.

The behaviour of AeA-FiResCrete was also verified on concrete slabs in the same way as verification of the IHT method. One-side heated, uniaxially loaded slabs with in-built thermocouples at the depths of 20, 40 and 60 mm from the heated surface were thermally loaded according to m-ISO curve, and temperature development monitored during the exposure, see Fig. 125.

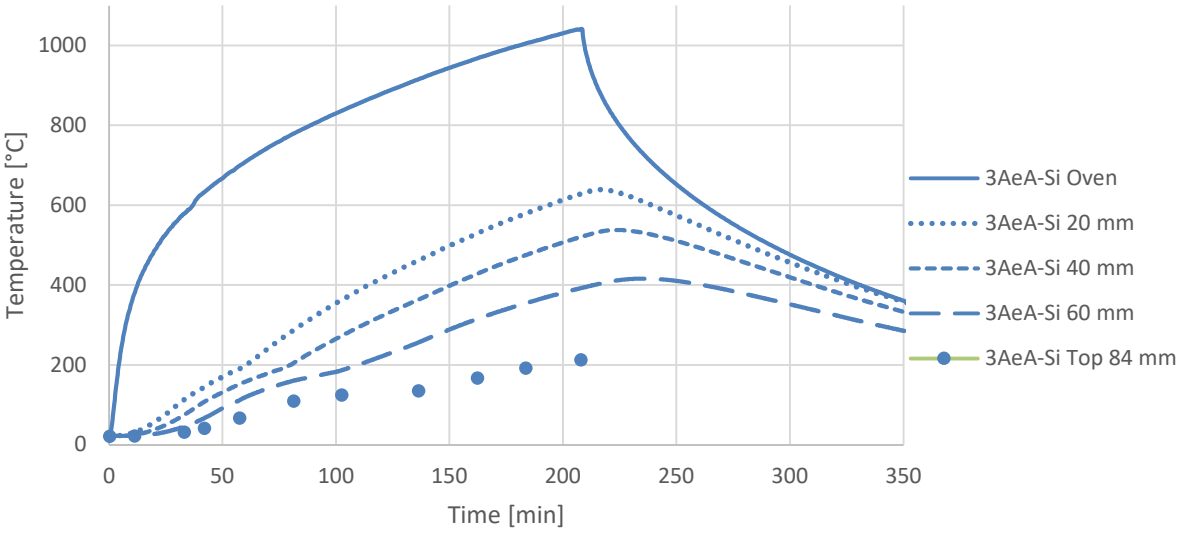

Fig. 125: Temperature development measured during the thermal exposure according to m-ISO curve of 3AeA-Si.

Development of heat in slab 1AeA-N and 3AeA-Si was similar, but temperature development in slab 2AeA-MC was significantly influenced by the melting of polymer microspheres, see Annex 4. Melting of polymer microspheres also influenced the temperature gradient and “moisture clog” is extremely visible from results of Tg (Fig. 127) and might be misleading.

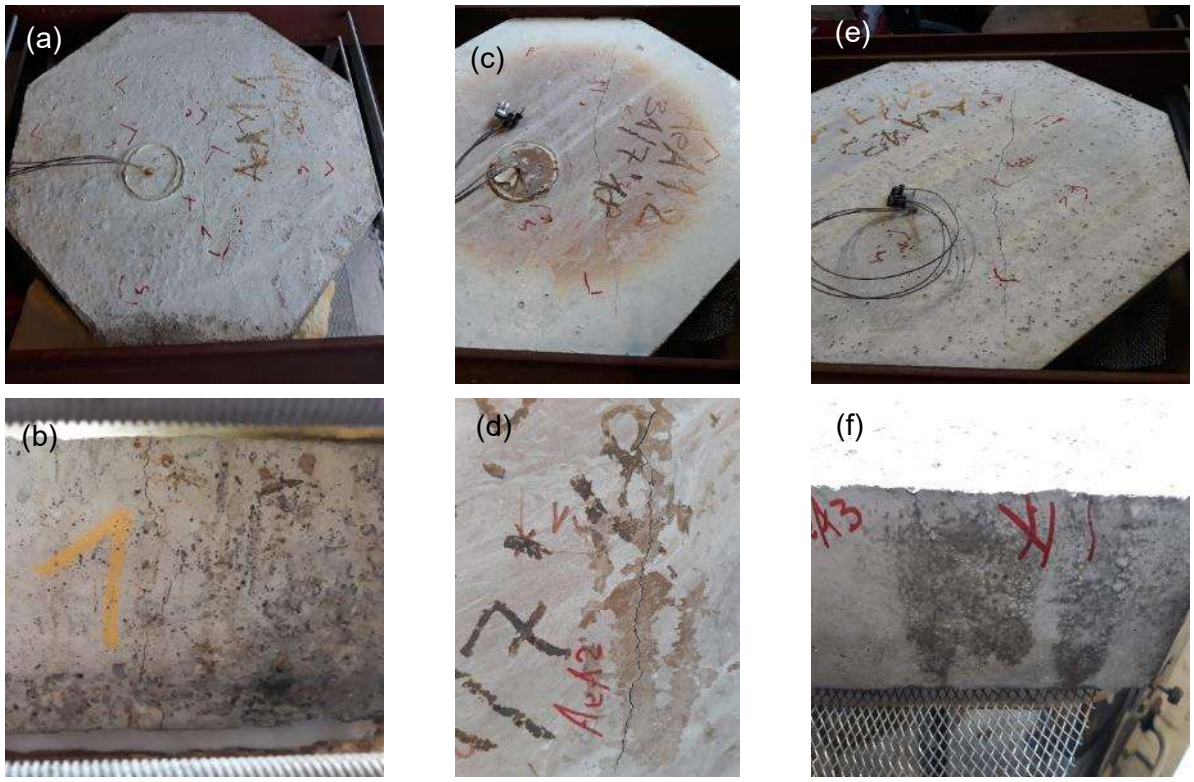

Fig. 126: Photo documentation of tested slabs. (a)1AeA-N crack formed over the whole slab during the cooling period; (b) 1AeA-N crack on the side of slab formed during the thermal exposure according to m-ISO curve; (c) 2AeA-MC discoloration due to melting of polymer microspheres; (d) 2AeA-MC heated surface where the polymer microspheres formed white powder coating; (e) 3AeA-Si cracked formed on the non-heated surface during the cooling period; (f) 3AeA-Si evaporation of water vapour from the side of the slab during the heating period.

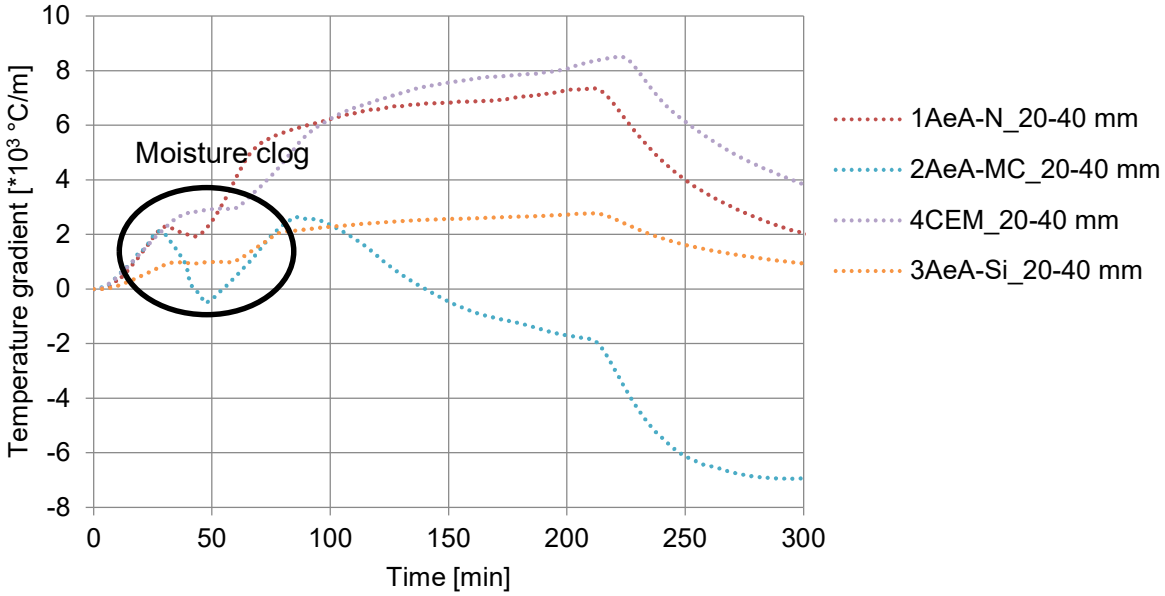

Fig. 127: Temperature gradients of individual slabs measured between 20 to 40 mm from a heated surface according to m-ISO curve.

Moisture clog was significant in the case of 1AeA-N and 2AeA-MC, while 3AeA-Si had a less dense and wider condensation zone demonstrated by temperature dwell and subsequent gain recorded by inbuilt thermocouples. Such a temperature dwell is expressed in Tg as drop and subsequently rapid increase of Tg. From Fig. 125 migration of moisture clog (vapour zone) towards the cold surface is visible, and from moisture content measured by contact moisture-meter TRAMEX CM4 on the top surface (Fig. 128) it can be concluded, that the moisture zone

migrated through the whole thickness of the test slab. Moisture content was the highest at 600°C (38 min from initiation of the test) and consequently decreased below the initial measured value.

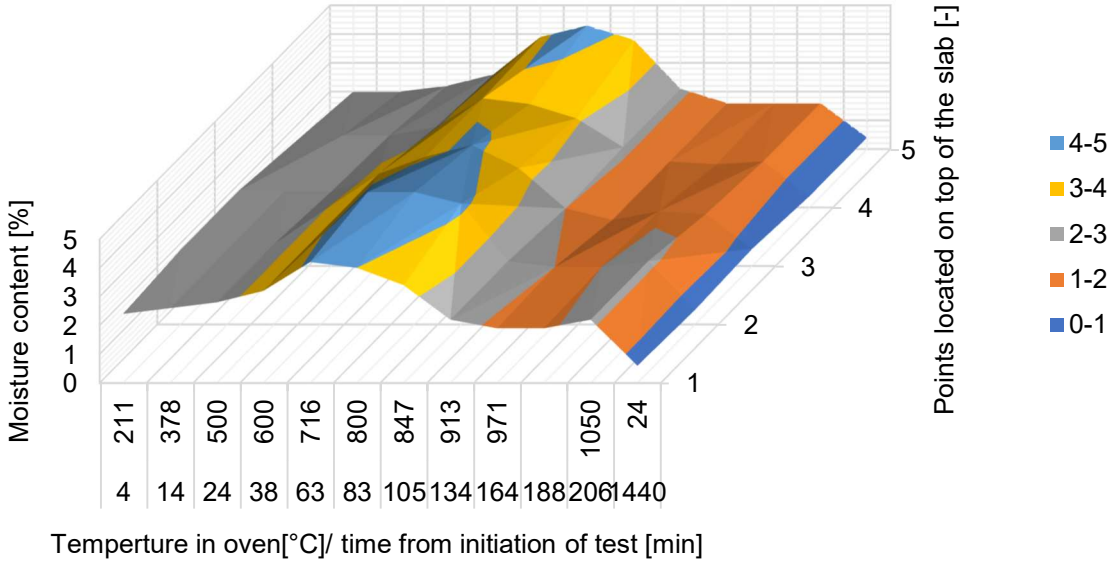

Fig. 128: Moisture development on the top surface of slab 2AeA-MC during thermal exposure according to m-ISO curve.

Explosive spalling has not occurred as the moisture was not restricted and could evaporate through a non-heated surface. In real situations would be further migration of moisture clog would be restricted, and extensive development of vapour pressure in the surface layer might cause crack formation and explosive spalling.

During the thermal exposure, according to m-ISO curve, cracks with a width of 0,2±0,1 mm were formed on the unloaded sides of the slab. Those cracks closed during the cooling phase, and one larger crack over the whole length in loading direction was formed. The width of the crack formed during cooling differs for individual slabs and was caused by uneven cooling signified by rapid reduction of thermal gradient in the zone 0-20 mm from the heated surface. Furthermore, volume changes of concrete at the time of cooling, expansion of cement paste, also contributed to single crack formation, and, as a consequence of uniaxial loading, expansion of slab was permitted only perpendicularly to the loading direction. The shape of the test sample was unique and a combination of a loaded and non-loaded section, see Fig. 81, which might contribute to unusual results, such as crack propagation and subsequent extermination, or single crack formation during the cooling phase. Additionally, test slabs were not reinforced; thus, expansion was not restricted by any inner component. In other words, it could be stated that the flexural strength of tested concrete is lower than forces created by volume changes of cooling concrete. Detailed investigation of cooling of the concrete slab after thermal exposure is not the subject of this work and will be published separately in a suitable journal.

8.2 Conclusion of AeA-FiResCrete

The assumed theory of the relation between freeze-thaw resistance and fire resistance of concrete was not fully confirmed, and only a small overlap of pore diameter suitable for both is registered and confirmed by pores structure evaluation in IHT method development 1st series, chapter 7.1. Concrete mixes prepared in this chapter serve for comparison to the IHT method, especially behaviour of slabs. The detailed evaluation of porous structure is subject to further study. For air content in fresh concrete Airvoid analyzer (AVA) might be suitable, and use of intrusion mercury porosimetry or 1H NMR analyser for analysis of the porous structure of hardened concrete might verify present conclusions.

Higher porosity suitable for freeze-thaw resistance of concrete is not necessarily improving fire resistance of concrete. The higher porosity is no assurance of the easier migration of water through the microstructure. If the porous structure is formed by larger pores characterised by a poor spacing factor, migrating water and vapour have difficulties in passing between individual pores through narrow “necks” explained by Bažant (83). Further investigation of the “new generation” AeA – Centrament Airpolymer (polymer microspheres) from MC-Bauchemie is adventurous as the number of detected air pores was insufficient.

Moisture clog was more significant in the case of higher air content (1AeA-N), while mix 4CEM with denser structure with applied IHT200/2 recorded a wider vapour zone with lower moisture cumulation. Also, AeA SikaControl AER-200 P from Sika in mix 3AeA-Si contributed to the extension of the vapour zone, which is favourable for mitigation of crack formation and fire spalling.

CONCLUSION

Fire resistance is a complex problem, which involves many variables and influencing parameters. Therefore, extensive literature review and theoretical explanation of the necessity of fire resistance, legislation connected to fire protection and presently used fire protection methods are described. Finally, a detailed description of individual components and subsequently concrete as a cementitious composite was described, to gain basic knowledge about mechanical, physical and chemical changes due to thermal exposure.

The subject of this PhD thesis was the development of two different approaches for enhancement of fire resistance of concrete structures, especially structures from the higher fire risk group such as tunnel lining, underground garages, and possibly nuclear power plants. The greatest attention was given to the development of a new method for enhancement of fire resistance of existing structures based on porous structure modification by intentional heat treatment. There is no completely suitable method for enhancement of fire resistance for existing tunnel lining and other structures with the higher fire risk level and restricted space and reduced ventilation possibilities. The second method AeA-FiResCrete is suitable for new constructions where modification of concrete design will lead to the improved fire resistance of the concrete structure.

For the development of both methods, smaller samples exposed entirely to elevated temperatures were used, and followed by large-scale testing. A final assessment of efficiency of developing method was performed on one-side heated uniaxially loaded slabs with inbuilt thermocouples for monitoring of temperature development in concrete mass. All samples, either for development or verification, were thermally exposed according to the modified ISO 834 curve. Equipment for the development of all three methods was not primarily adjusted for concrete with eventual explosive spalling. The electric oven performs excellently for pre-set regimes with defined ramp-dwell-cooling phase, but not for fire testing curve ISO 834, which has extremely steep temperature gain. In connection to the test oven, the one-side heated uniaxially loaded slabs were also designed to fit the oven, and due to this, shape and loading were unconventional, but still, inspired by test setups presented at the 5th International RILEM Workshop on Concrete Spalling due to Fire Exposure, Borås, Sweden. Equipment introduced for industrial application of the IHT method has not been tested, and therefore increase of ambient temperature in tunnels during application must be closely monitored.

IHT method development

The detailed description of the porous structure, chemical changes and mechanical changes were described in 4 series during the development of the IHT method. Based on the results from the 1st series, it was concluded that suitable pores are capillary pores with a diameter between 0,03 and 30 μm analysed by MIP and TGA-DTA, and if the exposure temperature exceeds 350°C, rehydration takes place, and porosity is reduced. Testing of normal strength concrete in the 2nd series showed the same trend of porous structure

modification and also chemical changes of individual compounds due to thermal load analysed by MIP and XRD. In the 3rd series, various configurations of the IHT method on 3 different binder types were verified as the surface layer is predominantly formed by cement paste. Analyses showed, that the IHT method has a positive influence on compressive and flexural strength, and the most suitable configurations are IHT200/2 and IHT250/1. Described in detail, the temperature ramp of 5°C/min until the requested temperature 200°C or 250°C held for 1 or 2 hours and naturally cooled to ambient temperature. Further testing was performed only with IHT200/2 as temperature 250°C might cause greater microcracking, especially in the case of concrete with the addition of silica fume and larger samples. Binder testing was followed by the application of IHT200/2 on 4 different concrete types. Based on results from remaining compressive strength after thermal exposure of samples with and without applied IHT method (IHT200/2) according to m-ISO curve, beneficial impact on concrete with blended cement (FA cement - CEM II/B-M) and concrete with the content of silica fume can be concluded. Contribution to CEM I is negligible even slightly negative, and in the case of Granite_NO aggregates, the effect of the IHT method was lost to the degradation of Granite aggregates.

Verification of IHT method efficiency was tested on one-side heated, uniaxially loaded slabs with integrated thermocouples for heat spread monitoring. From the results, it could be concluded that the vapour zone/drying zone is extended, and the risk of moisture clog formation reduced, as is also the case of explosive spalling and extensive crack formation. Furthermore, individual parameters and their connection to a thickness of the IHT zone and IHT transition zone were explained.

The total thickness of IHT method is between 25,5 and 43,0 mm, and consists of the IHT zone ranged from 14,5 till 16,0 mm, and thickness of the IHT transition zone was between 11,0 to 27,0 mm, which is in conformity to a thickness of the cover layer, and no impact on steel rebars is ensured. Finally, the method for industrial application is suggested, trucks with radiators on hydraulic arms.

The benefits of the new IHT method are (i) after treatment of the IHT method, fires can be extinguished by water and do not emit harmful and poisoning gasses; (ii) locations of installations such as tunnels do not need to be necessarily fully closed during the application period which is relatively short in comparison to other fire resistance methods; (iii) application of IHT method has a low environmental impact; (iv) its application does not have a negative impact on strength and durability of concrete and whole concrete structure; (v) calculation of cost for realisation of the IHT method is transparent as heat (energy) is the only requirement; (vi) IHT method is adjustable to various concrete types and different structure shapes.

Further development of IHT method would include a detailed investigation of (i) stability of IHT_T/t in natural ambient with relative humidity around 75% and exposure to exhaust gases; (ii) further investigation of the cooling phase; (iii) the development of the IHT method was highly comprehensive, and all results are interconnected, the set of data might serve for the development of a mathematical model for IHT method design, and also for prediction of crack formation in heated concrete.

AeA-FiResCrete

The second method investigated air-entraining agents (AeA) and their contribution to the fire resistance of newly produced concrete. Three types of AeA were tested, including two “new generation” AeA and conclusions are that pores formed by AeA are not entirely suitable for fire resistance. Moisture clog was visible from temperature gradient measured between individual thermocouples, and migration of moisture through the whole thickness of slab was recorded. Further investigation of porous structure and moisture migration is needed for a distinct conclusion of AeA’s contribution to the fire resistance of concrete. Despite that, results showed, that more moisture is captured with higher porosity, which could cause explosive spalling and extensive cracking if the non-heated surface is impermeable.

In general, the use of polymer fibres is not entirely environmentally friendly, and thus air-entraining agents might be a beneficial option for a sustainable method for enhancement of fire resistance of newly built concrete structures.

Contribution to science and practice

The following points were selected as a significant contribution to science, (i) a detailed description of chemical changes of cement paste exposed to elevated temperatures demonstrated by results from TGA-DTA, XRD, MIP and temperature measurements in concrete during the thermal exposure; (ii) detail description of porous structure modification of various concrete types. Definition of pores suitable for fire resistance; (iii) evaluation of 4 concrete types with 2 different aggregates, 3 binder types and 3 air-entraining agents; (iv) system for moisture clog monitoring and heat penetration based on temperature measurements and temperature gradient calculation.

The following points were selected as significant contribution to practice, (i) new method for enhancement of fire resistance of existing concrete structures with no need for additional materials and low environmental impact; (ii) innovative solution for the design of new concrete with improved fire resistance properties by “new generation” air-entraining agents, which is more ecological than the use of polypropylene fibres.

REFERENCES

1. TecEco - Newsletter 72. [online]. [Accessed 3 November 2019]. Available from: https://www.tececo.com.au/files/newsletters/Newsletter72.php
2. Concrete Helper- A Concrete Industry Resource – Concrete Facts. [online]. [Accessed 3 November 2019]. Available from: http://concretehelper.com/concrete-facts/
3. The History of Concrete | Giatec Scientific Inc. [online]. [Accessed 3 November 2019]. Available from: https://www.giatecscientific.com/education/the-history-of-concrete/
4. CBI. Ultra High Performance Concrete (Uhpc) – Development, Application, Sustainability. . 2016.
5. KHOURY, Gabriel Alexander. Effect of fire on concrete and concrete structures. *Progress in Structural Engineering and Materials*. October 2000. Vol. 2, no. 4, p. 429–447. DOI 10.1002/pse.51.
6. EN 1992-1-2: 2004 Eurocode 2: Design of concrete structures - Part 1-2: General rules - Structural fire design. [online]. 2004. [Accessed 4 November 2019]. Available from: https://archive.org/details/en.1992.1.2.2004
7. BS EN 1363-1:2012 - Fire resistance tests. General requirements. [online]. [Accessed 4 November 2019]. Available from: https://shop.bsigroup.com/ProductDetail/?pid=000000000030251439
8. BS EN 13823:2010+A1:2014 - Reaction to fire tests for building products. Building products excluding floorings exposed to the thermal attack by a single burning item. [online]. [Accessed 4 November 2019]. Available from: https://shop.bsigroup.com/ProductDetail/?pid=000000000030296479
9. KORTEN, A. and WETZIG, V. Spalling of concrete - Influence of porosity and specimen size and its critical factors regarding safety. *MATEC Web of Conferences*. 2013. Vol. 6. DOI 10.1051/matecconf/20130601010.
10. GEHANDLER, J., KARLSSON, P. and VYLUND, L. Risks associated with alternative fuels in road tunnels and underground garages. *Proceedings of Eighth International Symposium on Tunnel Safety and Security, Borås, Sweden, March 14-16, 2018*. 2018.
11. FUENTES-CANTILLANA, José Luis. Entrevista a José Luis Fuentes-Cantillana, director de Aitemin. *Interempresas.net* [online]. [Accessed 20 October 2019]. Available from: http://www.interempresas.net/Seguridad/Articulos/34907-Entrevista-a-Jose-Luis-Fuentes-Cantillana-director-de-Aitemin.html

12. ROMAN, Jesse. Ramp Risk. *NFPA Journal* [online]. [Accessed 20 October 2019]. Available from: https://www.nfpa.org/News-and-Research/Publications-and-media/NFPA-Journal/2019/March-April-2019/Features/Protecting-Parking-Garages

13. BEARD, Alan and CARVEL, Richard. *Handbook of Tunnel Fire Safety (2nd Edition) - Knovel* [online]. 2005. [Accessed 12 November 2019]. Available from: https://app.knovel.com/web/toc.v/cid:kpHTFSE002/viewerType:toc//root_slug:handbook-tunnel-fire/url_slug:hydrogen-powered-cars?=undefined&issue_id=kpHTFSE002&hierarchy=

14. THIENPONT, Thomas, VAN COILE, Ruben, DE CORTE, Wouter and CASPEELE, Robby. DETERMINING A GLOBAL RESISTANCE FACTOR FOR SYMPLY SUPPORTED FIRE EXPOSED RC SLABS. In : *fib Symposium 2019 Concrete-Innovations in Materials, Design and Structures*. 2019. p. 2191–2197.

15. BURLACU, D., ANGHEL, I., POPA, C. and CASARU, I. FIRE SAFETY EVALUATION OF AN UNDERGROUND CAR PARK USING NUMERICAL SIMULATION. *Mathematical Modelling in Civil Engineering*. 2018. Vol. 14, no. 2, p. 1–12. DOI 10.2478/mmce.

16. List of town and city fires - Wikipedia. [online]. [Accessed 13 November 2019]. Available from: https://en.wikipedia.org/wiki/List_of_town_and_city_fires

17. HUANG, Ping and ZHANG, Jingyuan. Facts related to August 12, 2015 explosion accident in Tianjin, China. *Process Safety Progress*. 1 December 2015. Vol. 34, no. 4, p. 313–314. DOI 10.1002/prs.11789.

18. Notre Dame fire was probably caused by electrical short circuit, police official says - Los Angeles Times. [online]. [Accessed 13 November 2019]. Available from: https://www.latimes.com/world/la-fg-notre-dame-fire-cause-short-circuit-20190418-story.html

19. Bushfire weather. *Australian Government* [online]. [Accessed 13 November 2019]. Available from: http://www.bom.gov.au/weather-services/fire-weather-centre/bushfire-weather/index.shtml

20. 2019 Fire Season | Welcome to CAL FIRE. [online]. [Accessed 13 November 2019]. Available from: https://www.fire.ca.gov/incidents/2019/

21. Bushfire basics: what you need to know - CSIROscope. [online]. [Accessed 13 November 2019]. Available from: https://blog.csiro.au/bushfire-basics/

22. Notre dame fire: “You’ve got to get out” 23 minutes to evacuate Paris cathedral. [online]. [Accessed 13 November 2019]. Available from:

https://www.9news.com.au/world/notre-dame-fire-millions-of-euros-pledged-to-rebuild-cathedral/1a4d87be-d04c-4762-aacd-892430029797

23. Grenfell Tower: What happened - BBC News. [online]. [Accessed 13 November 2019]. Available from: https://www.bbc.com/news/uk-40301289

24. IDA - Hem. [online]. [Accessed 13 November 2019]. Available from: https://ida.msb.se/ida2#page=3d635cdf-e7eb-4f49-b579-9612fb44c941

25. COLLIER, P. *Car parks - Fires involving modern car sand stacking systems* [online]. 2011. Available from: https://www.branz.co.nz/

26. 1,400 cars destroyed in Liverpool parking garage fire - UPI.com. [online]. [Accessed 13 November 2019]. Available from: https://www.upi.com/Top_News/World-News/2018/01/01/1400-cars-destroyed-in-Liverpool-parking-garage-fire/8321514854783/

27. *Kings Dock car park fire, protection report*. 2018.

28. Garage Ventilation System Design: CO Removal with Jet Fan Placement. [online]. [Accessed 13 November 2019]. Available from: https://www.simscale.com/blog/2018/02/garage-ventilation-system-jet-fan/

29. FORSBERG, S. Elbil brann i Helsingborg imorse. *Laddaelbilen.se* [online]. 2013. [Accessed 13 November 2019]. Available from: http://www.laddaelbilen.se/2013/10/13/elbil-brann-i-helsingborg-imorse-*update!*-18729893

30. Seven Swiss Firefighters Die in Collapsed Parking Garage. [online]. [Accessed 13 November 2019]. Available from: https://www.firehouse.com/lodds/news/10514192/seven-swiss-firefighters-die-in-collapsed-parking-garage

31. Fire in San Diego Underground Parking Garage - Firefighter Nation. [online]. [Accessed 29 November 2019]. Available from: https://www.firefighternation.com/2018/05/14/fire-in-san-diego-underground-parking-garage/#gref

32. NOLAN, Dennis P. *Handbook of fire and explosion protection engineering principles : for oil, gas, chemical and related facilities*. Elsevier Inc, 2011. ISBN 9781437778588.

33. BUVIK, Harald. *Vehicle fires in Norwegian road tunnels*. 2015.

34. NAEVESTAD, Tor-Olav, RANESTAD, Karen, ELVEBAKK, Beate and MEYER, Sunniva. *Vehicle fires in Norwegian road tunnels 2008-2015*. 2016.

35. The Accident Investigation Board Norway. [online]. [Accessed 29 November 2019]. Available from: https://www.aibn.no/home

36. BEARD, Alan and CARVEL, Richard. *The handbook of tunnel fire safety*. Thomas Telford, 2005. ISBN 0727731688.

37. Tauern Road Tunnel - Wikipedia. [online]. [Accessed 29 November 2019]. Available from: https://en.wikipedia.org/wiki/Tauern_Road_Tunnel

38. Tesla “Model S” Battery Fire Kills Teenagers | Watts Up With That? [online]. [Accessed 29 November 2019]. Available from: https://wattsupwiththat.com/2018/05/10/tesla-model-s-battery-fire-kills-teenagers/

39. *Fire classification of construction products and building elements – Part 1: Classification using test data from reaction to fire tests*. 2019.

40. *EN 1991-1-2: Eurocode 1: Actions on structures - Part 1-2: General actions - Action on structures exposed to fire*. 1991.

41. ALI, Msheer Hasan, DINKHA, Youkhanna Zayia and HAIDO, James H. Mechanical properties and spalling at elevated temperature of high performance concrete made with reactive and waste inert powders. *Engineering Science and Technology, an International Journal* [online]. 2017. Vol. 20, no. 2, p. 536–541. DOI 10.1016/j.jestch.2016.12.004. Available from: http://dx.doi.org/10.1016/j.jestch.2016.12.004

42. CRC Fire resistance - Full scale testing on simply supported slab. [online]. [Accessed 8 December 2019]. Available from: https://www.hi-con.com/concrete-blog/crc-fire-resistance-full-scale-testing-on-simply-supported-slab-3

43. BODNAROVA, Lenka, VALEK, Jaroslav and NOVOSAD, Petr. Testing of action of direct flame on concrete. *Scientific World Journal*. 2015. Vol. 2015. DOI 10.1155/2015/371913.

44. NMAI, Charles, BURY, Mark and DACZKO, Joseph. SHRINKAGE OF CONCRETE: MINIMIZING/ELIMINATING THE POTENTIAL FOR CRACKING. [online]. 2018. [Accessed 8 December 2019]. Available from: https://tilt-up.org/tilt-uptoday/2018/01/27/shrinkage-of-concrete-minimizingeliminating-the-potential-for-cracking/

45. LEIVO, Virpi. *Moisture Behavior of Slab-On-Ground Structures*. 2016. ISBN 9789521527494.

46. LERCH, W. Plastic Shrinkage. *Proceedings of the ACI Journal*. 1957. Vol. 53, no. 8,

p. 797–802.

47. BWALYA, A. C., LOUGHEED, G. S. D., KASHEF, A. and SABER, H. H. Survey Results of Combustible Contents and Floor Areas Canadian Dwellings. *FireTechnology*. 2008. No. 32, p. 120–136.

48. ARIYANAYAGAM, Anthony Deloge and MAHENDRAN, Mahen. Fire safety of buildings based on realistic fire time-temperature curves. *Proceedings of the 19th International CIB World Building Congress, Brisbane 2013: Construction and Society* [online]. 2013. P. 1–13. Available from: http://eprints.qut.edu.au/61929/

49. ISO 834-1:1999 - Fire-resistance tests — Elements of building construction — Part 1: General requirements. [online]. [Accessed 1 December 2019]. Available from: https://www.iso.org/standard/2576.html

50. Fire curves - Tunnel. [online]. [Accessed 1 December 2019]. Available from: https://www.promat-tunnel.com/en/advices/fire-protection/fire curves

51. WORKING PARTY 4.3-1. *Fire design of concrete structures - materials, structure and modelling*. 2007. ISBN 9782883940789.

52. *Thematic Network FIT – Fire in Tunnels* [online]. 2005. [Accessed 29 November 2019]. Available from: https://www.cstc.be/homepage/index.cfm?cat=services&sub=standards_regulations&pag=fire&art=library&niv01=fit

53. The METRO project 2009 – 2012. [online]. [Accessed 29 November 2019]. Available from: http://www.metroproject.se/

54. TORELLI, Giacomo, MANDAL, Parthasarathi, GILLIE, Martin and TRAN, Van Xuan. Concrete strains under transient thermal conditions: A state-of-the-art review. *Engineering Structures* [online]. 2016. Vol. 127, no. December, p. 172–188. DOI 10.1016/j.engstruct.2016.08.021. Available from: http://dx.doi.org/10.1016/j.engstruct.2016.08.021

55. RILEM TC 227-HPB. *Physical Properties and Behaviour of High-Performance Concrete at High Temperature - State-of-the-Art Report of the RILEM Technical Committee 227-HPB | Pierre Pimienta | Springer* [online]. 2019. ISBN ISBN 978-3-319-95432-5. Available from: https://www.springer.com/gp/book/9783319954318

56. KHOURY, GA, GRAINGER, BN and SULLIVAN, PJE. Strain of concrete during first heating to 600 °C under load. *Mag Concr Res*. 1985. Vol. 37, p. 195–215.

57. MINDEGUIA, J-C, HAGER, I, PIMIENTA, P, CARRÉ, H and LA BORDERIE, C.

Parametrical study of transient thermal strain of ordinary and high performance concrete. *Cem Concr Res*. 2013. P. 40–52.

58. SCHNEIDER, U and KASSEL, G. *Properties of materials in high temperatures: concrete*. Gesamthochschul-Bibliothek, 1985.

59. NIELSEN, C. V., PEARCE, C. J. and BIĆANIĆ, N. Theoretical model of high temperature effects on uniaxial concrete member under elastic restraint. *Magazine of Concrete Research*. 2002. Vol. 54, no. 4, p. 239–249. DOI 10.1680/macr.2002.54.4.239.

60. KHOURY, Ga Aa, GRAINGER, Ba Na and SULLIVAN, Pa Jaa Ea. Strain of concrete during first cooling from 600 °C under load. *Mag Concr Res*. 1986. P. 3–12.

61. ANDERBERG, Yngve and THELANDERSSON, Sven. *Stress and Deformation Characteristics of Concrete at High Temperatures. 2. Experimental Investigation and Material Behaviour Model*. 1976.

62. DIEDERICHS, Ulrich. Modelle zur Beschreibung der Betonverformung bei instantion {ä}ren Temperaturen. *Abschlu{ß}kolloquium–Bauwerke Unter. Brand*. 1987. P. 25–34.

63. THELANDERSSON, Sven. Modeling of Combined Thermal and Mechanical Action in Concrete. *Journal of Engineering Mechanics* [online]. June 1987. Vol. 113, no. 6, p. 893–906. [Accessed 14 December 2019]. DOI 10.1061/(ASCE)0733-9399(1987)113:6(893). Available from: http://ascelibrary.org/doi/10.1061/%28ASCE%290733-9399%281987%29113%3A6%28893%29

64. DE BORST, René and PEETERS, Paul P.J.M. Analysis of concrete structures under thermal loading. *Computer Methods in Applied Mechanics and Engineering*. 1989. Vol. 77, no. 3, p. 293–310. DOI 10.1016/0045-7825(89)90079-0.

65. PEARCE, Chris J., NIELSEN, Claus V. and BIĆANIĆ, N. Gradient enhanced thermo-mechanical damage model for concrete at high temperatures including transient thermal creep. *International Journal for Numerical and Analytical Methods in Geomechanics* [online]. June 2004. Vol. 28, no. 78, p. 715–735. [Accessed 14 December 2019]. DOI 10.1002/nag.376. Available from: http://doi.wiley.com/10.1002/nag.376

66. DAUTI, Dorjan, TENGATTINI, Alessandro, DAL PONT, Stefano, TOROPOVS, Nikolajs, BRIFFAUT, Matthieu and WEBER, Benedikt. Analysis of moisture migration in concrete at high temperature through in-situ neutron tomography. *Cement and Concrete Research*. 2018. Vol. 111, no. June, p. 41–55. DOI 10.1016/j.cemconres.2018.06.010.

67. *THE CONSTRUCTION PRODUCTS DIRECTIVE (COUNCIL DIRECTIVE*

89/106/EEC). [no date].

68. ISO 23932-1:2018 Fire safety engineering — General principles — Part 1: General. *ISO* [online]. 2018. [Accessed 28 April 2020]. Available from: https://www.iso.org/obp/ui/#iso:std:iso:23932:-1:ed-1:v1:en

69. Difference Between Passive and Active Fire Protection. [online]. [Accessed 14 December 2019]. Available from: http://news.lifesafetyservices.com/blog/difference-between-passive-and-active-fire-protection

70. Passive Fire Protection: A beginner's guide. [online]. [Accessed 14 December 2019]. Available from: https://www.ifsecglobal.com/fire/beginners-guide-to-passive-fire-protection/

71. Hypoxic Air Fire Preventive System Conteg. [online]. [Accessed 14 December 2019]. Available from: https://www.conteg.com/hypoxic-air-fire-preventive-system

72. ATHANASOPOULOU, A, BEZUIJEN, A, BOGUSZ, W, BOURNAS, D, BRANDTNER, M, BREUNESE, A, BURBAUM, U, DIMOVA, S, FRANK, R, GANZ, H, GRUNICKE, U, JUNG, H, LEWANDOWSKA, A, NUIJTEN, G, PECKER, A, PSOMAS, S, ROESSLER, K, SCIOTTI, A, SOUSA, M L, STILLE, H and SUBRIN, D. Standardisation needs for the design of underground structures. [online]. 2019. [Accessed 28 April 2020]. DOI 10.2760/760968. Available from: https://ec.europa.eu/jrc

73. *Directive 2004/54/EC of the European Parliament and of the Council of 29 April 2004 on minimum safety requirements for tunnels in the Trans-European Road Network* [online]. 2004. [Accessed 28 April 2020]. Available from: https://eur-lex.europa.eu/eli/dir/2004/54/oj

74. *TP229 Bezpečnost v tunelech pozemních komunikací*. 2010.

75. *TP98 Tech nologické Vybaven í tu nel ů pozemních komunikací*. 2003. Současně se ruší anahrazujiv celém rozsahu TP 98, schválené b)'v.

76. 264/2009 Sb. Nařízení vlády o bezpečnostních požadavcích na tunely pozemních komunikací delší než 500 metrů. [online]. [Accessed 28 April 2020]. Available from: https://www.zakonyprolidi.cz/cs/2009-264

77. SCHNÜTGEN, B. Design of precast steel fibre reinforced tunnel elements. In : . Springer Nature, 17 November 2006. p. 145–152.

78. *BEST PRACTICES FOR ROADWAY TUNNEL DESIGN, CONSTRUCTION, MAINTENANCE, INSPECTION, AND OPERATIONS* [online]. [no date].

[Accessed 27 April 2020]. Available from: http://144.171.11.40/cmsfeed/TRBNetProjectDisplay.asp?ProjectID=1570.

79. North American Tunneling 2018 Proceedings - Google Books. [online]. [Accessed 27 April 2020]. Available from: https://books.google.no/books?id=LMJqDwAAQBAJ&pg=PA586&lpg=PA586&dq=Pickett+A.,+Thomas+A.:+Where+Are+We+Now+with+Sprayed+Concrete+Lining+in+Tunnels?&source=bl&ots=iUToltK7iH&sig=ACfU3U06RilOEUx47ua-Yk_5OENiHA85GA&hl=en&sa=X&ved=2ahUKEwiAgeLOw4npAhV2AxAIHX

80. SRI LANKA, Japan. *Technical Assistance for Improvement of Capacity for Planning of Road Tunnels Guideline for Design of Road Tunnel*. 2018.

81. *Håndbok N500 Vegtunneler* [online]. Norwegian Public Roads Administration, 2020. [Accessed 28 April 2020]. Available from: www.vegvesen.no.

82. Home - Transport Research International Documentation - TRID. [online]. [Accessed 27 April 2020]. Available from: https://trid.trb.org/

83. BAZANT, Zdenek and THONGUTHAI, Werapol. Pore pressure in heated concrete walls: theoretical prediction. *Magazine of Concrete Research*. 1979.

84. BAZANT, Z. and KAPLAN, M. Concrete at high temperatures: material properties and mathematical models. *American Society of Mechanical Engineers*. 1996.

85. ALONSO, C. and FERNANDEZ, L. Dehydration and rehydration processes of cement paste exposed to high temperature environments. *Journal of Materials Science*. 2004. Vol. 39, no. 9, p. 3015–3024. DOI 10.1023/B:JMSC.0000025827.65956.18.

86. 256-SPF : Spalling of concrete due to fire: testing and modelling. [online]. [Accessed 15 December 2019]. Available from: https://www.rilem.net/groupe/256-spf-spalling-of-concrete-due-to-fire-testing-and-modelling-309

87. ANDERBERG, Yngve. Analytical fire engineering design of reinforced concrete structures based on real fire characteristics. *Proceedings of the FIP Congress*. 1978.

88. BECKER, J and BRESLER, B. *FIRES-RC, A computer program for the fire response of structures-reinforced concrete frames*. 1974.

89. KODUR, V., DWAIKAT, M and RAUT, N. Macroscopic FE model for tracing the fire response of reinforced concrete structures. *Engineering Structures*. 2009. Vol. 31, no. 10, p. 2368–2379.

90. ZHAO, J. *Fire-Induced Spalling Modeling of High-Performance Concrete*. Technical University Delft, 2012.

91. SCHREFLER, Bernhard A., KHOURY, Gabriel A., GAWIN, Dariusz and MAJORANA, Carmelo E. Thermo-hydro-mechanical modelling of high performance concrete at high temperatures. *Engineering Computations (Swansea, Wales)*. 2002. Vol. 19, no. 7–8, p. 787–819. DOI 10.1108/02644400210444320.

92. KHOURY, G. A., MAJORANA, C. E., PESAVENTO, F. and SCHREFLER, B. A. Modelling of heated concrete. *Magazine of Concrete Research* [online]. April 2002. Vol. 54, no. 2, p. 77–101. [Accessed 15 December 2019]. DOI 10.1680/macr.2002.54.2.77. Available from: http://www.icevirtuallibrary.com/doi/10.1680/macr.2002.54.2.77

93. PESAVENTO, Francesco. *Non-linear modelling of concrete as multiphase porous material in high temperature conditions* [online]. 2000. [Accessed 15 December 2019]. Available from: https://books.google.no/books/about/Non_linear_modelling_of_concrete_as_mult.html?id=QB6_oQEACAAJ&redir_esc=y

94. BOŠNJAK, Josipa. *Explosive spalling and permeability of high performance concrete under fire – numerical and experimental investigations, PhD thesis*. 2014.

95. LOTHENBACH, Barbara and ZAJAC, Maciej. Application of thermodynamic modelling to hydrated cements. *Cement and Concrete Research* [online]. 2019. Vol. 123, no. January, p. 105779. DOI 10.1016/j.cemconres.2019.105779. Available from: https://doi.org/10.1016/j.cemconres.2019.105779

96. PINSON, Matthew B., MASOERO, Enrico, BONNAUD, Patrick A., MANZANO, Hegoi, JI, Qing, YIP, Sidney, THOMAS, Jeffrey J., BAZANT, Martin Z., VAN VLIET, Krystyn J. and JENNINGS, Hamlin M. Hysteresis from multiscale porosity: Modeling water sorption and shrinkage in cement paste. *Physical Review Applied*. 2015. Vol. 3, no. 6. DOI 10.1103/PhysRevApplied.3.064009.

97. KHOURY, G. A. Polypropylene fibres in heated concrete. Part 2: Pressure relief mechanisms and modelling criteria. *Magazine of Concrete Research* [online]. 25 April 2008. Vol. 60, no. 3, p. 189–204. [Accessed 5 April 2020]. DOI 10.1680/macr.2007.00042. Available from: http://www.icevirtuallibrary.com/doi/10.1680/macr.2007.00042

98. CONSTANTINIDES, Georgios and ULM, Franz Josef. The nanogranular nature of C-S-H. *Journal of the Mechanics and Physics of Solids*. January 2007. Vol. 55, no. 1, p. 64–90. DOI 10.1016/j.jmps.2006.06.003.

99. ZENG, Qiang, LI, Kefei, FEN-CHONG, Teddy and DANGLA, Patrick. Determination of

cement hydration and pozzolanic reaction extents for fly-ash cement pastes. *Construction and Building Materials* [online]. 2012. Vol. 27, no. 1, p. 560–569. DOI 10.1016/j.conbuildmat.2011.07.007. Available from: http://dx.doi.org/10.1016/j.conbuildmat.2011.07.007

100. Thermal Properties of Concrete. [online]. [Accessed 10 April 2020]. Available from: https://www.scribd.com/doc/40130246/Thermal-Properties-of-Concrete

101. FRIDRICHOV, Marcela, NOVAK, Jan and DVORAK, Karel. *Maltoviny*. Studijní o. Vysoké učení technické v Brne, Fakulta stavební, [no date].

102. Composition of cement. [online]. [Accessed 28 March 2020]. Available from: https://www.engr.psu.edu/ce/courses/ce584/concrete/library/construction/curing/Composition of cement.htm

103. BLACK, Leon, BREEN, Chris, YARWOOD, Jack, DENG, C. S., PHIPPS, Jonathan and MAITLAND, Geoff. Hydration of tricalcium aluminate (C3A) in the presence and absence of gypsum - Studied by Raman spectroscopy and X-ray diffraction. *Journal of Materials Chemistry*. 17 March 2006. Vol. 16, no. 13, p. 1263–1272. DOI 10.1039/b509904h.

104. T., CARLSON, Elmer. *Some Properties of the Calcium Aluminoferrite Hydrates*. United States Department of Commerce, 1966.

105. RADWAN, M. and HEMALY, S. *Hydration characteristics of Tetracalcium aluminoferrite phase in the presence of Calcium Carbonate*. 2011.

106. COLLEPARDI, Mario, MONOSI, Saveria, MORICONI, Giacomo and CORRADI, Mario. Tetracalcium aluminoferrite hydration in the presence of lime and gypsum. *Cement and Concrete Research*. 1979. Vol. 9, no. 4, p. 431–437. DOI 10.1016/0008-8846(79)90040-1.

107. SCRIVENER, K. L., FÜLLMANN, T., GALLUCCI, E., WALENTA, G. and BERMEJO, E. Quantitative study of Portland cement hydration by X-ray diffraction/Rietveld analysis and independent methods. *Cement and Concrete Research*. 1 September 2004. Vol. 34, no. 9, p. 1541–1547. DOI 10.1016/j.cemconres.2004.04.014.

108. LAM, L., WONG, Y. L. and POON, C. S. Degree of hydration and gel/space ratio of high-volume fly ash/cement systems. *Cement and Concrete Research*. 1 May 2000. Vol. 30, no. 5, p. 747–756. DOI 10.1016/S0008-8846(00)00213-1.

109. TANG, Chao Wei. Hydration properties of cement pastes containing high-volume mineral admixtures. *Computers and Concrete*. 2010. Vol. 7, no. 1, p. 17–38. DOI 10.12989/cac.2010.7.1.017.

110. BALÁZS, György L and LUBLÓY, Éva. *Concrete in Fire Tűz hatása a betonra Acţiunea focului asupra betonului* [online]. [no date]. [Accessed 5 April 2020]. Available from: http://www.polizia.ti.ch

111. FERNANDES, B., GIL, A. M., BOLINA, F. L. and TUTIKIAN, B. F. Microstructure of concrete subjected to elevated temperatures: physico-chemical changes and analysis techniques. *Revista IBRACON de Estruturas e Materiais*. August 2017. Vol. 10, no. 4, p. 838–863. DOI 10.1590/s1983-41952017000400004.

112. HLAVIČKA, Viktor and LUBLÓY, Éva. Concrete cone failure of bonded anchors in thermally damaged concrete. *Construction and Building Materials*. 20 May 2018. Vol. 171, p. 588–597. DOI 10.1016/j.conbuildmat.2018.03.148.

113. HALL, Christopher, BARNES, Paul, BILLIMORE, Andrew D., JUPE, Andrew C. and TURRILLAS, Xavier. Thermal decomposition of ettringite Ca6 [Al(OH)6]2(SO4)3·26H 2O. *Journal of the Chemical Society - Faraday Transactions*. 21 June 1996. Vol. 92, no. 12, p. 2125–2129. DOI 10.1039/FT9969202125.

114. ZHANG, Qi and YE, Guang. Dehydration kinetics of Portland cement paste at high temperature. In : *Journal of Thermal Analysis and Calorimetry*. Springer, 19 October 2012. p. 153–158.

115. HAGER, I. Behaviour of cement concrete at high temperature. *Bulletin of the Polish Academy of Sciences: Technical Sciences*. March 2013. Vol. 61, no. 1, p. 145–154. DOI 10.2478/bpasts-2013-0013.

116. WYRZYKOWSKI, Mateusz, MCDONALD, Peter J., SCRIVENER, Karen L. and LURA, Pietro. Water Redistribution within the Microstructure of Cementitious Materials due to Temperature Changes Studied with 1H NMR. *Journal of Physical Chemistry C*. 21 December 2017. Vol. 121, no. 50, p. 27950–27962. DOI 10.1021/acs.jpcc.7b08141.

117. GAJEWICZ-JAROMIN, Agata M., MCDONALD, Peter J., MULLER, Arnaud C.A. and SCRIVENER, Karen L. Influence of curing temperature on cement paste microstructure measured by 1H NMR relaxometry. *Cement and Concrete Research*. 1 August 2019. Vol. 122, p. 147–156. DOI 10.1016/j.cemconres.2019.05.002.

118. DOVÁL, M., PALOU, M. and S.C., Mojumdar. *HYDRATION BEHAVIOR OF C2S AND C2AS NANOMATERIALS, SYNTHETIZED BY SOL–GEL METHOD*. 2006.

119. OKADA, Yoshihiko, SASAKI, Kaori, ZHONG, Baiqian, ISHIDA, Hideki and MITSUDA, Takeshi. Formation Processes of beta-C2S by the Decomposition of Hydrothermally Prepared C-S-H with Ca(OH)2. *Journal of the American Ceramic Society* [online]. May 1994. Vol. 77, no. 5, p. 1319–1323. [Accessed 11 April 2020]. DOI 10.1111/j.1151-

2916.1994.tb05409.x. Available from: http://doi.wiley.com/10.1111/j.1151-2916.1994.tb05409.x

120. EL-DIDAMONY, H., SHARARA, A. M., HELMY, I. M. and ABD EL-ALEEM, S. Hydration characteristics of β-C2S in the presence of some accelerators. *Cement and Concrete Research*. 1 August 1996. Vol. 26, no. 8, p. 1179–1187. DOI 10.1016/0008-8846(96)00103-2.

121. KHACHANI, M, HAMIDI, A El, HALIM, M and ARSALANE, S. Non-isothermal kinetic and thermodynamic studies of the dehydroxylation process of synthetic calcium hydroxide Ca(OH) 2. *J. Mater. Environ. Sci*. 2014. Vol. 5, no. 2, p. 615–624.

122. CRUZ, C. R. and GILLEN, M. Thermal expansion of Portland cement paste, mortar and concrete at high temperatures. *Fire and Materials* [online]. 1 June 1980. Vol. 4, no. 2, p. 66–70. [Accessed 11 April 2020]. DOI 10.1002/fam.810040203. Available from: http://doi.wiley.com/10.1002/fam.810040203

123. JOSEPH F. LAMOND, J. H. Pielert. Significance of Tests and Properties of Concrete and Concrete-making Materials. *ASTM International* [online]. 2006. [Accessed 11 April 2020]. Available from: https://books.google.no/books?id=isTMHD6yIy8C&pg=PA12&lpg=PA12&dq=coefficient+of+thermal+expansion+of+SCSH+gel&source=bl&ots=SWqCO9SBuQ&sig=ACfU3U38DoiAQZPdJ0Oh8SjwnJPiYVKExQ&hl=en&sa=X&ved=2ahUKEwi56Jaw7t3oAhUFqYsKHVaKBd4Q6AEwAHoECAkQKw#v=onepage&q&f=fal

124. SURANENI, Prannoy, HAJIBABAEE, Amir, RAMANATHAN, Sivakumar, WANG, Ying and WEISS, Jason. New insights from reactivity testing of supplementary cementitious materials. *Cement and Concrete Composites*. 1 October 2019. Vol. 103, p. 331–338. DOI 10.1016/j.cemconcomp.2019.05.017.

125. VAN DAMME, Henri. *Concrete material science: Past, present, and future innovations*. 1 October 2018. Elsevier Ltd.

126. Cements in Nebraska: NDOR Research Into FlyAsh Alternatives. [online]. [Accessed 6 April 2020]. Available from: https://www.slideshare.net/jillthepill81/cements-in-nebraska

127. ČSN EN 450-1 - Náhled. [online]. [Accessed 9 April 2020]. Available from: http://csnonlinefirmy.unmz.cz/html_nahledy/72/73985/73985_nahled.htm

128. ČSN EN 450-2 (722064) - Technické normy ČSN. [online]. [Accessed 9 April 2020]. Available from: http://www.technicke-normy-csn.cz/722064-csn-en-450-2_4_73984.html

129. ASTM. Standard Specification for Blended Supplementary Cementitious Materials, ASTM C1697-10. *Annual Book of ASTM Standards*. 2010. Vol. i, no. c, p. 1–5. DOI 10.1520/C1697-10.

130. SURANENI, Prannoy and WEISS, Jason. Examining the pozzolanicity of supplementary cementitious materials using isothermal calorimetry and thermogravimetric analysis. *Cement and Concrete Composites*. 1 October 2017. Vol. 83, p. 273–278. DOI 10.1016/j.cemconcomp.2017.07.009.

131. AVET, François, SNELLINGS, Ruben, ALUJAS DIAZ, Adrian, BEN HAHA, Mohsen and SCRIVENER, Karen. Development of a new rapid, relevant and reliable (R3) test method to evaluate the pozzolanic reactivity of calcined kaolinitic clays. *Cement and Concrete Research*. 1 July 2016. Vol. 85, p. 1–11. DOI 10.1016/j.cemconres.2016.02.015.

132. MARTIRENA-HERNANDEZ, Jose Fernando, ALUJAS-DÍAZ, Adrian and AMADOR-HERNANDEZ, Meylin. *Proceedings of the International Conference of Sustainable Production and Use of Cement and Concrete* [online]. 2020. ISBN 978-3-030-22033-4. Available from: http://link.springer.com/10.1007/978-3-030-22034-1

133. SINGH, Bhupinder. Rice husk ash. In : *Waste and Supplementary Cementitious Materials in Concrete: Characterisation, Properties and Applications*. Elsevier, 2018. p. 417–460. ISBN 9780081021569.

134. HAHA, M. Ben, LOTHENBACH, B., LE SAOUT, G. and WINNEFELD, F. Influence of slag chemistry on the hydration of alkali-activated blast-furnace slag - Part II: Effect of Al2O3. *Cement and Concrete Research*. January 2012. Vol. 42, no. 1, p. 74–83. DOI 10.1016/j.cemconres.2011.08.005.

135. Building Materials in Civil Engineering - Google Books. [online]. [Accessed 29 March 2020]. Available from: https://books.google.no/books?id=TZJwAgAAQBAJ&pg=PA47&lpg=PA47&dq=Portland+cement+is+the+hydraulic+binding+material+consisting+of+Portland+cement+clinker,+0~5%25+limestone+or+granulated+blast+furnace+slag,+and+a+limited+amount+of+...&source=bl&ots=aesgBha

136. DONATELLO, Shane, KUENZEL, Carsten, PALOMO, Angel and FERNÁNDEZ-JIMÉNEZ, Ana. High temperature resistance of a very high volume fly ash cement paste. *Cement and Concrete Composites*. 1 January 2014. Vol. 45, p. 234–242. DOI 10.1016/j.cemconcomp.2013.09.010.

137. SHANG, Huai-Shuai and YI, Ting-Hua. Behavior of HPC with Fly Ash after Elevated

Temperature. *Advances in Materials Science and Engineering* [online]. 2013. Vol. 2013. [Accessed 11 April 2020]. DOI 10.1155/2013/478421. Available from: http://dx.

138. LUBLÓY, Éva, BALÁZS, György L, CZOBOLY, Olivér and HARMAN, Béla. Influence of silica fume on fire resistance. *fib Symposium PRAGUE* [online]. 2011. [Accessed 11 April 2020]. Available from: https://www.researchgate.net/publication/268515417_Influence_of_silica_fume_on_fire_resistance

139. MORSY, M. M, SHELB, SS and RASHAD, AM. EFFECT OF FIRE ON MICROSTRUCTURE AND MECHANICAL PROPERTIES OF BLENDED CEMENT PASTES CONTAINING METAKAOLIN AND SILICA FUME. *ASIAN JOURNAL OF CIVIL ENGINEERING (BUILDING AND HOUSING) VOL. 9, NO. 2 (2008) PAGES 93-105* [online]. 2009. [Accessed 11 April 2020]. Available from: https://www.researchgate.net/publication/279713870_Effect_of_silica_fume_and_metakaoline_pozzolana_on_the_performance_of_blended_cement_pastes_against_fire

140. SIDDIQUE, Rafat and KAUR, Deepinder. Properties of concrete containing ground granulated blast furnace slag (GGBFS) at elevated temperatures. *Journal of Advanced Research*. January 2012. Vol. 3, no. 1, p. 45–51. DOI 10.1016/j.jare.2011.03.004.

141. Compressive Strength of High Volume Slag Cement Concrete in High Temperature Curing | Scientific.Net. [online]. [Accessed 11 April 2020]. Available from: https://www.scientific.net/AMR.287-290.793

142. MATHER, Bryant and HIME, William G. *Amount of Water Required for Complete Hydration of Portland Cement*. 2002.

143. PLUGIN, A.N., PLUGIN, A.A, WANG, W., KALININ, O.A. and MIROSHNICHENKO, S.V. The Long-Time Creep and Durability of the Concrete and Reinforced Concrete. [online]. 2003. [Accessed 9 April 2020]. Available from: https://www.researchgate.net/publication/331534209_The_Long-Time_Creep_and_Durability_of_the_Concrete_and_Reinforced_Concrete

144. BÜYÜKÖZTÜRK, Oral and LAU, Denvid. High performance concrete : fundamentals and application. *Proceedings of the International Conference on New Developments in Concrete Technologies*. 2007. P. 1–20.

145. CARUSO, Francesco, MANTELLATO, Sara, PALACIOS, Marta and FLATT, Robert J. ICP-OES method for the characterization of cement pore solutions and their modification by polycarboxylate-based superplasticizers. *Cement and Concrete Research*. 1 January 2017. Vol. 91, p. 52–60. DOI 10.1016/j.cemconres.2016.10.007.

146. ZHENG, J J, LI, C Q and ZHOU, X Z. *Thickness of interfacial transition zone and cement content profiles around aggregates*. [no date].

147. WONG, H. S., PAPPAS, A. M., ZIMMERMAN, R. W. and BUENFELD, N. R. Effect of entrained air voids on the microstructure and mass transport properties of concrete. *Cement and Concrete Research*. 1 October 2011. Vol. 41, no. 10, p. 1067–1077. DOI 10.1016/j.cemconres.2011.06.013.

148. SCHWOON, Oliver. A new efficient and safe admixture for freeze/thaw resistant concrete. In : *High Tech Concrete: Where Technology and Engineering Meet - Proceedings of the 2017 fib Symposium*. Springer International Publishing, 2017. p. 2162–2168. ISBN 9783319594705.

149. LI, Zongjin. *Advanced Concrete Technology* [online]. Hoboken, NJ, USA : John Wiley and Sons, 2011. [Accessed 12 April 2020]. ISBN 9780470437438. Available from: http://doi.wiley.com/10.1002/9780470950067

150. BRAMESHUBER, Wolfgang. Concrete An Example for Complex Porosity. . 2008. No. August, p. 1–19.

151. ANOVITZ, Lawrence M. and COLE, David R. Characterization and analysis of porosity and pore structures. *Reviews in Mineralogy and Geochemistry*. 1 January 2015. Vol. 80, no. 1, p. 61–164. DOI 10.2138/rmg.2015.80.04.

152. NOVÁKOVÁ, Iveta, DIEDERICHS, Ulrich and BODNÁROVÁ, Lenka. Usage of heat pretreatment for reduction of explosive spalling of high performance concrete. *Advanced Materials Research*. 2014. Vol. 1054, p. 37–42. DOI 10.4028/www.scientific.net/AMR.1054.37.

153. Innovative microsphere-based admixture technology for freeze-thaw durability eliminates the need for air-entrained concrete. [online]. [Accessed 12 April 2020]. Available from: https://www.basf.com/us/en/media/news-releases/2014/03/p-13-512.html

154. Readymix - MC-Bauchemie. [online]. [Accessed 12 April 2020]. Available from: https://www.mc-bauchemie.com/market-segments/concrete-industry/fields-of-expertise/readymix.html#/challenges-and-solutions

155. WAHEED, Farhan, KHALIQ, Wasim and KHUSHNOOD, Rao Arsalan. High-temperature residual strength and microstructure in air-entrained high-strength concrete. *ACI Materials Journal*. 1 May 2018. Vol. 115, no. 3, p. 425–436. DOI 10.14359/51702037.

156. KHALIQ, Wasim and WAHEED, Farhan. Mechanical response and spalling sensitivity

of air entrained high-strength concrete at elevated temperatures. *Construction and Building Materials*. 30 September 2017. Vol. 150, p. 747–757. DOI 10.1016/j.conbuildmat.2017.06.039.

157. HOLAN, J, NOVÁK, J and STEFAN, R ˇ. Air-entrainment as an alternative to polypropylene fibers and its effect on the compressive strength of concrete at high temperatures. . DOI 10.1088/1757-899X/596/1/012032.

158. POWERS, T.C. Structure and physical properties of hardened portland cement paste. *Journal of American ceramic society*. 1958. Vol. 41, no. 1, p. 1–6.

159. ALDRIDGE, L P, BORDALLO, H N, FERNANDO, K and BERTRAM, W K. *CRACKS AND PORES -THEIR ROLES IN THE TRANSMISSION OF WATER*.

160. THOMAS, Jeffrey J and JENNINGS, Hamlin M. Materials of Cement Science Primer: The Science of Concrete. . 2009.

161. DAVIE, Colin T., PEARCE, Chris J. and BIĆANIĆ, Nenad. Coupled heat and moisture transport in concrete at elevated temperatures - Effects of capillary pressure and adsorbed water. *Numerical Heat Transfer; Part A: Applications*. 2006. Vol. 49, no. 8, p. 733–763. DOI 10.1080/10407780500503854.

162. WANG, Yiyang, JIN, Feng and XIE, Yuetao. Experimental study on effects of casting procedures on compressive strength, water permeability, and interfacial transition zone porosity of rock-filled concrete. *Journal of Materials in Civil Engineering*. 1 August 2016. Vol. 28, no. 8. DOI 10.1061/(ASCE)MT.1943-5533.0001558.

163. ŠIMONOVÁ, H., VYHLÍDAL, M., KUCHARCZYKOVÁ, B., BAYER, P., KERŠNER, Z., MALÍKOVÁ, L. and KLUSÁK, J. Modelling of interfacial transition zone effect on resistance to crack propagation in fine-grained cement-based composites. *Frattura ed Integrita Strutturale*. 2017. Vol. 11, no. 41, p. 211–219. DOI 10.3221/IGF-ESIS.41.29.

164. WU, Kai. *Experimental Study on the Influence of ITZ on the Durability of Concrete Made with Different Kinds of Blended Materials*. 2013. ISBN 978-90-8578-701-3.

165. MEHTA, P K. CONCRETE. STRUCTURE, PROPERTIES AND MATERIALS. . 1986.

166. BEHBAHANI, Hamid, NEMATOLLAHI, Behzad and FARASATPOUR, Majid. Steel Fiber Reinforced Concrete: A Review. *ICSECM 2011 conference papaer* [online]. 2011. [Accessed 19 April 2020]. Available from: https://www.researchgate.net/publication/266174465_Steel_Fiber_Reinforced_Concrete_A_Review

167. KANSTAD, Terje and DOSSLAND, Ase Lyslo. *Publikasjon NB38: Fiberarmert betong i*

bærende konstruksjoner [online]. 2020. [Accessed 19 April 2020]. Available from: https://betong.net/aktuelt/horing-av-publikasjon-nb38-fiberarmert-betong-i-baerende-konstruksjoner/

168. KAHANJI, C, ALI, F and NADJAI, A. Explosive spalling of ultra-high performance fibre reinforced concrete beams under fire. [online]. [Accessed 18 April 2020]. DOI 10.1108/JSFE-12-2016-023. Available from: www.emeraldinsight.com/2040-2317.htm

169. BANERJI, Srishti, KODUR, Venkatesh and SOLHMIRZAEI, Roya. Experimental behavior of ultra high performance fiber reinforced concrete beams under fire conditions. *Engineering Structures*. 1 April 2020. Vol. 208. DOI 10.1016/j.engstruct.2020.110316.

170. Full range of composite reinforcement for concrete: MiniBars™ & BasBars™ | Reforcetech. [online]. [Accessed 19 April 2020]. Available from: https://reforcetech.com/full-range/

171. KODUR, V. K. R. Spalling in High Strength Concrete Exposed to Fire: Concerns, Causes, Critical Parameters and Cures. In : *Advanced Technology in Structural Engineering* [online]. Reston, VA : American Society of Civil Engineers, 27 April 2000. p. 1–9. [Accessed 18 April 2020]. ISBN 9780784404928. Available from: http://ascelibrary.org/doi/10.1061/40492%282000%29180

172. YERMAK, N., PLIYA, P., BEAUCOUR, A. L., SIMON, A. and NOUMOWÉ, A. Influence of steel and/or polypropylene fibres on the behaviour of concrete at high temperature: Spalling, transfer and mechanical properties. *Construction and Building Materials*. 1 February 2017. Vol. 132, p. 240–250. DOI 10.1016/j.conbuildmat.2016.11.120.

173. MOHAGHEGH, Ali Mohammadi, SILFWERBRAND, Johan, ARSKOG, Vemund and MCNAMEE, Robert Jansson. Fire Spalling of High-Performance Basalt Fibre Concrete. *Nordic Concrete Research* [online]. 2017. Vol. 57, no. 2, p. 89–102. [Accessed 19 April 2020]. Available from: http://www.diva-portal.org/smash/record.jsf?pid=diva2%3A1175721&dswid=206

174. KHOURY, G A and WILLOUGHBY, B. Polypropylene fibres in heated concrete. Part 1: Molecular structure and materials behaviour. [online]. [Accessed 19 April 2020]. DOI 10.1680/macr.2008.60.2.125. Available from: www.concrete-research.com

175. WANG, Wei Chien, WANG, Her Yung, CHANG, Kao Hao and WANG, Shao Yu. Effect of high temperature on the strength and thermal conductivity of glass fiber concrete. *Construction and Building Materials*. 10 June 2020. Vol. 245.

DOI 10.1016/j.conbuildmat.2020.118387.

176. ÇAVDAR, Ahmet. A study on the effects of high temperature on mechanical properties of fiber reinforced cementitious composites. *Composites Part B: Engineering*. July 2012. Vol. 43, no. 5, p. 2452–2463. DOI 10.1016/j.compositesb.2011.10.005.

177. LIU, X., YE, G., DE SCHUTTER, G., YUAN, Y. and TAERWE, L. On the mechanism of polypropylene fibres in preventing fire spalling in self-compacting and high-performance cement paste. *Cement and Concrete Research*. 1 April 2008. Vol. 38, no. 4, p. 487–499. DOI 10.1016/j.cemconres.2007.11.010.

178. SILFWERBRAND, J. *SWEDISH RECOMMENDATIONS FOR PREVENTING FIRE SPALLING IN CONCRETE STRUCTURES FOR CIVIL ENGINEERING PURPOSES*. [no date].

179. NATTA, Giulio and CORRADINI, Paolo. Conformation of linear chains and their mode of packing in the crystal state. *Journal of Polymer Science* [online]. 1 September 1959. Vol. 39, no. 135, p. 29–46. [Accessed 22 April 2020]. DOI 10.1002/pol.1959.1203913504. Available from: http://doi.wiley.com/10.1002/pol.1959.1203913504

180. MEARS, P. *Polymers : structure and bulk properties*. London : Van Nostrand Reinhold, 1965.

181. NEVILLE, A.M. *Properties of cocnrete*. Longman Group, 1995.

182. HUISMANN, Sven, WEISE, Frank, MENG, Birgit and SCHNEIDER, Ulrich. Influence of polypropylene fibres on the thermal strain of high strength concrete at high temperatures. In : *Journal of Structural Fire Engineering*. 1 September 2011. p. 173–179.

183. PISTOL, Klaus, WEISE, Frank, MENG, Birgit and DIEDERICHS, Ulrich. Polypropylene fibres and micro cracking in fire exposed concrete. In : *Advanced Materials Research* [online]. Trans Tech Publications, 2014. p. 284–289. [Accessed 16 August 2020]. ISBN 9783038350262. Available from: https://www.scientific.net/AMR.897.284

184. WANG, Wei Chien, WANG, Shao Yu and LIN, Cheng Hsun. EFFECT OF HIGH TEMPERATURE ON PROPERTIES OF GLASS CONCRETE. . DOI 10.1051/matecconf/201713801007.

185. TUFAIL, Muhammad, SHAHZADA, Khan, GENCTURK, Bora and WEI, Jianqiang. Effect of Elevated Temperature on Mechanical Properties of Limestone, Quartzite and Granite Concrete. *International Journal of Concrete Structures and Materials* [online]. 1 March 2017. Vol. 11, no. 1, p. 17–28. [Accessed 26 April 2020]. DOI 10.1007/s40069-

016-0175-2. Available from: http://link.springer.com/10.1007/s40069-016-0175-2

186. XING, Zhi, BEAUCOUR, Anne Lise, HEBERT, Ronan, NOUMOWE, Albert and LEDESERT, Béatrice. Influence of the nature of aggregates on the behaviour of concrete subjected to elevated temperature. *Cement and Concrete Research*. 1 April 2011. Vol. 41, no. 4, p. 392–402. DOI 10.1016/j.cemconres.2011.01.005.

187. XING, Zhi, HÉBERT, Ronan, BEAUCOUR, Anne-Lise, LEDÉSERT, Béatrice and NOUMOWÉ, Albert. Influence of chemical and mineralogical composition of concrete aggregates on their behaviour at elevated temperature. *Materials and Structures*. 2014. DOI 10.1617/s11527-013-0161-y.

188. XING, Zhi, BEAUCOUR, Anne Lise, HEBERT, Ronan, NOUMOWE, Albert and LEDESERT, Béatrice. Aggregate's influence on thermophysical concrete properties at elevated temperature. *Construction and Building Materials*. 21 July 2015. Vol. 95, p. 18–28. DOI 10.1016/j.conbuildmat.2015.07.060.

189. RAYSSAC, Erwann, AURIOL, Jean Claude, DENEELE, Dimitri, DE LARRARD, François, LEDEE, Vincent and PLATRET, Gérard. *Valorisation de laitiers d'acierie LD pour les infrastructures routières* [online]. [no date]. [Accessed 27 April 2020]. Available from: https://hal.archives-ouvertes.fr/hal-00451330

190. BODNAROVA, Lenka, HELA, Rudolf, HUBERTOVÁ, Michala and NOVÁKOVÁ, Iveta. Behaviour of Lightweight Expanded Clay Aggregate Concrete Exposed to High Temperatures. *International Journal of Civil and Environmental Engineering* [online]. 2014. Vol. 8, no. 12. [Accessed 27 April 2020]. Available from: https://publications.waset.org/9999750/behaviour-of-lightweight-expanded-clay-aggregate-concrete-exposed-to-high-temperatures

191. YILMAZ, M. and TURUL, A. The effects of different sandstone aggregates on concrete strength. *Construction and Building Materials*. October 2012. Vol. 35, p. 294–303. DOI 10.1016/j.conbuildmat.2012.04.014.

192. KOMPANÍKOVÁ, Z., GOMEZ-HERAS, M., MICHŇOVÁ, J., DURMEKOVÁ, T. and VLČKO, J. Sandstone alterations triggered by fire-related temperatures. *Environmental Earth Sciences*. 1 October 2014. Vol. 72, no. 7, p. 2569–2581. DOI 10.1007/s12665-014-3164-2.

193. ZOLDNERS, N.G. *Thermal Properties of Concrete Under Sustained Elevated Temperatures*. 1971.

194. KHOURY, Gabriel Alexander. *Effect of heat on cocnrete material*. 1995.

195. HUANG, Shan-Shan and BURGESS, Ian (eds.). Fire spalling 2019. In : HUANG, Shan-

Shan and BURGESS, Ian (eds.), *Proceedings of the 6th International Workshop on Concrete Spalling due to Fire Exposure*. The University of Sheffield Sheffield, UK, 2019.

196. PAN, Zhu, SANJAYAN, Jay G. and KONG, Daniel L.Y. Effect of aggregate size on spalling of geopolymer and Portland cement concretes subjected to elevated temperatures. *Construction and Building Materials*. 1 November 2012. Vol. 36, p. 365–372. DOI 10.1016/j.conbuildmat.2012.04.120.

197. JANSSON, R. Fire spalling of concrete - A historical overview. *MATEC Web of Conferences*. 2013. Vol. 6, no. August. DOI 10.1051/matecconf/20130601001.

198. BARRET. On the French and other methods of constructing iron floors. *Civil Engineering and Architect's Journal*. 1854. Vol. 17, p. 94.

199. HINRICHSMEYER, K. and ROSTASY, F.S. Analysis of thermal damage of concrete by aplication of the structural model. *HEFT 1990*. 1990. DOI 0863-0720.

200. MCNAMEE, Robert. FIRE SPALLING THEORIES – REALISTIC AND MORE EXOTIC ONES. *Proceedings of the 6th International Workshop on Concrete Spalling due to Fire Exposure*. 2019. No. September, p. 19–20.

201. JANSSON MCNAMEE, Robert and BOSTROM, L. Three experiments to validate basic functions in firespalling models. *The 4th International RILEM Workshop on Concrete Spalling due to Fire Exposure*. 2015.

202. WAUBKE, N. V. and SCHNEIDER, U. Tensile stress in concrete due to fast vapour flow. *Proceedings of the international RILEM symposium "Pore Structure and Properties of Materials*. 1973.

203. NOVÁKOVÁ, Iveta, ÞÓRHALLSSON, Eyþór Rafn, WALLEVIK, Olafur and BODNÁROVÁ, Lenka. Influence of porosity of basalt aggregates on fire resistance and freeze-thaw durability of fibre reinforced concrete. In : *The 11th High Performance Concrete (11th HPC) & The Second Concrete Innovation Conference (2nd CIC)* [online]. 2017. [Accessed 12 August 2020]. Available from: https://www.researchgate.net/publication/315443203_INFLUENCE_OF_POROSITY_OF_BASALT_AGGREGATES_ON_FIRE_RESISTANCE_AND_FREEZE-THAW_DURABILITY_OF_FIBRE_REINFORCED_CONCRETE

204. NOVÁKOVÁ, Iveta, ÞÓRHALLSSON, Eyþór Rafn and BODNÁROVÁ, Lenka. Behaviour of Basalt Fibre Reinforced Concrete Exposed to Elevated Temperatures. In : *5th International RILEM Workshop on Concrete Spalling due to Fire Exposure* [online]. 2017. [Accessed 12 August 2020]. Available from: https://www.researchgate.net/publication/327906392

205. NOVÁKOVÁ, Iveta and BODNÁROVÁ, Lenka. High strength concrete with enhanced properties by addition of chopped basalt fibres. In : *Materials Science Forum* [online]. Trans Tech Publications Ltd, 2017. p. 164–170. [Accessed 12 August 2020]. ISBN 9783035711578. Available from: https://www.scientific.net/MSF.908.164

206. DIEDERICHS, U, BODNAROVA, L and PETRANEK, V. Fire safety assessment and upgrading of existing traffic tunnels. *MATEC Web of Conferences* [online]. 2013. Vol. 6, p. 6001. [Accessed 16 August 2020]. DOI 10.1051/matecconf/20130606001. Available from: http://dx.doi.org/10.1051/matecconf/20130606001

207. FAQ: Boiling and altitude/pressure. [online]. [Accessed 30 May 2020]. Available from: http://www.iapws.org/faq1/boil.html

208. BUCK, A. L. New equations for computing vapor pressure and enhancement factor. *J. Appl. Meteorol.* [online]. 1981. Vol. 20, p. 1527–1532. [Accessed 30 May 2020]. Available from: http://ams.allenpress.com/perlserv/?request=get-pdf&doi=10.1175%2F1520-0450%281981%29020%3C1527%3ANEFCVP%3E2.0.CO%3B2

209. Tetens equation - Wikipedia. [online]. [Accessed 30 May 2020]. Available from: https://en.wikipedia.org/wiki/Tetens_equation

210. MIYAGI, Isoji, MATSUBAYA, Osamu and NAKASHIMA, Satoru. *Change in D/H ratio, water during dehydration of content and color hornblende*. 1998.

211. AABORGPORTLAND. Declaration of performance CEM I 42,5 N SR5. [online]. [Accessed 18 May 2020]. Available from: https://www.aalborgportland.dk/wp-content/uploads/2019/01/ydeevnedeklaration_lavalkali_sulfatbestandig_cement_nr_4_2016_DK.pdf

212. Norcem Standardsement FA | Norcem. [online]. [Accessed 31 May 2020]. Available from: https://www.norcem.no/en/standardsement_fa

213. DIAMOND, Sidney and SAHU, Sadananda. Densified silica fume: Particle sizes and dispersion in concrete. In : *Materials and Structures/Materiaux et Constructions*. Springer Netherlands, 2 August 2006. p. 849–859.

214. MasterGlenium SKY 615. [online]. [Accessed 1 June 2020]. Available from: https://www.master-builders-solutions.basf.no/nn-no/products/mastergleniumsky/masterglenium-sky-615

215. MasterGlenium SKY 830. [online]. [Accessed 1 June 2020]. Available from: https://www.master-builders-solutions.basf.no/nn-no/products/mastergleniumsky/masterglenium-sky-830

216. MasterAir 11. [online]. [Accessed 1 June 2020]. Available from: https://www.master-builders-solutions.basf.no/nn-no/products/masterair/masterair-11

217. *SikaControl® AER-200 P*. [no date].

218. BS EN 12620:2013 Aggregates for concrete. [online]. [Accessed 6 June 2020]. Available from: https://shop.bsigroup.com/ProductDetail/?pid=000000000030212560

219. BS EN 196 - Methods of testing cement. [online]. [Accessed 6 June 2020]. Available from: https://landingpage.bsigroup.com/LandingPage/Series?UPI=BS EN 196

220. BS EN 933-2:1996 - Tests for geometrical properties of aggregates. Determination of particle size distribution. Test sieves, nominal size of apertures – BSI British Standards. [online]. [Accessed 6 June 2020]. Available from: https://shop.bsigroup.com/ProductDetail/?pid=000000000000759331

221. BS EN 1097-6:2013 - Tests for mechanical and physical properties of aggregates. Determination of particle density and water absorption. [online]. [Accessed 6 June 2020]. Available from: https://shop.bsigroup.com/ProductDetail?pid=000000000030218643

222. BS EN 196-1:2016 - Methods of testing cement. Determination of strength. [online]. [Accessed 7 June 2020]. Available from: https://shop.bsigroup.com/ProductDetail/?pid=000000000030291447

223. BS EN 206:2013+A1:2016 Concrete. Specification, performance, production and conformity. [online]. [Accessed 7 June 2020]. Available from: https://shop.bsigroup.com/ProductDetail/?pid=000000000030326195

224. BS EN 12350-2:2019 - Testing fresh concrete. Slump test. [online]. [Accessed 7 June 2020]. Available from: https://shop.bsigroup.com/ProductDetail?pid=000000000030360058

225. BS EN 12350-6:2019 - Testing fresh concrete. Density. [online]. [Accessed 7 June 2020]. Available from: https://shop.bsigroup.com/ProductDetail?pid=000000000030360091

226. BS EN 12350-7:2019 - Testing fresh concrete. Air content. Pressure methods. [online]. [Accessed 7 June 2020]. Available from: https://shop.bsigroup.com/ProductDetail/?pid=000000000030360094

227. BS EN 12350-1:2019 - Testing fresh concrete. Sampling and common apparatus. [online]. [Accessed 7 June 2020]. Available from: https://shop.bsigroup.com/ProductDetail?pid=000000000030360061

228. BS EN 12390-1:2012 - Testing hardened concrete. Shape, dimensions and other requirements for specimens and moulds. [online]. [Accessed 7 June 2020]. Available from: https://shop.bsigroup.com/ProductDetail/?pid=000000000030254400

229. BS EN 12390-7:2019 - Testing hardened concrete. Density of hardened concrete. [online]. [Accessed 7 June 2020]. Available from: https://shop.bsigroup.com/ProductDetail?pid=000000000030360085

230. BS EN 12390-3:2019 - Testing hardened concrete. Compressive strength of test specimens. [online]. [Accessed 7 June 2020]. Available from: https://shop.bsigroup.com/ProductDetail?pid=000000000030360097

231. BS EN 12390-6:2009 - Testing hardened concrete. Tensile splitting strength of test specimens. [online]. [Accessed 7 June 2020]. Available from: https://shop.bsigroup.com/ProductDetail/?pid=000000000030200045

232. C457/C457M, ASTM. Standard Test Method for Microscopical Determination of Parameters of the Air-Void System in Hardened Concrete. *ASTM International, West Conshohocken, PA* [online]. 2016. [Accessed 7 June 2020]. DOI 10.1520/C0457_C0457M-16. Available from: www.astm.org

233. BS EN 480-11:2005 - Admixtures for concrete, mortar and grout. Test methods. Determination of air void characteristics in hardened concrete. [online]. [Accessed 7 June 2020]. Available from: https://shop.bsigroup.com/en/ProductDetail/?pid=000000000030129094

234. PD CEN/TS 12390-9:2016 - Testing hardened concrete. Freeze-thaw resistance with de-icing salts. Scaling. [online]. [Accessed 7 June 2020]. Available from: https://shop.bsigroup.com/ProductDetail?pid=000000000030332517

235. Mercury Intrusion Porosimetry - Particle Technology Labs. [online]. [Accessed 12 June 2020]. Available from: https://www.particletechlabs.com/analytical-testing/gas-adsorption-and-porosimetry/mercury-intrusion-porosimetry

236. STRUBLE, L. J. and BROWN, P.W. *An Evaluation of Ettringite and Related Compounds for Use in Solar Energy Storage*. 1984.

237. PÖLLMANN, Herbert. *Cementitious Materials: Composition, Properties, Application* [online]. 2017. [Accessed 2 July 2020]. Available from: https://books.google.cz/books?id=RZJdDwAAQBAJ&pg=SA3-PA36&lpg=SA3-PA36&dq=β–c2s+size&source=bl&ots=MEdJBnKque&sig=ACfU3U2euIkrdnc9bKoqNXIJA0Fh31zFEw&hl=en&sa=X&ved=2ahUKEwjMjdfek6_qAhWM-

KQKHfUaC4kQ6AEwAHoECAkQAQ#v=onepage&q=β–c2s size&f=false

238. BONAVETTI, V. L., RAHHAL, V. F. and IRASSAR, E. F. Studies on the carboaluminate formation in limestone filler-blended cements. *Cement and Concrete Research*. 1 May 2001. Vol. 31, no. 6, p. 853–859. DOI 10.1016/S0008-8846(01)00491-4.

239. Kinetic Hydration Heat Modeling for High-Performance Concrete Containing Limestone Powder. [online]. [Accessed 4 July 2020]. Available from: https://www.hindawi.com/journals/amse/2017/4090265/

240. *Can Excess Soluble Sulfates in Cement Cause Deleterious Expansions in Concrete?* [no date].

241. DRIESSCHE, Alexander E S Van, STAWSKI, Tomasz M, BENNING, Liane G, KELLERMEIER, Matthias, VAN DRIESSCHE, A E S, STAWSKI, T M, BENNING, L G and KELLERMEIER, M. Calcium Sulfate Precipitation Throughout Its Phase Diagram. *New Perspectives on Mineral Nucleation and Growth*. 2017. No. 3. DOI 10.1007/978-3-319-45669-0_12.

242. VAN DRIESSCHE, A. E.S., BENNING, L. G., RODRIGUEZ-BLANCO, J. D., OSSORIO, M., BOTS, P. and GARCÍA-RUIZ, J. M. The role and implications of bassanite as a stable precursor phase to gypsum precipitation. *Science* [online]. 6 April 2012. Vol. 335, no. 6077, p. 69–72. [Accessed 4 July 2020]. DOI 10.1126/science.1215648. Available from: www.sciencemag.orgSCIENCEVOL336

243. Match! - Phase Identification from Powder Diffraction. [online]. [Accessed 9 July 2020]. Available from: https://www.crystalimpact.com/match/

244. EN 450-1：2012 | FLY ASH FOR CONCRETE - PART 1: DEFINITION, SPECIFICATIONS AND CONFORMITY CRITERIA | SAI Global. [online]. [Accessed 14 July 2020]. Available from: https://infostore.saiglobal.com/en-us/Standards/EN-450-1-2012-334221_SAIG_CEN_CEN_767754/

ABBREVIATIONS

HPC	high-performance concrete
SCC	self-compacting concrete
FRC	fibre reinforced concrete
UHPC	Ultra-high performance concrete
CSH gel	calcium silicate hydrates gel
IHT method	intentional heat treatment method
CAFS	compressed air foam systems
HGV	heavy goods vehicles
RH	relative humidity
FRR	Fire Resistance Rating
HC	hydrocarbon
MHC	modified hydrocarbon
RWS	Rijkswaterstaat
HTL	head-then-load
LTH	load-then-head
LITS	load-induced thermal strain
ε ela,0ε	elastic strain at ambient temperature
ε lits	load-induced thermal strain
FTS	free thermal strain
ISAT	initial surface absorption test
RHR	rate head release
HSC	hight strength concrete
TRID	Transport Research Information Database
PbM	performance -based methods
^{29}Si MAS-NMR	^{29}Si magic-angle spinning nuclear magnetic resonance
RILEM	International Union of Laboratories and Experts in Construction Materials,Systems and Structures
Fib	The International Federation for Structural Concrete
HITECOSP	hight -temperature concrete spalling
ITZ	interfacial transition zone
SCM	supplementary cementitious material
CAH	calcium aluminates hydrates
TGA	thermogravimetry analysis
DTA	diffraction thermal analysis
XRD	X-rya diffraction analysis
BSE/IA	backscatter electron image analysis
NMR	nuclear magnetic resonance
TGA/DTA	thermal analysis
FA	fly ash
SL	slag (ground granulated blast furnace)
SF	silica fume
OPC	ordinary Portland cement
AeA	air-entraining agent
AeA- HSC	air-entraining agent hight strength concrete
PPF	polypropylene fibres
PITS	pressure-induced tangential space

PVA	polyvinyl alcohol
LWA	light-weight aggregates
BLEVE	Boiling Liquid expanding Vapour Explosion
AeA-FiResCrete	Air-Entraining Agent Fire Resistant Concrete
SP	superplasticizer
PCE	polycarboxylate
LA test	the Los Angeles test
MIP	mercury intrusion porosimatry
WS	water storage
LAB	laboratory condition curing
Tg	temperature gradient
DZ	dry zone
VZ	vapour zone
SZ	saturated zone
T	temperature
p_v	vapour pressure
w	moisture content

LIST OF FIGURES

LIST OF TABLES

ANNEXES

Annex 1

Fig. 129: Photo documentation of samples from the 3rd series after application of various configurations of IHT method and thermal exposure according to m-ISO curve. (a) Reference sample without IHT method; (b) IHT200/1; (c) IHT200/2; (d) IHT250/1; (e) IHT250/2; (f) Samples in oven before thermal exposure.

Annex 2

Tab. 46: Mix design of samples used during the development of IHT in the 4th series, namely mix 4CEM, 5FA, 6SF and 7NO.

Name	Aggregates		Cement		Supplementary cementitious materials		Admixtures		Water	
	Fraction	Dose [%]	Type	Dose [%]	Type	Dose [% of mc]	Type	Dose [% of m_c]	w/c ratio	Dose [l]
4CEM	0-8 mm Basalt_IS	70	CEM I 42,5N-SR5	340	-	-	MasterGlenium SKY 830	0,88	0,37	126
	8-22,4 mm Basalt_IS	30								
5FA	0-8 mm Basalt_IS	70	CEM II/B-M 42,5 R	340	-	-	MasterGlenium SKY 830	0,7	0,42	151
	8-22,4 mm Basalt_IS	30								
6SF	0-8 mm Basalt_IS	70	CEM I 42.5N-SR5	320	Silica Fume	6	MasterGlenium SKY 830	1,1	0,38	122
	8-22,4 mm Basalt_IS	30								
7NO	0-8 mm Granite_NO	62	CEM I 42.5N-SR5	340	-	-	MasterGlenium SKY 830	1,5	0,32	109
	8-16 mm Granite_NO	38								

Annex 3

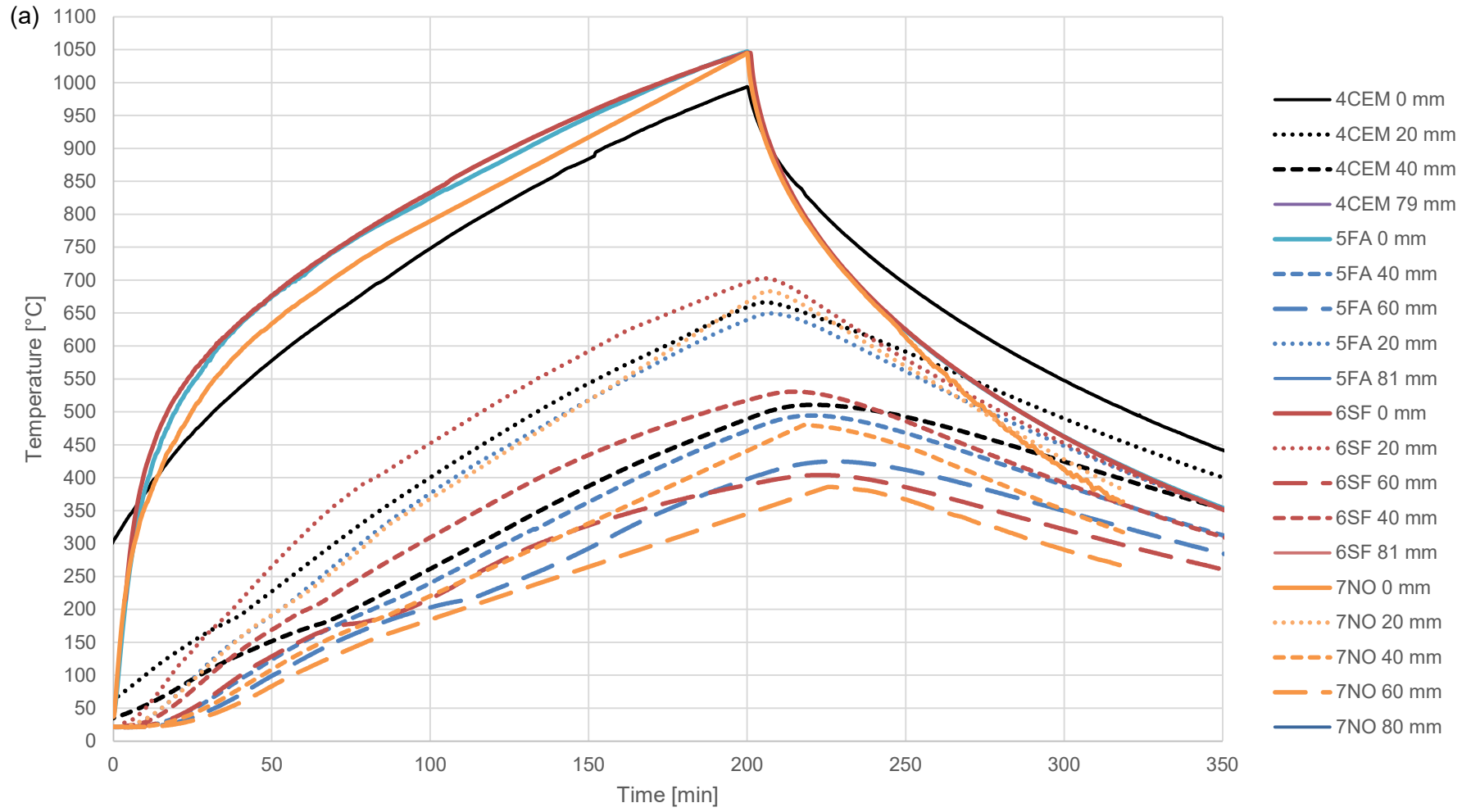
(a)
Temperature [°C]
Time [min]
0
50
100
150
200
250
300
350
0
50
100
150
200
250
300
350
400
450
500
550
600
650
700
750
800
850
900
950
1000
1050
1100
4CEM 0 mm
4CEM 20 mm
4CEM 40 mm
4CEM 79 mm
5FA 0 mm
5FA 40 mm
5FA 60 mm
5FA 20 mm
5FA 81 mm
6SF 0 mm
6SF 20 mm
6SF 60 mm
6SF 40 mm
6SF 81 mm
7NO 0 mm
7NO 20 mm
7NO 40 mm
7NO 60 mm
7NO 80 mm

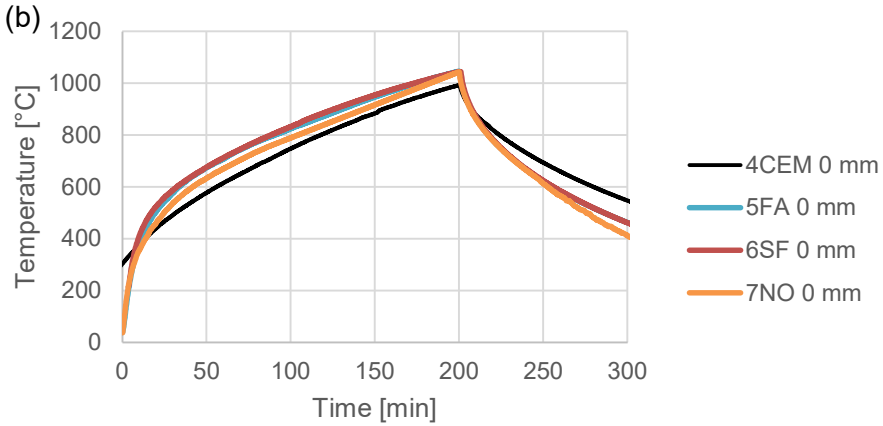
(b)
Temperature [°C]
Time [min]
4CEM 0 mm
5FA 0 mm
6SF 0 mm
7NO 0 mm

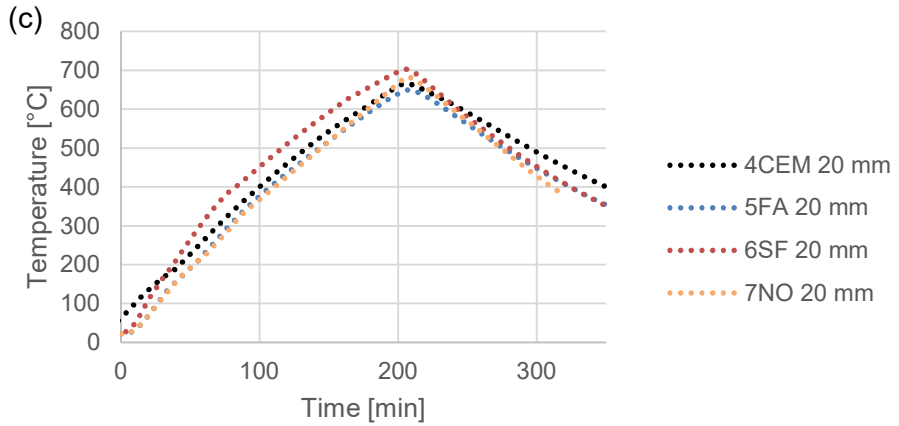
(c)
Temperature [°C]
Time [min]
4CEM 20 mm
5FA 20 mm
6SF 20 mm
7NO 20 mm

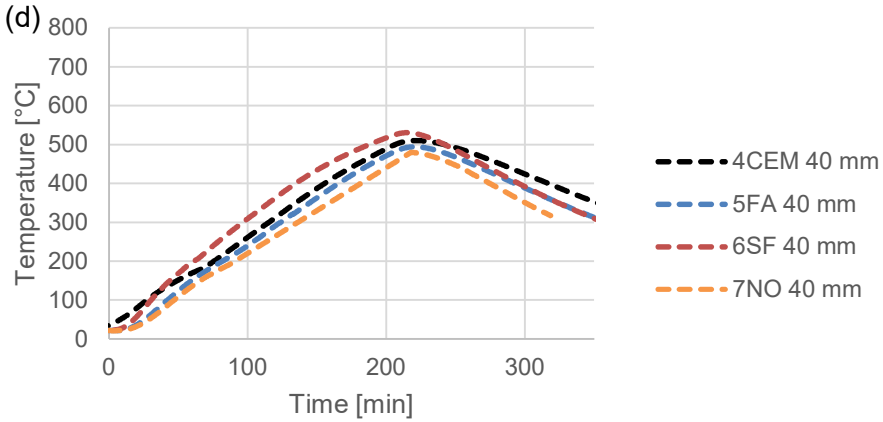
(d)
Temperature [°C]
Time [min]
4CEM 40 mm
5FA 40 mm
6SF 40 mm
7NO 40 mm

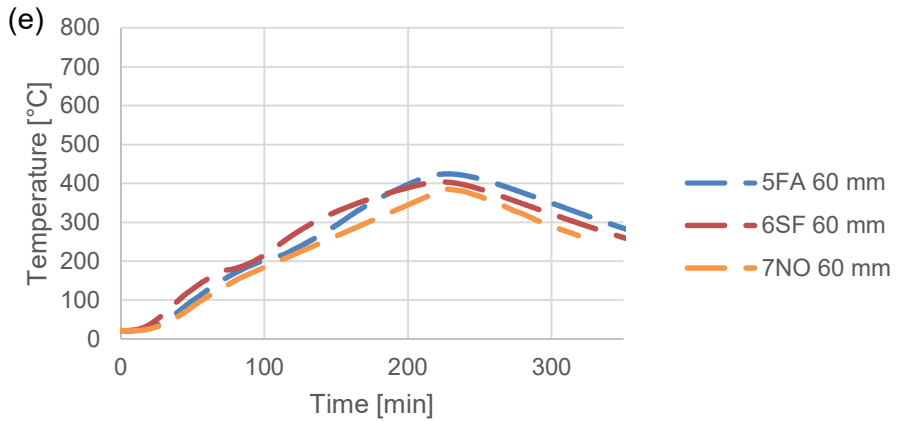
(e)
Temperature [°C]
Time [min]
5FA 60 mm
6SF 60 mm
7NO 60 mm

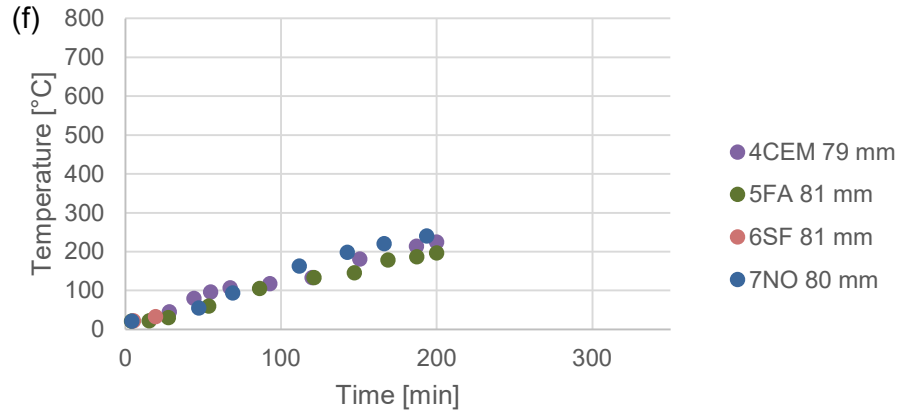

Fig. 130: Slab testing and validation of IHT200/2 on four different concrete types (4CEM, 5FA, 6SF, 7NO). Temperature development during exposure to m-ISO curve in the depth of 0, 20, 40, 60 mm and top of slabs. (a) Temperature curves of all samples in all depths; (b) Temperature curves of all samples in the depth of 0 mm form heated surface; (c) Temperature curves of all samples in the depth of 20 mm form heated surface; (d) Temperature curves of all samples in the depth of 40 mm form heated surface; (e) Temperature curves of all samples in the depth of 60 mm form heated surface; (f) Temperature curves of all samples measured on the top of slabs.

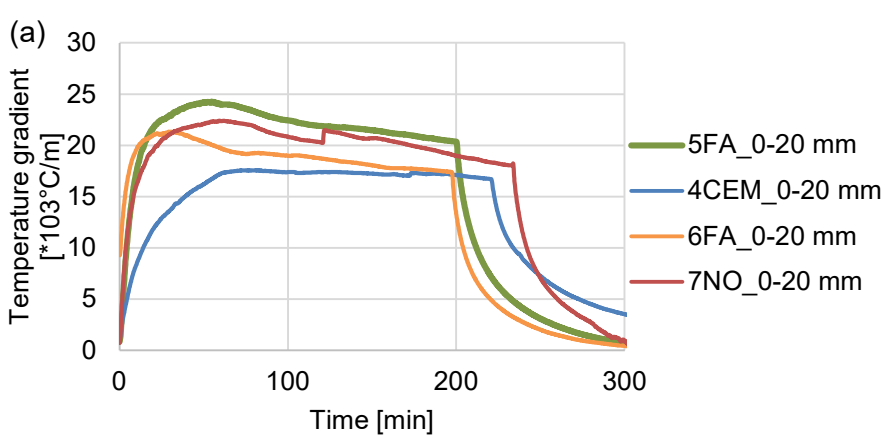

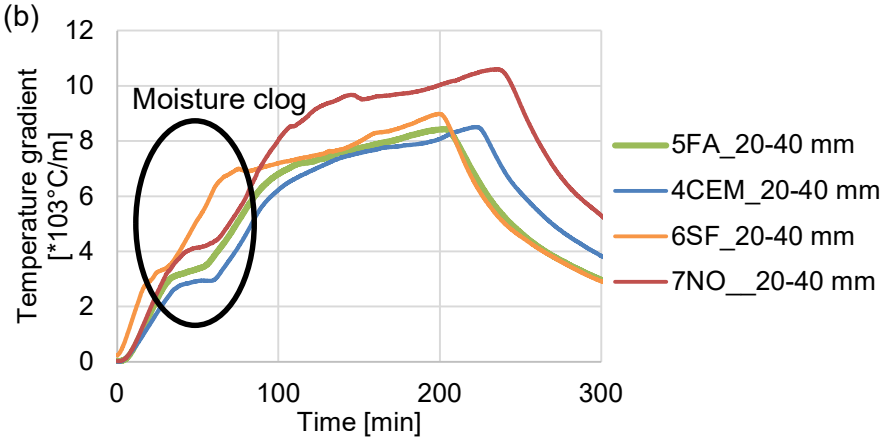

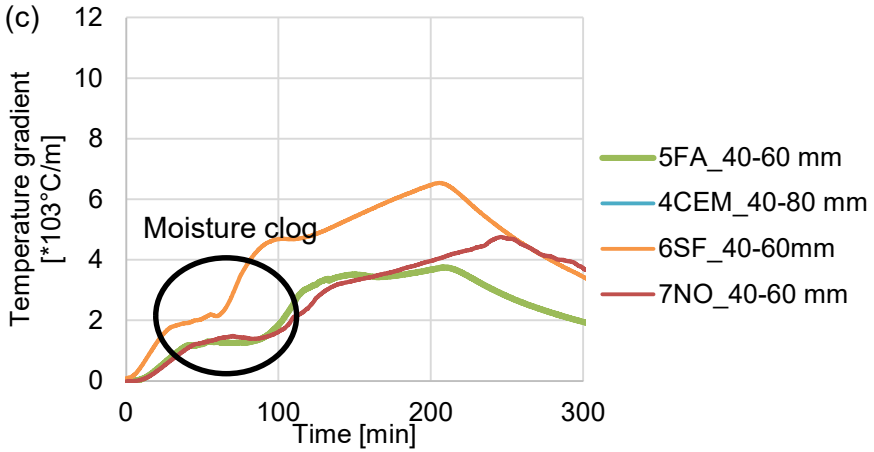

Fig. 131: Slab testing and validation of IHT200/2 on four different concrete types (4CEM, 5FA, 6SF, 7NO). The temperature gradient of slabs exposed to m-ISO curve calculated in between 0-20 mm, 20-40 mm, 40-60mm and 60mm to top from heated surface. (a) The temperature gradient between 0-20 mm from heated surface (b) The temperature gradient between 20-40 mm from heated surface; (c) The temperature gradient between 40-60 mm or 40-80 mm from heated surface.

Annex 4

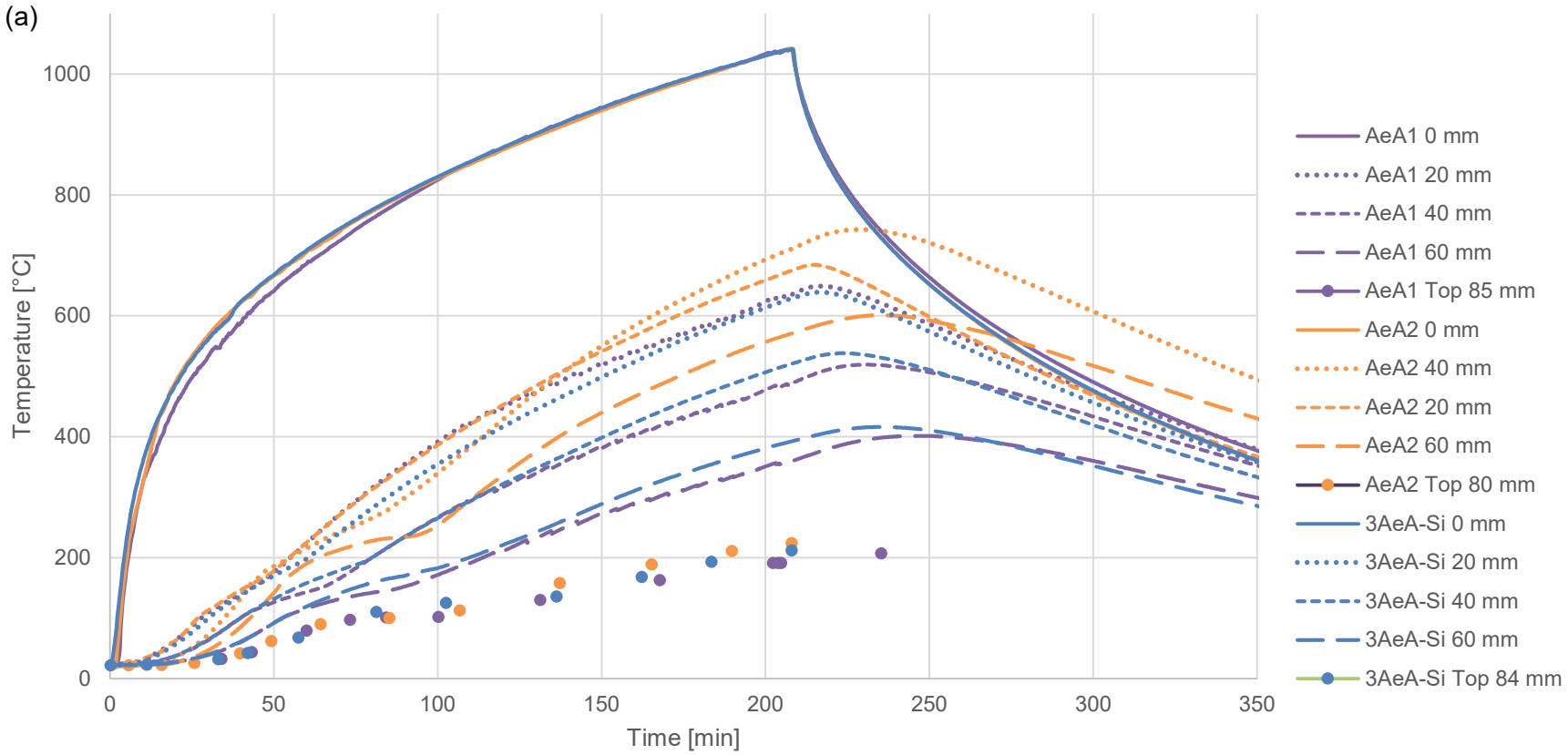
(a)
Temperature [°C]
Time [min]
0
200
400
600
800
1000
0
50
100
150
200
250
300
350
AeA1 0 mm
AeA1 20 mm
AeA1 40 mm
AeA1 60 mm
AeA1 Top 85 mm
AeA2 0 mm
AeA2 40 mm
AeA2 20 mm
AeA2 60 mm
AeA2 Top 80 mm
3AeA-Si 0 mm
3AeA-Si 20 mm
3AeA-Si 40 mm
3AeA-Si 60 mm
3AeA-Si Top 84 mm

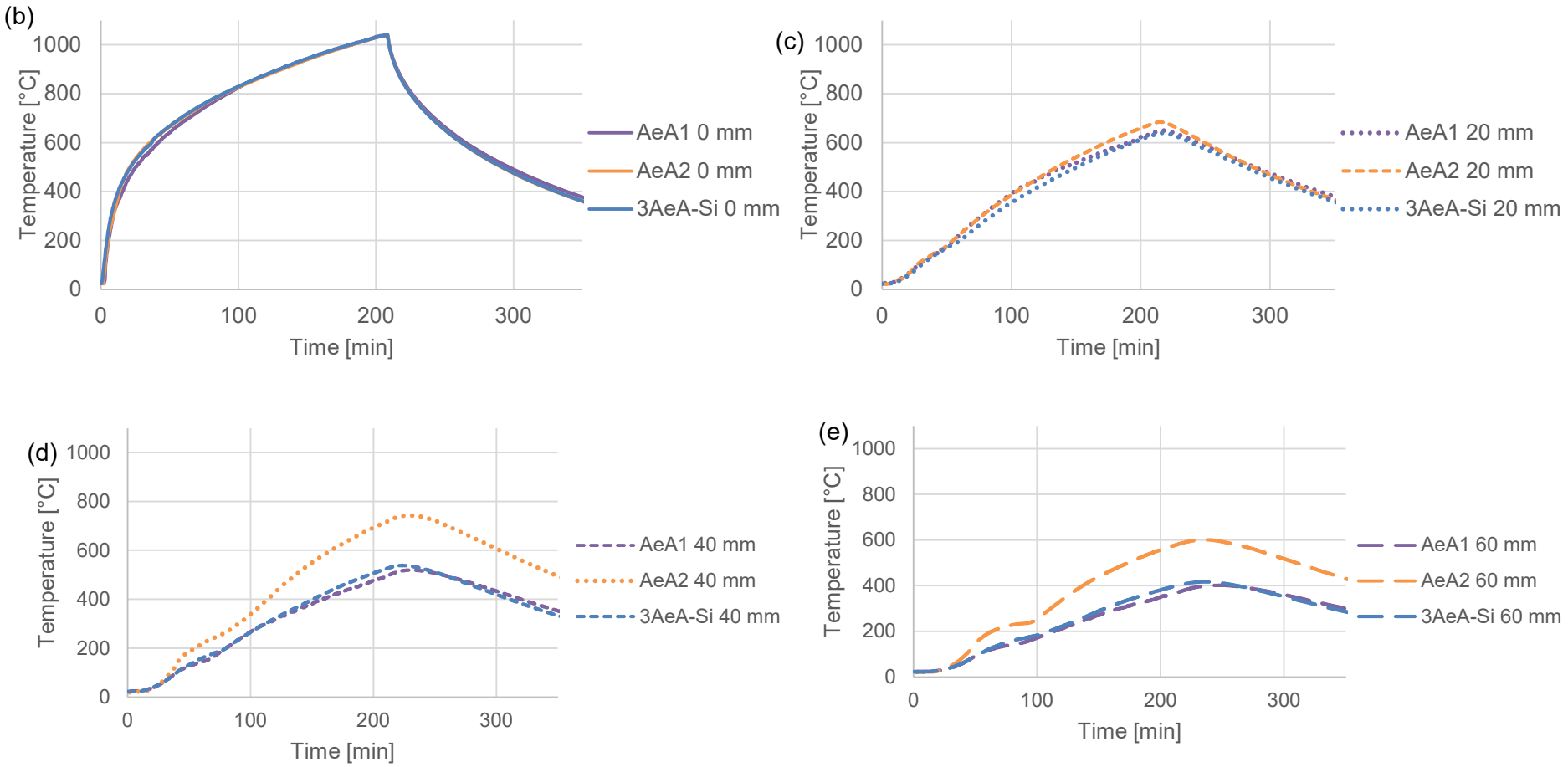

Fig. 132: Slab testing and validation of AeA-FiResCrete on three different concrete types (AeA1, AeA2, AeA3). Temperature development during exposure to m-ISO curve in the depth of 0, 20, 40, 60 mm and top of slabs. (a) Temperature curves of all samples in all depths; (b) Temperature curves of all samples in the depth of 0 mm form heated surface; (c) Temperature curves of all samples in the depth of 20 mm form heated surface; (d) Temperature curves of all samples in the depth of 40 mm form heated surface; (e) Temperature curves of all samples in the depth of 60 mm form heated surface.

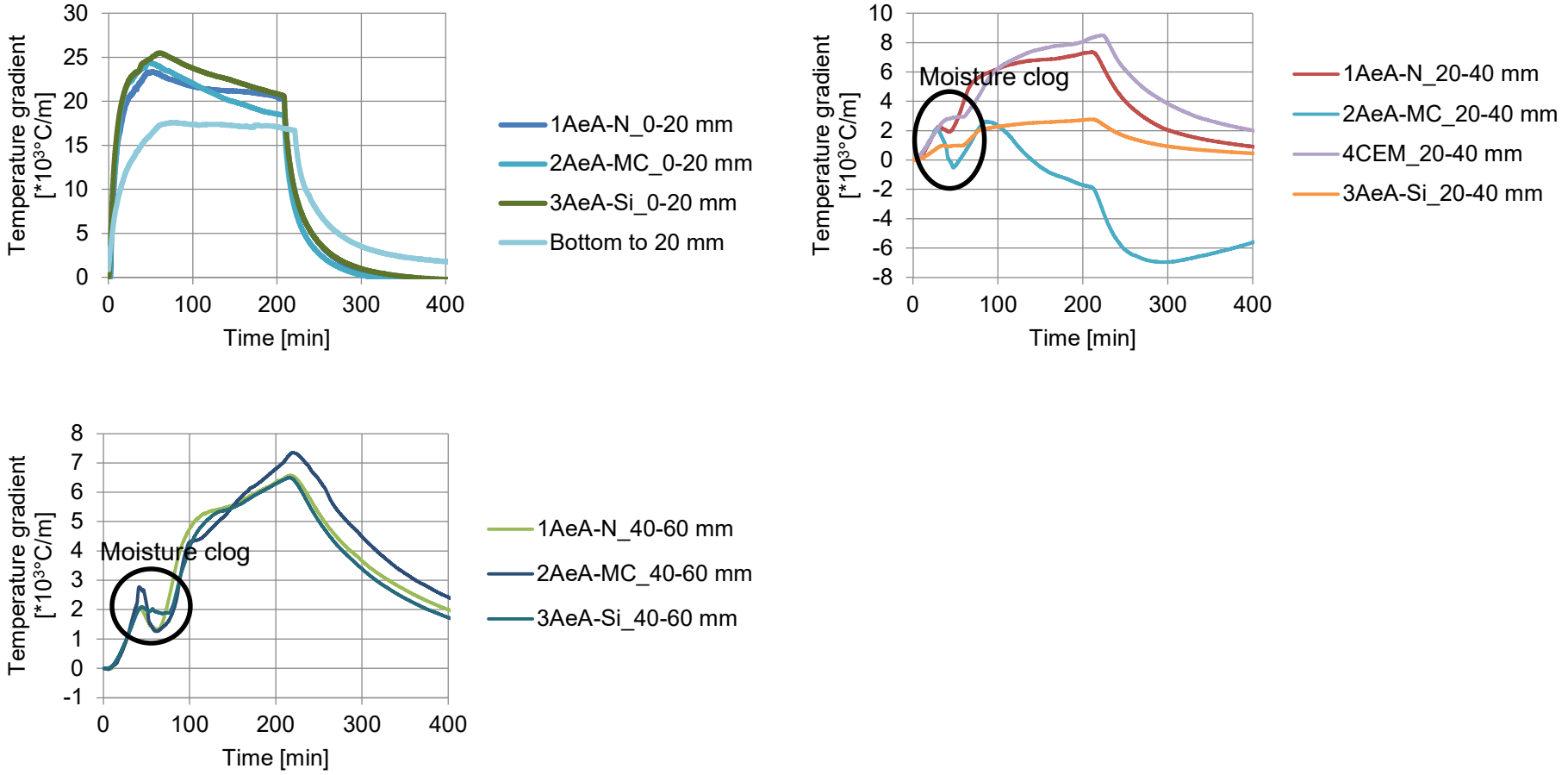

Fig. 133: Slab testing and validation of AeA-FiResCrete on three different concrete types (AeA1, AeA2, AeA3). The temperature gradient of slabs exposed to m-ISO curve calculated in between 0-20 mm, 20-40 mm, 40-60mm and 60mm to top from heated surface. (a) The temperature gradient between 0-20 mm from heated surface (b) The temperature gradient between 20-40 mm from heated surface; (c) The temperature gradient between 40-60 mm from heated surface.